"Polyelectrolyte multilayer nanotubes for drug delivery applications"

Saghazadeh, Saghi

Abstract

Recent advances in medicine and nanotechnology have inspired numerous researches in which nano-engineering is used for the development of optimal drug nanocarrier. Up to now, most efforts in this field have been focused on creating spherical nanocarriers such as liposomes, capsules, or polymersomes. However, anisotropic structures such as nanotubes are currently attracting considerable attention because they offer some promising advantages over isotropic structures. The size of nanotubes can be manipulated in two dimensions, giving the opportunity to construct nanotubes with different aspect ratios. They possess higher surface area compared to nanospheres of identical radius, resulting in more functional groups (antifouling, targeting…) assembled on their surface. Elaborated structures can be achieved by separately and selectively functionalizing the inner and outer surfaces of the nanotubes. The degree of sophistication can still be increased by assembling functional groups on the...

Document type : *Thèse (Dissertation)*

Université catholique de Louvain
École Polytechnique de Louvain
Institute of Condensed Matter and Nanosciences
Bio- and Soft Matter

Polyelectrolyte Multilayer Nanotubes for Drug Delivery Applications

Dissertation présentée en vue de l'obtention du grade de

Docteur en Sciences de l'ingénieur

par **Saghi Saghazadeh**

Membres du jury :

Prof. Sophie Demoustier-Champagne, promoteur

Prof. Alain Jonas, promoteur

Prof. Jacques Devaux, président

Prof. Karine Glinel

Prof. Bruno De Geest

Dr. Jessem Landoulsi

Louvain-la-Neuve, 2015

Abstract

Recent advances in medicine and nanotechnology have inspired numerous researches in which nano-engineering is used for the development of optimal drug nanocarriers. Up to now, most efforts in this field have been focused on creating spherical nanocarriers such as liposomes, capsules, or polymersomes. However, anisotropic structures such as nanotubes are currently attracting considerable attention because they offer some promising advantages over isotropic structures.

The size of nanotubes can be manipulated in two dimensions, giving the opportunity to construct nanotubes with different aspect ratios. They possess higher surface area compared to nanospheres of identical radius, resulting in more functional groups (antifouling, targeting…) assembled on their surface. Elaborated structures can be achieved by separately and selectively functionalizing the inner and outer surfaces of the nanotubes. The degree of sophistication can still be increased by assembling functional groups on the lateral and basal surfaces of nanotubes.

In the present work, layer-by-layer assembly method is combined with template synthesis to fabricate nanotubes composed of a therapeutic agent, namely, ovalbumin protein. A method for quantitative collection and transfer of nanotubes from the template to desired aqueous medium is developed. This method is applicable for collection of any template-synthesized nano-object independent of its nature and dimension and thus, is universal. The ability to functionalize nanotubular drug carriers with antifouling poly(ethylene glycol) chains was also reported.

Nanotubes of different chemistry, dimension and surface functionalization are then incubated with dendritic cells to study their interaction with cells. Results showed nanotubes phagocytosis is influenced by nanotubes surface function as well as size and rigidity.

Although many challenges are yet to be tackled to reach optimum nanotubular drug carriers, this study might pave the way towards the design and application of multifunctional nanotubular drug delivery systems.

Acknowledgement

I sincerely thank Prof. Sophie Demoustier-Champagne and Prof. Alain Jonas for their extensive support during the 4 years of my research and their enthusiastic and supportive supervision. Without their continuous critical and pedagogical guidance, I would not have been able to finish this dissertation. Together, we had hours of research planning and scientific discussions. I learnt a lot about planning experiments and having a methodological approach. Alain and Sophie always encouraged me to analyze the results more thoroughly, looking for details and always asking, "Why is this happening?" Their dedication to their students' development is unlimited. They walked me through different steps of this research. They taught me not to get discouraged when things do not work and celebrated my every bit of success. With Sophie and Alain, I always felt assured about the quality of my work and I am grateful for all they did for me.

I would like to thank Prof. Bruno De Geest who kindly accepted to be a member of my "comité d'accompagnement". I had lively discussions with Bruno, especially regarding the experiments with cells. His insight about bio-experiments enriched this dissertation. Without Bruno, and his PhD student's (Zhiyue Zhang) help it was not possible to conduct the cellular uptake tests. I appreciate the time and effort Prof. De Geest dedicated to this work and all his input on this dissertation.

Many thanks to Prof. Karine Glinel for kindly accepting to be a member of my "comité d'accompagnement" and for fruitful discussions about my work. I thank Karine for her detailed comments on this manuscript, which helped me improve the quality of the work. Karine also helped me to prepare for my FNRS-FRIA scholarship interview and for that, I am truly thankful.

My sincere thanks to Dr. Jessem Landoulsi, who accepted to be the reviewer of this work and studied my work thoroughly. Jessem gave me detailed comments and ideas that thoroughly enriched this manuscript.

I would like to thank Prof. Jacques Devaux, for serving as the president of my jury. Jacques helped me go through the defense procedure and was supportive during my defense. I am thankful for his support and kindness.

I would like to thank FNRS-FRIA (Fonds pour la Formation à la Recherche dans l'Industrie et dans l'Agriculture) committee for financing this research for 4 years. Without FRIA financial support, this work could not have been done.

I would like to thank Prof. Christine Dupont who helped me a lot at the beginning of this research, especially to prepare for FRIA scholarship interview. I also had several discussions with her regarding biomacromolecules, proteins and their applications and Christine patiently taught me the essentials.

I would like to thank Prof. Bernard Nysten and Prof. Alain Jonas who were both the presidents of BSMA laboratory at different periods. BSMA lab was always a warm and friendly environment. Not only we (the BSMA members) were colleagues, but also we were family; helping each other and cheering for everyone's success. I learnt many life lessons from my colleagues and I believe that BSMA's friendly environment is a fruit of Alain and Bernard's management.

My special thanks to Dr. Delphine Magnin who was not only a friend but also and amazing colleague with a lot of hand in experience with the research and the techniques available in the lab. Delphine gave me valuable advices about my research and life. I am very grateful for Delphine's kindness.

Many thanks to Pierre Eloy, for his assistance with XPS analysis. Pierre was very patient and always welcomed detailed discussions about XPS results. Despite his busy schedule, Pierre was always available and he always managed to free sometime for discussing the results. I am thankful for his patience and support.

Many thanks to Claude Poleunis, for his assistance with ToF-SIMS analysis. Clause walked me through the principles of ToF-SIMS and taught me how to interpret the data. He was always available for discussion and I sincerely thank him for his time and effort.

My sincere thanks to Dr. Etienne Ferain and It4ip company who provided me with templates and helped me with gas-flow porometry measurements. Etienne has been very helpful during this research and I have always enjoyed discussions with him.

Many thanks to Cécile D'Haese for her assistance with AFM experiments. I had many discussions with Cécile and I appreciate her kindness and helpfulness.

Many thanks to our secretary, Aurore Becquevort. She was always there to help me and I always felt assured that any administrative process will be handled amazingly by Aurore. Aurore also taught me a lot about living in Belgium and for that, I am very grateful.

I would like to thank Colette Douchamps who helped me with the purchase of chemical products and small instruments for my experiments. Colette was always helpful with my "urgent" orders and she truly saved several experiments.

Many thanks to my friends and fellow researchers in BSMA laboratory. Shouwei Zhang who set an example of hard work and never giving up especially during our struggle with "Nanotubes Collection". Dr. Alina Osypova who is a determined and dedicated fellow researcher with whom, I shared many moments. We three in the office formed a trio, trying to tame polyelectrolytes and nanotubes.

Thanks to Damien Lefèvre with whom I worked on surface functionalization of nanotubes. I am grateful for Damien's kindness and hard work.

Many thanks to Sabine Bebelmann, with whom I shared an office and had happy moments. Also many thanks to Pascale Lipnik for TEM imaging and Dr. Ali Dirani for helping me with the dipping robot and ellipsometry. My sincere thanks to Dr. Sabrine Belbekhouche, Dr. Aurélie Le Beulze, Dr. Nasima Afshar Imani, Dr. Moira Ciardi, Dr. Antony Fernandes, Dr. Florian Jurin, Vanina Cristaudo, Quentin Voleppe, Marion Galmiche, Dr. Camille Marie, Dr. Marie Henry, Catherine Philippart, Claire Chattaway, Supriya Surana, Amir Bahrami, Mohammad Zarshenas and Dr. Hadi Goldansaz, and all others who I have not mentioned. Many thanks to my friends Katia Plouznikoff, Mounia Bellaala, Pierre-Louis Alaux, Dr. Gregory Hislop, André Trybulowski, and Claire Haezeleer. "Thanks" is a small word to express my gratefulness towards all of you.

I am very grateful to my parents, Fariba and Mostafa and my brother, Soha. You three are always there for me and have always supported my life choices.

I am very blessed to have you in my life. Thanks for being patient and encouraging me to live the life the way I want. I would not have gotten this far without your help and I cannot thank you enough. Thank you for everything.

Many thanks to Sadegh for always seeing my true colors. With you, I am a better version of myself. Together, we have set a record for longest long distance relationship (distance and timewise!) Thanks a lot for your patience and support. Thanks for having faith in me, encouraging me and cheering me up. Thank you for everything you have done for me.

Contents

ABSTRACT I

ACKNOWLEDGEMENT III

LIST OF ABBREVIATIONS AND ACRONYMS XI

1. INTRODUCTION 1

THESIS STRUCTURE 5

BIBLIOGRAPHY 7

2 OVERVIEW 9

2.1 LBL ASSEMBLY 10

2.2 TEMPLATE SYNTHESIS 17

2.2.1 Nanoporous planar templates *20*

2.3 COMBINING TEMPLATE SYNTHESIS WITH LBL ASSEMBLY 21

2.4 DELIVERY OF THERAPEUTIC AGENTS TO DESIRED CELLS 24

2.5 PROTEINS AND BIOMACROMOLECULES IN LBL ASSEMBLY 30

2.5.1 Protein and biomacromolecule containing LbL assembled flat systems *30*

2.5.2 Protein and biomacromolecule-containing LbL assembled spherical systems *32*

2.5.3 Protein and biomacromolecule-containing LbL assembled nanotubular systems *34*

2.6 PARTICLES WITH ANTIFOULING PROPERTIES 40

2.7 CONCLUSION 42

2.8 BIBLIOGRAPHY 43

3 MULTILAYER LBL ASSEMBLED FILMS AND NANOTUBES 61

3.1 INTRODUCTION 62

3.2 MATERIALS AND METHODS 64

3.2.1 Materials *64*

3.2.2 Fabrication of LbL assembled flat films *65*

3.2.3 Fabrication of LbL assembled nanotubes *66*

3.2.4 Removing the polyelectrolyte crust from PC membrane *67*

3.2.5 Capping the nanotubes *67*

3.2.6 Releasing nanotubes from the template *68*

3.2.7 Characterization methods *68*

3.3 RESULTS AND DISCUSSION 73

3.3.1 Construction of multilayer films on flat surfaces *74*

3.3.2 Construction of multilayer nanotubes *80*

3.3.3 Capping nanotubes with nanoparticles ... *89*
3.4 CONCLUSION ... 90
3.5 BIBLIOGRAPHY ... 92

4 COLLECTION OF LBL ASSEMBLED NANOTUBES ... 99

4.1 INTRODUCTION ... 100
4.2 MATERIALS AND METHODS ... 101
4.2.1 Materials ... *101*
4.2.2 Fabrication of LbL assembled nanotubes ... *101*
4.2.3 Releasing nanotubes from the template ... *102*
4.2.4 Verifying the stability of nanotubes in aqueous medium ... *103*
4.2.5 Collection of nanotubes by precipitation and freeze-drying ... *103*
4.2.6 Collection by biphasic method ... *103*
4.2.7 Collection and re-dispersion of nanotubes with a virgin PET filter ... *104*
4.2.8 Collection and re-dispersion of nanotubes with a coated PET filter ... *104*
4.2.9 Collection by adjuvant assisted method ... *104*
4.2.10 Characterization methods ... *105*
4.3 RESULTS AND DISCUSSION ... 107
4.3.1 Nanotubes stability in aqueous medium ... *107*
4.3.2 Nanotubes collection by precipitation and freeze-drying ... *109*
4.3.3 Nanotubes collection based on an immiscible biphasic system ... *110*
4.3.4 Collection of nanotubes by filtration over a modified filter ... *114*
4.3.5 Collection of nanotubes by filtration in presence of an adjuvant ... *118*
4.3.6 Evaluating nanotubes rigidity after dispersion in aqueous medium ... *122*
4.4 CONCLUSION ... 125
4.5 BIBLIOGRAPHY ... 127

5. FUNCTIONALIZATION OF POLYELECTROLYTE MULTILAYER ASSEMBLED SYSTEMS WITH POLY(ETHYLENE GLYCOL) CHAINS ... 131

5.1 INTRODUCTION ... 132
5.2 MATERIALS AND METHODS ... 135
5.2.1 Materials ... *135*
5.2.2 Fabrication of LbL assembled flat films ... *136*
5.2.3 Fabrication of LbL assembled nanotubes ... *138*
5.2.4 Releasing nanotubes from the template ... *139*
5.2.5 Grafting PEG chains on the surface of nanotubes ... *139*
5.2.6 Characterization methods ... *140*
5.3 RESULTS AND DISCUSSION ... 145
5.3.1 Using polyelectrolyte-PEG copolymers as LbL assembly building blocks ... *145*
5.3.2 Grafting PEG chain by covalent bonding ... *159*

5.4 CONCLUSION 167
5.5 BIBLIOGRAPHY 168

6 CELLULAR UPTAKE OF MULTILAYER LBL ASSEMBLED NANOTUBES 173

6.1 INTRODUCTION 174
6.2 MATERIALS AND METHODS 177
6.2.1 Materials 177
6.2.2 Fabrication of LbL assembled nanotubes 178
6.2.3 Releasing nanotubes from the template 180
6.2.4 Checking the stability of nanotubes in aqueous medium 180
6.2.5 Collection and redispersion in aqueous solution 180
6.2.6 Checking the stability of free floating nanotubes in DPBS 181
6.2.7 Cell culture 181
6.2.8 Characterization methods 182
6.3 RESULTS AND DISCUSSION 183
6.3.1 Stability of free LbL assembled nanotubes in water 184
6.3.2 Stability of free floating LbL assembled nanotubes in culture medium 190
6.3.3 Fabrication of nanotubes with improved stability in culture medium 192
6.3.4 Cellular uptake of LbL assembled nanotubes 198
6.4 CONCLUSION 204
BIBLIOGRAPHY 206

7 CONCLUSIONS AND PERSPECTIVES 211

APPENDIX 215

DISSEMINATION 219

List of abbreviations and acronyms

AAO	Anodized aluminum oxide
AFM	Atomic force microscopy
APC	Antigen presenting cell
bFGF	Basic fibroblast growth factor
BMP	Bone morphogenetic proteins
CAT	Catalase
DEX	Dextran
DEXS	Dextran sulfate
DMF	Dimethylformamide
DNA	Deoxyribonucleic acid
DMEM	Dulbecco's modified eagle medium
DPBS	Dulbecco's Phosphate-Buffered Saline
EDC	1-Ethyl-3-(3-dimethylaminopropyl)carbodiimide
EDTA	Ethylenediaminetetraacetic acid
FBS	Fetal bovine serum
FDA	Food and Drug Administration
FITC	Fluorescein isothiocyanate
FWHM	Full width at half maximum
GOX	Glucose oxidase
GRAS	Generally recognized as safe
HA	Hyaluronic acid
HSA	Human serum albumin
HBV	Hepatitis B virus
HEPES	4-(2-hydroxyethyl)-1-piperazineethanesulfonic acid
LbL	Layer-by-layer
Lp	Persistence length
MES	2-(N-morpholino)ethanesulfonic acid
MHC	Major histocompatibility complex
MSC	Mesenchymal stem cells
OVA	Ovalbumin
PAH	Poly(allalyamine hydrochloride)
PBAE	Poly(beta-amino ester)
PBS	Phosphate-buffered saline
PC	Polycarbonate

PDADMAC	Poly(diallyldimethylammonium chloride)
PEG	Polyethylene glycol
PEI	Poly(ethyleneimine)
PET	Polyethylene terephthalate
pI	Isoelectric point
PLA	Poly-L-arginine hydrochloride
PLL	Poly-L-lysine
PSS	Poly(sodium 4-styrenesulfonate)
R_{EE}	End to end distance
SEM	Scanning electron microscopy
STEM	Scanning transmission electron microscopy
Sulfo-NHS	N-hydroxy sulfosuccinimide sodium salt
TEM	Transmission electron microscopy
ToF-Sims	Time-of-flight Secondary ion mass spectroscopy
XPS	X-ray photoelectron spectroscopy

1 Introduction

Nanotechnology is rapidly growing and has already highly affected our daily life. It is fair to say that Feynman revolutionized science by introducing the concept of nanotechnology [1,2]. During the past decades, nanotechnology has been applied in many different domains from electronics and mechanics to medicine and pharmaceutics. One of the main issues to tackle in medicine is to design and fabricate efficient drug delivery systems. In general terms, drug delivery refers to the process of transporting and introducing a pharmaceutical compound into cells in order to safely achieve its therapeutic effect. Conventionally, “free” drugs are used to be administrated to patients. Those “free” drugs suffered from some physico-chemical limitations such as instability in biologic media, undesired distribution in body, rapid clearance and removal by immune system, etc.

Novel drug delivery systems, benefiting from innovations in nanotechnology are mainly designed to overcome the limitations of traditional drugs while improving their biodistribution as well as enhancing their pharmacokinetics [3]. Nanotechnology provides the tools and possibility to fabricate biocompatible, biodegradable, stimuli-responsive and targeted delivery systems with a high control over their shape, size, chemistry and multi-functionality. A survey in 2013 reported that 247 nanomaterial-based medical products had been already approved by Food and Drug Administration (FDA) and were at different stages of clinical study [4,5].

Among them, nanoparticle-based drug delivery systems have gained a particular interest. Detailed researches proved indeed that by formulating biopharmaceutical components such as proteins, peptides and nucleic acids in nanoparticles, their therapeutic potential is highly increased. Nanoparticles should encapsulate the cargo with high efficiency and protect

them from premature drug release, undesired degradation while avoiding any triggers for unwanted immune responses. Nanoparticle drug delivery systems can be fabricated from a vast range of materials such as liposomes, polymersomes, polymer micelles, silica, gold and silver metals, silica, titanium oxide and iron oxides, dendrimers, synthetic macromolecules and biomacromolecules [6,7].

Nanoparticle based drug delivery systems may become more complex by fabricating particles of different shape, size, rigidity as well as surface function. In this respect, template synthesis combined with layer-by-layer assembly provides unique tools to fabricate anisotropic micro and nano-sized structures such as nano-disks, nano-platelets, nanotubes and nanowires. Among those anisotropic nanostructures, hollow nanotubes present some notable advantages compared to nanospheres.

- The size of nanotubes can be manipulated in at least two space directions, which increases the number of possibilities to engineer the nanocarriers [8,9].
- Cylindrical carriers can carry larger drug payloads than nanospheres of the same diameter [8–10].
- Likewise, for the same diameter, nanotubes may exhibit higher surface area than nanospheres. As a result, more agents (targeting, antifouling,...) can be assembled on the outer part of nanotubes than on nanospheres [8,9].
- Nanotubes exhibit more possibilities of tailoring the functionality of the nanocarriers. They have different inner and outer surfaces that can be separately and selectively functionalized and, they have lateral and basal surfaces that can also be tailored separately [8,9,11].

- Nanotubes have longer circulation in vivo. They have fewer collisions with blood vessels walls than nanospheres. Moreover, it was recently reported that cylindrically shaped particles were internalized in cells much faster than spherical particles of the same diameter [12–14].

In this context, the **general aim of the present research work** was to design and fabricate anisotropic multifunctional tubular nano-objects for the controlled delivery of proteins as therapeutic agent. To reach this aim, different key steps needed to be reached: (1) multifunctional nanotubes including various components (especially proteins) had to be reproducibly fabricated, (2) a rigorous methodology to functionalize the outer surfaces of the nanotubes had to be implemented, (3) a robust process to transfer and disperse the nanotubes into a proper medium for in vitro tests had to be developed and optimized and finally, (4) a study of nanotubes-targeted cells had to be carried out.

Apart from practical interests, **some fundamental objectives** were also envisioned:

1. To investigate possible combination of different materials and nano-assembly fabrication techniques to construct multifunctional nano-sized objects, with a high degree of control over the shape and the localization of chemical functions.
2. To provide an insight on nanotubes physical changes upon transfer from one medium to another.
3. To demonstrate how a complex charged surface could be functionalized with functional groups.
4. To investigate how the nanotubes shape, size and surface functionalization affect their stability and cellular uptake.

The developed **global strategy** to achieve these objectives is the following: The construction of nanotubes is based on membrane templating method, which means that the nanotubes are synthesized inside the pores of a nanoporous membrane. This approach is a unique strategy providing monodisperse nanotubes with controlled dimensions (size and diameters). The length of the nanotubes is indeed determined by the thickness of the template, while the outside diameter of the tubes is dictated by the diameter of the template pores. Moreover, a wide range of materials ranging from organic polymers to synthetic and natural polyelectrolytes can be deposited within the pores of the membrane [15–19].

To construct polyelectrolyte multilayer nanotubes, layer-by-layer (LbL) assembly is combined with membrane templating method. The LbL assembly simply consists of the alternative adsorption of interacting polymers (e.g. through electrostatic interactions and/or hydrogen bonds) into the pores of the template. Nanotubes composed of different polyelectrolyte building blocks are then released from the template by dissolving the template (polycarbonate membrane) in an organic solvent. By releasing the nanotubes from the membrane, their outer surface is exposed and available for further functionalization (e.g. grafting polyethylene glycol chains to achieve antifouling characteristics). Afterwards, nanotubes are transferred to aqueous medium suitable for biological applications and their interaction with immune dendritic cells is observed (**Error! Reference source not ound.**).

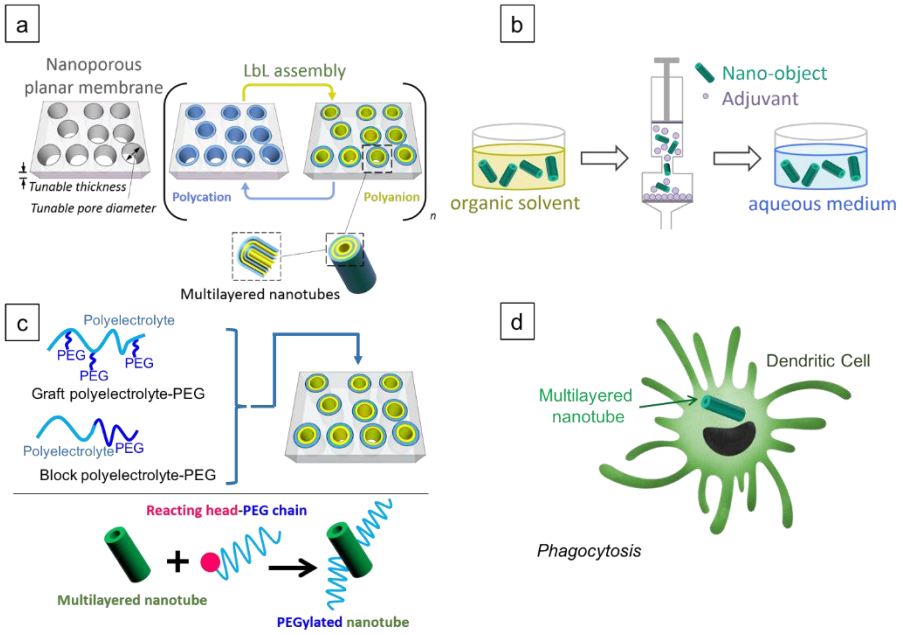

Figure 1.1. Schematic representation of strategies developed in this thesis. (a) LbL assembly is combined with template synthesis to fabricate multilayered nanotubes, (b) the template is dissolved in an organic solvent and nanotubes are released. Nanotubes are then collected and transferred to aqueous medium by an adjuvant-assisted method, (c) surface of nanotubes is functionalized with PEG chains, by using block and graft polyelectrolyte-PEG copolymers or by grafting PEG chain with covalent bonding on nanotubes surface, (d) dendritic cells uptake multilayered nanotubes by phagocytosis.

Thesis structure

The **second chapter** overviews the basis of this research. Layer-by-layer assembly and template synthesis methods are introduced and the outcome of combining these two methods is explained. Since the model drug in this research was a protein, a brief review of proteins and their structure is mentioned. Afterwards, the effect of surface functionalization with antifouling moieties is explained. In the end, possible interactions of micro- and nano-sized objects with cells are introduced.

The **third chapter** discusses the assembly of multilayer flat films and multilayer nanotubes and compares their growth. The possibility of capping nanotubes ends with nanoparticles is also explained.

The **fourth chapter** is dedicated to different processes to collect and transfer nanotubes in aqueous medium for further biological applications are studied. A universal method allowing the quantitative collection of membrane templated nanotubes of different compositions and rigidity is described. Changes in rigidity of nanotubes prior and after being dispersed in aqueous medium are also evaluated.

The **fifth chapter** focuses on surface functionalization of multilayer planar films and multilayer LbL assembled nanotubes with antifouling poly(ethylene glycol) chains.

The **sixth chapter** reports on stability of nanotubes in cell culture medium and their phagocytosis by dendritic cells.

Finally, the thesis is concluded in the **seventh chapter** by a brief summary of the results and some perspectives on the use of multilayered LbL assembled nanotubes for further biological applications are suggested.

Bibliography

(1) "Plenty of Room" Revisited. Editorial. *Nat. Nanotechnol.* **2009**, *4*, 781–781.

(2) Roukes, M. Plenty of Room Indeed. *Sci. Am.* **2007**, *17*, 4–11.

(3) Allen, T. M.; Cullis, P. R. Drug Delivery Systems: Entering the Mainstream. *Science* **2004**, *303*, 1818–1822.

(4) Etheridge, M. L.; Campbell, S. a; Erdman, A. G.; Haynes, C. L.; Wolf, S. M.; McCullough, J. The Big Picture on Nanomedicine: The State of Investigational and Approved Nanomedicine Products. *Nanomedicine* **2013**, *9*, 1–14.

(5) Mitragotri, S.; Anderson, D. G.; Chen, X.; Chow, E. K.; Ho, D.; Kabanov, A. V; Karp, J. M.; Kataoka, K.; Mirkin, C. A.; Petrosko, S. H.; *et al.* Accelerating the Translation of Nanomaterials in Biomedicine. *ACS Nano* **2015**, *9*, 6644–6654.

(6) Goldberg, M.; Langer, R.; Jia, X. Nanostructured Materials for Applications in Drug Delivery and Tissue Engineering. *J. Biomater. Sci. Polym. Ed.* **2011**, *18*, 241–268.

(7) Doshi, N.; Mitragotri, S. Designer Biomaterials for Nanomedicine. *Adv. Funct. Mater.* **2009**, *19*, 3843–3854.

(8) Sahoo, S. K.; Labhasetwar, V. Nanotech Approaches to Drug Delivery and Imaging. *Drug Discov. Today* **2003**, *8*, 1112–1120.

(9) Qu, X.; Komatsu, T. Molecular Capture in Protein Nanotubes. *ACS Nano* **2010**, *4*, 563–573.

(10) Komatsu, T.; Qu, X.; Ihara, H.; Fujihara, M.; Azuma, H.; Ikeda, H. Virus Trap in Human Serum Albumin Nanotube. *J. Am. Chem. Soc.* **2011**, *133*, 3246–3248.

(11) Lee, D.; Cohen, R. E.; Rubner, M. F. Heterostructured Magnetic Nanotubes. *Langmuir* **2007**, *23*, 123–129.

(12) Moghimi, S. M.; Porter, C. J.; Muir, I. S.; Illum, L.; Davis, S. S. Non-Phagocytic Uptake of Intravenously Injected Microspheres in Rat Spleen: Influence of Particle Size and Hydrophilic Coating. *Biochem. Biophys. Res. Commun.* **1991**, *177*, 861–866.

(13) Simone, E. A.; Dziubla, T. D.; Muzykantov, V. R. Polymeric Carriers: Role of Geometry in Drug Delivery. *Expert Opin. Drug Deliv.* **2008**, *5*, 1283–1300.

(14) He, Q.; Cui, Y.; Ai, S.; Tian, Y.; Li, J. Self-Assembly of Composite Nanotubes and Their Applications. *Curr. Opin. Colloid Interface Sci.* **2009**, *14*, 115–125.

(15) Landoulsi, J.; Roy, C. J. C. J.; Dupont-Gillain, C.; Demoustier-Champagne, S. Synthesis of Collagen Nanotubes with Highly Regular Dimensions through Membrane-Templated Layer-by-Layer Assembly. *Biomacromolecules* **2009**, *10*, 1021–1024.

(16) Callegari, V.; Gence, L.; Melinte, S.; Demoustier-Champagne, S. Electrochemically Template-Grown Multi-Segmented Gold-Conducting Polymer Nanowires with Tunable Electronic Behavior. *Chem. Mater.* **2009**, *21*, 4241–4247.

(17) Callegari, V.; Demoustier-Champagne, S. Using the Hard Templating Method for the Synthesis of Metal-Conducting Polymer Multi-Segmented Nanowires. *Macromol. Rapid Commun.* **2011**, *32*, 25–34.

(18) Perry, J. L.; Martin, C. R.; Stewart, J. D. Drug-Delivery Strategies by Using Template-Synthesized Nanotubes. *Chemistry* **2011**, *17*, 6296–6302.

(19) Roy, C. J.; Chorine, N.; De Geest, B. G.; De Smedt, S.; Jonas, A. M.; Demoustier-Champagne, S. Highly Versatile Approach for Preparing Functional Hybrid Multisegmented Nanotubes and Nanowires. *Chem. Mater.* **2012**, *24*, 1562–1567.

2 Overview

This chapter aims to overview the fundamental basis of this research. Layer-by-layer (LbL) assembly technique as well as template synthesis method are described and their main advantages are pointed out. Followed by discussing the combination of these two versatile techniques. Focus is made on combining LbL assembly and template synthesis within the pores of porous planar templates to fabricate nanotubes. Next, we move on towards delivery of therapeutic agents to cells and the uptake process by dendritic cells is briefly discussed. Since the model drug in this research is a protein, an overview of using protein-containing multilayer assembled structures for biological applications is discussed. We emphasize protein-containing LbL assembled nanotubes, give a summary of the latest advances in this particular subject, and then briefly point out the missing techniques in order to use such nanotubes for biomedical applications. In the end, the interest of assembling different anti-fouling moieties on the desired surfaces and their potential for biological applications is briefly discussed.

2.1 LbL assembly

The root of this research lies in layer-by-layer assembly (LbL) methodology. LbL assembly was introduced in 1991 by Decher et al. as a simple, versatile and inexpensive bottom-up method to fabricate multilayered structures [1–5]. Since then, it has been rapidly expanded to become a method of choice for the preparation of nanoscaled materials with tailored properties.

In this method, a solid support with a charged surface is exposed to a solution containing a species of opposite charge. Opposite charges are adsorbed on the surface of the support, due to electrostatic interactions. Since the adsorption is non-stoichiometric, the sign of the surface charge is reversed promoting the adsorption of the next layer. A rinsing step is performed to remove unbound material and avoid contamination of the next deposition solution. The substrate is exposed to the second solution, containing opposite charged species followed by another rinsing step. The electrostatic adsorption occurs once again and another layer is added to the substrate (Figure 2.1). A couple of positive and negative layer is called a bilayer. The whole cycle can be repeated until the desired number of bilayers is achieved [6].

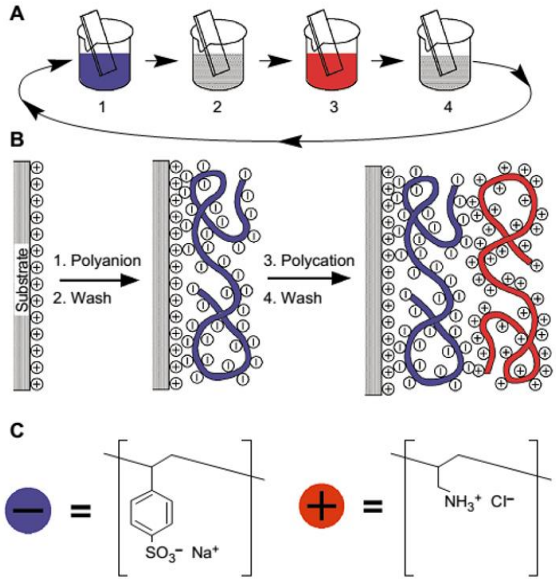

Figure 2.1. Schematic representation of LbL assembly; (a) immersing the positively charged substrate in polyanion solution, reversing the surface charge of the substrate, followed by a rinsing step. Then, the coated substrate is immersed in a polycation solution followed by another rinsing step, (b) simplified representation of surface charges during the LbL assembly, (c) chemical structure of two typical polyelectrolytes, polystyrene sodium salt (PSS) and poly(allylamine) hydrochloride [1].

The LbL assembly is extremely versatile and a broad range of materials such as polymers, lipids, DNAs, proteins and organic or inorganic small molecules can be assembled on different substrates [7–13]. Such a wide choice of materials allows the multilayers to be engineered for different applications ranging from optics and catalysis to biomedicine (Figure 2.2).

LbL assembly is not restricted to electrostatic interactions only. In fact, LbL assembly can be operated successfully based on hydrogen bonding, hydrophobic interactions, covalent bonding and complementary base pairing [14–17].

Several parameters influence the growth of polyelectrolyte multilayers such as the nature of the substrate, the polyelectrolyte molar mass and concentration, the depositing solutions pH and ionic strength, dipping duration and last but not least, the introduction of an intermediate drying step.

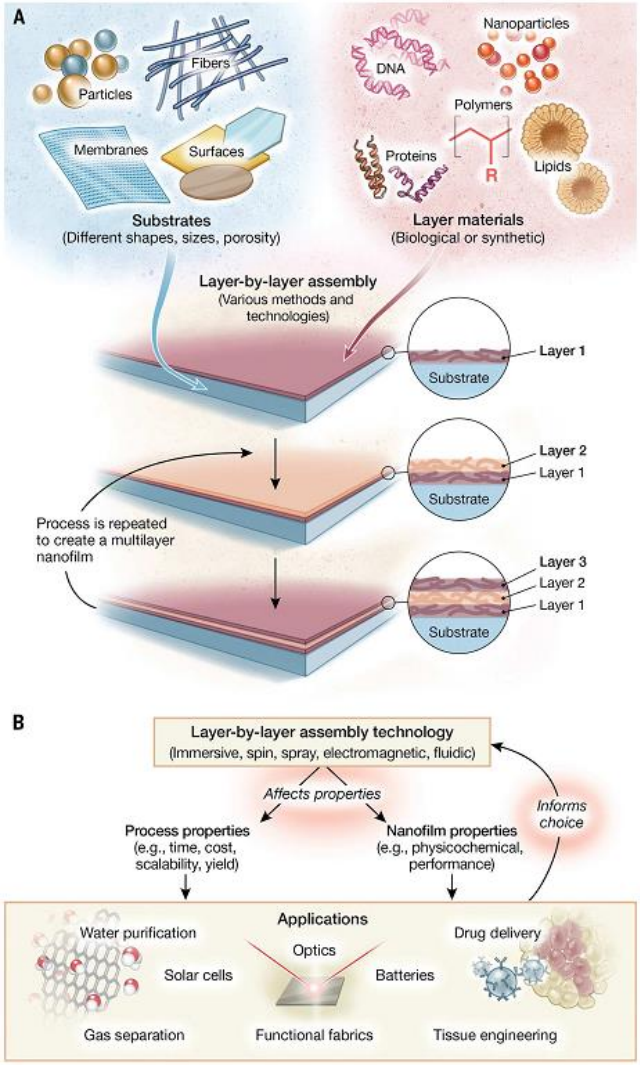

Figure 2.2. An overview of LbL assembly versatility. (a) Substrates with different shape, size and morphology can be used while the building components can be chosen among a wide range of materials, (b) Schematic view of assembly over a planar surface, (c) how the assembly method affects the properties of fabricated multilayered structure as well as application area [18].

The effect of pH on LbL assembly is complex. Shiratori et al [19] studied the effect of pH on the thickness of weak polyelectrolyte layers deposited on a

flat surface. They proved that the thickness of the absorbed layer depends on the charge density of adsorbing polymers, the charge density of the surface on which adsorption is taking place as well as the conformation of the polymer chains.

When a free polymer chain is adsorbed on the surface, there will be an entropic loss because the previously free chain has to be spread into a flat conformation on the surface. In the same time, the system will have an enthalpic gain due to the free energy of adsorption [19]. However, the enthalpic gain by electrostatic interactions cannot be the main driving force of multilayers build-up. The first reason is that electrostatic interactions can occur between charged polyelectrolytes and small counter ions or between two oppositely charged polyelectrolytes. In both cases, polyelectrolyte charges are compensated. The former case leads to no growth while the latter leads to growth of multilayers. Second, it is known that during the assembly, oppositely charged polyelectrolytes interact and the surface charge is reversed. Such a reversal in charge needs a high energy and the adsorption should probably stop at zero surface charge. Finally yet importantly, multilayers growth has been observed at high ionic strength solutions where most of electrostatic interactions are screened. Considering these cases, it must be admitted that enthalpic gain is probably playing a role but is not the sole cause of multilayers assembly. Indeed, the gain in entropy due to the release of counterions acts as a driving force in assembly and has a crucial impact on multilayers build-up as well [20].

In one particular study, the effect of temperature on growth of strong polyelectrolyte pair (polydiallyldimethylammonium chloride and polystyrene sulfonate) (PDADMAC/PSS) was observed. It was shown that by increasing the temperature the thickness of those multilayers was strongly increased.

This is probably due to overcoming activation barriers and the higher mobility of polyelectrolyte chains in solution towards the surface leading to higher amount of released counterions [21]. This proves that indeed entropic gain plays a major role in multilayers build-up.

Counterions are able to screen the charges along the polyelectrolyte chains. In a solution with a high ionic strength, polyelectrolytes have a more coiled conformation with a lower net charge, resulting in formation of thicker multilayers. In contrast, at low ionic strength, the polymer coils tend to decoil during adsorption, creating thin flat films [6,15,22–25].

The type of ions can also affect the multilayers buildup and the properties of the obtained films [21]. Ions have been previously classified according to their ability to precipitate certain proteins from an aqueous solution by Hofmeister [26]. The ion specific effect on multilayers growth occurs in solutions with ionic strength higher than 0.1 M in which the interaction between polyelectrolytes and counterions is dominant and follows the "Hofmeister series" [21,27]. According to Hofmeister series, some ions have stronger interactions with water molecules than water molecules themselves. These ions are called kosmotropes or structure makers. Ions such as sulfates, F^- or Na^+ are kosmotropes and have a large hydration shell. In contrast, other ions have weaker interaction with water molecules and are called chaotropes or structure breakers. Ions such as I^- or Cs^+ are chaotropes and have a smaller hydration shell that can easily be replaced by other species. Chaotropic ions interact strongly with opposite charged polyelectrolytes and cause stronger screening of charges along the polyelectrolyte chain, leading to higher coiling and formation of thicker multilayers [20,27]. It is observed that ion specific effects are more significant for anions than cations however; both must be taken into account when

multilayer assembly is carried out at high ionic strength solutions. The case becomes more complicated when monovalent and divalent ions are compared. It should be pointed out that the effect of ions cannot be exclusively studied and the ensemble of ion-macromolecule pairs must be taken into account [27,28].

Polyelectrolytes molar mass plays an important and yet complex role during the assembly. One should keep an eye on charged groups as well as hydrophobic domains along the polyelectrolyte chains. In order to assemble multilayers, there must be a minimum charge density along the chains and in order to stabilize the newly formed layers, hydrophobic domains must interact with each other. Short highly charged polyelectrolyte chains produce thin layers that are much less interconnected compared to highly interlocked multilayers obtained from long chain polyelectrolytes. In addition, soluble polyelectrolyte complexes might form at the solid/liquid interface when assembly is carried out from short chain polyelectrolytes resulting in the loss of matter during the assembly process [29,30]. To stabilize such systems and increase the growth, it is suggested to increase the ionic strength of assembly and rinsing solution [31]. Indeed, non-electrostatic short range hydrophobic interactions play an important role in formation and stabilization of the multilayers [32]. Polyelectrolytes with a high molar mass composed of charged groups and long hydrophobic segments produce stable and thick multilayers. During the buildup, charged groups interact electrostatically while a large amount of matter is also deposited due to the presence of hydrophobic segments. However, if the length of uncharged hydrophobic segment is larger than a certain value, small aggregates may occur in solution because of intramolecular interactions and thus, multilayer growth is hindered [32]. Considering all this, it is concluded that there exists a critical charge density for each polyelectrolyte for any polyelectrolyte pair. Below this critical

charge density value, oppositely charged polyelectrolytes form unstable complexes that may disassemble resulting in no growth [33,34]. Above this charge threshold, assembly occurs and the thickness of resulting multilayers depends on the conformation of polyelectrolyte chains in solution as well as their interactions upon adsorption [35].

Applying a drying step during the assembly also affects the film growth. It has been observed that thinner, less dense multilayers are obtained when the adsorbed layers were always kept wet during the assembly [6].

Overall, the growth of multilayers can be tuned by playing with different parameters, providing the opportunity to fabricate films of desired structures.

2.2 Template synthesis

LbL assembly can be operated on the outer surface of colloidal particles. These particles can be either isotropic (spherical particles) or anisotropic with high aspect ratio (rods, fibers).

To obtain isotropic colloidal particles coated with multilayers LbL assembly is carried out on the surfaces of solid spheres of calcium carbonate ($CaCO_3$), melamine formaldehyde, polystyrene or silica or gold particles. These particles are mostly in the range of 0.1 - 10 µm [11,36]. However, in one particular case, gold nanoparticles of 13.5 nm diameter were successfully coated with PAH/PSS multilayers [37]. These spherical templates can be subsequently removed in order to obtain hollow capsules with a polyelectrolyte shell (Figure 2.3). Polystyrene core is removed by using tetrahydrofuran, while melamine formaldehyde is decomposed under strong acidic conditions and gold nanoparticles are dissolved in aqueous solution containing potassium cyanide. $CaCO_3$ particles are removed by

ethylenediaminetetraacetic acid (EDTA) and silica particles are removed by HF/ammonium fluoride [11,37,38]. Two methods are available to load desired macromolecules in these capsules. In the first method, the capsule membrane is reversibly permeabilized by specific stimuli so that the desired molecule can diffuse through the capsule structure and then the capsule membrane is closed in order to trap the macromolecule within the structure. In the second method, porous colloidal templates such as silica or $CaCO_3$ are preloaded with the desired molecule and then coated by LbL assembly [11,36]. During the dissolution of the core, these macromolecules remain entrapped in the hollow capsule. Micrometer sized capsules have a broad application range including encapsulation and controlled release of drugs, genes, cosmetics, as well as sensing and catalysis [39–44].

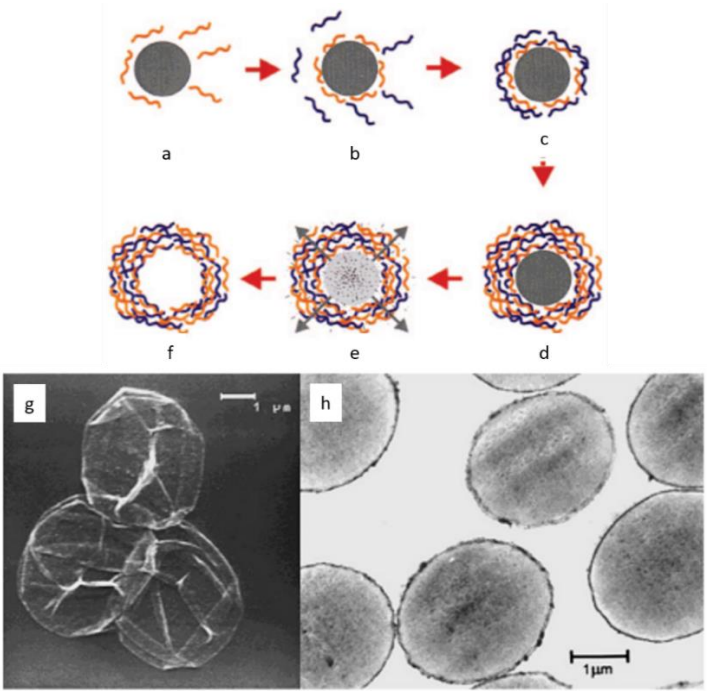

Figure 2.3. (a - f) Schematic representation of LbL assembly over a spherical particle, followed by subsequent removal of the core, resulting in formation of a multilayered shell. (g) SEM image of $(PAH/PSS)_4/PSS$ shells, (h) TEM image of stained $(PAH/PSS)_4/PSS$ shell [44].

Filamentous structures are obtained from LbL assembly on anisotropic colloidal templates that have high aspect ratio. Nickel nanorods with an average diameter of 65 nm and average length of 1.5 µm were successfully coated with PDADMAC/PSS multilayers [45]. Carbon microfibers with a diameter of 8 – 12 µm were also coated by PDADMAC/silicalite-1. Hollow tubular shell is obtained after calcination and removal of the carbon microfiber core (Figure 2.4) [46].

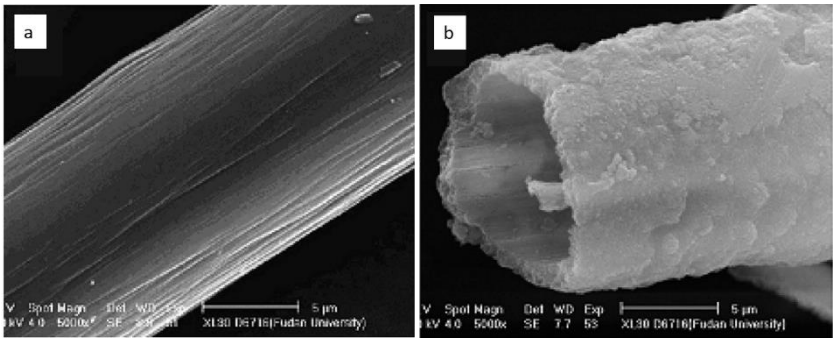

Figure 2.4. SEM images of (a) a carbon microfiber, (b) microtube obtained by LbL assembly over the carbon microfiber [46].

Halloysite, tubular alluminosilicate clay with 15 nm inner diameter and 0.5 – 1 µm length has also been used as a template for multilayer assembly [47,48]. The outer surface of halloysite tubes is composed of silicon oxide while their inner surface is composed of aluminum oxide. Thus, at the pH range of 2 – 8, halloysite tubes have a negatively charged outer surface and a positively charged inner surface that are suitable for multilayer assembly.

Although advantages of using colloidal particles as templates for multilayer assembly are numerous, they suffer from a main disadvantage: their tedious preparation procedure [36]. For each layer deposition, strong centrifugation and sonication steps must be applied. These steps may result in irreversible

aggregation especially for small, nano-sized particles. Therefore, developing an alternative method that eliminates those steps is highly favorable.

2.2.1 Nanoporous planar templates

About 20 years ago, Martin et al. reported on the fabrication of well-defined cylindrical hollow structures from a variety of materials using supramolecular templating synthesis. Tubular structures are constructed inside the pores of a nanoporous planar membrane, such as anodic aluminum oxide (AAO) or track etched polycarbonate (PC) membranes, and can be released by dissolving the template [49]. This hard templating method is highly advantageous due to its simplicity, versatility, and robustness. A wide range of materials from metals to semiconductors, organic polymers, and synthetic and natural polyelectrolytes as will be shown here, can be deposited within the pores of the membrane [10,50–56]. Deposition methods vary from chemical vapor deposition (CVD) to electrochemical deposition, sol−gel, chemical polymerization, electroless plating, and, more recently, layer-by-layer (LbL) assembly [57–61].

Anodic Aluminum oxide (AAO) templates are commercially available in various dimensions (template thickness ~ 10 - 200 µm; pore diameter ~ 10 - 150 nm; pore density ~ 10^9 - 10^{11} pores.cm^{-2}) (Figure 2.5.a). To create the nano-sized pores within the film of alumina the film is subjected to a two-step anodization. The pore dimensions of AAO templates are strictly dependent on the synthesis conditions. The template thickness is controlled by the anodization time and the pore diameters can be tailored by varying the conditions of anodization. However, it must be noted that there is a dependency between the pore size and pore density in AAO templates. The higher the pore density, the smaller their size and vice versa [62–65].

Nanoporous track-etched polycarbonate (PC) membranes with controlled pore geometry, pore size and density are commercially available (template thickness ~ 10 - 25 µm; pore diameter ~ 0.1 - 12 µm; pore density ~ 1.10^{5}-6.10^{8} pores.cm^{-2}) (Figure 2.5.b) [66]. In contrary to AAO templates, pore size and pore density of PC membranes are independent.

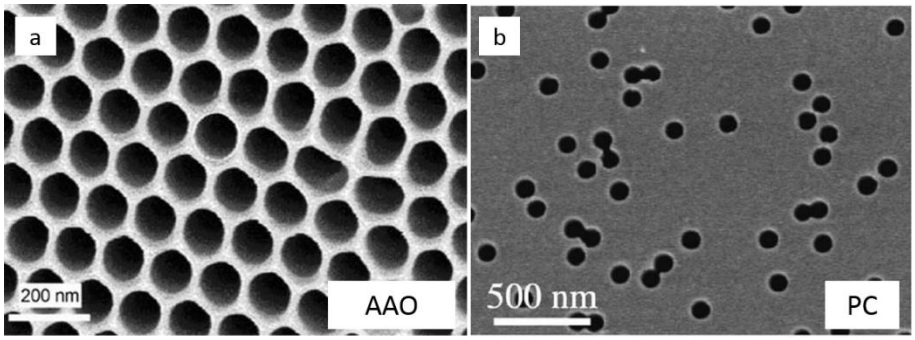

Figure 2.5. SEM images of nanoporous planar templates (a) AAO, (b) track-etched PC [66,67].

Fabrication of track-etched membranes consists of a two-step process. First, the PC film is bombarded with energetic heavy ions accelerated in a cyclotron. Because of this bombardment, the polymer chemical bonds are damaged, leading to the creation of linear damaged tracks. In the second step, these tracks are chemically etched. This etching process is performed in successive temperature-regulated baths filled with hydrogen peroxide, caustic soda and acetic acid solutions. At the end of this etching process, the so-called "track-etched" membranes are obtained [66,68].

2.3 Combining template synthesis with LbL assembly

The innovative idea of LbL assembly within the pores of a nanoporous planar membrane was introduced around 2003 [7,88]. By combining LbL assembly with template synthesis, a variety of species such as polyelectrolytes, charged

biomacromolecules, and nanoparticles can be deposited within the pores of membranes, resulting in the formation of cylindrical nanotubes with well controlled and tunable outer diameter, length, composition and wall thickness [9,69–73] (Figure 2.6). In this work, this flexibility will be used to fabricate anisotropic carriers for biomedical applications.

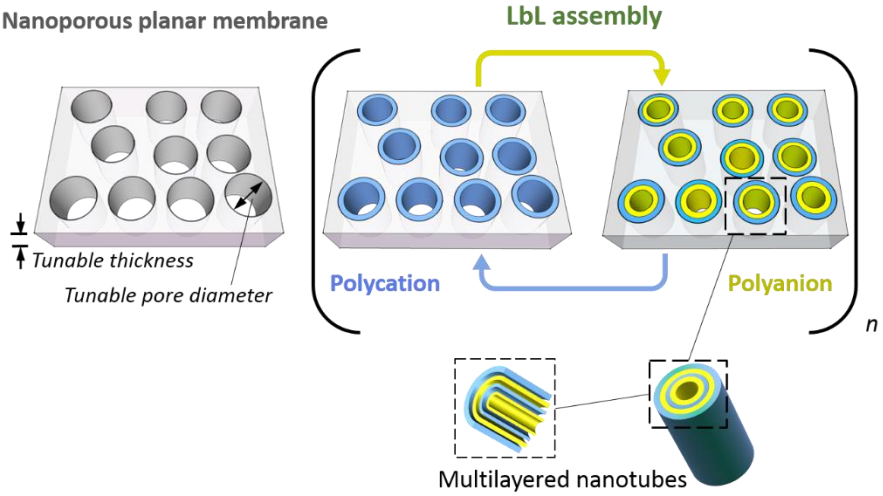

Figure 2.6. Schematic representation of multilayer PE nanotube construction via LbL assembly within the pores of a nanoporous planar template.

Multilayer nanotubes are released from the template by dissolving (sacrificing) the template. AAO templates can be etched in aqueous solutions of either pH ≤ 4.5 or pH ≥ 8.5. PC can be dissolved in common organic solvents such as dichloromethane (CH_2Cl_2) and dimethylformamide (DMF). Usually, PC templates are preferred to AAO templates, considering their gentler dissolution conditions.

Many groups have managed to fabricate these nanotubes by template-assisted LbL assembly with different polyelectrolytes and have studied their structure thoroughly [52,71,74–78]. It is generally shown that the thickness of

multilayer polyelectrolytes in the nanoporous membranes is higher than on flat surfaces [77,79]. Alem et al. demonstrated that the multilayers growth within the pores of a membrane is independent of the molecular weight or the ionic strength of the solutions and is solely dependent of the membrane pore size at pore diameters smaller than 250 nm [77].

Roy et al. [80] showed the existence of two growth regimes for multilayer polyelectrolyte structures in nanopores. The first regime is similar to the growth on flat surfaces. Polyelectrolyte chains approach the pore walls and are adsorbed as on flat surfaces. After deposition of a certain number of bilayers, the polymer chains start to entangle inside the pores. At this moment, the second growth regime begins. The second regime is slower in terms of kinetics since diffusion becomes a limiting mechanism. The interconnection between polyelectrolyte chains inside the pores results in the formation of a dense gel that may clog the pore and prevent any further deposition. One must not forget that multilayer polyelectrolytes are highly hydrated thus, when brought to the dry state, these hydrated structures will shrink and the layer thickness will be decreased (Figure 2.7).

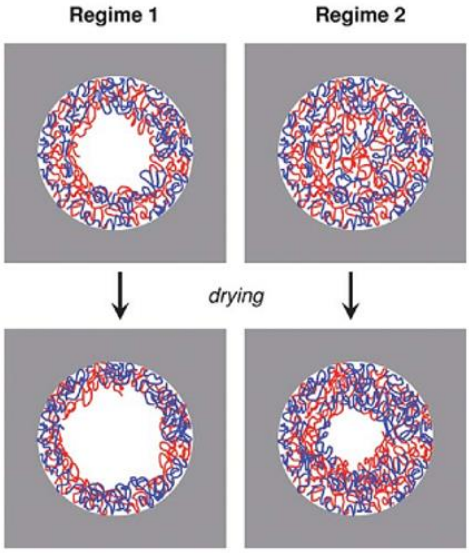

Figure 2.7. Schematic representation of multilayer polyelectrolyte structures within the pores of the membrane corresponding to regime 1 and 2, prior and after drying [80].

2.4 Delivery of therapeutic agents to desired cells

One of the main objectives of this work is to deliver a specific macromolecular cargo to cells. Hereby, a few studied cell types and their interest in drug delivery applications are introduced and then focus is made on dendritic cells as model cells for vaccine-delivery studies and the model antigen to be delivered to these cells.

Mesenchymal stem cells (MSC) are adult stem cells and are mostly found in the bone marrow. These cells can differentiate to form several types of cells belonging to our skeletal tissues such adipocytes (fat), cartilage, bone, tendons, muscle and skin. These cells are highly interesting for cellular therapeutics especially for regenerative medicine [81]. In contrast, malignant cell lines are also quite interesting since they are easy to culture and can be used to observe the effect of therapeutic substance on malignant tumors.

HeLa cell line is widely used as a model cell line for cancer research. Jurkat cells are used as a model for T cells. They are mostly used to study the response of cancerous T cells to radiation and therapeutic agents [81].

Immune cells such as B cells, macrophages and dendritic cells are studied for immunobioengineering since they are all antigen presenting cells (APC) [82]. Among all, dendritic cells are the most specialized since they are capable of presenting antigens to naïve T-cells. Pathogens are recognized and uptaken by dendritic cells. Next, dendritic cells mature and express major histocompatibility complex (MHC) molecules on their surface. These molecules are recognized by T-cells and result in the production of memory T-cells, helper T-cell and cytotoxic T-cells [83–86] (Figure 2.8). Significant amount of research has been dedicated to modulation of immune response by introducing pathogens to dendritic cells. For instance, dendritic cells can be isolated and specific antigens can be presented to dendritic cells in vitro. After ingestion and further processing of those antigens, dendritic cells with antigens expressed on their surface can be introduced to the organs in vivo in order to communicate with T cells [87,88].

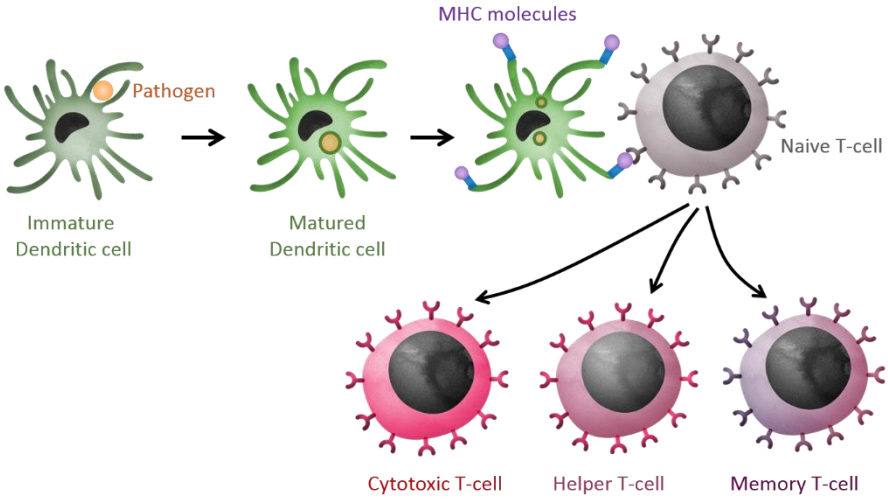

Figure 2.8. Schematic representation of dendritic cells interaction with pathogens. The pathogen is first recognized by immature dendritic cells and is then uptaken. The pathogen is degraded by immature dendritic cell upon maturation and some fragments of the pathogen are expressed on the surface of matured dendritic cell using MHC molecules. Naïve T-cells recognize MHC molecules and become activated to form cytotoxic T-cells, helper T-cells and memory T-cells (Images are extracted and modified from [89]).

Nanoparticles can be used as carriers to encapsulate and protect vaccine antigen and deliver the cargo to dendritic cells. These nanoparticles are internalized by dendritic cells through different pathways and are then processed inside the cell. The mechanism of cell internalization is important and may affect the induced immune response [83]. These mechanisms are mostly influenced by the physicochemical properties of the nanoparticles. Depending on these properties, there are two main internalization pathways: phagocytosis (cell-eating) or the other endocytic pathways (cell-drinking). Colloidal particles are mostly internalized via phagocytosis [90].

Phagocytosis plays a major mechanism in an organism immune system against non-self elements such as pathogens (most bacteria and some viruses) as well as exogenous particles (such as colloidal drug carrying particles). Phagocytosis occurs mainly in specific cell-types, such as macrophages, monocytes, neutrophils and dendritic cells. During the phagocytic activity, three steps take place. First, the particle is recognized and identified as a foreign object in the blood stream by the opsonization process. During the opsonization process, the foreign object is tagged by proteins (such as immunoglobulins) called opsonins in order to make the foreign object visible for the macrophages. Afterwards, the opsonized particle adheres to the macrophages; third, the particle is ingested by the macrophages (Figure 2.9) [91].

In most cases, colloidal particles should have a minimum size of 250 nm to undergo phagocytosis. However, macrophages are well capable of eating much bigger particles [92].

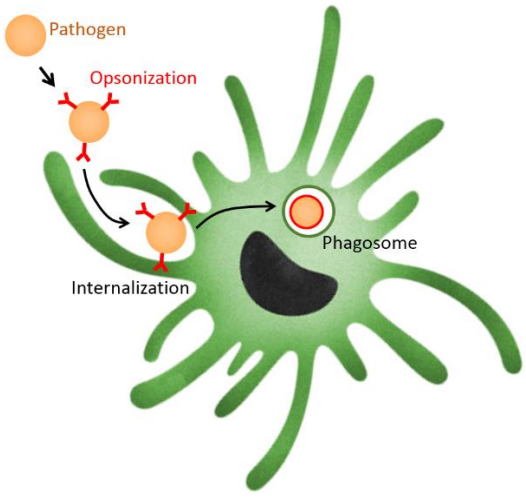

Figure 2.9. Schematic representation of particle internalization into cells by phagocytosis. (Images are extracted and modified from [89]).

The shape of particles also affects the phagocytosis process. A study was dedicated to phagocytosis of disk-shaped particles. It was found out that the local particle shape at the contact point with the cell dictates whether the phagocytosis will take place. For instance, if the particle touches the cell by its pointy-head, it will be internalized. On the other hand, if the particle lays with its flat face on the cell surface, internalization does not take place even after 12 hours [93]. Another interesting parameter that affects phagocytosis is the rigidity of the particle. Macrophages have a higher preference for rigid particles. This could be related to the fact the cell walls of bacteria and other pathogens is mostly more rigid than their targeting tissue [91].

Nanoparticles containing different antigens such as DNA and proteins have been introduced to dendritic cells to observe their phagocytosis process and dendritic cell activation [94]. Using a well-known model antigen is favored since the main interactions and responses are known. One of the well-known protein families are the albumins. These globular proteins are mostly found in blood. Ovalbumin in the major protein component of chicken egg white and is available for a rather cheap price. By studying antibodies binding to ovalbumin, the immunogenic epitopes of ovalbumin were mapped. All in all, ovalbumin is one of the most characterized and studied antigens and is widely used as an antigen for immunization experiments [95–100].

The primary, secondary and quaternary structures of multimeric ovalbumin complex are shown in Figure 2.10. Ovalbumin is composed of amino acids with, depending on the pH, positively charged side chains as well as amino acids with negative side chains. Thus, ovalbumin can be used as a building block for LbL assembly and depending on the solution pH, ovalbumin acts as either a polycation or a polyanion [101].

Due to the particular interest in using dendritic cells to develop novel vaccine-delivery system and to use ovalbumin as a model antigen, we opted to use ovalbumin as the therapeutic agent to be delivered to dendritic cells. To this aim, ovalbumin must be incorporated within the designed drug-carrier structure.

10	20	30	40	50
MGSIGAASME	FCFDVFKELK	VHHANENIFY	CPIAIMSALA	MVYLGAKDST
60	70	80	90	100
RTQINKVVRF	DKLPGFGDSI	EAQCGTSVNV	HSSLRDILNQ	ITKPNDVYSF
110	120	130	140	150
SLASRLYAEE	RYPILPEYLQ	CVKELYRGGL	EPINFQTAAD	QARELINSWV
160	170	180	190	200
ESQTNGIIRN	VLQPSSVDSQ	TAMVLVNAIV	FKGLWEKAFK	DEDTQAMPFR
210	220	230	240	250
VTEQESKPVQ	MMYQIGLFRV	ASMASEKMKI	LELPFASGTM	SMLVLLPDEV
260	270	280	290	300
SGLEQLESII	NFEKLTEWTS	SNVMEERKIK	VYLPRMKMEE	KYNLTSVLMA
310	320	330	340	350
MGITDVFSSS	ANLSGISSAE	SLKISQAVHA	AHAEINEAGR	EVVGSAEAGV
360	370	380		
DAASVSEEFR	ADHPFLFCIK	HIATNAVLFF	GRCVSP	

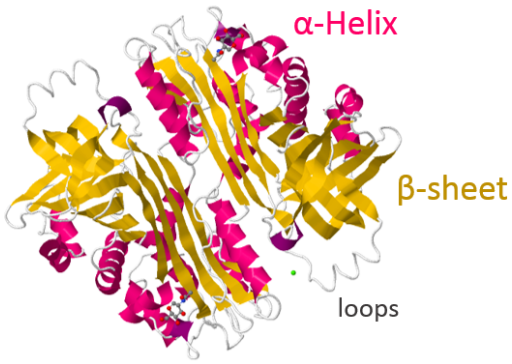

Figure 2.10. Top: Amino acid sequence of ovalbumin. Amino acids with negatively charged side chains (D: aspartic acid, E: glutamic acid) are marked with blue. Amino acids with positively charged side chains (K: lysine, R: arginine, H: histidine) are marked with red. Bottom: The secondary structure of ovalbumin is shown (α-helices and β-sheets), two ovalbumin proteins are associated with each other to form a multimeric structure [101].

2.5 Proteins and biomacromolecules in LbL assembly

2.5.1 Protein and biomacromolecule containing LbL assembled flat systems

Incorporating proteins as biomacromolecules in multilayer assembled structures has been extensively studied. It is shown that water soluble proteins such as cytochrome c, myoglobin, lysozyme, histone, hemoglobin and glucose oxidase can be used to construct multilayer assembled films [102]. These proteins remained stable and retained their functionality after assembly [103].

Multilayers of glucose oxidase (GOX) enzyme and polyethylenimine (PEI) were fabricated and the enzymatic activity of GOX was evaluated. It was shown that GOX maintained its oxidative activity for 14 days. In addition, it was found that by incorporating the enzyme in multilayers, its tolerance towards fluctuations in temperature is significantly enhanced. GOX containing films retained 90 % of their activity after being incubated at 50 °C, while the activity of GOX aqueous solution was almost zero after incubation [104].

Hammond et al. [105] constructed LbL assembled multilayer flat films composed of ovalbumin and hydrolytically degradable poly-β-amino ester (PBAE) polycations as a model for transcutaneous protein delivery system. Upon degradation of PBAE, non-aggregated and non-degraded ovalbumin protein is released and is uptaken by skin-resident antigen presenting Langerhans cells (Figure 2.11).

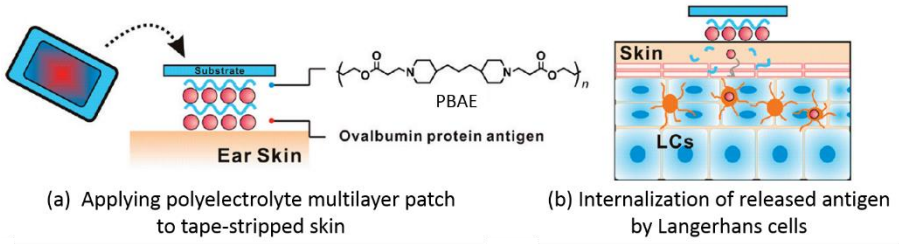

Figure 2.11. Schematic representation of (a) applying hydrolytically degradable polyelectrolyte multilayers containing ovalbumin model antigen on tape-stripped skin, (b) upon degradation of PBAE component, ovalbumin is release and is uptaken by skin-resident Langerhans cells [105].

Other systems for tunable release of ovalbumin protein were also developed by using different combinations of two pH sensitive polycations with different pKa and charge density (poly-L-lysine (PLL) and PBAE), and ovalbumin as polyanion. The release kinetics of ovalbumin can be fine-tuned by varying order and the ratio of these two polycations from 0.3 to 79 hours [106].

Proteins can also be loaded within the structure of a multilayer assembled film. In a particular case, PLL was used as polycation and hyaluronic acid (HA) was used a polyanion for LbL assembly of a multilayer film over a titanium substrate. These layers were then crosslinked at different degrees and were loaded with bone morphogenetic proteins (BMP-2). It was observed that both protein loaded and unloaded multilayers were stable for almost one year at 4 °C [107]. Another LbL assembled system composed of chitosan (polycation) and poly(β-L malic acid) (polyanion) was fabricated and loaded with either lysozyme or fibroblast growth factor-2 (bFGF). The sustained release of these proteins was carefully monitored. Lysozyme showed a tunable release from 30 minutes to more than 5 days while bFGF had a sustained release up to 2 weeks [108,109].

2.5.2 Protein and biomacromolecule-containing LbL assembled spherical systems

Microcapsules containing biomacromolecules have been developed and their application has been studied thoroughly. Multilayers of protamine and dextran sulfate were assembled on melamine formaldehyde microparticles. Protamine is a strong basic protein and has a high content of arginine thus, was chosen as polycation while dextran sulfate was chosen as polyanion. The core was dissolved at low pH and a swollen hollow shell was obtained. Hollow capsules were next loaded with horseradish peroxidase. Those capsules demonstrated high oxidative activity and were stable for 12 months [110].

Hollow capsules with stimuli responsive shells were developed by Li et al [111]. Multilayers of GOX and catalase (CAT) were deposited on insulin particles via LbL assembly and were crosslinked by glutaraldehyde resulting into formation of microcapsules with glucose sensitive shell and insulin cargo. When these capsules come in contact with glucose, the shell undergoes an oxidative reaction which results into production of H^+ and therefore, the pH of the microenvironment is decreased, leading to an increase in the permeability of these capsules and release of insulin cargo [111].

Biodegradable microcapsules were fabricated by LbL assembly of poly-L-arginine (PLA) (as polycation) and dextran sulfate (DEXS) (as polyanion) over $CaCO_3$ microparticles. Hollow capsules were obtained by removing $CaCO_3$ core and were loaded with fluorescent-tagged ovalbumin. The capsules were next incubated in an aqueous pronase solution. Pronase is a mixture of different proteases and is able to cleave amino acids. It was observed that capsules degraded overtime and ovalbumin cargo was released in a timely fashion [112,113].

In another work, (PLA/DEXS) hollow capsules were loaded with self-quenched fluorescent-tagged ovalbumin (DQ-OVA) and were incubated with dendritic cells. After being uptaken by dendritic cells, the capsule shell is degraded and intracellular protease can reach and cleave DQ-OVA cargo, resulting into relieving the self-quenching and obtaining fluorescence emission. Control capsules composed of (PAH/PSS) shell, loaded with DQ-OVA were also incubated with dendritic cells and retained their integrity upon uptake and the DQ-ovalbumin remained self-quenched (Figure 2.12) [114–116].

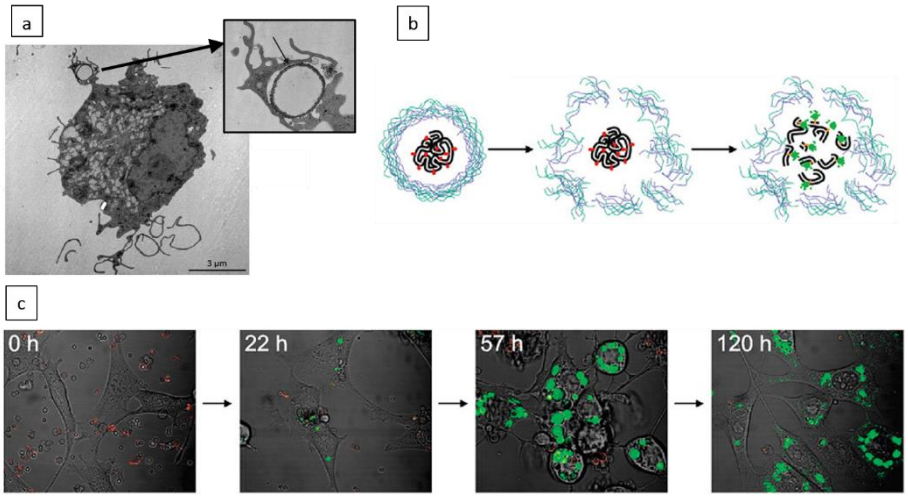

Figure 2.12. (a) TEM image of a dendritic cell stretching out to capture a hollow microcapsule, (b) schematic representation of capsule shell degradation, followed by cleaving fluorescent self-quenched ovalbumin cargo and revoking the fluorescence signal, (c) Intracellular degradation of (dextran sulfate/poly-L-arginine) capsules containing fluorescently quenched ovalbumin protein (DQ-OVA) over time [116].

Microcapsules can also be fabricated from hydrogen-bonding interacting species. Microcapsules composed of poly(vinylpyrrolidone) and tannic acid were fabricated by LbL assembly over a porous mannitol core. Next, fluorescent-tagged ovalbumin was loaded within the pores of mannitol. The

mannitol core was dissolved upon dispersion in aqueous solution resulting in formation of ovalbumin loaded hollow capsules Figure 2.13.a and Figure 2.13.b. These capsules are successfully uptaken by dendritic cells as shown in Figure 2.13.c. It is observed that encapsulation of protein antigens compared to soluble antigen, promotes humoral and cellular immune response in vivo [117].

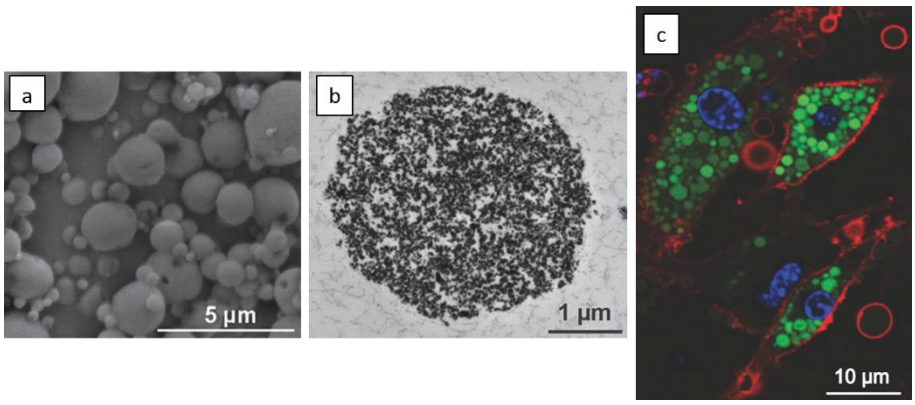

Figure 2.13. (a) SEM and (b) TEM images of a (ovalbumin/ tannic acid/ poly(vinylpyrrolidone) microcapsules, (c) confocal microscopy images of these microcapsules after phagocytosis by dendritic cells. The cell nuclei were stained blue, the cell membrane was conjugated with a red fluorescent dye, and microparticles contained green fluorescent conjugated ovalbumin [117].

2.5.3 Protein and biomacromolecule-containing LbL assembled nanotubular systems

Incorporation of biomacromolecules in fabrication of LbL assembled template synthesized nanotubes was first suggested by Martin et al [74]. They fabricated glucose oxidase/glutaraldehyde and hemoglobin/glutaraldehyde containing nanotubes by vacuum filtration of proteins through the pores of AAO templates. Nanotubes were freed by dissolving the AAO template in an acidic solution and were collected by vacuum filtration. Liberated glucose

oxidase containing nanotubes showed higher oxidation activity compared to nanotubes embedded in the pores of the template. Hemoglobin containing nanotubes also retained their heme electroactivity. This study showed that biomolecules can successfully be integrated in multilayer nanotubes while retaining their structure and biological activity [74]. Nanotubes containing other proteins such as cytochrome C or synthetic hemoprotein were also fabricated and it was shown that they retained the electronic activity as well as biochemical activity of the proteins [69,71].

Since the release of nanotubes from AAO template demands an etching process in highly acidic or basic solutions, the use of PC membranes became more in fashion due to their milder dissolution process. Nanotubes composed of peroxidase and synthetic polyelectrolytes were fabricated within the pores of a PC membrane. Bioactivity of template-embedded tubes was measured and it was observed that such activity depends on the number of enzyme layers deposited inside the pores [118]. Our group has also extensively studied enzyme containing LbL assembled nanotubes. It was observed that very active surfaces are obtained by assembling a very few number of enzyme multilayers (chitosan/β-lactamase) within the pores of a membrane [79]. In our most recent study, it was shown that liberated enzyme-containing nanotubes (polyethylenimine/glucose oxidase) had a higher enzymatic activity compared to template-embedded nanotubes and this higher activity is in proportion to their larger exposed surface (Figure 2.14) [119]. These results promote the potential of LbL assembled template synthesized nanotubes for biocatalytic applications. Hemoglobin-based nanotubes with an interior surface of catalase showed promising H_2O_2-scavenging capacity in vitro, proving their potential application in the treatment of oxidative stress [120].

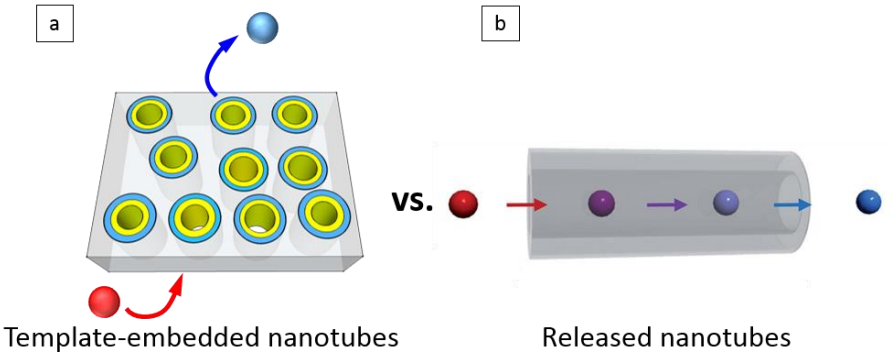

Figure 2.14. Schematic representation of an enzymatic reaction in (a) template-embedded nanotubes, (b) released nanotubes [121].

Apart from enzyme containing systems, multilayered nanotubes containing fibrillar and globular proteins were also developed. Collagen-based nanotubes were successfully fabricated in our group by assembling multilayers of collagen and synthetic polyelectrolytes within the pores of a PC membrane. It was observed that membrane dissolution in CH_2Cl_2 does not affect the structure and morphology of nanotubes [52,122]. After release from the template, those collagen-based nanotubes were deposited on a flat surface and were put in contact with preosteoblast cells, resulting in remarkable changes in cell morphology while the cell behavior was not altered [123].

Globular proteins of different size were incorporated in the structure of LbL assembled nanotubes. To that aim, polyelectrolyte solutions of a polycation (poly-L-arginine) and different polyanions (myoglobin, human serum albumin (HSA) and ferritin) were deposited in the pores of PC membrane by pressure filtration (Figure 2.15). It must be pointed out that in most cases, when assembly is carried out by filtering polyelectrolyte solutions inside the

pores, the wall-thickness of fabricated nanotubes is higher than nanotubes fabricated by simple immersion of equal number of bilayers. Nevertheless, it was shown that the wall-thickness of protein-based nanotubes depends on the globular size of the utilized protein (ferritin > HSA > myoglobin) [124].

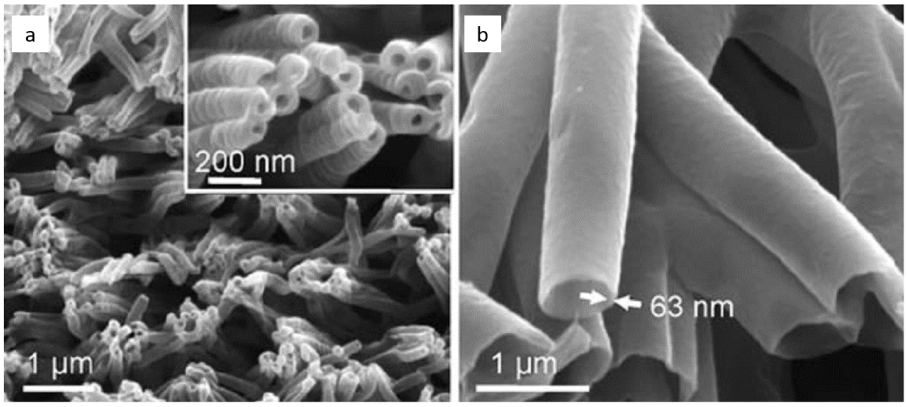

Figure 2.15. SEM images of (poly-L-arginine/human serum albumin) nanotubes prepared by (a) assembling 3 bilayers in a 200 nm porous PC template; (b) assembling 6 bilayers in a 800 nm porous PC template [124].

Protein-based nanotubes with a PLA/HSA core and functional inner or outer surfaces were fabricated within the pores of PC membrane. In one example [125], the innermost layer of these nanotubes contained a protein, avidin, that strongly complexed with biotinylated fluorescent nanoparticles (biotin-FNP). Biotin-FNPs of 100 nm size were able to enter the hollow tubes of 200 nm diameter, while 250 nm biotin-FNP particles did not enter the tubes due to their bigger size (Figure 2.16.a and Figure 2.16.b). Another interesting system was designed with an inner layer of hepatitis B antigen that was able to trap human hepatitis B virus (HBV) particles [121,126,127]. Nanotubes with an outer layer of magnetic Fe_3O_4 and PLA/HSA core were also fabricated by LbL assembly. It was observed that those nanotubes could successfully be collected at a certain place by using a small magnet [121,128]. Microtubes with

25 µm length, 1 µm outer diameter and 150 nm wall thickness composed of PLA/HSA were used to trap Escherichia coli bacteria (0.4 – 0.7 µm width and 2 – 4 µm length) inside the tubes. While some E.coli bacteria could not enter the tubes, other smaller bacteria were able to reach the depth of the tubes (Figure 2.16.c-e) [129].

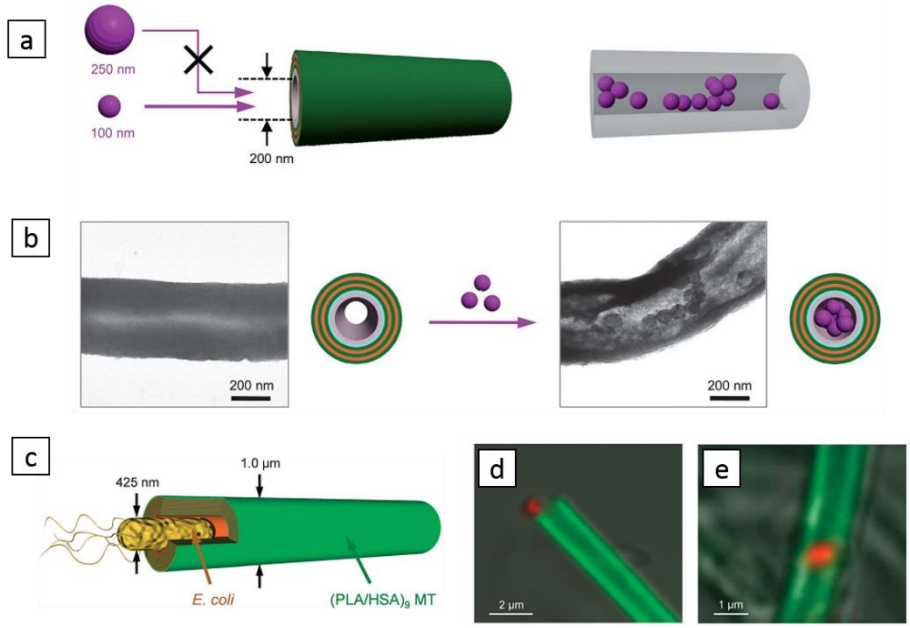

Figure 2.16. (a) Schematic representation of (biotin-FNP) nanoparticles capture in hollow nanotubes of (PLA/HSA) of 200 nm inner diameter containing avidin innermost layer. Biotin-FNP with 250 nm diameter cannot enter the nanotubes while biotin-FNP with 100 nm can enter the tubes, (b) TEM image of avidin containing (PLA/HSA) nanotubes prior and after internalization of 100 nm biotin-FNP [121], (c) Schematic representation of E.coli bacteria trapped inside microtubes, (d) and (e) An overlap of DIC and CLSM images of fluorescent microtubes (green) with red fluorescent-labeled E.coli. (d) E.coli with 700 nm width could not enter the tube and remained stuck on the tube end, (e) E.coli with 425 nm width reached the depth of the tube [129].

Core-shell structured microtubes with cell adhesive (chitosan/hyaluronic acid) and cell resistive (PAH/PSS) surfaces were fabricated by Rubner et al [130]. They demonstrated that depending on the position of the cell adhesive and cell resistive layers, those microtubes attach on the cell surfaces with different orientations.

These results are solid proofs of the possibility of incorporating biomacromolecules such as polysaccharides, nucleic acids and proteins in the structure of nanotubes [131–134]. Nevertheless, the key point for using these nanotubes for biomedical application is their proper release from the membrane and redispersion in an appropriate medium. However, available methods for transferring these nanotubes from the membrane to an aqueous medium are very limited. Rubner et al. extracted nanotubes from the PC membrane by dissolving the membrane in CH_2Cl_2 followed by a subsequent filtration over a hydrophilic polytetrafluoroethylene filter. The collected microtubes were then scraped off the filter surface and transferred to aqueous medium [130].

Komatsu et al. used another methodology to collect and transfer the nanotubes. First, the PC template is dissolved immediately in a polar amide solvent (dimethylformamide, DMF), and the precipitated nanotubes are washed several times with DMF. Second, the obtained tubes are quickly freeze-dried in vacuum to yield the lyophilized nanotubes [125]. Although efficient, this method sometimes leads to formation of aggregates. We believed that a universal method should be developed for collection and dispersion of nanotubes in high yield, which will be done in this thesis.

2.6 Particles with antifouling properties

On our quest to fabricate an ideal drug carrier, it is important to have some understanding of the way carriers can be made to circulate longer in a living organism.

In 1994, Langer et al.[135] demonstrated that by forming a diblock copolymer containing a PEG block, the in vivo circulation half-lives of nanoparticles is dramatically increased. Since that time, PEGylated nanoparticles have been extensively developed, studied and even commercialized (ex. Doxil®, a PEGylated liposomal formulation of doxorubicin). Right now, PEG is FDA approved and is listed as "Generally Recognized as Safe" (GRAS). PEG provides stealth properties to particle surfaces and prevents non-specific binding of blood components to the particles reducing their uptake and clearance by the cells of the mononuclear phagocytic system [136].

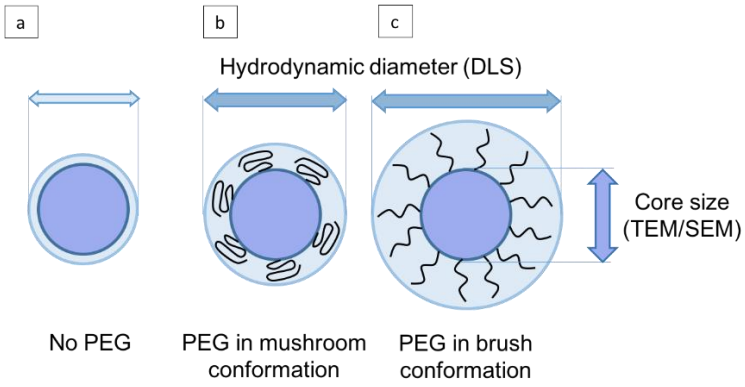

Figure 2.17. Schematic representation of (a) non-grafted particle, (b) PEGylated particle (mushroom regime), (c) PEGylated particle (brush regime). The core size of particles can be characterized by SEM or TEM, while their hydrodynamic diameter can be measured by dynamic light scattering. (Images are extracted and modified from [137].)

The PEG chain coverage density plays a major role in providing antifouling properties. Proper antifouling effect is achieved at a high coverage density that is mainly when chains adopt a brush morphology (Figure 2.17). Thus, the conformation of PEG chain over the surface is an important parameter to be taken into account when antifouling properties are needed [137,138].

Although PEG is commonly used to fabricate non-fouling surfaces, it has some limitations. For instance, PEG may auto-oxidaze in presence of oxygen resulting into formation of ethers and aldehydes that the surface might lose its non-fouling properties. Therefore, development of alternative systems is becoming more and more attractive. The key points that must be taken into account are hydrophilicity, making hydrogen bonds with water molecules and conformational stability of developed surfaces. Self-assembled monolayers presenting oligomers of propylene sulfoxide showed antifouling properties and resisted the adsorption of fibrinogen [139]. Other research groups developed phospholipids bearing zwitterions head groups. These structures are highly remarkable since zwitterions can bind strongly to water molecules and thus, avoid adsorption of proteins [140]. Zwitterions-containing polymeric surfaces and brushes as well as self-assembled monolayers composed of zwitterions showed a significant protein resistance and were strongly non-fouling. Here again, the coverage density and conformation of groups on the surface are very important and must be controlled [139–142].

Since PEG is already widely used and thoroughly studied to develop anti-fouling surfaces, we also aim on fabricating anti-fouling properties by PEGylating the surface of studied particles.

2.7 Conclusion

Without any doubts, fabricating an ideal nano-sized drug carrier demands a combination of techniques and methodologies. It is clear that LbL assembly combined with template synthesis method give us the proper tools to fabricate multilayer nanotubes of our desired compositions, dimensions and functionalities. These methods are highly versatile; however, care must be taken while choosing fabrication conditions. The system becomes even more complex when biomacromolecules, especially proteins, are used.

The proper growth of multilayers within the pores of the template must be ensured in order to take the study into further steps (i.e. functionalizing the surface, transferring tubes to aqueous medium, studying interactions with cell, etc.). Indeed, one should master the fabrication techniques mentioned in this chapter and laboriously put them together in order to achieve our ultimate goal: “fabrication of anisotropic multifunctional tubular nano-objects for the controlled delivery of proteins as therapeutic agent”.

2.8 Bibliography

(1) Decher, G. Fuzzy Nanoassemblies: Toward Layered Polymeric Multicomposites. *Science* **1997**, *277*, 1232–1237.

(2) Decher, G.; Hong, J. D. Buildup of Ultrathin Multilayer Films by a Self-Assembly Process: II. Consecutive Adsorption of Anionic and Cationic Bipolar Amphiphiles and Polyelectrolytes on Charged Surfaces. *Ben. Bunsengens. Phys. Chem.* **1991**, *95*, 1430–1434.

(3) Decher, G.; Hong, J. D.; Schmitt, J. Buildup of Ultrathin Multilayer Films by a Self-Assembly Process: III. Consecutively Alternating Adsorption of Anionic and Cationic Polyelectrolytes on Charged Surfaces. *Thin Solid Films* **1992**, *210/211*, 831–835.

(4) Decher, G.; Hong, J.-D. Buildup of Ultrathin Multilayer Films by a Self-Assembly Process: I. Consecutive Adsorption of Anionic and Cationic Bipolar Amphiphiles on Charged Surfaces. *Makromol. Chemie. Macromol. Symp.* **1991**, *46*, 321–327.

(5) Decher, G.; Schmitt, J. Fine-Tuning of the Film Thickness of Ultrathin Multilayer Films Composed of Consecutively Alternating Layers of Anionic and Cationic Polyelectrolytes. In *Trends in Colloid and Interface Science VI*; Helm, C.; Lösche, M.; Möhwald, H., Eds.; Progress in Colloid & Polymer Science; Steinkopff: Darmstadt, 1992; Vol. 89, pp. 160–164.

(6) Bertrand, P.; Jonas, A.; Laschewsky, A.; Legras, R. Ultrathin Polymer Coatings by Complexation of Polyelectrolytes at Interfaces : Suitable Materials, Structure and Properties. *Macromol. Rapid Commun.* **2000**, *21*, 319–348.

(7) Liang, Z.; Susha, A. S.; Yu, A.; Caruso, F. Nanotubes Prepared by Layer-by-Layer Coating of Porous Membrane Templates. *Adv. Mater.* **2003**, *15*, 1849–1853.

(8) Ai, S.; Lu, G.; He, Q.; Li, J. Highly Flexible Polyelectrolyte Nanotubes. *J. Am. Chem. Soc.* **2003**, *125*, 11140–11141.

(9) Lu, G.; Ai, S.; Li, J. Layer-by-Layer Assembly of Human Serum Albumin and Phospholipid Nanotubes Based on a Template. *Langmuir* **2005**, *21*, 1679–1682.

(10) Ai, S.; He, Q.; Tao, C.; Zheng, S.; Li, J. Conductive Polypyrrole and Poly(allylamine Hydrochloride) Nanotubes Fabricated with Layer-by-Layer Assembly. *Macromol. Rapid Commun.* **2005**, *26*, 1965–1969.

(11) Wang, Y.; Angelatos, A. S.; Caruso, F. Template Synthesis of Nanostructured Materials via Layer-by-Layer Assembly. *Chem. Mater.* **2008**, *20*, 848–858.

(12) Tian, Y.; He, Q.; Tao, C.; Li, J. Fabrication of Fluorescent Nanotubes Based on Layer-by-Layer Assembly via Covalent Bond. *Langmuir* **2006**, *22*, 360–362.

(13) Guo, Y.-G.; Hu, J.-S.; Liang, H.-P.; Wan, L.-J.; Bai, C.-L. TiO2-Based Composite Nanotube Arrays Prepared via Layer-by-Layer Assembly. *Adv. Funct. Mater.* **2005**, *15*, 196–202.

(14) Caruso, F. Nanoengineering of Particle Surfaces. *Adv. Mater.* **2001**, *13*, 11–22.

(15) Ariga, K.; Hill, J. P.; Ji, Q. Layer-by-Layer Assembly as a Versatile Bottom-up Nanofabrication Technique for Exploratory Research and Realistic Application. *Phys. Chem. Chem. Phys.* **2007**, *9*, 2319–2340.

(16) Peyratout, C. S.; Dähne, L. Tailor-Made Polyelectrolyte Microcapsules: From Multilayers to Smart Containers. *Angew. Chem. Int. Ed. Engl.* **2004**, *43*, 3762–3783.

(17) Quinn, J. F.; Johnston, A. P. R.; Such, G. K.; Zelikin, A. N.; Caruso, F.

Next Generation, Sequentially Assembled Ultrathin Films: Beyond Electrostatics. *Chem. Soc. Rev.* **2007**, *36*, 707–718.

(18) Richardson, J. J.; Bjornmalm, M.; Caruso, F. Technology-Driven Layer-by-Layer Assembly of Nanofilms. *Science* **2015**, *348*, 411–424.

(19) Shiratori, S. S.; Rubner, M. F. pH-Dependent Thickness Behavior of Sequentially Adsorbed Layers of Weak Polyelectrolytes. *Macromolecules* **2000**, *33*, 4213–4219.

(20) Von Klitzing, R. v. Internal Structure of Polyelectrolyte Multilayer Assemblies. *Phys. Chem. Chem. Phys.* **2006**, *8*, 5012–5033.

(21) Salomäki, M.; Laiho, T.; Kankare, J. Counteranion-Controlled Properties of Polyelectrolyte Multilayers. *Macromolecules* **2004**, *37*, 9585–9590.

(22) *Trends in Colloid and Interface Science VI*; Helm, C.; Lösche, M.; Möhwald, H., Eds.; Progress in Colloid & Polymer Science; Steinkopff: Darmstadt, 1992; Vol. 89.

(23) Arys, X.; Fischer, P.; Jonas, A. M.; Koetse, M. M.; Laschewsky, A.; Legras, R.; Wischerhoff, E. Ordered Polyelectrolyte Multilayers. Rules Governing Layering in Organic Binary Multilayers. *J. Am. Chem. Soc.* **2003**, *125*, 1859–1865.

(24) Linford, M. R.; Auch, M.; Möhwald, H. Nonmonotonic Effect of Ionic Strength on Surface Dye Extraction during Dye-Polyelectrolyte Multilayer Formation. *J. Am. Chem. Soc.* **1998**, *120*, 178–182.

(25) Hammond, P. T. Recent Explorations in Electrostatic Multilayer Thin Film Assembly. *Curr. Opin. Colloid Interface Sci.* **1999**, *4*, 430–442.

(26) Leontidis, E. Hofmeister Anion Effects on Surfactant Self-Assembly and the Formation of Mesoporous Solids. *Curr. Opin. Colloid*

Interface Sci. **2002**, *7*, 81–91.

(27) Volodkin, D.; von Klitzing, R.; Moehwald, H. Polyelectrolyte Multilayers: Towards Single Cell Studies. *Polymers (Basel).* **2014**, *6*, 1502–1527.

(28) Wong, J. E.; Zastrow, H.; Jaeger, W.; Von Klitzing, R. Specific Ion versus Electrostatic Effects on the Construction of Polyelectrolyte Multilayers †. *Langmuir* **2009**, *25*, 14061–14070.

(29) Sukhishvili, S. a.; Kharlampieva, E.; Izumrudov, V. Where Polyelectrolyte Multilayers and Polyelectrolyte Complexes Meet. *Macromolecules* **2006**, *39*, 8873–8881.

(30) Nestler, P.; Paßvogel, M.; Helm, C. a. Influence of Polymer Molecular Weight on the Parabolic and Linear Growth Regime of PDADMAC/PSS Multilayers. *Macromolecules* **2013**, *46*, 5622–5629.

(31) Micciulla, S.; Dodoo, S.; Chevigny, C.; Laschewsky, A.; Von Klitzing, R. Short versus Long Chain Polyelectrolyte Multilayers: A Direct Comparison of Self-Assembly and Structural Properties. *Phys. Chem. Chem. Phys.* **2014**, *16*, 21988–21998.

(32) Guyomard, A.; Muller, G.; Glinel, K. Buildup of Multilayers Based on Amphiphilic Polyelectrolytes. *Macromolecules* **2005**, *38*, 5737–5742.

(33) Kotov, N. a. Layer-by-Layer Self-Assembly: The Contribution of Hidrophobic Interactions. *NanoStructured Mater.* **1999**, *12*, 789–796.

(34) Glinel, K.; Moussa, A.; Jonas, A. M.; Laschewsky, A. Influence of Polyelectrolyte Charge Density on the Formation of Multilayers of Strong Polyelectrolytes at Low Ionic Strength. *Langmuir* **2002**, *18*, 1408–1412.

(35) Schoeler, B.; Kumaraswamy, G.; Caruso, F. Investigation of the Influence of Polyelectrolyte Charge Density on the Growth of Multilayer Thin Films Prepared by the Layer-by-Layer Technique. *Macromolecules* **2002**, *35*, 889–897.

(36) De Geest, B. G.; Sukhorukov, G. B.; Möhwald, H. The Pros and Cons of Polyelectrolyte Capsules in Drug Delivery. *Expert Opin. Drug Deliv.* **2009**, *6*, 613–624.

(37) Schneider, G.; Decher, G. From Functional Core/shell Nanoparticles Prepared via Layer-by-Layer Deposition to Empty Nanospheres. *Nano Lett.* **2004**, *4*, 1833–1839.

(38) De Koker, S.; De Geest, B. G.; Cuvelier, C.; Ferdinande, L.; Deckers, W.; Hennink, W. E. W. E.; Smedt, S. De; Mertens, N. In Vivo Cellular Uptake , Degradation , and Biocompatibility of Polyelectrolyte Microcapsules. *Adv. Funct. Mater.* **2007**, *17*, 3754–3763.

(39) Such, G. K.; Tjipto, E.; Postma, A.; Johnston, A. P. R.; Caruso, F. Ultrathin, Responsive Polymer Click Capsules. *Nano Lett.* **2007**, *7*, 1706–1710.

(40) Itoh, Y.; Matsusaki, M.; Kida, T.; Akashi, M. Enzyme-Responsive Release of Encapsulated Proteins from Biodegradable Hollow Capsules. *Biomacromolecules* **2006**, *7*, 2715–2718.

(41) Yu, A.; Wang, Y.; Barlow, E.; Caruso, F. Mesoporous Silica Particles as Templates for Preparing Enzyme-Loaded Biocompatible Microcapsules. *Adv. Mater.* **2005**, *17*, 1737–1741.

(42) Shchukin, D. G.; Patel, A. A.; Sukhorukov, G. B.; Lvov, Y. M. Nanoassembly of Biodegradable Microcapsules for DNA Encasing. *J. Am. Chem. Soc.* **2004**, *126*, 3374–3375.

(43) Zelikin, A. N.; Li, Q.; Caruso, F. Degradable Polyelectrolyte Capsules Filled with Oligonucleotide Sequences. *Angew. Chem. Int. Ed. Engl.*

2006, *118*, 7907–7909.

(44) Donath, E.; Sukhorukov, G. B.; Caruso, F.; Davis, S. a; Möhwald, H. Novel Hollow Polymer Shells by Colloid-Templated Assembly of Polyelectrolytes. *Angew. Chem. Int. Ed. Engl.* **1998**, *37*, 2201–2205.

(45) Mayya, K. S.; Gittins, D. I.; Dibaj, A. M.; Caruso, F. Nanotubes Prepared by Templating Sacrificial Nickel Nanorods. *Nano Lett.* **2001**, *1*, 727–730.

(46) Wang, Y. J.; Tang, Y.; Wang, X. D.; Yang, W. L.; Gao, Z. Fabrication of Hollow Zeolite Fibers through Layer-by-Layer Adsorption Method. *Chem. Lett.* **2000**, 1344–1345.

(47) Shutava, T. G.; Fakhrullin, R. F.; Lvov, Y. M. Spherical and Tubule Nanocarriers for Sustained Drug Release. *Curr. Opin. Pharmacol.* **2014**, *18C*, 141–148.

(48) Veerabadran, N. G.; Mongayt, D.; Torchilin, V.; Price, R. R.; Lvov, Y. M. Organized Shells on Clay Nanotubes for Controlled Release of Macromolecules. *Macromol. Rapid Commun.* **2009**, *30*, 99–103.

(49) Cepak, V. M.; Martin, C. R. Preparation of Polymeric Micro- and Nanostructures Using a Template-Based Deposition Method. *Chem. Mater.* **1999**, *11*, 1363–1367.

(50) Kovtyukhova, N. I.; Martin, B. R.; Mbindyo, J. K. N.; Smith, P. A.; Razavi, B.; Mayer, T. S.; Mallouk, T. E. Layer-by-Layer Assembly of Rectifying Junctions in and on Metal Nanowires. *J. Phys. Chem. B* **2001**, *105*, 8762–8769.

(51) Sander, M. S.; Prieto, A. L.; Gronsky, R.; Sands, T.; Stacy, A. M. Fabrication of High-Density, High Aspect Ratio, Large-Area Bismuth Telluride Nanowire Arrays by Electrodeposition into Porous Anodic Alumina Templates. *Adv. Mater.* **2002**, *14*, 665–667.

(52) Landoulsi, J.; Roy, C. J. C. J.; Dupont-Gillain, C.; Demoustier-Champagne, S. Synthesis of Collagen Nanotubes with Highly Regular Dimensions through Membrane-Templated Layer-by-Layer Assembly. *Biomacromolecules* **2009**, *10*, 1021–1024.

(53) Callegari, V.; Gence, L.; Melinte, S.; Demoustier-Champagne, S. Electrochemically Template-Grown Multi-Segmented Gold-Conducting Polymer Nanowires with Tunable Electronic Behavior. *Chem. Mater.* **2009**, *21*, 4241–4247.

(54) Callegari, V.; Demoustier-Champagne, S. Using the Hard Templating Method for the Synthesis of Metal-Conducting Polymer Multi-Segmented Nanowires. *Macromol. Rapid Commun.* **2011**, *32*, 25–34.

(55) Perry, J. L.; Martin, C. R.; Stewart, J. D. Drug-Delivery Strategies by Using Template-Synthesized Nanotubes. *Chemistry* **2011**, *17*, 6296–6302.

(56) Roy, C. J.; Chorine, N.; Geest, B. De; Smedt, S. De; Jonas, A. M.; Demoustier-champagne, S. Highly Versatile Approach for Preparing Hybrid Multisegmented Nanotubes and Nanowires with Tailored Properties. *Chem. Mater.* **2012**, *24*, 1562–1567.

(57) Shen, X.-P.; Liu, H.-J.; Fan, X.; Jiang, Y.; Hong, J.-M.; Xu, Z. Construction and Photoluminescence of In2O3 Nanotube Array by CVD-Template Method. *J. Cryst. Growth* **2005**, *276*, 471–477.

(58) Callegari, V.; Demoustier-Champagne, S. Interfacing Conjugated Polymers with Magnetic Nanowires. *ACS Appl. Mater. Interfaces* **2010**, *2*, 1369–1376.

(59) Lakshmi, B. B.; Patrissi, C. J.; Martin, C. R. Sol−Gel Template Synthesis of Semiconductor Oxide Micro- and Nanostructures. *Chem. Mater.* **1997**, *9*, 2544–2550.

(60) Yabu, H.; Hirai, Y.; Shimomura, M. Electroless Plating of Honeycomb

and Pincushion Polymer Films Prepared by Self-Organization. *Langmuir* **2006**, *22*, 9760–9764.

(61) Cui, Y.; Tao, C.; Zheng, S.; He, Q.; Ai, S.; Li, J. Synthesis of Thermosensitive PNIPAM-Co-MBAA Nanotubes by Atom Transfer Radical Polymerization within a Porous Membrane. *Macromol. Rapid Commun.* **2005**, *26*, 1552–1556.

(62) Furneaux, R. C.; Rigby, W. R.; Davidson, A. P. The Formation of Controlled-Porosity Membranes from Anodically Oxidized Aluminium. *Nature* **1989**, *337*, 147–149.

(63) Thompson, G. . Porous Anodic Alumina: Fabrication, Characterization and Applications. *Thin Solid Films* **1997**, *297*, 192–201.

(64) AlMawlawi, D.; Coombs, N.; Moskovits, M. Magnetic Properties of Fe Deposited into Anodic Aluminum Oxide Pores as a Function of Particle Size. *J. Appl. Phys.* **1991**, *70*, 4421.

(65) Hurst, S. J.; Payne, E. K.; Qin, L.; Mirkin, C. A. Multisegmented One-Dimensional Nanorods Prepared by Hard-Template Synthetic Methods. *Angew. Chem. Int. Ed. Engl.* **2006**, *45*, 2672–2692.

(66) Ferain, E.; Legras, R. Track-Etch Templates Designed for Micro- and Nanofabrication. *Nucl. Instr. Meth. Phys. Res.* **2003**, *208*, 115–122.

(67) Ye, Z.; Liu, H.; Schultz, I.; Wu, W.; Naugle, D. G.; Lyuksyutov, I. Template-Based Fabrication of Nanowire-Nanotube Hybrid Arrays. *Nanotechnology* **2008**, *19*, 325303.

(68) Hanot, H.; Ferain, E. Industrial Applications of Ion Track Technology. *The Seventh International Symposium on Swift Heavy Ions in Matter*, 2008.

(69) Lu, G.; Komatsu, T.; Tsuchida, E. Artificial Hemoprotein Nanotubes. *Chem. Commun.* **2007**, 2980–2982.

(70) Perry, J. L.; Guo, P.; Johnson, S. K.; Mukaibo, H.; Stewart, J. D.; Martin, C. R. Fabrication of Biodegradable Nano Test Tubes by Template Synthesis. *Nanomedicine (Lond).* **2010**, *5*, 1151–1160.

(71) Tian, Y.; He, Q.; Cui, Y.; Li, J. Fabrication of Protein Nanotubes Based on Layer-by-Layer Assembly. *Biomacromolecules* **2006**, *7*, 2539–2542.

(72) Silva, J. M.; Duarte, A. R. C.; Custódio, C. A.; Sher, P.; Neto, A. I.; Pinho, A. C. M.; Fonseca, J.; Reis, R. L.; Mano, J. F. Nanostructured Hollow Tubes Based on Chitosan and Alginate Multilayers. *Adv. Healthc. Mater.* **2014**, *3*, 433–440.

(73) Kohler, D.; Schneider, M.; Krüger, M.; Lehr, C.-M.; Möhwald, H.; Wang, D. Template-Assisted Polyelectrolyte Encapsulation of Nanoparticles into Dispersible, Hierarchically Nanostructured Microfibers. *Adv. Mater.* **2011**, *23*, 1376–1379.

(74) Hou, S.; Wang, J.; Martin, C. R. Template-Synthesized Protein Nanotubes. *Nano Lett.* **2005**, *5*, 231–234.

(75) Hou, S.; Wang, J.; Martin, C. R. Template-Synthesized DNA Nanotubes. *J. Am. Chem. Soc.* **2005**, *127*, 8586–8587.

(76) Yang, Y.; He, Q.; Duan, L.; Cui, Y.; Li, J. Assembled Alginate/chitosan Nanotubes for Biological Application. *Biomaterials* **2007**, *28*, 3083–3090.

(77) Alem, H.; Blondeau, F.; Glinel, K.; Demoustier-champagne, S.; Jonas, A. M. Layer-by-Layer Assembly of Polyelectrolytes in Nanopores. *Macromolecules* **2007**, *40*, 3366–3372.

(78) He, Q.; Cui, Y.; Ai, S.; Tian, Y.; Li, J. Self-Assembly of Composite Nanotubes and Their Applications. *Curr. Opin. Colloid Interface Sci.* **2009**, *14*, 115–125.

(79) Ramírez-Wong, D. G.; Coelho-diogo, C.; Aimé, C.; Bonhomme, C.; Jonas, A. M.; Demoustier-champagne, S. Effects of Geometrical Confinement in Membrane Pores on Enzyme-Based Layer-by-Layer Assemblies. *Appl. Surf. Sci.* **2015**, *338*, 154–162.

(80) Roy, C. J.; Dupont-Gillain, C.; Demoustier-Champagne, S.; Jonas, a M.; Landoulsi, J. Growth Mechanism of Confined Polyelectrolyte Multilayers in Nanoporous Templates. *Langmuir* **2010**, *26*, 3350–3355.

(81) Mailänder, V.; Landfester, K. Interaction of Nanoparticles with Cells. *Biomacromolecules* **2009**, *10*, 2379–2400.

(82) Singh, A.; Pradhan, P.; Roy, K. *Novel Immune Potentiators and Delivery Technologies for Next Generation Vaccines*; Singh, M., Ed.; Springer US: Boston, MA, 2013.

(83) Gregory, A. E.; Titball, R.; Williamson, D. Vaccine Delivery Using Nanoparticles. *Front. Cell. Infect. Microbiol.* **2013**, *3*, 1–13.

(84) Silva, J. M.; Videira, M.; Gaspar, R.; Préat, V.; Florindo, H. F. Immune System Targeting by Biodegradable Nanoparticles for Cancer Vaccines. *J. Control. Release* **2013**, *168*, 179–199.

(85) Hubbell, J. a; Thomas, S. N.; Swartz, M. a. Materials Engineering for Immunomodulation. *Nature* **2009**, *462*, 449–460.

(86) Devriendt, B.; De Geest, B. G.; Cox, E. Designing Oral Vaccines Targeting Intestinal Dendritic Cells. *Expert Opin. Drug Deliv.* **2011**, *8*, 467–483.

(87) Lipscomb, M. F.; Masten, B. J. Dendritic Cells: Immune Regulators in Health and Disease. *Physiol. Rev.* **2002**, *82*, 97–130.

(88) Palucka, K.; Banchereau, J. Cancer Immunotherapy via Dendritic Cells. *Nat. Rev. Cancer* **2012**, *12*, 265–277.

(89) Syfert, B. http://bigpictureeducation.com/immune-response-component-images http://bigpictureeducation.com/immune-response-component-images (accessed Nov 20, 2015).

(90) Johnston, A. P. R. R.; Such, G. K.; Ng, S. L.; Caruso, F. Challenges Facing Colloidal Delivery Systems : From Synthesis to the Clinic. *Curr. Opin. Colloid Interface Sci.* **2011**, *16*, 171–181.

(91) Hillaireau, H.; Couvreur, P. Nanocarriers' Entry into the Cell: Relevance to Drug Delivery. *Cell. Mol. Life Sci.* **2009**, *66*, 2873–2896.

(92) Aderem, A. How to Eat Something Bigger than Your Head. *Cell* **2002**, *110*, 5–8.

(93) Champion, J. a; Mitragotri, S. Role of Target Geometry in Phagocytosis. *Proc. Natl. Acad. Sci. U. S. A.* **2006**, *103*, 4930–4934.

(94) Singh, M.; Chakrapani, A.; O'Hagan, D. Nanoparticles and Microparticles as Vaccine-Delivery Systems. *Expert Rev. Vaccines* **2007**, *6*, 797–808.

(95) Standley, S. M.; Kwon, Y. J.; Murthy, N.; Kunisawa, J.; Shastri, N.; Guillaudeu, S. J.; Lau, L.; Fréchet, J. M. J. Acid-Degradable Particles for Protein-Based Vaccines: Enhanced Survival Rate for Tumor-Challenged Mice Using Ovalbumin Model. *Bioconjug. Chem.* **2004**, *15*, 1281–1288.

(96) Mahony, D.; Cavallaro, A. S.; Stahr, F.; Mahony, T. J.; Qiao, S. Z.; Mitter, N. Mesoporous Silica Nanoparticles Act as a Self-Adjuvant for

Ovalbumin Model Antigen in Mice. *Small* **2013**, *9*, 3138–3146.

(97) O'Hagan, D. T.; Rahman, D.; McGee, J. P.; Jeffery, H.; Davies, M. C.; Williams, P.; Davis, S. S.; Challacombe, S. J. Biodegradable Microparticles as Controlled Release Antigen Delivery Systems. *Immunology* **1991**, *73*, 239–242.

(98) Widera, G.; Johnson, J.; Kim, L.; Libiran, L.; Nyam, K.; Daddona, P. E.; Cormier, M. Effect of Delivery Parameters on Immunization to Ovalbumin Following Intracutaneous Administration by a Coated Microneedle Array Patch System. *Vaccine* **2006**, *24*, 1653–1664.

(99) Kwon, Y. J.; James, E.; Shastri, N.; Fréchet, J. M. J. In Vivo Targeting of Dendritic Cells for Activation of Cellular Immunity Using Vaccine Carriers Based on pH-Responsive Microparticles. *Proc. Natl. Acad. Sci. U. S. A.* **2005**, *102*, 18264–18268.

(100) Bandyopadhyay, A.; Fine, R. L.; Demento, S.; Bockenstedt, L. K.; Fahmy, T. M. The Impact of Nanoparticle Ligand Density on Dendritic-Cell Targeted Vaccines. *Biomaterials* **2011**, *32*, 3094–3105.

(101) Stein, P.E., Leslie, A.G., Finch, J.T., Carrell, R. W. E.; Leslie, A. G.; Finch, J. T.; Carrell, R. W. Crystal Structure of Uncleaved Ovalbumin at 1.95 Å Resolution. *J.Mol.Biol.* **1991**, *221*, 941–959.

(102) Lvov, Y.; Ariga, K.; Ichinose, I.; Kunitake, T. Assembly of Multicomponent Protein Films by Means of Electrostatic Layer-by-Layer Adsorption. *J. Am. Chem. Soc.* **1995**, *117*, 6117–6123.

(103) Tang, Z.; Wang, Y.; Podsiadlo, P.; Kotov, N. a. Biomedical Applications of Layer-by-Layer Assembly: From Biomimetics to Tissue Engineering. *Adv. Mater.* **2006**, *18*, 3203–3224.

(104) Onda, M.; Ariga, K.; Kunitake, T. Activity and Stability of Glucose Oxidase in Molecular Films Assembled Alternately with Polyions. *J. Biosci. Bioeng.* **1999**, *87*, 69–75.

(105) Su, X.; Kim, B.; Kim, S. R.; Hammond, P. T.; Irvine, D. J. Layer-by-Layer-Assembled Multilayer Films for Transcutaneous Drug and Vaccine Delivery. *ACS Nano* **2009**, *3*, 3719–3729.

(106) Hong, J.; Kim, B.-S.; Char, K.; Hammond, P. T. Inherent Charge-Shifting Polyelectrolyte Multilayer Blends: A Facile Route for Tunable Protein Release from Surfaces. *Biomacromolecules* **2011**, *12*, 2975–2981.

(107) Guillot, R.; Gilde, F.; Becquart, P.; Sailhan, F.; Lapeyrere, A.; Logeart-avramoglou, D.; Picart, C. Biomaterials The Stability of BMP Loaded Polyelectrolyte Multilayer Coatings on Titanium. *Biomaterials* **2013**, *34*, 5737–5746.

(108) Hsu, B. B.; Jamieson, K. S.; Hagerman, S. R.; Holler, E.; Ljubimova, J. Y.; Hammond, P. T. Ordered and Kinetically Discrete Sequential Protein Release from Biodegradable Thin Films. *Angew. Chemie* **2014**, *53*, 8231–8236.

(109) Hsu, B. B.; Hagerman, S. R.; Jamieson, K.; Veselinovic, J.; O'Neill, N.; Holler, E.; Ljubimova, J. Y.; Hammond, P. T. Multilayer Films Assembled from Naturally-Derived Materials for Controlled Protein Release. *Biomacromolecules* **2014**.

(110) Balabushevich, N. G.; Tiourina, O. P.; Volodkin, D. V.; Larionova, N. I.; Sukhorukov, G. B. Loading the Multilayer Dextran Sulfate/protamine Microsized Capsules with Peroxidase. *Biomacromolecules* **2003**, *4*, 1191–1197.

(111) Qi, W.; Yan, X.; Fei, J.; Wang, A.; Cui, Y.; Li, J. Triggered Release of Insulin from Glucose-Sensitive Enzyme Multilayer Shells. *Biomaterials* **2009**, *30*, 2799–2806.

(112) Dierendonck, M.; De Koker, S.; Vervaet, C.; Remon, J. P.; De Geest, B. G. Interaction between Polymeric Multilayer Capsules and Immune

Cells. *J. Control. Release* **2012**, *161*, 592–599.

(113) De Geest, B. G.; Vandenbroucke, R. E.; Guenther, A. M.; Sukhorukov, G. B.; Hennink, W. E.; Sanders, N. N.; Demeester, J.; De Smedt, S. C. Intracellularly Degradable Polyelectrolyte Microcapsules. *Adv. Mater.* **2006**, *18*, 1005–1009.

(114) Rivera-Gil, P.; De Koker, S.; De Geest, B. G.; Parak, W. J. Intracellular Processing of Proteins Mediated by Biodegradable Polyelectrolyte Capsules. *Nano Lett.* **2009**, *9*, 4398–4402.

(115) Devriendt, B.; Baert, K.; Dierendonck, M.; Favoreel, H.; De Koker, S.; Remon, J. P.; De Geest, B. G.; Cox, E. One-Step Spray-Dried Polyelectrolyte Microparticles Enhance the Antigen Cross-Presentation Capacity of Porcine Dendritic Cells. *Eur. J. Pharm. Biopharm.* **2012**, 1–9.

(116) De Cock, L. J.; De Koker, S.; De Geest, B. G.; Grooten, J.; Vervaet, C.; Remon, J. P.; Sukhorukov, G. B.; Antipina, M. N.; Cock, L. J. De; Koker, S. De; *et al.* Polymeric Multilayer Capsules in Drug Delivery. *Angew. Chem. Int. Ed. Engl.* **2010**, *49*, 6954–6973.

(117) Dierendonck, M.; Fierens, K.; De Rycke, R.; Lybaert, L.; Maji, S.; Zhang, Z.; Zhang, Q.; Hoogenboom, R.; Lambrecht, B. N.; Grooten, J.; *et al.* Nanoporous Hydrogen Bonded Polymeric Microparticles: Facile and Economic Production of Cross Presentation Promoting Vaccine Carriers. *Adv. Funct. Mater.* **2014**, *24*, 4634–4644.

(118) Yu, A.; Liang, Z.; Caruso, F. Enzyme Multilayer-Modified Porous Membranes as Biocatalysts. *Chem. Mater.* **2005**, *17*, 171–175.

(119) Zhang, S.; Demoustier-champagne, S.; Jonas, A. M. Quantitative Collection and Enzymatic Activity of Glucose Oxidase Nanotubes Fabricated by Templated Layer-by-Layer Assembly. *Biomacromolecules* **2015**, *16*, 2382–2393.

(120) Chen, B.; Jia, Y.; Zhao, J.; Li, H.; Dong, W.; Li, J. Assembled Hemoglobin and Catalase Nanotubes for the Treatment of Oxidative Stress. *J. Phys. Chem. C* **2013**, *117*, 19751–19758.

(121) Komatsu, T. Protein-Based Nanotubes for Biomedical Applications. *Nanoscale* **2012**, *4*, 1910–1918.

(122) Poleunis, C.; Dupont-Gillain, C.; Demoustier-Champagne, S.; Delcorte, A.; Kalaskar, D. Characterisation of Protein Nanotubes by ToF-SIMS Imaging. *Surf. Interface Anal.* **2013**, *45*, 333–337.

(123) Kalaskar, D. M.; Demoustier-champagne, S.; Dupont-Gillain, C. C. Interaction of Preosteoblasts with Surface-Immobilized Collagen-Based Nanotubes. *Colloids Surfaces B Biointerfaces* **2013**, *111*, 134–141.

(124) Qu, X.; Lu, G.; Tsuchida, E.; Komatsu, T. Protein Nanotubes Comprised of an Alternate Layer-by-Layer Assembly Using a Polycation as an Electrostatic Glue. *Chemistry* **2008**, *14*, 10303–10308.

(125) Qu, X.; Komatsu, T. Molecular Capture in Protein Nanotubes. *ACS Nano* **2010**, *4*, 563–573.

(126) Komatsu, T.; Qu, X.; Ihara, H.; Fujihara, M.; Azuma, H.; Ikeda, H. Virus Trap in Human Serum Albumin Nanotube. *J. Am. Chem. Soc.* **2011**, *133*, 3246–3248.

(127) Komatsu, T.; Terada, H.; Kobayashi, N. Protein Nanotubes with an Enzyme Interior Surface. *Chemistry* **2011**, *17*, 1849–1854.

(128) Komatsu, T.; Kobayashi, N. Protein Nanotubes Bearing a Magnetite Surface Exterior. *Polym. Adv. Technol.* **2011**, *22*, 1315–1318.

(129) Yuge, S.; Akiyama, M.; Komatsu, T. An Escherichia Coli Trap in

Human Serum Albumin Microtubes. *Chem. Commun. (Camb).* **2014**, *50*, 9640–9643.

(130) Gilbert, J. B.; O'Brien, J. S.; Suresh, H. S.; Cohen, R. E.; Rubner, M. F.; Brien, J. S. O. Orientation-Specific Attachment of Polymeric Microtubes on Cell Surfaces. *Adv. Mater.* **2013**, *25*, 5948–5952.

(131) Kato, R.; Komatsu, T. Structure and Photocatalytic Activity of Iron Oxide Nanotubes Prepared from Ferritin. *J. Inorg. Organomet. Polym. Mater.* **2012**, *23*, 167–171.

(132) Goto, S.; Amano, Y.; Akiyama, M.; Böttcher, C.; Komatsu, T. Gold Nanoparticle Inclusion into Protein Nanotube as a Layered Wall Component. *Langmuir* **2013**, *29*, 14293–14300.

(133) Nair, B. G.; Nakano, Y.; Ito, Y.; Abe, H. Transmembrane Molecular Transport through Nanopores Formed by Protein Nanotubes. *Chem. Commun.* **2014**, *50*, 602–604.

(134) Shiraishi, Y.; Akiyama, M.; Sato, T.; Hattori, M.; Komatsu, T. Size-Dependent Dextran Loading in Protein Nanotube with an Interior Wall of Concanavalin A. *Polym. Adv. Technol.* **2014**, *25*, 1247–1251.

(135) Gref, R.; Minamitake, Y.; Peracchia, M. T.; Trubetskoy, V.; Torchilin, V.; Langer, R. Biodegradable Long-Circulating Polymeric Nanospheres. *Science* **1994**, *263*, 1600–1603.

(136) Kamaly, N.; Xiao, Z.; Valencia, P. M.; Radovic-Moreno, A. F.; Farokhzad, O. C. Targeted Polymeric Therapeutic Nanoparticles: Design, Development and Clinical Translation. *Chem. Soc. Rev.* **2012**, *41*, 2971–3010.

(137) Rabanel, J.-M.; Hildgen, P.; Banquy, X. Assessment of PEG on Polymeric Particles Surface, a Key Step in Drug Carrier Translation. *J. Control. Release* **2014**, *185C*, 71–87.

(138) Louguet, S.; Kumar, A. C.; Guidolin, N.; Sigaud, G.; Duguet, E.; Lecommandoux, S.; Schatz, C. Control of the PEO Chain Conformation on Nanoparticles by Adsorption of PEO-Block-poly(L-Lysine) Copolymers and Its Significance on Colloidal Stability and Protein Repellency. *Langmuir* **2011**, *27*, 12891–12901.

(139) Banerjee, I.; Pangule, R. C.; Kane, R. S. Antifouling Coatings: Recent Developments in the Design of Surfaces That Prevent Fouling by Proteins, Bacteria, and Marine Organisms. *Adv. Mater.* **2011**, *23*, 690–718.

(140) Schlenoff, J. B. Zwitteration: Coating Surfaces with Zwitterionic Functionality to Reduce Nonspecific Adsorption. *Langmuir* **2014**, *30*, 9625–9636.

(141) Tegoulia, V. A.; Rao, W.; Kalambur, A. T.; Rabolt, J. F.; Cooper, S. L. Surface Properties, Fibrinogen Adsorption, and Cellular Interactions of a Novel Phosphorylcholine-Containing Self-Assembled Monolayer on Gold. *Langmuir* **2001**, *17*, 4396–4404.

(142) Feng, W.; Brash, J. L.; Zhu, S. Non-Biofouling Materials Prepared by Atom Transfer Radical Polymerization Grafting of 2-Methacryloloxyethyl Phosphorylcholine: Separate Effects of Graft Density and Chain Length on Protein Repulsion. *Biomaterials* **2006**, *27*, 847–855.

3 Multilayer LbL assembled films and nanotubes

This chapter is dedicated to fabrication of multilayer assembled flat films and nanotubes of different nature. The growth of the films over flat surfaces are studied and compared with the growth of multilayers inside the nano-sized pores of a membrane. This study provides practical information to fabricate layer-by-layer assembled template synthesized nanotubes and gives further information about their structure.

3.1 Introduction

Anisotropic nano-objects, such as nanowires and nanotubes have recently gained attention especially the field of nanomedicine [1–4]. Nanotubes present several advantages, particularly as nanocarriers for drug delivery applications. First, similar to shell structures, they have interior and exterior surfaces that can each be specifically functionalized. Second, nanotubes possess open ends that are useful for loading and delivery of the therapeutic load. Third, nanotubes have a larger inner volume compared to nanospheres of diameter equal to the nanotube diameter, resulting in possibly higher payloads. Finally, nanotubes have a longer circulation time in vivo and a higher cell internalization rate [5,6].

To fabricate these anisotropic nanotubes with a precise control over their dimension and properties, template synthesis method can be used. This simple yet versatile method is mainly based on depositing desired materials within the pores of a template. A wide range of materials from metals and semiconductors to synthetic and biological polyelectrolytes can be deposited within the pores [7–14]. Layer-by-layer (LbL) assembly is an inexpensive and versatile method based on alternative adsorption of interacting species [15–19]. By combining LbL assembly with template synthesis method, polyelectrolyte based nanotubes with well-controlled and tunable outer diameter, length, composition and wall thickness can be fabricated [20–24].

In this chapter, we focus on the growth of LbL assembled films on flat surfaces as well as fabricating multilayer LbL assembled nanotubes inside the pores of a PC membrane by combining LbL assembly and template synthesis. We study flat multilayers and nanotubes made from a variety of materials including synthetic strong and weak polyelectrolytes as well as natural polyelectrolytes such as proteins and polyaminoacids. Optimal deposition

conditions are investigated for different systems and their growth is monitored. The growth of studied multilayers is compared to similar systems in the literature and the effect of confinement is demonstrated by comparing the thickness of multilayer flat films and multilayers deposited within nano-sized pores of PC membrane. The behavior of nanotubes upon drying on a flat surface is studied and related to their building blocks (Figure 3.1). In the end, more sophisticated nanotubes with nanoparticles capping the tubes ends were fabricated.

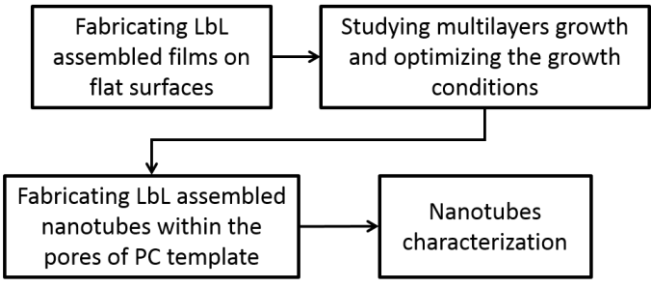

Figure 3.1. A flowchart of the main steps in this chapter.

3.2 Materials and Methods

3.2.1 Materials

Dichloromethane (CH_2Cl_2), sodium chloride (NaCl), 2-(N-morpholino) ethane sulfonic acid (MES) monohydrate, 4-(2- hydroxyethyl) piperazine-1- ethane sulfonic acid (HEPES), Polyallylamine hydrochloride (PAH, M_W: 58 kDa), poly(sodium 4-styrenesulfonate) (PSS, M_W: 70 kDa), polyacrylic acid (PAA, M_W: 100 kDa), poly-L-arginine (PLA, M_W > 70 kDa), ovalbumin (OVA, M_W: 45 kDa) and poly(allylamine hydrochloride) fluorescein isothiocyanate (PAH-FITC, M_W: 15 kDa maximum excitation at 495 nm and a maximum emission at 521 nm) with a monomer to dye ratio (PAH:FITC) of (50:1) were purchased from Sigma-Aldrich. Fluorescent ovalbumin (OVA Alexa Fluor Fluor 488) was purchased from Life Technologies. The Alexa Fluor Fluor 488 fluorophore has a maximum excitation peak at 495 nm and a maximum emission peak at 519 nm. Aluminum oxide (Al_2O_3, alumina) particles with an average particle diameter of 300 nm were provided by BASi. Milli-Q water with 18.2 MΩ.cm resistivity was used in all experiments. All products were used as received.

Sheets of track-etched polycarbonate membranes were provided by It4ip (Louvain-la-Neuve, Belgium, http://www.it4ip.be) with pore diameters of namely 500 nm. The pore diameter of the PC membrane is not exactly as given by the supplier and a 5 – 10 % variation is observed among the pores. All membranes had a thickness of 21 µm and a pore density of 10^8 pores.cm^{-2}. Hydrophilic poly(ethylene terephtalate) (PET) membranes with a pore size of 200 nm, thickness of 23 µm and pore density of about 5.10^8 pores.cm^{-2} were provided by It4ip as well.

Preparation of polyelectrolyte solutions for assembly on flat surfaces

Except for fluorescent-tagged polyelectrolytes, all polyelectrolyte solutions were prepared at 1 mg.mL^{-1} concentration. OVA Alexa Fluor 488 and

PAH-FITC polyelectrolytes were prepared at 0.1 $mg.mL^{-1}$ and 0.5 $mg.mL^{-1}$ concentration respectively. The PAH and PSS solutions used to grow PAH/PSS multilayers were prepared in water containing 150 mM NaCl (or 500 mM NaCl). The PAH and PAA solutions used to grow PAH/PAA multilayers were prepared in 150 mM MES buffer at pH = 5.5. To determine the optimum conditions for the growth of PAH/OVA multilayers, polyelectrolyte solutions were prepared in milli-Q water and the pH was fixed at 5.5, 7 and 8 with no added buffer (pH was adjusted with HCl and NaOH) and 10 mM HEPES buffer at pH = 8 as well. PLA/OVA multilayers were grown in milli-Q water with 150 mM NaCl (or 500 mM NaCl).

3.2.2 Fabrication of LbL assembled flat films

Single-side polished silicon wafers (Si, <100> orientation, ACM) were cleaned for 20 minutes in piranha solution (H_2SO_4 (98%) / H_2O_2 (32%), 1/1 v/v) before use. The wafers were then rinsed abundantly with milli-Q water and dried. The substrates were then immersed in the polycation solution for 5 minutes, followed by three rinsing steps to ensure the removal of loosely attached polyelectrolyte chains on the surface. The rinsing bath for each system was an aqueous solution of same ionic strength and composition as used for the polyelectrolytes. The three step rinsing process consisted of dipping the substrate for 45 seconds in first rinsing bath, 70 seconds in second rinsing bath and 30 seconds in the last rinsing bath. Afterwards, the substrate was dipped in the polyanion solution for 5 minutes, followed by similar rinsing steps. The whole process was cycled until the desired number of layer pairs was obtained. In the end, samples were abundantly rinsed with milli-Q water to eliminate the salt on their surface and were then dried by nitrogen and stored at room temperature.

3.2.3 Fabrication of LbL assembled nanotubes

All polyelectrolyte solutions were prepared at 1 $mg.mL^{-1}$ concentration except for OVA Alexa Fluor 488 and PAH-FITC polyelectrolytes that were prepared at 0.1 $mg.mL^{-1}$ and 0.5 $mg.mL^{-1}$ concentration respectively. PAH/PSS pairs were prepared in water containing 150 mM NaCl at neutral pH. PAH/PAA pairs were prepared in 150 mM MES at pH = 5.5. PAH/OVA pair was fabricated in 10 mM HEPES buffer at pH = 8 and PLA/OVA pair were prepared in milli-Q water containing 150 mM NaCl at neutral pH.

Fabrication of LbL assembled nanotubes by dipping

Multilayer LbL assembled nanotubes were formed within the pores of a nanoporous PC membrane by alternately dipping the membrane in polyelectrolyte solutions for 30 minutes. Since the PC membrane is negatively charged, the membrane is first immersed in polycation solution followed by an intermediate two-step rinsing process (2 minutes each) in two baths of aqueous solution of same ionic strength and composition as used for the polyelectrolytes. Next, the membrane was dipped in polyanion solution and rinsed again. This process was repeated until the desired number of layer pairs (mostly 6) was obtained. In the end, the PC membrane containing nanotubes was rinsed abundantly with milli-Q water.

Fabrication of LbL assembled nanotubes by filtration

The nanoporous PC membrane was placed into a stainless steel syringe holder filtration gasket and 3 mL polycation solution was filtered through the membrane with 1 $mL.min^{-1}$ rate by pressure filtration. Excess polyelectrolyte was washed away by filtering the rinsing solution of same ionic strength and composition as used for the polyelectrolytes was at 1 $mL.min^{-1}$ rate. The PC membrane was taken out and the surface of the membrane was rinsed with the rinsing solution. Afterwards, 3 mL polyanion solution was filtered

through the membrane at 1 mL.min^{-1} rate followed by the same rinsing process. This process was repeated until the desired number of layer pairs (= 3) was achieved. In the end, the PC membrane containing the nanotubes was rinsed abundantly with milli-Q water.

3.2.4 Removing the polyelectrolyte crust from PC membrane

During the LbL process, a polyelectrolyte multilayer crust forms on the top and bottom surfaces of the PC template. This film blocks the access to pores and prevents nanotubes proper release from the membrane and thus, must be removed.

Removal by plasma etching

K1050X Plasma Asher (Quorum Technologies) was used to remove the residual polyelectrolyte crust. Substrates (silicon wafer and PC membrane) with multilayers deposited on their surfaces were put inside the etching chamber followed by introducing vacuum and decreasing the pressure in the chamber. Plasma was produced by 100 watts and the etching process was carried out at desired duration. Samples were then stored at room temperature.

Removal by gentle mechanical rubbing

To remove the polyelectrolyte crust, the top and bottom surfaces of the PC membrane containing nanotubes were gently scrubbed with a cell scraper after each bilayer deposition to eliminate the adherent polyelectrolyte layer. Samples were rinsed abundantly with milli-Q water to eliminate buffer salts, and dried and stored at room temperature.

3.2.5 Capping the nanotubes

Aluminum oxide (Al_2O_3, alumina) particles with an average particle diameter of 300 nm were used for capping the nanotubes. For each case, a little

amount of powder was deposited on velvet polishing disk and some drops of water was added to the powder in order to make slurry. The PC membrane containing nanotubes was rubbed against this slurry for 6 minutes (3 minutes each side) and was then rinsed for 1 min with milli-Q water. Next, the PC membrane was immersed in a 10 ml solution of milli-Q water and sonication was applied for 3 minutes. Afterwards, each face of the PC membrane was rinsed again for about 1 min with milli-Q water. The PC membrane was dried overnight.

3.2.6 Releasing nanotubes from the template

To release the nanotubes from the template, the PC membrane was dissolved in CH_2Cl_2, resulting in a colloidal suspension of nanotubes and dissolved PC in CH_2Cl_2. The nanotubes were then recovered by filtration of this colloidal suspension over a hydrophilic PET membrane. To maximize the removal of remnant PC, fresh CH_2Cl_2 was flushed through the PET filter for several times.

3.2.7 Characterization methods

SEM, STEM observations and EDX analysis

Samples were observed with a field emission scanning electron microscope (JSM-7600F, JEOL Ltd.), equipped with a transmission detector. Energy dispersive X-ray (EDX) spectra were acquired using a detection unit attached to the microscope. SEM measurements were performed at 15 keV for the scanning mode and 30 keV for the scanning transmission mode. To obtain EDX element maps, samples prepared for STEM imaging were scanned at 30 keV for 200 seconds.

For SEM imaging, the CH_2Cl_2 or aqueous suspension of nano-objects was filtered through a PET filter coated with a 20 nm layer of gold. For scanning

transmission electron microscopy (STEM), a few drops of the colloidal suspension (either in water or CH_2Cl_2) was dropped over a carbon-coated copper TEM grid (200 mesh, Electron Microscopy Sciences) and air-dried at room temperature.

Fluorescence microscopy

The suspension of fluorescent-tagged nanotubes was filtered through a PET filter for epi-fluorescence optical microscopy. Fluorescence images were obtained by an Olympus IX2 inverted microscope equipped with a FITC filter set.

Image analysis for determining flattening of nanotubes

The pore diameter of PC membranes as well as the outer diameter of the nanotubes prior and after being in contact with the aqueous solution was determined from SEM and STEM images using ImageJ software (developed by Wayne Rasband, National Institutes of Health, Bethesda, MD). 30 measurements for each system were taken to obtain the average and standard deviation values.

AFM imaging

Atomic force imaging was performed using a Bruker Multimode III A microscope operating in tapping mode. Acquired data were analyzed by Nanoscope Analysis v.1.4 software (Bruker). Images have been flattened using 1^{st} order polynomials in a line-by-line flattening process one after another. Root-mean-square roughness values are reported for 1x1 μm^2 images.

Ellipsometry

The thickness of LbL assembled multilayers on silicon wafers were measured by a spectroscopic ellipsometer (Uvisel, Horiba-Jobin-Yvon) at an incident

angle of 70° in a wavelength range from 300 to 800 nm. Measurements were carried out with the analyzer at +45° and -45° (with respect to the plane of incidence) to compensate for systematic errors (imperfections and residual misalignment of optical components) [25,26].

Ellipsometric data were fitted with DeltaPsi 2 software (Horiba Scientific) in a wavelength range of 550-750 nm based on an optical model consisting of two layers:

1. bulk silicon substrate;
2. homogenous isotropic single layer on top of the substrate.

Since the refractive index of silicon oxide ($n = 1.46$) is close to the refractive index of multilayers ($n \sim 1.45 - 1.55$) at the wavelengths of measurement, the native silicon oxide layer cannot be distinguished from the polyelectrolyte multilayer [26–28]. Therefore, the multilayer thickness was obtained by subtraction of the thickness of the native oxide (determined to be around 1.5 nm from measurements on a bare silicon wafer right after cleaning). The complex index of refraction of Si was taken from tabulated data provided by the manufacturer. The complex index of refraction ($n^* = n + i\,k$) of the multilayer film was modeled by a transparent Cauchy layer with $n(\lambda) = A + {}^{B}/_{\lambda^2} + {}^{C}/_{\lambda^4}$ and $k(\lambda) = 0$ with *A*, *B* and *C* as the fitting parameters. To ensure the validity of the data, the goodness of the fit was verified (minimizing the sum of squares, χ^2) and the refractive index was kept between 1.45 and 1.57 (in the wavelength range of 550 - 750 nm) for all analyzed thin films. All thickness values correspond to an average of five different measurements taken on each sample.

Porometry

The average diameter of PC membrane pores before and after nanotubes construction was measured by gas-flow porometry at room temperature. The air-dried samples are firmly fixed inside the sample holder with an effective section area of 0.138 cm^2. Nitrogen gas was flown upstream with pressure ranging from 4-11 psi. The gas flow rate ($mL.min^{-1}$) downstream from the sample was measured by a flow meter (Agilent). Having this value, one can calculate the average inner diameter of the pores by using relationships based on the Knudsen diffusion and the viscous or Hagen Poiseuille flow relationship as previously reported by our group [29].

The Knudsen diffusion flux, J_{diff} ($mole.m^2s^{-1}$) and viscous flux J_{visc} ($mole.m^2s^{-1}$) are expressed respectively by

$$J_{diff} = \frac{4}{3}\frac{d}{l}\frac{\left(P_{up} - P_{down}\right)}{\sqrt{2\pi MRT}} \quad (3.1)$$

$$J_{visc} = \frac{d^2}{l}\frac{({P_{up}}^2 - {P_{down}}^2)}{64\mu RT} \quad (3.2)$$

where d is the pore diameter (m), l is the thickness of the membrane (m), P_{up} and P_{down} are the pressures (Pa) upstream and downstream from the membrane respectively, M is the gas molar mass ($kg.mol^{-1}$), μ is the dynamic viscosity of the gas ($kg.m^{-1}s^{-1}$), R is the ideal gas constant ($J.K^{-1}mol^{-1}$) and T is the gas temperature (K). The total volume flow rate Φ (m^3s^{-1}) from equations (*3.1* and 3.2 can be expressed by

$$\Phi = SP\frac{RT}{P_{atm}}\left(J_{diff} + J_{visc}\right) \quad (3.3)$$

where S is the effective section area of the membrane (m^2), P_{atm} is the atmospheric pressure (Pa) and P is the transparency of the membrane, defined by

$$P = N\frac{\pi d^2}{4} \quad (3.4)$$

where N is the pore density (m^{-2}). The dried film thickness of nanotubes inside the pores was calculated as half of the difference between the pore diameter of the virgin membrane and the pore diameter after LbL deposition.

3.3 Results and Discussion

Multilayer self-assembled flat films of different polyelectrolytes were fabricated prior to fabrication of nanotubes in order to compare different growth conditions and optimize the assembly condition for each system. The chemical structures of multilayers constructing components used in this study are displayed in Table *3.1*. It was decided to start with polyelectrolytes that are well known in the literature and are commercially available such as poly(allylamine hydrochloride) (PAH), poly(acrylic acid) (PAA) and poly(sodium 4-styrenesulfonate) (PSS). Protein-based systems were also fabricated by using ovalbumin protein as a polyelectrolyte. Biological multilayers were composed of ovalbumin and a polyamino acid (poly-L-arginine) (PLA).

Table 3.1 Chemical Structure and respective pKa and pI of organic components of the studied systems: Synthetic Polyelectrolytes: Poly(allylamine) (PAH), Poly(fluorescein isothiocyanate allylamine hydrochloride) (PAH-FITC), Poly(acrylic acid) (PAA), and Poly(sodium 4-styrenesulfonate) (PSS), Poly(amino acid): Poly-L arginine (PLA), and Protein: Ovalbumin [30] (OVA).

<table>
<tr><td colspan="4">Synthetic polyelectrolytes</td></tr>
<tr><td>PAH
 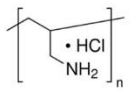
pKa: 9</td><td>PAH-FITC
 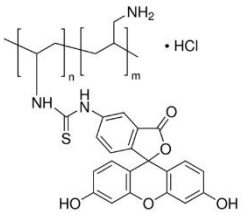 </td><td>PSS
 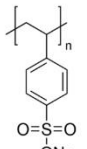 </td><td>PAA
 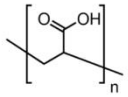
pKa: 4.5</td></tr>
<tr><td colspan="2">Polyamino acid</td><td colspan="2">Protein</td></tr>
<tr><td colspan="2">PLA
 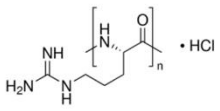
pKa: 12.5</td><td colspan="2">OVA
 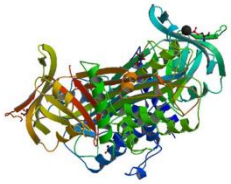
Globular structure
M_w: 45 kDa
pI: 4.5</td></tr>
</table>

3.3.1 Construction of multilayer films on flat surfaces

Multilayer polyelectrolyte films were assembled on top of silicon wafers. The build-up of multilayers was monitored by measuring the dried film thickness by ellipsometry. A summary of all studied systems and their LbL assembly condition is displayed in Table 3.2.

Table 3.2. LbL Assembled multilayer films of different composition, their construction pH value and their deposition condition. (The pH of buffered solutions is measured by a pH meter (with ± 0.1 error) while the pH of NaCl-containing solutions are assumed to be neutral.)

LbL assembled systems	Polycation	polyanion	Construction pH	Construction medium	Amount of buffer or salt
Synthetic	PAH	PSS	Neutral pH	Milli-Q water + NaCl	150 mM NaCl, 500 mM NaCl
	PAH	PAA	5.5 [measured]	MES Buffer	150 mM MES
Protein-based	PAH	OVA	5, 7, 8 [measured]	Milli-Q water	No added buffer or salt
			8 [measured]	HEPES Buffer	10 mM HEPES
	PLA	OVA	Neutral pH	Milli-Q water + NaCl	150 mM NaCl

PAH and PSS are two common synthetic polyelectrolytes and are well known in the literature and commercially available [31–33]. PSS is a strong polyacid while PAH has a pKa = 9. At pH = 5.5, PSS is fully negatively charged and PAH is fully positively charged as well. Therefore, the former acts as a polyanion while the latter is a polycation. Deposition of polyelectrolytes on an oppositely charged surface is based on an ion exchange and entropic gain. Charged polyelectrolytes approach the oppositely charged surface and replace small salt counterions, compensating the surface charge. In parallel,

when counterions are released the system entropy is increased and therefore, there is a gain in entropy [34,35].

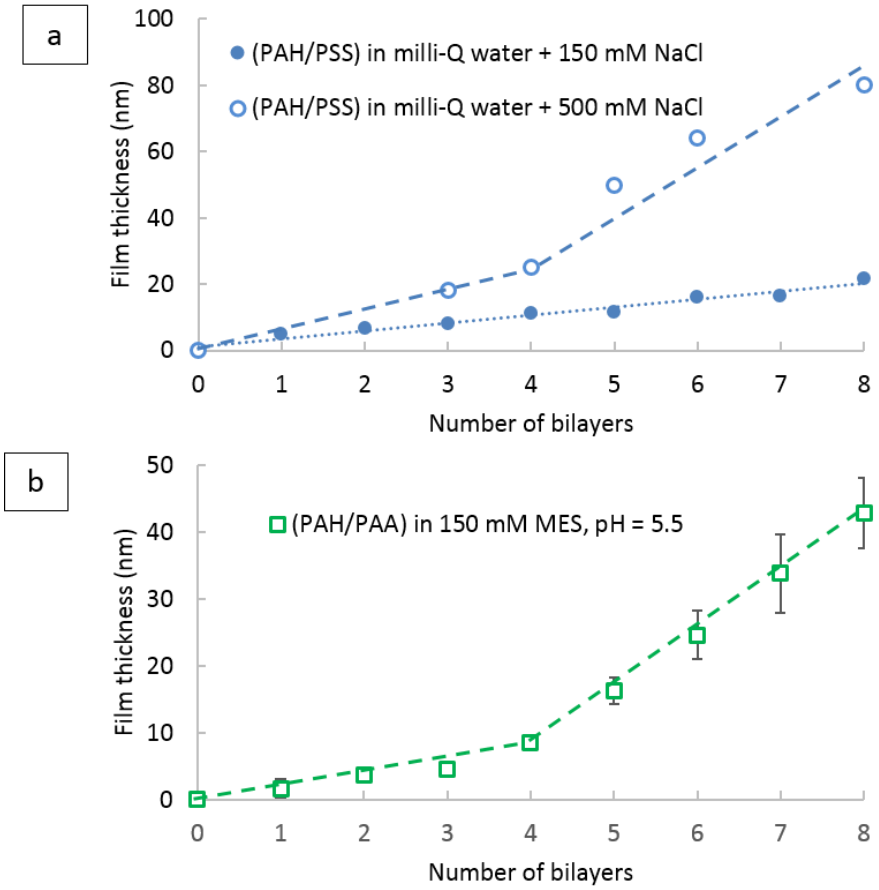

Figure 3.2. Evolution of dried film thickness as a function of the number of cycles, (a) $(PAH/PSS)_n$ deposited on silicon substrates in: (●) milli-Q water + 150 mM NaCl and (○) milli-Q water + 500 mM NaCl. Error bars were less than 4% and thus are not shown, (b) $(PAH/PAA)_n$ deposited on silicon substrates in 150 mM MES buffer. (Dashed and dotted lines are guides to the eye.)

Figure 3.2 demonstrates the evolution of dried film thickness of assembled multilayers at each bilayer deposition. It is observed that the growth of (PAH/PSS) multilayer films strongly depends to the ionic strength of the

deposition solution. The growth rate is rather low when the deposition is carried out in milli-Q water containing 150 mM NaCl. By increasing the amount of NaCl salt to 500 mM the growth rate is increased. The effect of salt concentration and ionic strength on the growth of LbL assembled polyelectrolyte multilayers has been well discussed in literature (see Chapter.2.1.). Briefly, added salt screens the charges along the polymer chain. Therefore, the polymer chains are more coiled with increasing the salt concentration, leading to the formation of thicker and rougher films [34–36].

The growth of (PAH/PSS) multilayers in 500 mM NaCl solution can be divided in two-steps linear growth. The first segment ($0 \leq n \leq 4$) has a less steep slope while the second segment ($4 \leq n \leq 8$) has a higher slope. This two-step linear-like growth was previously observed in our group [37]. Ladam et al. suggested that the slower growth at the early stages of the multilayer build-up can be related to the influence of the support [32]. During the adsorption of the very first bilayers, the macromolecules have strong interaction with the substrate surface and thus, will adopt a flatter conformation [17,38]. The growth of (PAH/PAA) multilayers can also be divided in two segments. However, to have a full understanding of the multilayers growth kinetics, a larger number of bilayers must be deposited on the surface and the resulting film must be characterized by different techniques as previously done by many groups. Here, we only aimed to show that (PAH/PSS) and (PAH/PAA) multilayers can be assembled on flat substrates at the chosen conditions.

To construct multilayers with biological components, PAH and OVA were chosen as polyelectrolyte building blocks. This system holds a special interest since the model antigen protein (OVA) is included in the structure of the multilayer and PAH provides the possibility of further functionalization due

to presence of primary amine side chains. Such system has not been studied previously. Therefore, the build-up of (PAH/OVA) multilayers was studied in solutions of different pH and ionic strength.

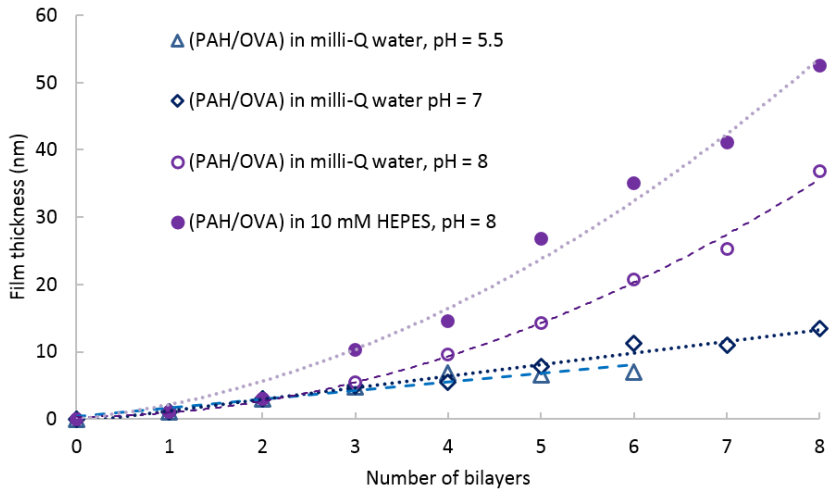

Figure 3.3. Evolution of dried film thickness as a function of the number of cycles $(PAH/OVA)_n$ deposited on silicon substrates in (Δ) milli-Q water with fixed pH = 5.5, (◊) milli-Q water with fixed pH = 7, (○) milli-Q water with fixed pH = 8, (●) 10 mM HEPES buffer at pH = 8. Error bars were less than 4% and thus are not shown. (Dashed and dotted lines are guides to the eyes.)

Figure 3.3 shows the growth of (PAH/OVA) multilayers at different conditions. The build-up of (PAH/OVA) was first studied in milli-Q water at different fixed pHs with no added buffer. OVA has an isoelectric point = 4.5, therefore, at pHs higher than 4.5, it has an excess negative charge and interacts electrostatically with PAH. However, it is observed that at pHs = 5 and 7, there is a very low deposition hardly exceeding 10 nm after 6 bilayer deposition. At pH = 8, the thickness of the multilayers increases. Much thicker multilayers are obtained when the deposition is carried out at 10 mM HEPES buffer solution. We cannot comment whether the growth of

(PAH/OVA) multilayers is linear or non-linear. For that aim, a larger number of bilayers should have been assembled. Nevertheless, we have shown that (PAH/OVA) multilayers can be grown at pH = 8 and by conducting the assembly in 10 mM HEPES buffer at pH = 8, thicker multilayers can be obtained while the pH is more controlled due to the presence of buffer.

Biological multilayers composed of PLA and OVA were assembled in milli-Q water with 150 mM NaCl at neutral pH. It is preferable to construct (PLA/OVA) multilayers in milli-Q water because, PLA aggregates in PBS buffer (with a buffer concentration higher than 10 mM) due to interactions between arginine and phosphate groups.

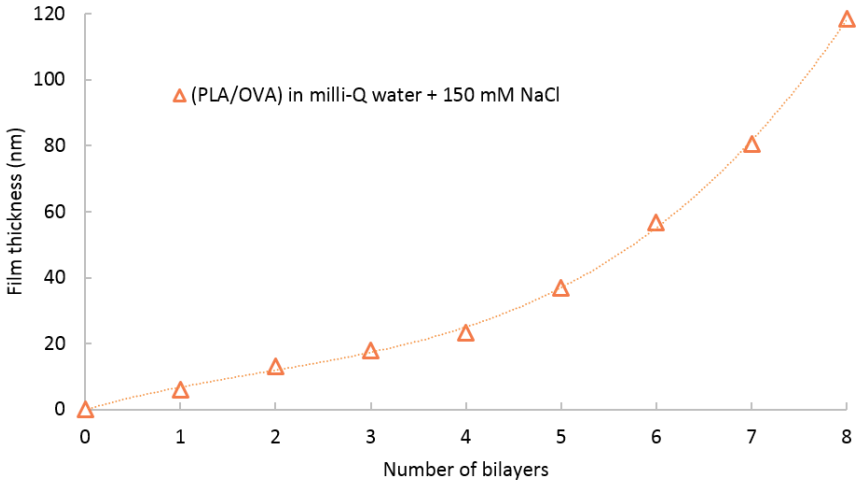

Figure 3.4. Evolution of dried film thickness as a function of the number of cycles deposited on silicon substrates for (**Δ**) (PLA/OVA) in milli-Q water with 150 mM NaCl. Error bars were less than 4% and thus are not shown. (Dotted line is a guide to the eyes.)

The growth of (PLA/OVA) multilayers is shown in *Figure 3.4*. (PLA/OVA) multilayers have the highest thickness amongst all studied systems. The

effect of ionic strength on the growth of (PLA/OVA) multilayers was investigated by AFM (Figure 3.5).

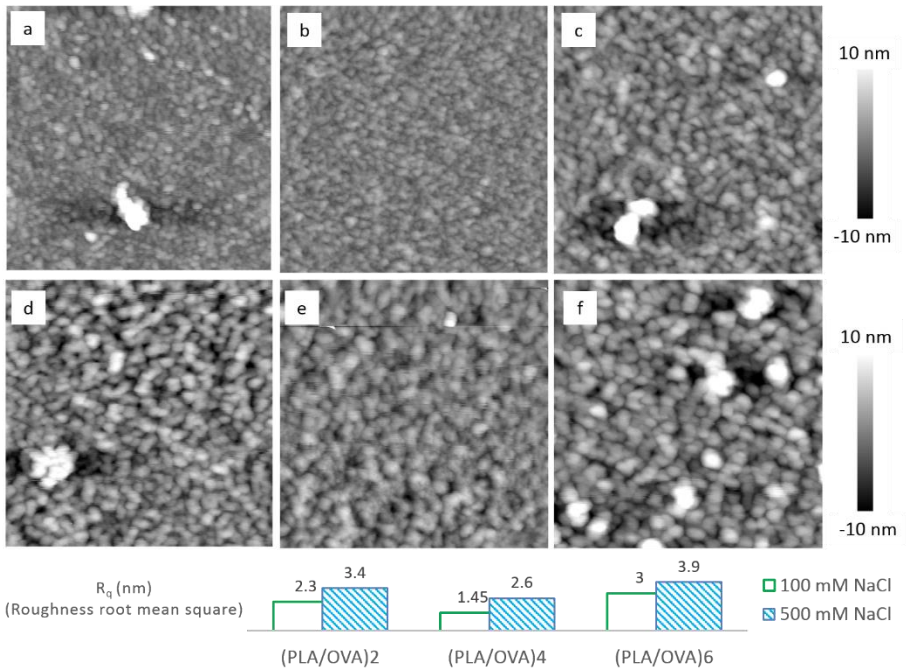

Figure 3.5. AFM height image of (PLA/OVA) multilayers deposited on a surface of a flat silicon wafer at different number of bilayers and in different deposition mediums. (a-c) 2, 4, 6 bilayers in milli-Q water with 100 mM NaCl, (d-f) 2, 4, 6 bilayers in milli-Q water with 500 mM NaCl. Z-scale is 20 nm for all images. The bar chart beneath the images shows root-mean-square roughness (R_q) values calculated from the images. (The analyzed surface of each sample is 1 μm^2).

As observed in Figure 3.5, multilayer assembled films form small island-shaped patches on the surface. By increasing the number of bilayers (Figure *3.5*.a-c), these islands grow in size as well. At the same time, by increasing the amount of salt in deposition solution, the ionic strength is increased and the islands grow bigger. Multilayers deposited from high ionic-strength solutions have a higher root-mean-square roughness (R_q) values. As

mentioned before, this is probably due to changes in the chains conformation as the amount of salt in the solution is increased [26,36].

Since the objective of this research was to prepare nanotubes suitable for biological applications, it was decided to keep the ionic strength of all future deposition solutions close to physiological value (150 mM). The only exception was for (PAH/OVA) system, which was assembled at a lower ionic strength (10 mM HEPES buffer) since an odd aggregate formation was observed when HEPES buffer of higher ionic strength was used for (PAH/OVA) system.

3.3.2 Construction of multilayer nanotubes

Multilayer nanotubes were constructed by combining LbL assembly and template synthesis method. Track-etched nanoporous PC membranes are chosen as templates and the LbL assembly is carried out inside the pores of the PC membranes. The deposition process can be carried out in two different ways. Either the polyelectrolyte solution is filtered through the pores by pressure filtration or the membrane is dipped in polyelectrolyte solutions and the polyelectrolyte molecules diffuse through the pores. By injecting the polyelectrolytes through the pores, molecules are forced to come in contact and will interact electrostatically with each other forming a polyelectrolyte complex inside the pores. During the rinsing step, when the rinsing solution is injected through the pores, un-bounded polyelectrolytes are washed off and removed. For all studied systems, after 3 bilayers, the pores were clogged and no more matter could be injected through the pores. In contrast, when assembly is carried-out by dipping the membrane in polyelectrolyte solutions, a larger number of bilayers can be deposited inside the pores (6 bilayers). The PC sacrificial template was dissolved in CH_2Cl_2 to characterize the resulting nano-objects by epi-fluorescence microscopy and

electron microscopy, resulting in an organic suspension of PC and released nanotubes. Nanotubes were then simply collected by filtration of this suspension over a polyethylene terephthalate (PET) membrane. One can further flush a large amount of solvent through the filter to maximize the PC removal.

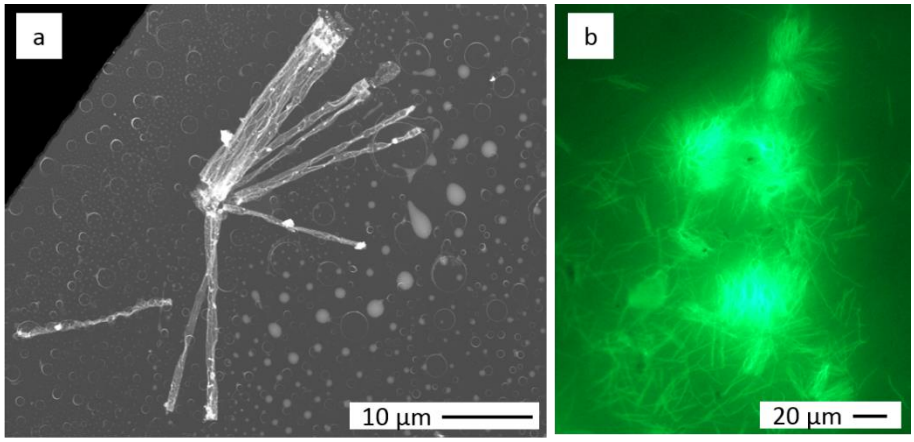

Figure 3.6. (a) STEM and (b) epi-fluorescence microscopy images of $(PLA/OVA\ Alexa\ Fluor\ 488)_6$ nanotubes deposited over a TEM grid or filtered over a PET filter respectively.

Figure 3.6.a and Figure 3.6.b show $(PLA/OVA\ Alexa\ Fluor\ 488)_6$ nanotubes released from a PC membrane. In both images, bundle of nanotubes are observed. These nanotubes are attached to each other due to the presence of a crust layer. Indeed, during the LbL process, a PE multilayer crust forms on the top and bottom surfaces of the PC template. This film blocks the access to nanopores and prevents future dispersion of nanotubes as observed in Figure 3.6.

There have been different approaches for the removal of this crust. One option is to remove this layer by plasma etching [42–44].

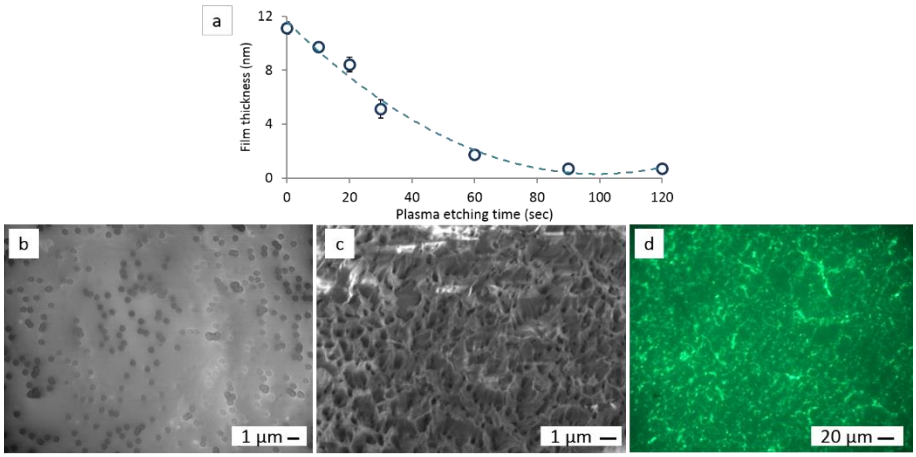

Figure 3.7. Effect of plasma etching on polyelectrolyte crust removal, (a) Monitoring the removal of 12 nm $(PAH/PSS)_6$ multilayers from a flat silicon wafer by plasma etching at different time periods. Dashed line is to guide the eyes, (b) SEM images of PC membrane containing $(PLA/OVA\ Alexa\ Fluor\ 488)_6$ nanotubes before plasma etching, (c) after 60 seconds of plasma etching, (d) Epi-fluorescence microscopy image of extracted $(PLA/OVA\ Alexa\ Fluor\ 488)_6$ nanotubes from the plasma etched PC membrane, filtered on a PET filter.

The effectiveness of plasma etching for removing deposited layers was investigated by monitoring the thickness of 6 bilayers of (PAH/PSS) deposited over a Si wafer after different etching times (Figure 3.7.a). According to Figure *3.7.*a, the whole deposited matter is removed after 2 minutes of plasma etching. When the PC membrane containing nanotubes is plasma etched, the surface of the membrane is highly disturbed and becomes rougher (Figure 3.7.b and Figure 3.7.c).

Figure 3.7.d is an epi-fluorescence image of $(PLA/OVA\ Alexa\ Fluor\ 488)_6$ nanotubes released from a plasma etched PC membrane. Nanotubes are deformed and have lost their tubular shape. It is probable that nanotubes inside the membrane pores were damaged and became more fragile during plasma etching process. Upon releasing the nanotubes by dissolving the

membrane and filtering the obtained suspension over a PET filter, damaged nanotubes could not hold their tubular shape and were deformed. Therefore, an alternative crust removal method must be used. Roy et al. and Ramirez Wong et al. suggested removing this crust by rubbing the surface with a cotton swab immersed in a basic aqueous solution (NaOH, pH = 12) of high ionic strength (NaCl, 3 M) and followed by abundant rinsing of the membrane. By using such solution, deposited multilayers will swell and be disturbed due to combination of two effects. First, at pH = 12, the positive charge density of PAH is strongly decreased and second, by using high salt concentration, the electrostatic repulsion of charges along the polyelectrolyte chains is reduced [29,37]. Although effective for certain polyelectrolyte combinations, the pH of this solution must be adjusted depending on the nature of assembled multilayers and the amount of salt must be adjusted, so that it will not disturb the nanotubes. For instance, for (PLA/OVA) nanotubes, using an acidic solution of high ionic strength (pH = 3) is more effective compared to basic (pH = 12) solution, since at pH = 3, both PLA and OVA are positively charged and therefore, repel each other much more. Moreover, we observed that using high amount of salt affected the nanotubes and caused some deformation in their structure. It was essential to opt for a milder approach of crust removal. It was observed that by simply mechanically rubbing the surface of the membrane with the rinsing solution after each bilayer deposition, the crust is adequately removed. Although this means more labor during the LbL process, a full crust removal is achieved without deforming nanotubes; this method was thus selected and used for any nanotubes fabrication in this study.

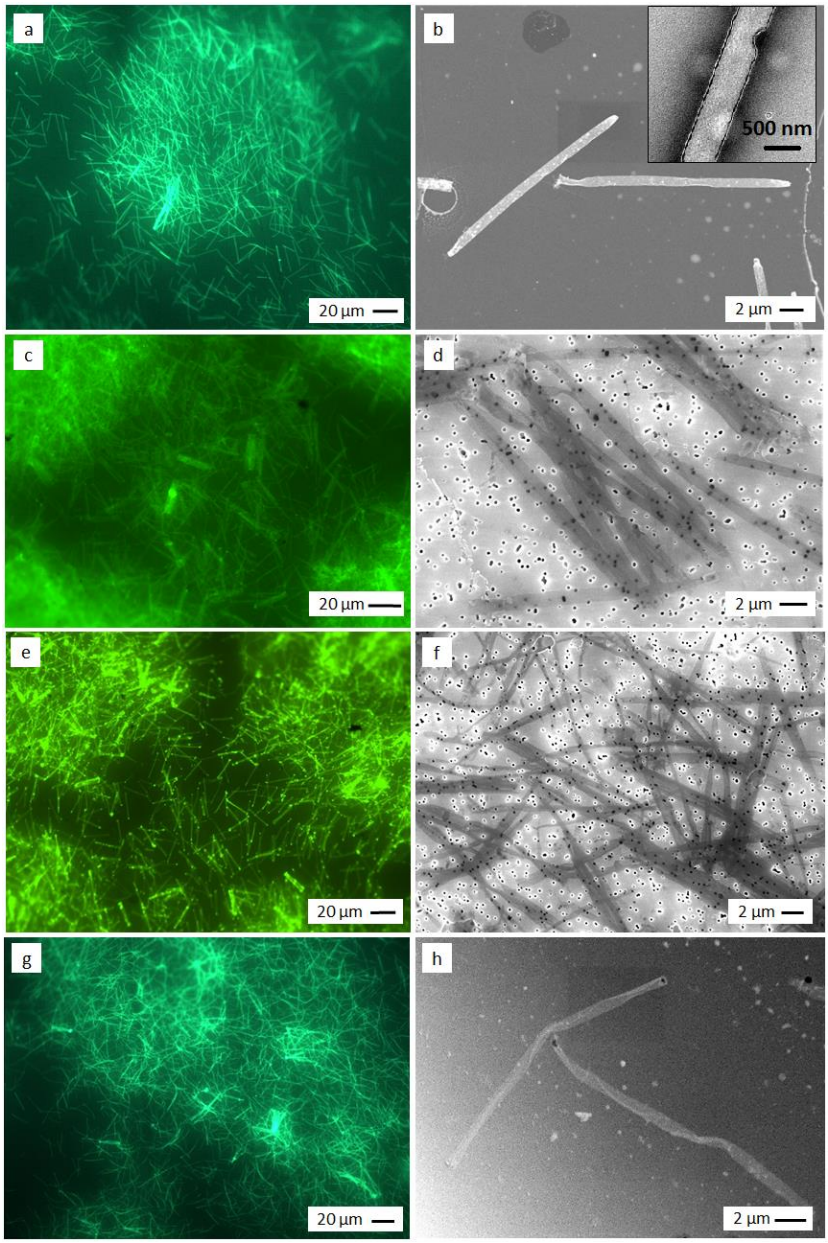

Figure 3.8. Left column: (a,c,e,g) epi-fluorescence microscopy images of nanotubes filtered over a PET filter, right column: (b,h) STEM and (d,f) SEM images of nanotubes on a TEM grid or on a PET filter respectively. (a, b) (PAH-FITC/PSS)$_6$, (c, d) (PAH-FITC/PAA)$_6$, (e , f) (PAH/ OVA Alexa Fluor 488)$_6$, (g, h) (PLA/ OVA Alexa Fluor 488)$_6$. The inset in (b) is a TEM image of a (PAH-FITC/PSS)$_6$ nanotube. (The acquisition conditions of fluorescence images were different and thus, the intensity of images could not be compared.)

Figure *3.8* shows typical STEM, SEM and epi-fluorescence images of LbL assembled nanotubes: synthetic strong polyelectrolyte (PAH/PSS), synthetic weak polyelectrolyte (PAH/PAA), protein-based (PAH/OVA) and biological (PLA/OVA) nanotubes. Nanotubes were constructed in a PC membrane with, namely, 500 nm pore diameter and 21 μm thickness, yielding nanotubes with an aspect ratio of $\sim$ 45. The inset image in Figure 3.8.b shows the hollow structure of $(PAH\text{-}FITC/PSS)_6$ nanotubes. Polyelectrolyte nanotubes are soft and prone to breakage and might be broken during the template removal process. We should also mention that the PC templates may contain a few interconnected pores through the membrane, resulting in shorter forked nanotubes. An interesting point is the high fluorescence intensity at the ends of the nanotubes for some cases, suggesting that the nanotubes are clogged at their ends with fluorescent polyelectrolyte. However, gas-flow porometry proved that nanotubes are hollow. Therefore, one can deduce that although there is a higher amount of polyelectrolytes at the ends of the tubes, they are not clogged. The higher fluorescent intensity at the ends of those tubes is most probably due to the presence of a small amount of residual crust at the tubes ends.

Since in some cases, nanotubes were observed to flatten when deposited on the grids for STEM characterization, this method was not appropriate to provide reliable values for the inner diameter from the imaged nanotubes. Hence, gas-flow porometry was used to determine the average diameter of PC membranes before and after nanotube construction. Half the difference between these two values gives the dry wall thickness (d_{wall}) reported in Table 3.3.

Table 3.3. Summary of the dimensions (outer diameter and dry wall thickness) of the studied nanotubes. (The membrane pore diameter D_{pore} is 440 ± 40 nm for all cases).

Type of system	Nanotubes outer diameter D_{tube} (nm)	Dry wall thickness d_{wall} (nm)		D_{tube}/D_{pore}
		3 bilayers LbL by filtration	6 bilayers LbL by dipping	
PAH/PSS	570 ± 35	35	45	1.29 ± 0.22
PAH/PAA	530 ± 81	23	40	1.17 ± 0.18
PAH/OVA	781 ± 84	60	60	1.77 ± 0.4
PLA/OVA	736 ± 61	60	63	1.67 ± 0.32

It should be taken into account that porometry measurements are operated on dried samples and that the drying process might cause some shrinking of nanotube walls. STEM images of all nanotubes were analyzed to determine the outer diameter variation among the nanotubes (D_{tube}). The ratio between the outer diameter of dried tubes D_{tube} and the diameter of the pores of the template, D_{pore} (both measured from STEM or SEM images) were calculated for all systems (Table 3.3) to evaluate the shrinking or flattening behavior of tubes after being extracted from the template and deposited over a flat filter surface. D_{tube}/D_{pore} values show that protein-based LbL assembled nanotubes (PAH/OVA) and (PLA/OVA) have the highest tendency to flatten when deposited and dried over a flat surface, indicating a higher softness.

Comparing the dry wall thickness of nanotubes deposited either by pressure-filtration (3 cycles) or by dipping (6 cycles), the final thickness value is very close. As mentioned before, after 3 bilayers deposition via pressure-filtration, pores are clogged and no more matter can be deposited inside the

pores. In contrast, deposition can be cycled many times when assembly is carried out by dipping.

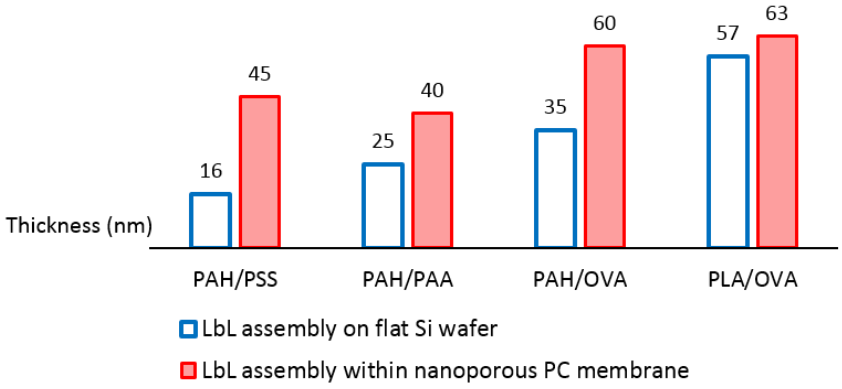

Figure 3.9. Comparison of the dried film thickness of (left columns) LbL multilayers assembled on silicon wafer with (right columns) LbL assembled nanotubes within the pores of a PC membrane. (6 bilayers are assembled for each system.)

Figure *3.9* compares the dried film thickness of multilayers assembled over a flat silicon wafer and multilayers assembled in nanotubes. Although the number of bilayers is equal, multilayers assembled in nanotubes have a higher thickness compared to flat films. Indeed, confinement in nanoporous membrane results in the formation of thicker multilayers [26,45–48]. As discussed in Chapter 2.3., this is mainly due to the existence of two growth regimes during the assembly of multilayers in nanotubes. During the first regime, polyelectrolyte chains enter the pores and are adsorbed on the pore walls. By increasing the number of deposited bilayers, polyelectrolyte chains start to entangle across the pores and thus, the second regime begins in which, polyelectrolytes diffusion becomes a limiting factor. The interconnection of polyelectrolytes across the pores will eventually lead to formation of a dense gel within the pores that may clog the pores and prevents any further

deposition. This difference in thickness is more pronounced for synthetic polyelectrolyte pairs (PAH/PSS) and (PAH/PAA) and less for biological systems (PAH/OVA) and (PLA/OVA). This could probably be due to the more compact globular form of OVA protein.

Alem et al. investigated multilayers build-up in a nanoporous PC by pressure-filtration and proposed that polyelectrolyte chains entangle during their passage through the pores and because of a locally increased concentration, they are no longer in the dilute regime. They pile-up in the pores and form a dense gel that almost fills the pore in the wet-state [26]. It must be noted that synthetic and biological polyelectrolytes are highly hydrophilic and have a swelling ratio (thickness at swollen state/ thickness at dried state) of 1.2 - 4.0 [31,35,49–51]. Upon drying, the dense gel inside the pores loses its water content, shrinks and thus a hollow tube is formed inside the pores. Roy et al. investigated the growth of (PAH/PSS) multilayers inside a nanoporous PC membrane by dipping and suggested the presence of two regimes. During the first regime, a linear growth is observed while in the second regime the growth rate is strongly reduced. During this second regime, adsorbed polyelectrolytes start to interconnect across the pores and again a gel is formed inside the pores. As a result, diffusion becomes the controlling factor in multilayers formation and the growth is slowed down.

For the systems studied in this chapter, the dried wall thickness (d_{wall}) of nanotubes is very close for the two methods, despite using different number of deposition cycles. This might be associated to the formation of a dense polyelectrolyte gel that would block the pores in the wet-state after 3 bilayers deposition by filtration and 6 bilayers deposition by dipping. Upon drying, this gel-like structure should shrink and hollow nanotubes of similar wall thickness would be formed.

3.3.3 Capping nanotubes with nanoparticles

Capping the ends of the nanotubes could have a particular interest for further applications [52]. Here, it was decided to benefit from electrostatic interactions between nanoparticles and the nanotubes. The nanoparticle size should be in the range of the hollow nanotubes inner diameter and to limit their interactions with nanotubes surface, the capping was carried out when nanotubes are still inside the PC membrane.

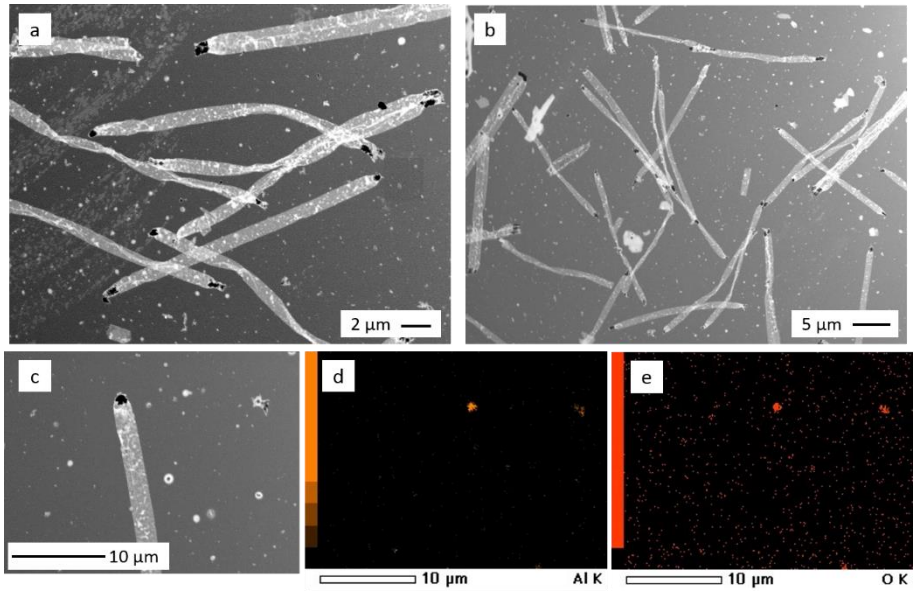

Figure 3.10. (a,b,c) STEM images of $(PLA/OVA)_6$ nanotubes capped with Al_2O_3 nanoparticles, (d,e) element map of Al and O respectively obtained by EDX analysis of (c).

To this aim, 300 nm alumina particles were gently rubbed over the surface of a PC membrane containing $(PLA/OVA)_6$ nanotubes followed by a short sonication and rinsing step. The PC membranes were then dissolved in dichloromethane and the tubes were observed by STEM (Figure 3.10 a, b). Figure 3.10.b shows that the length of the tubes still corresponds to the

thickness of the PC membrane, which means rubbing the PC surface with nanoparticles does not reduce the length of the tubes. Element maps obtained from energy-dispersive X-ray spectroscopy (EDX) measurements showed that alumina particles were attached to the ends of the tubes and cap the tubes ends (Figure 3.10.c-e). The number of capped nanotubes was counted in at least 20 images and it was observed that 80 % of nanotubes were successfully capped.

One can interpret the results by the fact that there are some interactions between the tubes and the particles. Indeed, alumina particles are negatively charged and the ends of the tubes carry a mix of positive and negative charges due to the nature of the multilayer.

3.4 Conclusion

LbL assembled multilayer flat films and nanotubes were fabricated either by LbL deposition over a flat substrate or combining LbL assembly with template synthesis method. The studied systems have different chemistry ranging from strong polyelectrolytes to weak polyelectrolytes and biological macromolecules. Optimal deposition conditions are investigated for each system and obtained multilayers are characterized by different methods. Linear growth is observed for synthetic pairs while non-linear growth is observed for systems containing proteins and polyaminoacids. The salt concentration affects the thickness of the layers and results in thicker and rougher multilayers.

Nanotubes have a tendency to flatten when deposited and dried over a flat surface. Biological nanotubes had the highest flattening amongst other studied systems indicating higher softness. The dry wall thickness of the nanotubes was measured by porometry, suggesting that during both deposition methods (3 bilayers of deposition by filtration or 6 bilayers of

deposition by dipping) the growth was stopped due to the formation of a dense gel inside the pores. When such a dense gel is formed due to the interconnection of chains across the pores, diffusion becomes the controlling parameter in growth and the growth rate is drastically slowed down. Upon drying, highly hydrated nanotubes lose their water and hollow nanotubes are formed inside the pores.

The ends of the tubes can be further manipulated. Here, we demonstrated capping by alumina nanoparticles due to electrostatic interactions between negatively charged alumina nanoparticles and the mixed-charged ends of the nanotubes.

Now that we mastered the process of fabricating multilayer assembled nanotubes by combining LbL assembly with template synthesis, we can move on with preparing functional nanotubes carrying a specific therapeutic cargo for biomedical applications.

3.5 Bibliography

(1) Geng, Y.; Dalhaimer, P.; Cai, S.; Tsai, R.; Tewari, M.; Minko, T.; Discher, D. E. Shape Effects of Filaments versus Spherical Particles in Flow and Drug Delivery. *Nat. Nanotechnol.* **2007**, *2*, 249–255.

(2) Buyukserin, F.; Medley, C. D.; Mota, M. O.; Kececi, K.; Rogers, R. R.; Tan, W.; Martin, C. R. Antibody-Functionalized Nano Test Tubes Target Breast Cancer Cells. *Nanomedicine (Lond).* **2008**, *3*, 283–292.

(3) Chen, B.; Jia, Y.; Zhao, J.; Li, H.; Dong, W.; Li, J. Assembled Hemoglobin and Catalase Nanotubes for the Treatment of Oxidative Stress. *J. Phys. Chem. C* **2013**, *117*, 19751–19758.

(4) Yuge, S.; Akiyama, M.; Komatsu, T. An Escherichia Coli Trap in Human Serum Albumin Microtubes. *Chem. Commun. (Camb).* **2014**, *50*, 9640–9643.

(5) Cepak, V. M.; Martin, C. R. Preparation of Polymeric Micro- and Nanostructures Using a Template-Based Deposition Method. *Chem. Mater.* **1999**, *11*, 1363–1367.

(6) Gratton, S. E. A.; Ropp, P. A.; Pohlhaus, P. D.; Luft, J. C.; Madden, V. J.; Napier, M. E.; DeSimone, J. M. The Effect of Particle Design on Cellular Internalization Pathways. *Proc. Natl. Acad. Sci. U. S. A.* **2008**, *105*, 11613–11618.

(7) Ai, S.; He, Q.; Tao, C.; Zheng, S.; Li, J. Conductive Polypyrrole and Poly(allylamine Hydrochloride) Nanotubes Fabricated with Layer-by-Layer Assembly. *Macromol. Rapid Commun.* **2005**, *26*, 1965–1969.

(8) Yabu, H.; Hirai, Y.; Shimomura, M. Electroless Plating of Honeycomb and Pincushion Polymer Films Prepared by Self-Organization. *Langmuir* **2006**, *22*, 9760–9764.

(9) Landoulsi, J.; Roy, C. J. C. J.; Dupont-Gillain, C.; Demoustier-Champagne, S. Synthesis of Collagen Nanotubes with Highly Regular Dimensions through Membrane-Templated Layer-by-Layer Assembly. *Biomacromolecules* **2009**, *10*, 1021–1024.

(10) Callegari, V.; Gence, L.; Melinte, S.; Demoustier-Champagne, S. Electrochemically Template-Grown Multi-Segmented Gold-Conducting Polymer Nanowires with Tunable Electronic Behavior. *Chem. Mater.* **2009**, *21*, 4241–4247.

(11) Callegari, V.; Demoustier-Champagne, S. Using the Hard Templating Method for the Synthesis of Metal-Conducting Polymer Multi-Segmented Nanowires. *Macromol. Rapid Commun.* **2011**, *32*, 25–34.

(12) Callegari, V.; Demoustier-Champagne, S. Interfacing Conjugated Polymers with Magnetic Nanowires. *ACS Appl. Mater. Interfaces* **2010**, *2*, 1369–1376.

(13) Perry, J. L.; Martin, C. R.; Stewart, J. D. Drug-Delivery Strategies by Using Template-Synthesized Nanotubes. *Chemistry* **2011**, *17*, 6296–6302.

(14) Roy, C. J.; Chorine, N.; Geest, B. De; Smedt, S. De; Jonas, A. M.; Demoustier-champagne, S. Highly Versatile Approach for Preparing Hybrid Multisegmented Nanotubes and Nanowires with Tailored Properties. *Chem. Mater.* **2012**, *24*, 1562–1567.

(15) Decher, G.; Hong, J. D.; Schmitt, J. Buildup of Ultrathin Multilayer Films by a Self-Assembly Process: III. Consecutively Alternating Adsorption of Anionic and Cationic Polyelectrolytes on Charged Surfaces. *Thin Solid Films* **1992**, *210/211*, 831–835.

(16) Decher, G. Fuzzy Nanoassemblies: Toward Layered Polymeric Multicomposites. *Science* **1997**, *277*, 1232–1237.

(17) Guyomard, A.; Muller, G.; Glinel, K. Buildup of Multilayers Based on

Amphiphilic Polyelectrolytes. *Macromolecules* **2005**, *38*, 5737–5742.

(18) Boudou, B. T.; Crouzier, T.; Ren, K.; Blin, G.; Picart, C.; Boudou, T. Multiple Functionalities of Polyelectrolyte Multilayer Films: New Biomedical Applications. *Adv. Mater.* **2010**, *22*, 441–467.

(19) Matsusaki, M.; Ajiro, H.; Kida, T.; Serizawa, T.; Akashi, M. Layer-by-Layer Assembly through Weak Interactions and Their Biomedical Applications. *Adv. Mater.* **2012**, *24*, 454–474.

(20) Tian, Y.; He, Q.; Cui, Y.; Li, J. Fabrication of Protein Nanotubes Based on Layer-by-Layer Assembly. *Biomacromolecules* **2006**, *7*, 2539–2542.

(21) Lu, G.; Komatsu, T.; Tsuchida, E. Artificial Hemoprotein Nanotubes. *Chem. Commun.* **2007**, 2980–2982.

(22) Perry, J. L.; Guo, P.; Johnson, S. K.; Mukaibo, H.; Stewart, J. D.; Martin, C. R. Fabrication of Biodegradable Nano Test Tubes by Template Synthesis. *Nanomedicine (Lond).* **2010**, *5*, 1151–1160.

(23) Kohler, D.; Schneider, M.; Krüger, M.; Lehr, C.-M.; Möhwald, H.; Wang, D. Template-Assisted Polyelectrolyte Encapsulation of Nanoparticles into Dispersible, Hierarchically Nanostructured Microfibers. *Adv. Mater.* **2011**, *23*, 1376–1379.

(24) Silva, J. M.; Duarte, A. R. C.; Custódio, C. A.; Sher, P.; Neto, A. I.; Pinho, A. C. M.; Fonseca, J.; Reis, R. L.; Mano, J. F. Nanostructured Hollow Tubes Based on Chitosan and Alginate Multilayers. *Adv. Healthc. Mater.* **2014**, *3*, 433–440.

(25) Kleim, R.; Kuntzler, L.; Ghemmaz, A. El. Systematic Errors in Rotating-Compensator Ellipsometry. *J. Opt. Soc. Am. A* **1994**, *11*, 2550.

(26) Alem, H.; Blondeau, F.; Glinel, K.; Demoustier-champagne, S.; Jonas,

A. M. Layer-by-Layer Assembly of Polyelectrolytes in Nanopores. *Macromolecules* **2007**, *40*, 3366–3372.

(27) Schwarz, S.; Eichhorn, K.-J.; Wischerhoff, E.; Laschewsky, A. Polyelectrolyte Adsorption onto Planar Surfaces: A Study by Streaming Potential and Ellipsometry Measurements. *Colloids Surfaces A Physicochem. Eng. Asp.* **1999**, *159*, 491–501.

(28) Dekeyser, C. M.; Buron, C. C.; Derclaye, S. R.; Jonas, A. M.; Rouxhet, P. G. Degradation of Bare and Silanized Silicon Wafer Surfaces by Constituents of Biological Fluids. *J. Colloid Interface Sci.* **2012**, *378*, 77–82.

(29) Roy, C. J.; Dupont-Gillain, C.; Demoustier-Champagne, S.; Jonas, a M.; Landoulsi, J. Growth Mechanism of Confined Polyelectrolyte Multilayers in Nanoporous Templates. *Langmuir* **2010**, *26*, 3350–3355.

(30) Stein, P.E., Leslie, A.G., Finch, J.T., Carrell, R. W. E.; Leslie, A. G.; Finch, J. T.; Carrell, R. W. Crystal Structure of Uncleaved Ovalbumin at 1.95 Å Resolution. *J.Mol.Biol.* **1991**, *221*, 941–959.

(31) Lösche, M.; Schmitt, J.; Decher, G.; Bouwman, W. G.; Kjaer, K.; Lo, M. Detailed Structure of Molecularly Thin Polyelectrolyte Multilayer Films on Solid Substrates as Revealed by Neutron Reflectometry. *Macromolecules* **1998**, *31*, 8893–8906.

(32) Ladam, G.; Schaad, P.; Voegel, J. C.; Schaaf, P.; Decher, G.; Europe, Ä.; Cuisinier, F. In Situ Determination of the Structural Properties of Initially Deposited Polyelectrolyte Multilayers. *Langmuir* **2000**, *16*, 1249–1255.

(33) He, Q.; Cui, Y.; Ai, S.; Tian, Y.; Li, J. Self-Assembly of Composite Nanotubes and Their Applications. *Curr. Opin. Colloid Interface Sci.* **2009**, *14*, 115–125.

(34) Dubas, S. T.; Schlenoff, J. B. Factors Controlling the Growth of Polyelectrolyte Multilayers. *Macromolecules* **1999**, *32*, 8153–8160.

(35) Von Klitzing, R. v. Internal Structure of Polyelectrolyte Multilayer Assemblies. *Phys. Chem. Chem. Phys.* **2006**, *8*, 5012–5033.

(36) Bertrand, P.; Jonas, A.; Laschewsky, A.; Legras, R. Ultrathin Polymer Coatings by Complexation of Polyelectrolytes at Interfaces : Suitable Materials, Structure and Properties. *Macromol. Rapid Commun.* **2000**, *21*, 319–348.

(37) Ramírez-Wong, D. G.; Coelho-diogo, C.; Aimé, C.; Bonhomme, C.; Jonas, A. M.; Demoustier-champagne, S. Effects of Geometrical Confinement in Membrane Pores on Enzyme-Based Layer-by-Layer Assemblies. *Appl. Surf. Sci.* **2015**, *338*, 154–162.

(38) Porcel, C.; Lavalle, P.; Ball, V.; Decher, G.; Senger, B.; Voegel, J.-C.; Schaaf, P. From Exponential to Linear Growth in Polyelectrolyte Multilayers. *Langmuir* **2006**, *22*, 4376–4383.

(39) Shiratori, S. S.; Rubner, M. F. pH-Dependent Thickness Behavior of Sequentially Adsorbed Layers of Weak Polyelectrolytes. *Macromolecules* **2000**, *33*, 4213–4219.

(40) Picart, C.; Mutterer, J.; Richert, L.; Luo, Y.; Prestwich, G. D.; Schaaf, P.; Voegel, J.-C.; Lavalle, P. Molecular Basis for the Explanation of the Exponential Growth of Polyelectrolyte Multilayers. *Proc. Natl. Acad. Sci. U. S. A.* **2002**, *99*, 12531–12535.

(41) Lavalle, P.; Gergely, C.; Cuisinier, F. J. G.; Decher, G.; Schaaf, P.; Voegel, J. C.; Picart, C. Comparison of the Structure of Polyelectrolyte Multilayer Films Exhibiting a Linear and an Exponential Growth Regime: An in Situ Atomic Force Microscopy Study. *Macromolecules* **2002**, *35*, 4458–4465.

(42) Chia, K.-K.; Rubner, M. F.; Cohen, R. E. pH-Responsive Reversibly

Swellable Nanotube Arrays. *Langmuir* **2009**, *25*, 14044–14052.

(43) Gilbert, J. B.; O'Brien, J. S.; Suresh, H. S.; Cohen, R. E.; Rubner, M. F.; Brien, J. S. O. Orientation-Specific Attachment of Polymeric Microtubes on Cell Surfaces. *Adv. Mater.* **2013**, *25*, 5948–5952.

(44) He, Q.; Tian, Y.; Cui, Y.; Möhwald, H.; Li, J.; Mohwald, H.; Li, J. Layer-by-Layer Assembly of Magnetic Polypeptide Nanotubes as a DNA Carrier. *J. Mater. Chem.* **2008**, *18*, 784–754.

(45) Lee, D.; Nolte, A. J.; Kunz, A. L.; Rubner, M. F.; Cohen, R. E. pH-Induced Hysteretic Gating of Track-Etched Polycarbonate Membranes: Swelling/deswelling Behavior of Polyelectrolyte Multilayers in Confined Geometry. *J. Am. Chem. Soc.* **2006**, *128*, 8521–8529.

(46) Liang, Z.; Susha, A. S.; Yu, A.; Caruso, F. Nanotubes Prepared by Layer-by-Layer Coating of Porous Membrane Templates. *Adv. Mater.* **2003**, *15*, 1849–1853.

(47) Azzaroni, O.; Lau, K. H. A. Layer-by-Layer Assemblies in Nanoporous Templates: Nano-Organized Design and Applications of Soft Nanotechnology. *Soft Matter* **2011**, *7*, 8709–8724.

(48) Lazzara, T. D.; Aaron Lau, K. H.; Knoll, W.; Janshoff, A.; Steinem, C. Macromolecular Shape and Interactions in Layer-by-Layer Assemblies within Cylindrical Nanopores. *Beilstein J. Nanotechnol.* **2012**, *3*, 475–484.

(49) Dubas, S. T.; Schlenoff, J. B. Swelling and Smoothing of Polyelectrolyte Multilayers by Salt. *Langmuir* **2001**, *17*, 7725–7727.

(50) Miller, M. D.; Bruening, M. L. Correlation of the Swelling and Permeability of Polyelectrolyte Multilayer Films. *Chem. Mater.* **2005**, *17*, 5375–5381.

(51) Harris, J. J.; Bruening, M. L. Electrochemical and in Situ Ellipsometric Investigation of the Permeability and Stability of Layered Polyelectrolyte Films. *Langmuir* **2000**, *16*, 2006–2013.

(52) Roy, C. J.; Chorine, N.; De Geest, B. G.; De Smedt, S.; Jonas, A. M.; Demoustier-Champagne, S. Highly Versatile Approach for Preparing Functional Hybrid Multisegmented Nanotubes and Nanowires. *Chem. Mater.* **2012**, *24*, 1562–1567.

4 Collection of LbL assembled nanotubes

In this chapter, different methods to collect LbL assembled template-synthesized nanotubes and disperse them in aqueous medium. Among them, a method based on simple filtration of nanotubes in the presence of a powdered dextran adjuvant leads to the collection and dispersion of any template-synthesized nano-object independent of its nature (polyelectrolyte nanotubes as well as gold nanowires and organic polypyrrole nanotubes). This universal method to collect membrane templated nano-objects with a high yield paves the way to further characterization of a large variety of nanotubes in aqueous solution and to their potential use as nanocarriers for therapeutic cargo.

*The results of this chapter are already published in Langmuir (**2015**)* [1].

4.1 Introduction

Over the last decade, template assisted LbL assembly became a popular strategy to fabricate various kind of nanotubes, especially, polymer and protein nanotubular structures and a lot of research has been dedicated to this field [2–16]. However, although the key point for using these interesting nanotubular objects in biomedical applications is to efficiently extract them from the membrane without damage and to redisperse them in an appropriate medium, there are very few reports on the liberation of LbL nanotubes from the template and on their collection in an aqueous medium. Rubner et al. extracted hybrid tubes of micrometer size by dissolving the PC template in dichloromethane (CH_2Cl_2), a conventional solvent for PC, followed by a filtration step. The collected microtubes were then scraped off the filter surface and transferred to aqueous solution [17]. Komatsu et al. managed to separate nanotubes from the template by a two-steps process. First, the PC template is dissolved immediately in a polar amide solvent (DMF), and the precipitated nanotubes are washed several times with DMF. Second, the obtained tubes were quickly freeze-dried in vacuum to yield the lyophilized nanotubes [18–30]. Although efficient, this procedure sometimes leads to the formation of aggregates of nanotubes, which cannot be further redispersed in water.

In the present study, different methods to collect and transfer membrane template-synthesized LbL assembled nanotubes to aqueous solution are tested. The efficiency of each method is evaluated and the reasons why a method excels or fails the nanotubes collection and dispersion process are investigated, our final goal being to develop a universal method allowing the quantitative collection of membrane template-synthesized nanotubes of different sizes, composition, and rigidity. Finally, the change in nanotubes rigidity after dispersion in aqueous solution was also evaluated.

4.2 Materials and Methods

4.2.1 Materials

Dichloromethane (CH_2Cl_2), dimethylformamide (DMF), sodium chloride (NaCl) and dextran (from Leuconostoc spp., M_W: 40 kDa), N-hydroxy sulfosuccinimide sodium salt (sulfo-NHS), N-(3-Dimethylaminopropyl)-N'-ethyl carbodiimide hydrochloride (EDC), Polyallylamine hydrochloride (PAH, M_W: 58 kDa), poly(sodium 4-styrenesulfonate) (PSS, M_W: 70 kDa), polyacrylic acid (PAA, M_W: 100 kDa), poly-L-arginine (PLA, M_W > 70 kDa), ovalbumin (OVA, M_W: 45 kDa) and poly(allylamine hydrochloride) fluorescein isothiocyanate (PAH-FITC, M_W: 15 kDa maximum excitation at 495 nm and an maximum emission at 521 nm) with a monomer to dye ratio (PAH:FITC) of (50:1) were purchased from Sigma-Aldrich. Fluorescent ovalbumin (OVA Alexa Fluor Fluor 488) was purchased from Life Technologies. The Alexa Fluor Fluor 488 fluorophore has a maximum excitation peak at 495 nm and a maximum emission peak at 519 nm. Milli-Q water with 18.2 MΩ.cm resistivity was used in all experiments. All products were used as received.

Sheets of track-etched polycarbonate membranes were provided by It4ip (Louvain-la-Neuve, Belgium, http://www.it4ip.be) with pore diameters of namely 100, 300 and 500 nm. The pore diameter of the PC membrane is not exactly as given by the supplier and a 5-10% variation is observed among the pores. All membranes had a thickness of 21 µm and a pore density of 10^8 pores.cm^{-2}. Hydrophilic poly(ethylene terephtalate) (PET) membranes with a pore size of 200 nm, thickness of 23 µm and pore density of about 5.10^8 pores.cm^{-2} were provided by It4ip as well.

4.2.2 Fabrication of LbL assembled nanotubes

Except for fluorescent-tagged polyelectrolytes, all polyelectrolyte solutions were prepared at 1 mg.mL^{-1} concentration. OVA Alexa Fluor 488 and PAH-

FITC polyelectrolytes were prepared at 0.1 $mg.mL^{-1}$ and 0.5 $mg.mL^{-1}$ concentration, respectively. The PAH and PSS solutions used to grow PAH/PSS multilayers were prepared in water containing 150 mM NaCl. The PAH and PAA solutions used to grow PAH/PAA multilayers were prepared in 100 mM acetate buffer at pH = 5.5. The PAH and OVA solutions used to grow PAH/OVA multilayers were prepared in 10 mM HEPES buffer at pH = 8, whereas the PLA and OVA solutions used to grow PLA/OVA multilayers were prepared in milli-Q water. These buffers and pH conditions were chosen based on the pKa of the polyelectrolytes and the isoelectric points of the proteins to obtain a polycation/polyanion system in each case. PC membranes were immersed for 30 minutes in each polyelectrolyte solution followed by an intermediate rinsing step of 5 minutes by immersion in an aqueous solution of same ionic strength and composition as used for the polyelectrolytes. These steps were cycled until 6 bilayers were achieved for all systems. During the LbL process, a polyelectrolyte multilayer crust forms on the top and bottom surfaces of the PC template. This film blocks the access to nanopores, and thus must be removed. Therefore, after every bilayer deposition, the top and bottom surfaces of the PC membranes were gently scrubbed with a cell scraper to eliminate this adherent layer. Optional crosslinking of PAH/PAA nanotubes was carried out by immersing the nanotube-containing PC membrane in a 100 mM MES buffer solution (pH = 5.5) containing 25 mM EDC and 48 mM sulfo-NHS for approximately 24 hours at 4 °C. In the end, all samples were rinsed abundantly with milli-Q water to eliminate buffer salts, and dried and stored at room temperature.

4.2.3 Releasing nanotubes from the template

To release the nanotubes from the template, the PC membrane was dissolved in CH_2Cl_2, resulting in a colloidal suspension of nanotubes and dissolved PC in CH_2Cl_2. The nanotubes were then recovered by filtration of

this colloidal suspension over a hydrophilic PET membrane. To maximize the removal of remnant PC, fresh CH_2Cl_2, was flushed through the PET filter for several times.

4.2.4 Verifying the stability of nanotubes in aqueous medium

The stability of nanotubes in aqueous medium was verified by dissolving the PC template in CH_2Cl_2 and filtering the resulting suspension over a PET filter. The filter was then immersed in an aqueous medium for 24 hours. Nanotubes deposited on the filter surface were imaged by epi-fluorescence microscopy prior and after immersion in aqueous medium, to analyze the stability of nanotubes.

4.2.5 Collection of nanotubes by precipitation and freeze-drying

PC membrane containing nanotubes was dissolved in DMF. There was no immediate precipitation of nanotubes, therefore, the solution was centrifuged at 4000 rpm for 3 to 10 minutes. Nanotubes precipitated at the bottom of the container, forming a droplet separable from the rest of the solution. Excess solvent containing PC is removed and replaced by fresh solvent. The precipitate is then dispersed by agitation and sonicated for 5 seconds and fresh DMF is added to the recipient (washing step). Once again, the sample is centrifuged and the whole cycle (washing step) is repeated for 2-3 times. After the last washing step, samples are quickly freeze-dried in vacuum.

4.2.6 Collection by biphasic method

PC membrane holding the nanotubes was dissolved in CH_2Cl_2. The same volume of milli-Q water was then added to this organic solution in order to create a biphasic immiscible system with CH_2Cl_2 as the bottom phase and milli-Q water as the top phase. The mixture was stirred for 30 seconds and set aside to stabilize for 3 minutes. CH_2Cl_2 solution below the interface was

ejected out and removed and fresh CH_2Cl_2 was introduced to the solution (washing step). This washing step is repeated five times to maximize the PC removal. Afterwards, in order to remove the remaining CH_2Cl_2 from the bottom of the recipient, air was injected in the recipient to create air bubbles. These bubbles perturb the biphasic system and facilitate the CH_2Cl_2 arrival at the surface of the solution. After reaching the surface, CH_2Cl_2 evaporates rapidly due to its low boiling point (~40 °C). Finally, an aqueous solution containing liberated nanotubes remains in the test tube.

4.2.7 Collection and re-dispersion of nanotubes with a virgin PET filter

The suspension of fluorescent-tagged nanotubes was filtered through a PET filter. The PET filter with nanotubes deposited on top was then immersed in 2mL milli-Q water and stirred for 24 hours, before being stored at 4 °C.

4.2.8 Collection and re-dispersion of nanotubes with a coated PET filter

The PET filter was spin coated with an aqueous solution of 50 $mg.mL^{-1}$ dextran. The spin-coating process was carried out for 1 min at a speed of 1000 rpm followed by 4 minutes at a speed of 4000 rpm. The PET filter coated with dextran was then heated at 150 °C for 2 minutes. The filter was set aside to dry overnight. The colloidal suspension of nanotubes in CH_2Cl_2 was then filtered through the filter. The filter was finally immersed in 2 mL milli-Q water and stirred for 24 hours before being stored at 4 °C.

4.2.9 Collection by adjuvant assisted method

NaCl or dextran were used as water-soluble and CH_2Cl_2 -insoluble adjuvants in the collection process. NaCl was milled for 20 seconds to obtain a fine powder of 1-2 µm size. Dextran was already available as a fine powder and needed no further milling. 20-25 mg of adjuvant was first dispersed in pure CH_2Cl_2 and filtered over a PET filter, leading to formation of a thin porous

pellet over the PET filter inside the filtration gasket. This layer aims to mask interactions between the nano-objects and the filter surface. Next, another 20-25 mg of adjuvant was added to and dispersed in the colloidal suspension of nanotubes in CH_2Cl_2. The colloidal suspension was filtered through the previously prepared PET filter, thereby building a porous pellet with trapped nanotubes, lying over the pure adjuvant bottom layer. We found that it is crucial to have nanotubes trapped in the whole volume of the pellet. If this step is not followed properly, nanotubes will stack over the surface of the porous adjuvant pellet, resulting in the formation of clusters of nanotubes upon dispersing the pellet in the aqueous solution. To ensure the total removal of PC traces, CH_2Cl_2 was flushed gently several times through the whole system. The adjuvant pellet was then removed from the filtration gasket and immersed in 2 mL milli-Q water. The aqueous suspension containing the nanotubes and the dissolved adjuvant was then stirred for 15 minutes before being stored at 4 °C.

4.2.10 Characterization methods

SEM and STEM observations

Samples were observed with a field emission scanning electron microscope (JSM-7600F, JEOL Ltd.), equipped with a transmission detector. SEM measurements were performed at 15 keV for the scanning mode and 30 keV for the scanning transmission mode.

For SEM imaging, the CH_2Cl_2 or aqueous suspension of nano-objects was filtered through a PET filter coated with a 20 nm layer of gold. For scanning transmission electron microscopy (STEM), a few drops of the colloidal suspension (either in water or in CH_2Cl_2) was dropped over a carbon-coated copper TEM grid (200 mesh, Electron Microscopy Sciences) and air-dried at room temperature.

Fluorescence microscopy

The suspension of fluorescent-tagged nanotubes was filtered through a PET filter for epi-fluorescence optical microscopy. Fluorescence images were obtained by an Olympus IX2 inverted epi- microscope equipped with a FITC filter set.

Image analysis for determining flattening and flexibility of nanotubes

The pore diameter of PC membranes as well as the outer diameter of the nanotubes prior and after being in contact with the aqueous solution was determined from SEM and STEM images using ImageJ software (developed by Wayne Rasband, National Institutes of Health, Bethesda, MD). 30 measurements for each system were taken to obtain the average and standard deviation values. The root-mean-square end-to-end distance of nanotubes $< {R_{EE}}^2 >$ as well as their average contour length L were calculated by homemade routines written in Igor Pro v.6.3 (WaveMetrics, Inc), measuring about 25 different nanotubes for each system.

4.3 Results and Discussion

4.3.1 Nanotubes stability in aqueous medium

Before testing different strategies for collecting and dispersing LbL nanotubes in aqueous medium, we first evaluated the stability of these nanotubes in water.

To this aim, two types of nanotubes (PLA/OVA Alexa Fluor 488)$_6$ and (PAH-FITC/OVA)$_6$ were assembled inside the pores of a PC membrane. Tubes were released from the template by dissolving PC in CH_2Cl_2 solvent and the obtained nanotube suspension was filtered over a PET filter. This filter was then immersed in milli-Q water and was stirred for 5 days.

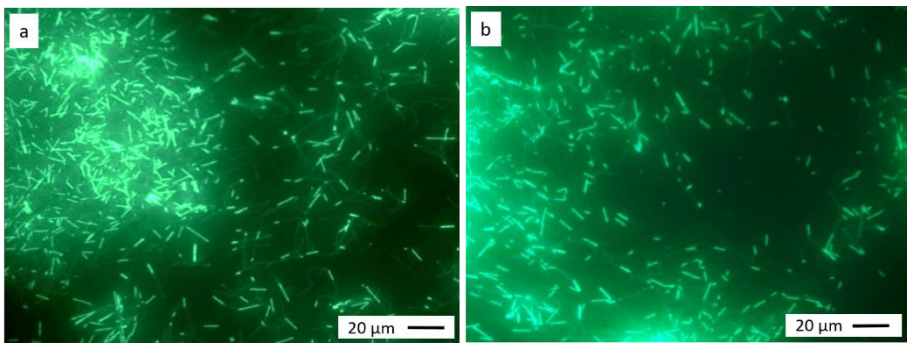

Figure 4.1.Epi-fluorescence microscopy images of (PLA/OVA Alexa Fluor Fluor 488)$_6$ nanotubes (a) after filtration over a PET filter and prior to immersion in aqueous solution, (b) after immersion in aqueous solution for 5 days (b).

Figure 4.1 shows fluorescence microscopy images of (PLA/OVA Alexa Fluor 488)$_6$ nanotubes deposited over PET filter prior and after being immersed in milli-Q water for 5 consecutive days. It is observed that under these conditions nanotubes retain their tubular structure and are not disassembled. Next, stability of nanotubes in aqueous solutions of different ionic strengths was examined. Organic suspension of nanotubes was again

filtered over a PET filter and the filter was immersed in aqueous solutions containing 100 mM, 200 mM and 500 mM of NaCl.

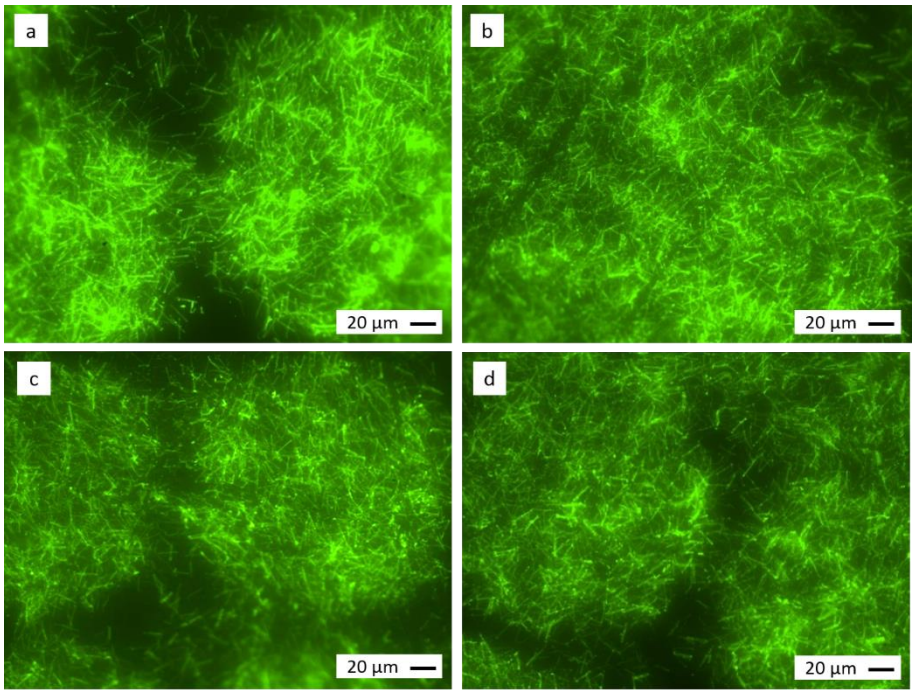

Figure 4.2. Epi-fluorescence microscopy images of (PLA/OVA Alexa Fluor 488)$_6$ nanotubes filtered over a PET filter and immerse for 30 minutes in milli-Q water containing: (a) no salt, (b) 100 mM NaCl, (c) 200 mM NaCl and (d) 500 mM NaCl. (The acquisition conditions of fluorescence images are different and thus, the intensity of the images could not be compared.)

Figure 4.2 shows fluorescence microscopy images of (PLA/OVA Alexa Fluor 488)$_6$ nanotubes prior to immersion in aqueous solution and after immersion in NaCl solutions of different ionic strengths.

From these results, we can conclude that these protein-based nanotubes are stable in aqueous medium and are thus adequate for applications requiring nanotubes dispersed in water.

4.3.2 Nanotubes collection by precipitation and freeze-drying

Transferring membrane template-synthesized LbL assembled nanotubes to aqueous solution is very challenging. At first, we tried to reproduce the method reported by Komatsu et al who collected $(PLA/HSA)_3$ nanotubes and redispersed them in aqueous solution. For that purpose, we used a simple and well-known system based on synthetic polyelectrolytes (PAH/PSS). The method consists in two steps. First, the PC template is dissolved in a polar amide solvent (DMF) resulting in instantaneous precipitation of nanotubes. The precipitated nanotubes are then washed several times with DMF to maximize the PC removal. Second, the obtained tubes are quickly freeze-dried in vacuum to yield lyophilized nanotubes. This lyophilized powder is then redispersed in aqueous medium of choice. We followed this method step-by-step and obtained a lyophilized powder of nanotubes. However, we were not able to disperse the powder in aqueous medium. When the powder was added to the aqueous solution, it broke into smaller insoluble aggregates. It was essential to determine why the lyophilized powder of nanotubes was not dispersible in aqueous medium. To that aim, the lyophilized powder was imaged by SEM (Figure 4.3.a).

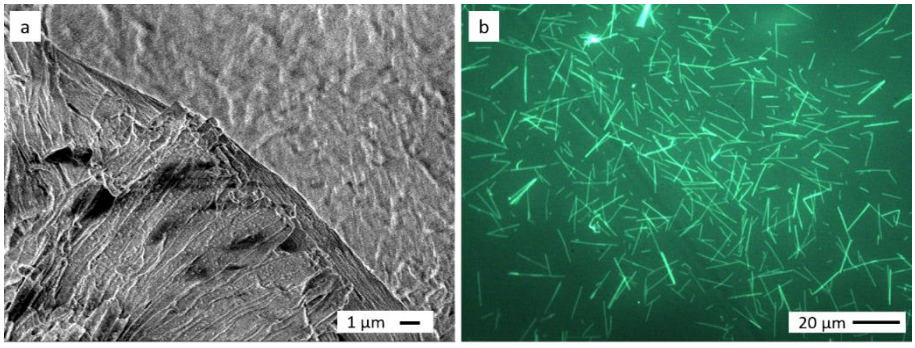

Figure 4.3. (a) SEM image of $(PAH\text{-}FITC/PSS)_6$ nanotubes after collection by precipitation and freeze-drying, (b) Epi-fluorescence microscopy image of $(PAH\text{-}FITC/PSS)_6$ nanotubes after dissolving some lyophilized nanotubes powder in CH_2Cl_2.

From Figure 4.3.a one can observe a bundle of nanotubes that are sticking together probably due to the presence of remaining PC. To verify this hypothesis, some lyophilized powder was added to CH_2Cl_2 and the suspension was filtered through a virgin PET filter. The deposited matter on the filter was then imaged by epi-fluorescence microscopy, revealing well-separated fluorescent nanotubes (Figure 4.3.b). These results suggest that some residual PC was indeed present in the lyophilized powder, inhibiting nanotubes separation and dispersion in aqueous medium. The difficulty in proper removal of PC is the major drawback of Komatsu's method for efficient collection and dispersion of nanotubes in aqueous medium. We therefore try to develop another strategy.

4.3.3 Nanotubes collection based on an immiscible biphasic system

As nanotubes are composed of hydrophilic polyelectrolytes and PC is soluble in many organic solvents, we tried to separate them using a biphasic collection system made of two compartments: one compartment (organic phase) dedicated to the dissolution of PC and another one dedicated to the collection of the tubes (aqueous medium, suitable for further biological applications). To this aim, CH_2Cl_2 was selected as PC dissolving compartment and milli-Q water was chosen as the nanotubes collecting compartment. CH_2Cl_2 has a very low miscibility in water (0.24% at 20 °C) and consequently, a biphasic system can be obtained with CH_2Cl_2 in the bottom and water on top due to higher density of CH_2Cl_2 (1.3 $g.cm^{-3}$).

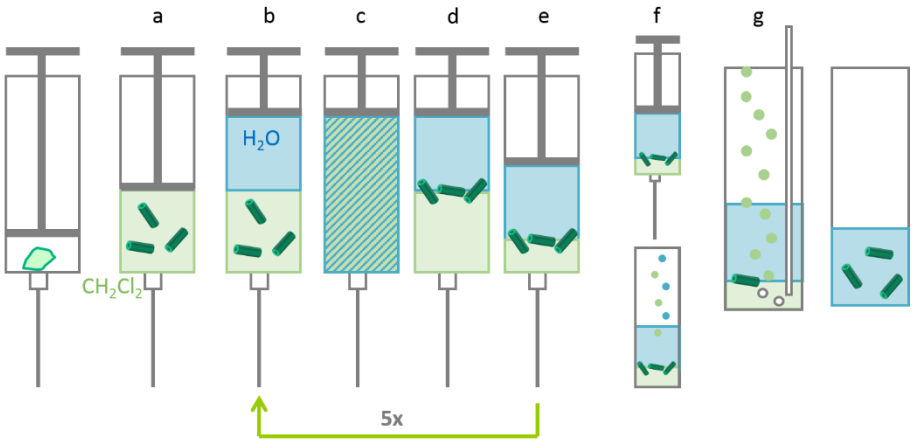

Figure 4.4. Schematic representation of PC separation and nanotube collection by creating an immiscible biphasic system. (a) dissolution of PC membrane containing LbL assembled nanotubes in CH_2Cl_2, (b) addition of water to the solution, (c) mixing the whole system, (d) setting the mixture aside to stabilize, (e) partial removal of CH_2Cl_2 and addition of fresh CH_2Cl_2, steps b-e (washing steps) were repeated 5 times, (f) ejecting the remaining solution to a glass test tube, (g) injecting air to create bubbles and remove the remaining CH_2Cl_2.

A schematic representation of the developed immiscible biphasic system process for collecting $(PLA/OVA\ Alexa\ Fluor\ 488)_6$ nanotubes is shown in Figure 4.4. PC membrane containing LbL assembled nanotubes was dissolved in dichloromethane and then milli-Q water was added to nanotubes suspension creating an immiscible biphasic solution. The mixture was agitated in order to put nanotubes in contact with aqueous medium and then set aside to stabilize. A few drops from water compartment, CH_2Cl_2 compartment and their interface were separately filtered through PET filters in order to detect if nanotubes have migrated from the organic phase to the aqueous phase. There were almost no nanotubes detected in the organic phase and a very low number of nanotubes detected in aqueous

compartment. However, a large number of nanotubes were detected at the water/CH_2Cl_2 interface.

Figure 4.5.a shows epi-fluorescence microscopy image of (PLA/OVA Alexa Fluor 488)$_6$ nanotubes trapped at water/organic solvent interface. Nanotubes migrate towards the interface to reduce the tension between the two phases. After being in contact with water, these tubes became highly flexible and formed loops.

To maximize the PC removal, organic compartment of dissolved PC in CH_2Cl_2 was ejected away while aqueous compartment and the interface were kept. Next, fresh CH_2Cl_2 was again added to this solution followed by agitation and stirring (washing step). This process was repeated 5 times to increase PC dissolution and removal. In the end, a final biphasic system constituted of the aqueous phase and a very little amount of CH_2Cl_2 was obtained. To completely remove CH_2Cl_2, air was injected in this solution, creating bubbles and perturbing the biphasic system. This perturbation facilitates the solvent arrival at the air/liquid interface. After reaching the interface, CH_2Cl_2 evaporates rapidly due to its low boiling point (~ 40 °C). Finally, an aqueous solution containing liberated tubes remained.

In order to determine the behavior of the nanotubes during the whole collection process, the solution was analyzed at different points:

1. The water/ CH_2Cl_2 interface;
2. The solution at water/glass interface after complete removal of CH_2Cl_2;
3. The final aqueous collection solution.

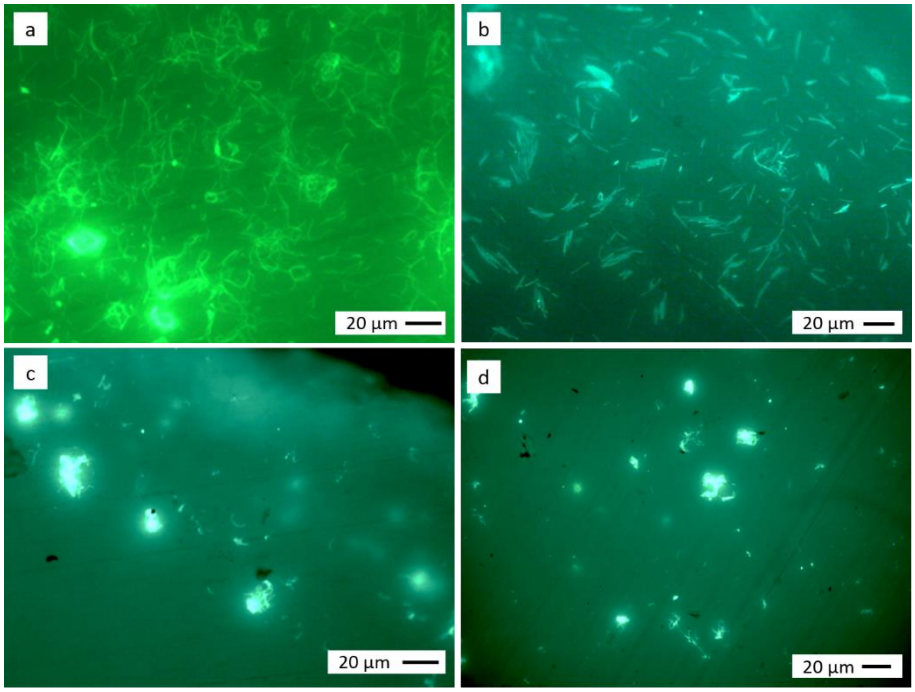

Figure 4.5. Epi-fluorescence microscopy images of (a) $(PLA/OVA\ Alexa\ 488)_6$ at the water/CH_2Cl_2 interface, (b) $(PAH\text{-}FITC/PSS)_6$ nanotubes at the water/CH_2Cl_2 interface, (c) $(PAH\text{-}FITC)_6$ nanotubes at the water/glass interface, (d) $(PAH\text{-}FITC/PSS)_6$ nanotubes collected in water. (The acquisition conditions of fluorescence images are different and thus, the intensity of the images could not be compared.)

Figure 4.5.b shows $(PAH\text{-}FITC/PSS)_6$ nanotubes at water/CH_2Cl_2 interface. Nanotubes have migrated to the interface. However, they appear to be stiffer and less deformed compared to $(PLA/OVA\ Alexa\ Fluor\ 488)_6$ nanotubes (Figure 4.5.a). Figure 4.5.c shows $(PAH\text{-}FITC/PSS)_6$ nanotubes at water/glass interface after complete evaporation of CH_2Cl_2. It was observed that a considerable amount of nanotubes stuck on the recipient surface. Figure 4.5.d showing collected nanotubes in the final aqueous solution demonstrated that the number of collected nanotubes in water is quite low. The same collection process was repeated for $(PLA/OVA\ Alexa\ Fluor\ 488)_6$

nanotubes and again, large amounts of nanotubes were lost during the rinsing process. This might be caused by the presence of LbL crust, which was not completely removed during the nanotubes build-up process. This crust prevents nanotubes migration from the interface to the aqueous solution.

Although trapping the nanotubes at the interface of an immiscible biphasic system appeared to be a promising approach for nanotubes collection in water, the process proved to be rather inefficient. This results from the existence of numerous attractive interactions between nanotubes and the recipient surfaces and between nanotubes themselves that interfere with the collection process. As those interacting forces can hardly be fully controlled, another strategy was envisaged for collecting nanotubes.

4.3.4 Collection of nanotubes by filtration over a modified filter

Filtration appears to be an easy process and leads to the collection of a large number of nanotubes over the PET filter. We therefore tried to benefit from a simple two-step process, consisting of first filtering a CH_2Cl_2 suspension of dissolved PC and liberated nanotubes over a PET filter, followed by immersing the PET filter in an aqueous solution and stirring the system to gently detach the nanotubes from the PET filter surface and disperse them in aqueous medium. Looking back to Figure 4.1, epi-fluorescence microscopy image of (PLA/OVA Alexa Fluor 488)$_6$ nanotubes prior and after being immersed and stirred in aqueous medium, it is evident that nanotubes do not leave the PET filter surface. There exist interactions between nanotubes and PET filter as well as between nanotubes themselves, which inhibit their detachment from filter and collection in aqueous medium.

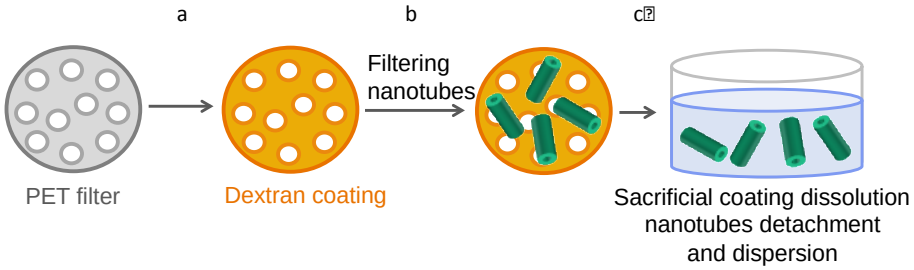

Figure 4.6. Schematic representation of nanotubes collection by filtration over a PET filter coated with a sacrificial layer, (a) dextran was coated on the surface of PET filter, (b) nanotubes were filtered over this modified filter, (c) immersing the filter in aqueous solution for further detachment of nanotubes from the surface and release in aqueous solution.

A simple approach to completely mask interactions between nanotubes and the filter could be coating the PET filter surface with a thin sacrificial layer (Figure 4.6). The collection procedure consists of filtering the nanotubes over this sacrificial later and then releasing them in aqueous medium by dissolving the coated layer. The sacrificial layer must be resistant to CH_2Cl_2 but highly soluble in aqueous solution to release the deposited nanotubes upon immersion in aqueous solution. Dextran was chosen as the sacrificial layer to be deposited on the surface of PET filter as it has already been demonstrated that dextran can act as water-soluble sacrificial later especially for micromachining applications [31].

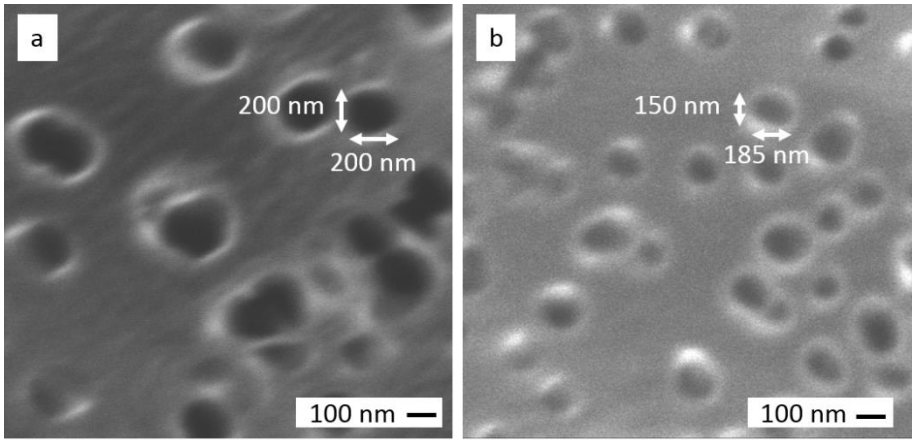

Figure 4.7. (a) SEM image of 200 nm pore diameter PET membrane before and (b) after being coated with dextran.

Considering conditions suggested by Linder et al.[31] we deposited about 50 nm of dextran on PET surface. Figure 4.7.a and Figure 4.7.b show SEM images of PET filter prior and after dextran layer deposition. As shown in Figure 4.7 the pore size of the PET filter did not change a lot after dextran deposition. The pore sizes was found to be 137 ± 22 nm after measuring the dimensions of about 100 pores and also there were no observable cracks on the filter surface. Considering these, the dextran coated PET filter could still be used as a filter and the collection procedure could be carried on.

PC membrane with (PLA/OVA Alexa Fluor 488)$_6$ nanotubes assembled within its pores was first dissolved in CH_2Cl_2 and then filtered through dextran-coated PET filter. The filter was then immersed in aqueous solution and stirred for 24h.

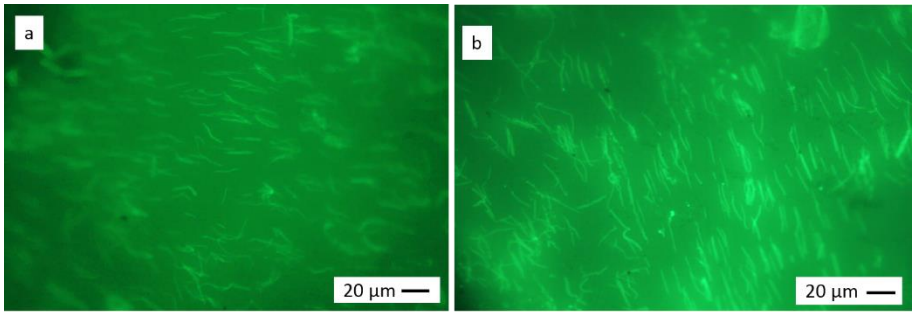

Figure 4.8. Epi-fluorescence microscopy image of (PLA/OVA Alexa 488)$_6$ nanotubes, (a) after being filtered over a dextran-coated PET filter, (b) still remaining on the surface of filter, after being immersed and stirred in aqueous solution for 24 hours.

Epi-fluorescence microscopy images (Figure 4.8) showed that nanotubes remained stuck on the filter surface and no nanotubes were collected in aqueous solution. This behavior can be explained by attractive interactions between the LbL nanotubes. Positive charged surfaces of one tube may interact with negative charged surface of another tube in addition to other short-range interactions between the tubes, resulting in the formation of a bundle of tubes, unable to detach from the filter surface.

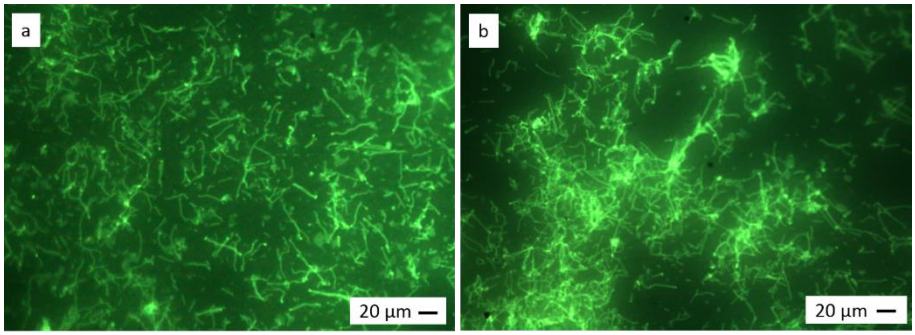

Figure 4.9. Epi-fluorescence microscopy image of (PLA/OVA Alexa 488)$_6$ nanotubes, (a) remained on the surface modified PET filter after being immersed and stirred in aqueous solution for 24 hours, (b) remained on the surface of the PET filter after being immersed and stirred in CH_2Cl_2 solution.

To demonstrate the extent of nanotubes interactions among themselves in the release process, the PET filter with nanotubes remaining on top was immersed back in fresh CH_2Cl_2 and stirred for 2 days (Figure 4.9). By comparing Figure 4.9.a and Figure 4.9.b, it is again observed that nanotubes did not detach from the PET surface. We can therefore conclude that nanotubes are indeed interacting with each other and that those interactions are irreversible.

4.3.5 Collection of nanotubes by filtration in presence of an adjuvant

As our previous attempts to overcome the short-range forces between the nanotubes were inefficient, a new strategy consisting in first creating a masking porous layer over the PET filter and then trapping the nanotubes in porous "protective cages" on top of the filter surface was considered. The porous cages must be resistant to CH_2Cl_2 while being highly soluble in aqueous solution so that trapped nanotubes can be released in aqueous solution; in addition, the material of the cages must be biologically innocuous for medical applications.

To create the porous masking layer, a powdered adjuvant was dispersed in pure CH_2Cl_2 and then filtered over a PET filter, forming a thin disk-shaped porous pellet. This masking layer will minimize the chances of nanotubes becoming in contact with the filter surface.

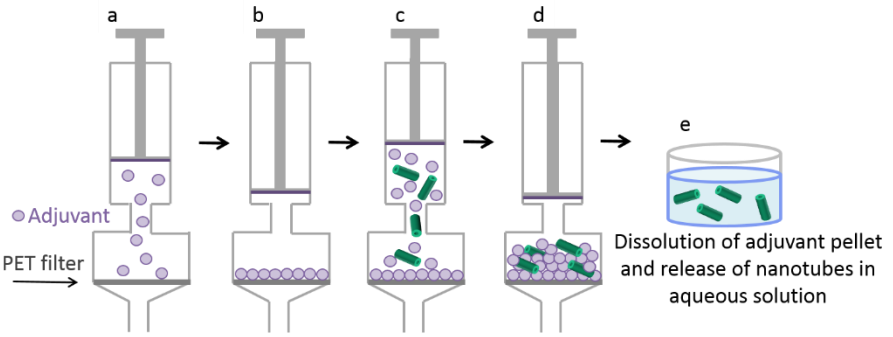

Figure 4.10. Schematic representation of nanotube collection by the adjuvant-assisted filtration method, (a) the adjuvant powder is dispersed in CH_2Cl_2 and filtered over a PET filter, (b) a thin disk-shaped pellet of adjuvant forms over the PET filter, (c) the adjuvant powder is added to the colloidal suspension of nanotubes in CH_2Cl_2 and filtered through the adjuvant-masked PET filter, (d) the nanotubes are trapped inside the newly formed adjuvant pellet, (e) the adjuvant pellet is dissolved in aqueous solution and the nanotubes are released.

To build the porous trapping cage, more powdered adjuvant was added to the CH_2Cl_2 colloidal suspension. By filtering the CH_2Cl_2 solution (containing nanotubes, dissolved PC, and adjuvant) through the adjuvant-masked PET filter, a new porous pellet of adjuvant is formed over the previous one. It is important to mix nanotubes with the adjuvant prior to filtration in order to minimize interactions between nanotubes and avoid clustering. Indeed, if the nanotubes are not evenly dispersed through the porous pellet a mat of nanotubes will be formed that will not be further dispersed in aqueous solution. After filtration, the nanotube-containing adjuvant pellet was dissolved in aqueous solution leading to release of the nanotubes (Figure 4.10).

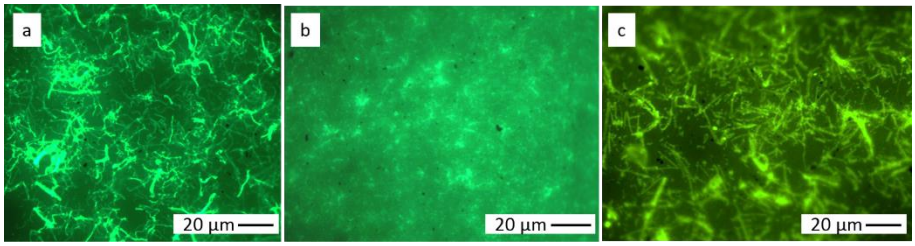

Figure 4.11. Epi-fluorescence images of (a) $(PAH\text{-}FITC/PSS)_6$ nanotubes, (b) non-crosslinked $(PAH\text{-}FITC/PAA)_6$ nanotubes and (c) crosslinked $(PAH\text{-}FITC/PAA)_6$ nanotubes, collected in aqueous solution by NaCl adjuvant-assisted collection method.

Sodium chloride was chosen as a potential adjuvant as it is not soluble in CH_2Cl_2 and yet highly soluble in aqueous solution. As shown in Figure 4.11.a, $(PAH\text{-}FITC/PSS)_6$ nanotubes were successfully collected and dispersed in aqueous solution by this method. Moving forward to the $(PAH\text{-}FITC/PAA)_6$ system, it was observed that the nanotubes lose their tubular structure when placed in contact with the aqueous solution (Figure 4.11.b).This deformation can be explained by the ionic shock induced by the dissolution of the NaCl powder that holds the nanotubes. To increase the ionic strength resistance of the $(PAH\text{-}FITC/PAA)_6$ structures, the nanotubes were chemically crosslinked with EDC/sulfo-NHS. Figure 4.11.c demonstrates that chemical crosslinking is efficient in reinforcing $(PAH\text{-}FITC/PAA)_6$ nanotubes against ionic shock, since well-shaped $(PAH\text{-}FITC/PAA)_6$ nanotubes were successfully collected.

To suppress this ionic shock and the subsequent need to crosslink the nanotubes, the collection process was slightly modified by replacing NaCl by dextran as adjuvant. Dextran is uncharged in aqueous solution and consequently does not modify the ionic strength of the aqueous solution.

Protein-based nanotubes were therefore trapped inside dextran pellets and further released in aqueous solution.

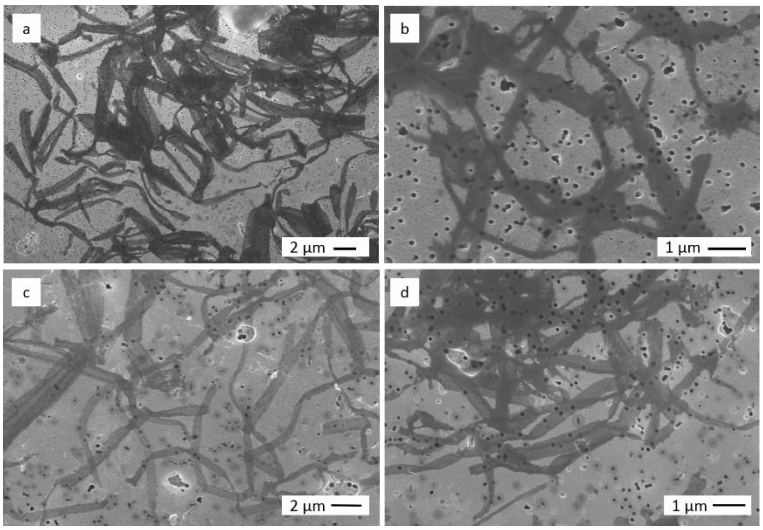

Figure 4.12. Nanotubes were imaged after collection in aqueous solution by the dextran adjuvant-assisted method. SEM images of (a) $(PAH/OVA)_6$, (b) $(PLA/OVA)_6$, (c) $(PAH/PSS)_6$, (d) $(PAH/PAA)_6$ nanotubes.

SEM pictures in Figure 4.12.a and Figure 4.12.b show $(PAH/OVA)_6$ and $(PLA/OVA)_6$ nanotubes after successful collection in aqueous solution. These protein-based nanotubes keep their tubular form but are highly flexible after contact with water. $(PLA/OVA)_6$ nanotubes are punctured at some points. This probably results from the high swelling of these nanotubes upon contact with water. Synthetic polyelectrolyte LbL nanotubes of $(PAH/PSS)_6$ and $(PAH/PAA)_6$ were also successfully collected in aqueous solution by dextran adjuvant-assisted method (Figure 4.12.c and Figure 4.12.d).

4.3.6 Evaluating nanotubes rigidity after dispersion in aqueous medium

As observed in Figure 4.12, LbL assembled nanotubes have a tendency to bend, fold and form loops after being dispersed in aqueous solution. In other words, there is a difference in nanotubes rigidity prior and after being dispersed in aqueous solution. To quantify the extent of rigidity modification, the root-mean-square (rms) end-to-end distance $< {R_{EE}}^2 >^{1/2}$ of each type of nanotubes as well as their average contour length L were measured. For wormlike objects such as our nanotubes in water, $< {R_{EE}}^2 > = 2L.L_P$ when the persistence length of the tube, L_P, is much smaller than the contour length [32]. In contrast, when $L_P \gg L$, , $< {R_{EE}}^2 > = L^2$. Therefore, the ratio $< {R_{EE}}^2 > / L^2$ can be taken as an index quantifying the rigidity of the nanotubes, ranging from 1 for very rigid nanotubes of long persistence length, to $2L_P < 1$ for softer ones. Because the persistence length is proportional to the bending rigidity of the tubes the ratio $< {R_{EE}}^2 > / L^2$ is actually indicative of the rigidity of the tubes per unit length [33]. This ratio was calculated for each system and the results gathered in *Figure 4.13* give us an idea about how flexible nanotubes become after being dispersed in aqueous solution.

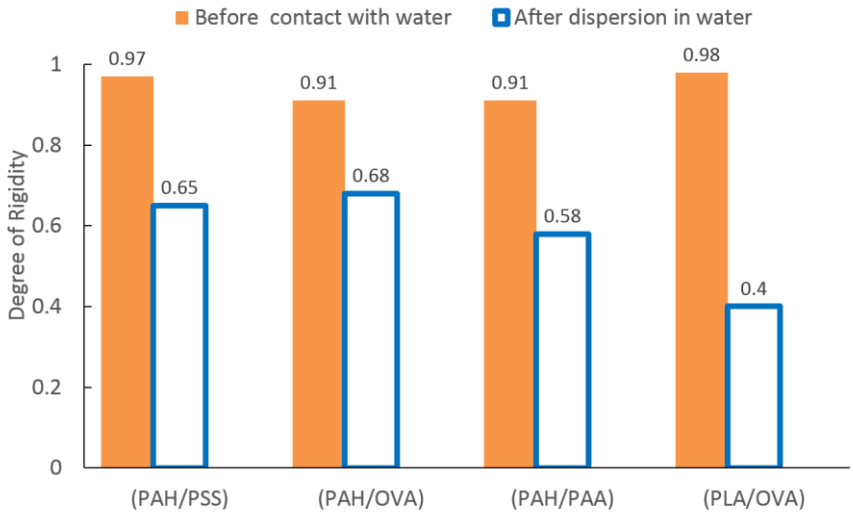

Figure 4.13.Comparison of the degree of rigidity of studied nanotubes before and after being dispersed in aqueous solution (left and right columns, respectively). The degree of rigidity is defined as $\langle R_{EE}^2 \rangle / L^2$. (Values are calculated from 25 nanotubes for each system).

It is observed that the index of rigidity of LbL assembled nanotubes is close to 1 when they are just liberated from the PC template and dispersed in organic solvent (CH_2Cl_2), meaning that nanotubes are mostly rod-shaped. However, the rigidity index drops drastically after being in contact with water. Different parameters can affect the persistence length of the nanotubes [34]. The persistence length can be expressed by

$$L_P = \frac{B_s}{k_b T} \quad (4.1)$$

where L_P is the persistence length (m), B_s is the bending stiffness (N.m), k_B is Boltzmann's constant ($J.K^{-1}$) and T is the temperature (K). The bending stiffness is also related to the young modulus and area momentum of inertia of the beam cross-section as expressed below

$$B_s = E.I \quad (4.2)$$

where E is the Young's modulus (N.m^{-2}), and I the area moment of inertia (m^4) which for a hollow cylinder can be expressed by

$$I = \frac{\pi}{4}({r_{outer}}^4 - {r_{inner}}^4) \quad (4.3)$$

where r_{inner} and r_{outer} are the inner and outer radius (m) of the hollow cylinder. Therefore, the persistence length of the nanotubes can be expressed by

$$L_P = \frac{\pi}{4k_BT} E({r_{outer}}^4 - {r_{inner}}^4) \quad (4.4)$$

Taking Equation 4.4 into account, one can clearly understand why there is a drastic decrease in nanotubes rigidity degree upon dispersion in aqueous medium. Due to hydrophilic nature of the polyelectrolytes used as nanotubes building blocks, nanotubes swell upon dispersion in aqueous solution, leading to an increase of both r_{outer} and r_{inner}; this factor should contribute to an increase of the persistence length. However, the Young's modulus of swollen nanotubes is very strongly decreased, which dominates the effects, resulting in a decrease of L_P. Finally, temperature also affects the persistence length.

Comparing the studied systems, $(PAH/OVA)_6$ and $(PAH/PSS)_6$ have a lower rigidity loss. $(PAH/PAA)_6$ nanotubes became more flexible upon dispersion in water. These nanotubes have a lower wall thickness comparing to other PAH containing nanotubes (see table 3.3) and thus cannot resist the deformation caused by swelling. Biological $(PLA/OVA)_6$ nanotubes lose their rigidity by 60% upon dispersion in aqueous medium. Such a high loss in rigidity can explain the rupture and punctured points observed in these tubes after being immersed in water.

4.4 Conclusion

In this chapter, we focused on different methods to collect and disperse LbL assembled nanotubes in aqueous medium. Our very first attempt was based on previously proposed methods in the literature, which was dissolving the membrane and obtaining a precipitate of nanotubes. We observed that this method might result in formation of nanotubes aggregates sticking to each other with the remnants of undissolved membrane, which could not be dispersed in aqueous solution. Further efforts were based on making a 2-compartment organic solvent/ aqueous medium system with nanotubes trapped at their interface. Nevertheless, this method also did not result in proper collection of tubes. Next, we focused on filtering nanotubes over a filter and aiming for their further detachment. To do so, the filter surface was coated with an organic-solvent resistant yet water-soluble dextran film. This sacrificial layer was expected to mask interactions between nanotubes and the filter surface while facilitating their detachment and dispersion in aqueous medium. However, it was proved that nanotubes did not leave the filter surface and their collection process failed. This was explained by the interactions amongst nanotubes themselves. Therefore, we came to conclusion that an extra measure has to be taken to minimize interactions as much as possible.

A new method was developed based on simple filtration while using a powdered adjuvant to form a protective cage and trap nanotubes within its volume. This method was proved successful in collection of nanotubes independent of their nature. In a parallel work (not mentioned here) organic polypyrrole nanotubes and metallic gold nanowires were also collected and dispersed in aqueous medium by this universal method. This adjuvant-assisted collection method presents several advantages. First, because the method is based on a very simple filtration process, it allows maximizing the

PC template removal by increasing the amount of CH_2Cl_2 solvent. Second, the method gives the opportunity of collecting a large number of nanotubes in one single filtration process. This method is especially applicable and interesting for systems where there is only a small amount of nanotubes to collect (for instance, a low amount of nanotubes composed of expensive molecules).

The morphology of nanotubes was studied in order to determine how they react upon dispersion in aqueous medium. To this aim, the root mean square end-to-end distance of nanotubes $< {R_{EE}}^2 > / L^2$ as well as their contour length L were measured. We assigned $< {R_{EE}}^2 > / L^2$ as an indicator of nanotubes rigidity. It was observed that before being dispersed in aqueous medium, all nanotubes were rod-shaped and they became flexible upon contact with water. Protein-based nanotubes had the highest loss in rigidity upon contact with water and were the most flexible of the bunch. This increased flexibility and associated softness is the reason of the difficulty to collect the LbL nanotubes, a problem successfully overcame by the adjuvant-assisted collection method.

4.5 Bibliography

(1) Saghazadeh, S.; Zhang, S.; Lefèvre, D.; Le Beulze, A.; Jonas, A. M.; Demoustier-Champagne, S. Universal Method to Transfer Membrane-Templated Nano-Objects to Aqueous Solutions. *Langmuir* **2015**, *31*, 7264–7273.

(2) Ai, S.; Lu, G.; He, Q.; Li, J. Highly Flexible Polyelectrolyte Nanotubes. *J. Am. Chem. Soc.* **2003**, *125*, 11140–11141.

(3) Alem, H.; Blondeau, F.; Glinel, K.; Demoustier-champagne, S.; Jonas, A. M. Layer-by-Layer Assembly of Polyelectrolytes in Nanopores. *Macromolecules* **2007**, *40*, 3366–3372.

(4) Azzaroni, O.; Lau, K. H. A. Layer-by-Layer Assemblies in Nanoporous Templates: Nano-Organized Design and Applications of Soft Nanotechnology. *Soft Matter* **2011**, *7*, 8709–8724.

(5) Cho, Y.; Lee, C.; Hong, J. Pore Size Effect on the Formation of Polymer Nanotubular Structures within Nanoporous Templates. *Colloids Surfaces A Physicochem. Eng. Asp.* **2014**, *443*, 195–200.

(6) Gasparac, R.; Kohli, P.; Mota, M. O.; Trofin, L.; Martin, C. R. Template Synthesis of Nano Test Tubes. *Nano Lett.* **2004**, *4*, 513–516.

(7) Hou, S.; Wang, J.; Martin, C. R. Template-Synthesized Protein Nanotubes. *Nano Lett.* **2005**, *5*, 231–234.

(8) Kalaskar, D. M.; Poleunis, C.; Dupont-Gillain, C.; Demoustier-Champagne, S. Elaboration of Nanostructured Biointerfaces with Tunable Degree of Coverage by Protein Nanotubes Using Electrophoretic Deposition. *Biomacromolecules* **2011**, *12*, 4104–4111.

(9) Landoulsi, J.; Roy, C. J. C. J.; Dupont-Gillain, C.; Demoustier-

Champagne, S. Synthesis of Collagen Nanotubes with Highly Regular Dimensions through Membrane-Templated Layer-by-Layer Assembly. *Biomacromolecules* **2009**, *10*, 1021–1024.

(10) Nair, B. G.; Nakano, Y.; Ito, Y.; Abe, H. Transmembrane Molecular Transport through Nanopores Formed by Protein Nanotubes. *Chem. Commun.* **2014**, *50*, 602–604.

(11) Perry, J. L.; Guo, P.; Johnson, S. K.; Mukaibo, H.; Stewart, J. D.; Martin, C. R. Fabrication of Biodegradable Nano Test Tubes by Template Synthesis. *Nanomedicine (Lond).* **2010**, *5*, 1151–1160.

(12) Roy, C. J.; Dupont-Gillain, C.; Demoustier-Champagne, S.; Jonas, a M.; Landoulsi, J. Growth Mechanism of Confined Polyelectrolyte Multilayers in Nanoporous Templates. *Langmuir* **2010**, *26*, 3350–3355.

(13) Roy, C. J.; Chorine, N.; De Geest, B. G.; De Smedt, S.; Jonas, A. M.; Demoustier-Champagne, S. Highly Versatile Approach for Preparing Functional Hybrid Multisegmented Nanotubes and Nanowires. *Chem. Mater.* **2012**, *24*, 1562–1567.

(14) Wang, Y.; Angelatos, A. S.; Caruso, F. Template Synthesis of Nanostructured Materials via Layer-by-Layer Assembly. *Chem. Mater.* **2008**, *20*, 848–858.

(15) Liang, Z.; Susha, A. S.; Yu, A.; Caruso, F. Nanotubes Prepared by Layer-by-Layer Coating of Porous Membrane Templates. *Adv. Mater.* **2003**, *15*, 1849–1853.

(16) Poleunis, C.; Dupont-Gillain, C.; Demoustier-Champagne, S.; Delcorte, A.; Kalaskar, D. Characterisation of Protein Nanotubes by ToF-SIMS Imaging. *Surf. Interface Anal.* **2013**, *45*, 333–337.

(17) Gilbert, J. B.; O'Brien, J. S.; Suresh, H. S.; Cohen, R. E.; Rubner, M. F.; Brien, J. S. O. Orientation-Specific Attachment of Polymeric

Microtubes on Cell Surfaces. *Adv. Mater.* **2013**, *25*, 5948–5952.

(18) Goto, S.; Amano, Y.; Akiyama, M.; Böttcher, C.; Komatsu, T. Gold Nanoparticle Inclusion into Protein Nanotube as a Layered Wall Component. *Langmuir* **2013**, *29*, 14293–14300.

(19) Kato, R.; Komatsu, T. Structure and Photocatalytic Activity of Iron Oxide Nanotubes Prepared from Ferritin. *J. Inorg. Organomet. Polym. Mater.* **2012**, *23*, 167–171.

(20) Komatsu, T. Protein-Based Nanotubes for Biomedical Applications. *Nanoscale* **2012**, *4*, 1910–1918.

(21) Komatsu, T.; Kobayashi, N. Protein Nanotubes Bearing a Magnetite Surface Exterior. *Polym. Adv. Technol.* **2011**, *22*, 1315–1318.

(22) Komatsu, T.; Qu, X.; Ihara, H.; Fujihara, M.; Azuma, H.; Ikeda, H. Virus Trap in Human Serum Albumin Nanotube. *J. Am. Chem. Soc.* **2011**, *133*, 3246–3248.

(23) Komatsu, T.; Sato, T.; Boettcher, C. Human Serum Albumin Nanotubes with Esterase Activity. *Chem. Asian J.* **2012**, *7*, 201–206.

(24) Komatsu, T.; Terada, H.; Kobayashi, N. Protein Nanotubes with an Enzyme Interior Surface. *Chemistry* **2011**, *17*, 1849–1854.

(25) Lu, G.; Komatsu, T.; Tsuchida, E. Artificial Hemoprotein Nanotubes. *Chem. Commun.* **2007**, 2980–2982.

(26) Qu, X.; Kobayashi, N.; Komatsu, T. Solid Nanotubes Comprising Alfa-Fe 2O3 Nanoparticles Prepared from Ferritin Protein. *ACS Nano* **2010**, *4*, 1732–1738.

(27) Qu, X.; Komatsu, T. Molecular Capture in Protein Nanotubes. *ACS Nano* **2010**, *4*, 563–573.

(28) Qu, X.; Lu, G.; Tsuchida, E.; Komatsu, T. Protein Nanotubes Comprised of an Alternate Layer-by-Layer Assembly Using a Polycation as an Electrostatic Glue. *Chemistry* **2008**, *14*, 10303–10308.

(29) Shiraishi, Y.; Akiyama, M.; Sato, T.; Hattori, M.; Komatsu, T. Size-Dependent Dextran Loading in Protein Nanotube with an Interior Wall of Concanavalin A. *Polym. Adv. Technol.* **2014**, *25*, 1247–1251.

(30) Yuge, S.; Akiyama, M.; Komatsu, T. An Escherichia Coli Trap in Human Serum Albumin Microtubes. *Chem. Commun. (Camb).* **2014**, *50*, 9640–9643.

(31) Linder, V.; Gates, B. D.; Ryan, D.; Parviz, B. a; Whitesides, G. M. Water-Soluble Sacrificial Layers for Surface Micromachining. *Small* **2005**, *1*, 730–736.

(32) Hiemenz, P. C.; Lodge, T. P. *Polymer Chemistry, Second Edition*; 2nd ed.; CRC Press: Boca Raton, 2007.

(33) Grosberg, A. Y.; Khokhlov, A. R. *Statistical Physics of Macromolecules*; AIP-Press: New York, 1994.

(34) Mofrad, M. R. K.; Kamm, R. D. *Cytoskeletal Mechanics: Models and Measurements in Cell Mechanics*; Cambridge University Press, 2006.

5 Functionalization of polyelectrolyte multilayer assembled systems with poly(ethylene glycol) chains

This chapter aims for functionalizing the LbL assembled multilayers with antifouling PEG chains. Block and graft polyelectrolyte-PEG copolymers were used both on flat surfaces and inside the pores to incorporate PEG chains in the structure of multilayer films. The presence of PEG chains was analyzed by different characterization methods. An additional alternative method based on direct grafting of PEG chains via covalent bonding was also introduced and the success of grafting was evaluated.

5.1 Introduction

When preparing carriers for drug delivery applications, there is a crucial need to protect the carrier and the cargo from undesired reactions or interactions that may result in degradation of the cargo or elimination of the carrier before its arrival at target destination. For instance, it is known that plasma proteins interact with the surface of carriers directly after their entrance in the body. Such interactions might cause unspecific uptake and removal by the mononuclear phagocytic system, which comprises migrating phagocytes, such as dendritic cells and macrophages. Therefore, reducing the amount of adsorbed protein on the surface of the carrier plays a big role in the stability of drug carriers and will decrease undesirable phagocytosis [1–9].

Highly hydrophilic poly(ethylene glycol) (PEG) has been widely used as a surface modifier that provides antifouling properties which results in reduction of protein and serum adsorption on the surface of drug carriers and ultimately improves their circulation by providing antifouling characteristics to the particle. PEG has low toxicity and is thus a very attractive substance for biomedical applications, although its immunogenicity is increasingly questioned [10–12].

Extensive research has been dedicated to the application of PEG in biomedical engineering. It has been observed both in vitro and in vivo that a dense and strongly attached layer of PEG exhibits low degrees of blood serum and protein adsorption as well as reduction in cell adhesion leading to a reduced risk of thrombus formation [13–15]. It is generally understood that the protein rejecting ability of PEG is due to the fact that PEG is hydrophilic and strongly hydrated, free of charged groups, flexible and mobile which results in steric stabilization [16–19].

One of the most common methods of introducing PEG chains on a target surface involves a controlled covalent coupling of reactive PEG derivatives to anchoring surface groups, or adsorption of surface-active PEG derivatives which consist of PEG molecules coupled to functional groups that have an affinity for the target surface [15,16,20].

Most recently, polyelectrolyte-*g*-PEG graft copolymers have been incorporated in polyelectrolyte multilayer capsules, as a protective shell in order to provide antifouling and stealth properties to LbL assembled capsules. It was observed that the presence of the PEG shell prevented the aggregation of capsules and reduced the inflammatory response as well [21–25]. Incorporation of polyelectrolyte-*b*-PEG block copolymers on the surface of nanoparticles has also been studied and the effect of different parameters such as the blocks length on surface antifouling properties has been investigated [26].

In this study, we aim to functionalize with PEG chains the surface of multilayer LbL assembled flat films as well as the surface of template synthesized LbL assembled nanotubes with PEG chains by different methodologies. Block and graft polyelectrolyte-PEG copolymers are incorporated as the building blocks during the LbL assembly and the presence of PEG chains on the surface is analyzed by different methods. Other grafting methods, such as reacting the surface of LbL assembled flat films or LbL assembled nanotubes with PEG-containing reagents are also studied. In the end, we propose an effective method to functionalize the surface of nanotubes with PEG chains (Figure 5.1). Such PEG-functionalized nanotubes with antifouling properties will be strong candidates for drug delivery applications.

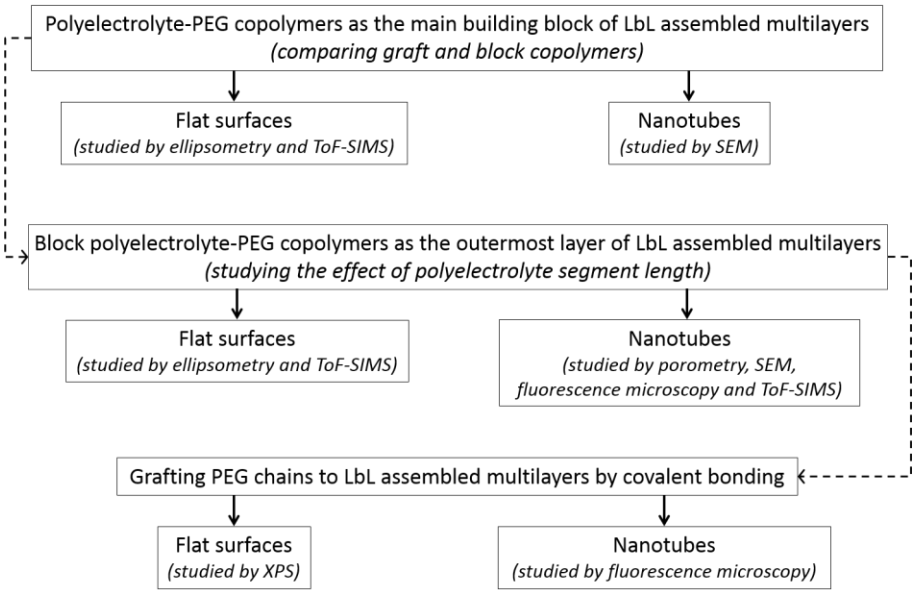

Figure 5.1. A flowchart of the main steps in this chapter.

5.2 Materials and Methods

5.2.1 Materials

Dichloromethane (CH_2Cl_2), chloroform ($CHCl_3$), sodium chloride (NaCl), 2-(N-morpholino) ethanesulfonic acid (MES) monohydrate, 4-(2-hydroxyethyl) piperazine-1-ethane sulfonic acid (HEPES), Polyallylamine hydrochloride (PAH, M_W: 58 kDa), poly(sodium 4-styrenesulfonate) (PSS, M_W: 70 kDa), polyacrylic acid (PAA, M_W: 100 kDa), poly-L-arginine (PLA, M_W > 70 kDa), ovalbumin (OVA, M_W: 45 kDa), poly-L-lysine hydrobromide (PLL, M_W: 30 - 70 kDa), fluorescein isothiocyanate tagged PAH (PAH-FITC, M_W: 15 kDa maximum excitation at 495 nm and a maximum emission at 521 nm) with a monomer to dye ratio of 50:1 were purchased from Sigma Aldrich. Poly-L-lysine (PLL, M_W ~ 20 kDa) grafted with polyethylene glycol (PEG, M_W ~ 2 kDa) (PLL-*g*-PEG) with a grafting ratio of PLL units to PEG chains (PLL : PEG = 3.5) was purchased from SuSoS. Block copolymers of poly-L-lysine hydrochloride (PLL) and polyethylene glycol (PEG, M_W ~ 5 kDa, degree of polymerization (n) = 113) with either a polymerization degree of 10 (PLL_{10}-*b*-PEG, M_W ~ 6.6 kDa) or 50 (PLL_{50}-*b*-PEG, M_W ~ 13 kDa) for the poly-L-lysine block, were purchased from Alamanda Polymers. Methoxyl poly(ethylene glycol) succinimidyl ester (PEG-NHS, M_w = 2 kDa), fluorescein isothiocyanate poly(ethylene glycol) succinimidyl ester (FITC-PEG-NHS) (M_w: 2 kDa, maximum excitation at 495 nm and a maximum emission at 521 nm) was purchased from NANOCS. Milli-Q water with 18.2 MΩ.cm resistivity was used in all experiments. All products were used as received.

Sheets of track-etched polycarbonate membranes were provided by It4ip (Louvain-la-Neuve, Belgium, http://www.it4ip.be) with pore diameters of namely 500 nm. The pore diameter of the PC membrane is not exactly as given by the supplier and a 5-10% variation is observed among the pores. All

membranes had a thickness of 21 µm and a pore density of 10^8 pores.cm^{-2}. Hydrophilic poly(ethylene terephtalate) (PET) membranes with a pore size of 200 nm, thickness of 23 µm and pore density of about 5.10^8 pores.cm^{-2} were provided by It4ip as well.

5.2.2 Fabrication of LbL assembled flat films

All polyelectrolyte solutions were prepared at 1 mg.mL^{-1} concentration.

Flat multilayers composed of polyelectrolytes only

PAH and PSS solutions used to grow PAH/PSS multilayers were prepared in water containing 150 mM NaCl. The PAH and PAA solutions used to grow PAH/PAA multilayers were prepared in 150 mM MES buffer at pH = 5.5. PLA/OVA multilayers were grown in milli-Q water with 150 mM NaCl. PLL polyelectrolyte was also prepared in milli-Q water containing 150 mM NaCl. Optional crosslinking of PAH/PAA nanotubes was carried out by immersing the nanotube-containing PC membrane in a 100 mM MES buffer solution (pH = 5.5) containing 25 mM EDC and 48 mM sulfo-NHS for approximately 24 hours at 4 °C.

Flat multilayers composed of polyelectrolyte-PEG copolymers and a polyanion

Multilayer flat films composed of PLL-PEG copolymers were constructed as follows: PLL-*g*-PEG and PSS solutions were prepared in 150 mM NaCl in milli-Q water to grow PLL-*g*-PEG/PSS multilayers. PLL_{50}-*b*-PEG and PSS solutions were also prepared in 150 mM NaCl in milli-Q water to grow PLL_{50}-*b*-PEG/PSS multilayer.

Flat multilayers composed of polyelectrolytes topped with single a layer of block polyelectrolyte-PEG copolymer (PLL-b-PEG)

Multilayers of PAH/PSS were first fabricated, terminating with the last PSS deposition. PLL-*b*-PEG copolymers with different PLL segment length (PLL_{10}-

b-PEG or PLL_{50}-*b*-PEG) were dissolved in milli-Q water containing 150 mM NaCl. Afterwards, a single layer of PLL-*b*-PEG was deposited on the surface by LbL assembly.

LbL assembly on flat silicon substrate

Single-side polished silicon wafers (Si, <100> orientation, ACM) were cleaned for 20 minutes in piranha solution (H_2SO_4 (98%) / H_2O_2 (32%), 1/1 v/v) before use. The wafers were then rinsed abundantly with milli-Q water and dried. The substrates were then immersed in the polycation solution for 5 minutes, followed by three rinsing steps to ensure the removal of loosely attached polyelectrolyte chains on the surface. The rinsing bath for each system was an aqueous solution of same ionic strength and composition as used for the polyelectrolytes. The three step rinsing process was composed of dipping the substrate for 45 seconds in the first rinsing bath, for 70 seconds in the second rinsing bath and for 30 seconds in the last rinsing bath. Afterwards, the substrate was dipped in the polyanion solution for 5 minutes, followed by similar rinsing steps.

The whole process was cycled until the desired number of layer pairs was obtained. The number of bilayers is shown by an integer (n) in $(polycation/polyanion)_n$. If an additional half cycle is carried out the (n) value would be shown as n+0.5 (example: 3 full cycles of polycation and polyanion deposition by LbL assembly is carried on, followed by 1 additional half cycle of polycation deposition. Therefore, the system would be presented as $(polycation/polyanion)_{3.5}$.)

In the end, samples were abundantly rinsed with milli-Q water to eliminate the salt on their surface and were then dried by nitrogen and stored at room temperature.

5.2.3 Fabrication of LbL assembled nanotubes

All polyelectrolyte solutions were prepared at 1 mg.mL^{-1} concentration.

LbL assembled nanotubes composed of polyelectrolytes only

The PAH and PSS solutions used to grow PAH/PSS multilayers were prepared in milli-Q water containing 150 mM NaCl. The PAH and PAA solutions used to grow PAH/PAA multilayers were prepared in 100 mM acetate buffer at pH = 5.3. The PAH and OVA solutions used to grow PAH/OVA multilayers were prepared in 10 mM HEPES buffer at pH = 8.

LbL assembled nanotubes composed of polyelectrolyte-PEG copolymers and a polyanion

PLL-*g*-PEG, PLL_{50}-*b*-PEG and PSS solutions were prepared in water containing 150 mM NaCl and were used to fabricate (PLL-*g*-PEG/PSS) as well as (PLL-*b*-PEG/PSS) nanotubes.

Core-shell nanotubes composed of a block PLL-b-PEG copolymer shell and a fluorescent polyelectrolyte inner core

Core-shell structured nanotubes were fabricated by forming a shell of PLL-*b*-PEG/PSS on their outer surface with different PLL segment lengths (thus: PLL_{10}-*b*-PEG/PSS or PLL_{50}-*b*-PEG/PSS), then filling the shell with the core material which consists of two layers of PAH and PSS, followed by three layers of PAH-FITC and PSS. This results in the formation of (PLL-*b*-PEG/PSS)$_1$(PAH/PSS)$_2$(PAH-FITC/PSS)$_3$.

LbL assembly within the pores of PC membranes

PC membranes were immersed for 30 minutes in each polyelectrolyte solution followed by an intermediate rinsing step of 5 minutes by immersion in an aqueous solution of same ionic strength and composition as used for the polyelectrolytes. These steps were cycled until the desired number of

bilayers was achieved for all systems. During the LbL process, a polyelectrolyte multilayer crust forms on the top and bottom surfaces of the PC template. This film blocks the access to nanopores, and must thus be removed. Therefore, after every bilayer deposition, the top and bottom surfaces of the PC membranes were gently scrubbed with a cell scraper to eliminate this adherent layer. Optional crosslinking of PAH/PAA nanotubes was carried out by immersing the nanotube-containing PC membrane in a 100 mM MES buffer solution (pH = 5.5) containing 25 mM EDC and 48 mM sulfo-NHS for approximately 24 hours at 4 °C. In the end, all samples were rinsed abundantly with milli-Q water to eliminate buffer salts, and dried and stored at room temperature.

5.2.4 Releasing nanotubes from the template

To release the nanotubes from the template, the PC membrane was dissolved in CH_2Cl_2, resulting in a colloidal suspension of nanotubes and dissolved PC in CH_2Cl_2. The nanotubes were then recovered by filtration of this colloidal suspension over a hydrophilic PET membrane. To maximize the removal of remnant PC, fresh CH_2Cl_2 was flushed through the PET filter for several times.

5.2.5 Grafting PEG chains on the surface of nanotubes

Nanotubes with PAH on their outermost layer were capable of further grafting with PEG-NHS ester reagent since succinimidyl groups react with primary amines, forming amide groups. A PC membrane containing nanotubes was dissolved in solvent (either CH_2Cl_2 or $CHCl_3$) containing 1 $mg.mL^{-1}$ PEG_{2kDa}-NHS ester reagent or 1 $mg.mL^{-1}$ of FITC-PEG_{2kDa}-NHS ester reagent. The suspension was set aside for 24 hours at 4 °C.

5.2.6 Characterization methods

Ellipsometry

The thickness of LbL assembled multilayers on silicon wafers were measured by a spectroscopic ellipsometer (Uvisel, Horiba-Jobin-Yvon) at an incident angle of 70° in a wavelength range from 300 to 800 nm. Measurements were carried out with the analyzer at +45° and -45° (with respect to the plane of incidence) to compensate for systematic errors (imperfections and residual misalignment of optical components [27,28].)

Ellipsometric data were fitted with the DeltaPsi 2 software (Horiba Scientific) in a wavelength range of 550-750 nm based on an optical model consisting of two layers:

3. bulk silicon substrate;
4. homogenous isotropic single layer on top of the substrate.

Since the refractive index of silicon oxide ($n = 1.46$) is close to the refractive index of multilayers ($n \sim 1.45 – 1.55$) at the wavelengths of measurement, the native silicon oxide layer cannot be distinguished from the polyelectrolyte multilayer [28–30]. Therefore, the multilayer thickness was obtained by subtraction of the thickness of the native oxide (determined to be around 1.5 nm from measurements on bare silicon wafer right after cleaning). The complex index of refraction of Si was taken from tabulated data provided by the manufacturer. The complex index of refraction ($n^* = n + i\,k$) of the multilayer film was modeled by a transparent Cauchy layer with $n(\lambda) = A + {}^{B}/_{\lambda^2} + {}^{C}/_{\lambda^4}$ and $k(\lambda) = 0$ with *A*, *B* and *C* as the fitting parameters. To ensure the validity of the data, the goodness of the fit was verified (minimizing the sum of squares, χ^2) and the refractive index was kept between 1.45 and 1.57 (in the wavelength range of 550 - 750 nm) for all

analyzed thin films. All thickness values correspond to an average of five different measurements taken on each sample.

Gas-flow porometry

The average diameter of PC membrane pores before and after nanotubes construction was measured by gas flow porometry at room temperature. Air-dried samples were firmly fixed inside the sample holder with an effective section area of 0.396 cm^2. Nitrogen gas was flown upstream with a pressure ranging from 4 - 10 psi. The gas flow rate (mL/min) downstream from the sample was measured by a flowmeter (Agilent). The inner diameter of the pores was calculated by using Knudsen diffusion and the viscous or Hagen-Poiseuille flow relationship as previously described in Chapter 3.

Time-of-flight secondary ion mass spectroscopy (ToF-SIMS)

Chemical characterization and imaging of flat multilayers as well as nanotubes were carried out by using ToF-SIMS. An Ion-TOF ToF-SIMS V instrument (IONTOF, GmbH, Münster, Germany) was used. To analyze flat multilayers, a silicon substrate with LbL assembled multilayer flat films deposited on its surface was mounted on the sample holder. To analyze nanotubes, a few drops of nanotube suspension was dropped on the silicon substrate and the silicon substrate was again mounted on the sample holder.

A bismuth cluster (Bi_3^+ or Bi_5^+) liquid metal ion source was used to produce a primary ion beam using an acceleration voltage of 60 keV or 30 keV to obtain SIMS images and spectra respectively. An AC target current of 0.43 pA was used with a bunched pulse width of less than 1.4 ns. Both positive and negative secondary ions species were analyzed. For imaging, a raster of 256 × 256 data points over an area of 100 × 100 μm^2 was used. The total ion beam dose for each analyzed area was always kept below 10^{12} $ions.cm^{-2}$, ensuring static conditions. Two different surface areas were analyzed for each sample.

All data analysis was carried out using the software supplied by the instrument manufacturer, SurfaceLab (version 6.1).

Mass spectral data of multilayer flat films were processed and quantified by calculating the area below the spectral peak of each particular compound of interest and dividing it by the summed area of all the assigned peaks, yielding a so-called relative intensity, specific to this substance of interest (5.1).

$$\text{Relative intensity of x } (\%) = \frac{\text{area under the peak of the x component}}{\sum \text{area of each assigned peak}} \times 100 \quad (5.1)$$

X-ray photoelectron spectroscopy (XPS)

XPS analyses were performed on a Kratos Axis Ultra spectrometer (Kratos Analytical – Manchester – UK) equipped with a monochromatized aluminum X-ray source (powered at 10 mA and 15 kV). The samples were fixed on a standard stainless steel multispecimen holder by using a piece of double sided insulating tape. The pressure in the analysis chamber was about 10^{-6} Pa. The angle between the normal to the sample surface and the direction of photoelectrons collection was about 0°. Analysis was performed in the hybrid lens mode with the slot aperture, so that the resulting analyzed area was 700 µm x 300 µm. The pass energy was set at 160 eV for the survey scan and 40 eV for narrow scans. In the latter conditions, the full width at half maximum (FWHM) of the Ag 3d5/2 peak of a standard silver sample was about 0.9 eV.

Charge stabilization was achieved by using the Kratos Axis device. The following sequence of spectra was recorded: survey spectrum, C 1s, O 1s, N 1s, Si 2p and C 1s again to check for charge stability as a function of time and the absence of degradation of the sample during the analyses.

The data treatment is performed with CasaXPS software (Casa Software Ltd., UK). The peaks are decomposed using a linear baseline and a component shape is defined by the product of a Gauss and Lorentz function, in 70:30 ratio respectively. The C-(C,H) component of the C1s peak of carbon has been fixed to 284.8 eV to set the binding energy scale. In Table 5.1, binding energy of carbon and nitrogen elements in chemical functions is reported (reproduced from Genet et al. [31]).

Table 5.1. Binding energy of carbon and nitrogen in chemical functions of biochemical compounds.

Element and function	Position (ev)	Compound of reference
Carbon		
C-(C,H)	284.8	Hydrocarbon, adventitious contamination
C-N, (C=O)-N-**C**	286.1	Amine; amide, peptidic link
C-O	286.3	Alcohol
(C=O)-O-**C**	286.8	Ester
C=O, O-**C**-O	287.8	Aldehyde, (hemi)acetal
(**C**=O)-N-C, O=**C**-O^-	288.0	Amide, peptidic link; carboxylate
(**C**=O)-O-C	289.0	Ester
(**C**=O)-OH	289.0	Carboxylic acid
Nitrogen		
C-**N**H_2	399.3	Amine
(C=O)-**N**H	399.8	Amide, peptidic link
C-**N**H_3^+	401.3	Protonated amine

SEM observations

Samples were observed with a field emission scanning electron microscope (JSM-7600F, JEOL Ltd.), equipped with a transmission detector. SEM

measurements were performed at 15 keV for the scanning mode and 30 keV for the scanning transmission mode.

For SEM imaging, the CH_2Cl_2 or aqueous suspension of nano-objects was filtered through a PET filter coated with a 20 nm layer of gold.

Fluorescence microscopy

The suspension of fluorescent-tagged nanotubes was filtered through a PET filter for epi-fluorescence optical microscopy. Fluorescence images were obtained by an Olympus IX2 inverted epi- microscope equipped with a FITC filter set.

5.3 Results and Discussion

5.3.1 Using polyelectrolyte-PEG copolymers as LbL assembly building blocks

Graft (PLL-*g*-PEG) and diblock (PLL_{50}-*b*-PEG) polyelectrolyte-PEG copolymers were used as building blocks during LbL assembly of multilayered flat films. The polyelectrolyte block (PLL) plays the role of polycation during the assembly and PEG chains are directly incorporated in the structure of the multilayered film. Since PSS is a strong polyacid, it is chosen as polyanion in order to provide negative charges and increase the probability of LbL assembly.

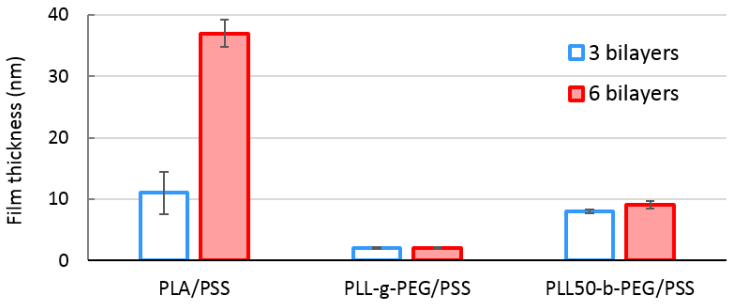

Figure 5.2. Dried film thickness of multilayer assembled films after 3 (left columns) and 6 (right columns) bilayers deposition on silicon substrates.

The growth of multilayer assembled films containing polyelectrolyte-PEG copolymers as polycation was studied by ellipsometry and is shown in Figure 5.2. The growth of such systems is compared with the growth of simple multilayered system composed of a model polyamino acid (PLA) and PSS. It is observed that the (PLA/PSS) system grows when increasing the number deposited bilayers. In contrast, there is almost no build-up for the (PLL-*g*-PEG/PSS) system. At the same time, the (PLL_{50}-*b*-PEG/PSS) system grows during the very first bilayers deposition and then the growth is

stopped after 3 bilayers. This is probably due to the structure of the copolymers. When using the graft copolymer in the structure, the polycationic backbone interacts with the negative charged surface of the silicon substrate, and the grafted PEG chains accumulate at the water interface. Since the assembly is carried on in aqueous medium, PEG chains are highly hydrated and prevent PSS from reaching the PLL segments, thereby inhibiting their further interactions. The diblock PLL_{50}-*b*-PEG polyelectrolyte interacts rather differently since the PEG chains are less densely packed. The PLL block adsorbs on the silicon substrate and the PEG blocks incompletely cover the surface. During the assembly of the very first bilayers, the PSS chains are thus, able to interact with the incompletely shielded PLL block and multilayers are formed. However, by increasing the number of bilayers the density of PEG chains available on the surface is increased. These PEG chains progressively cause a steric barrier and prevent further growth of the multilayers. Therefore, the growth is eventually stopped.

Multilayer flat films consisting of polyelectrolyte-PEG copolymers were constructed over silicon substrates. Six bilayers were deposited to fabricate the typical system and to have the copolymer as top layer, an additional half cycle of polycation deposition was carried on as well. The flat films were analyzed by ToF-SIIMS in order to define the chemical composition of their surface.

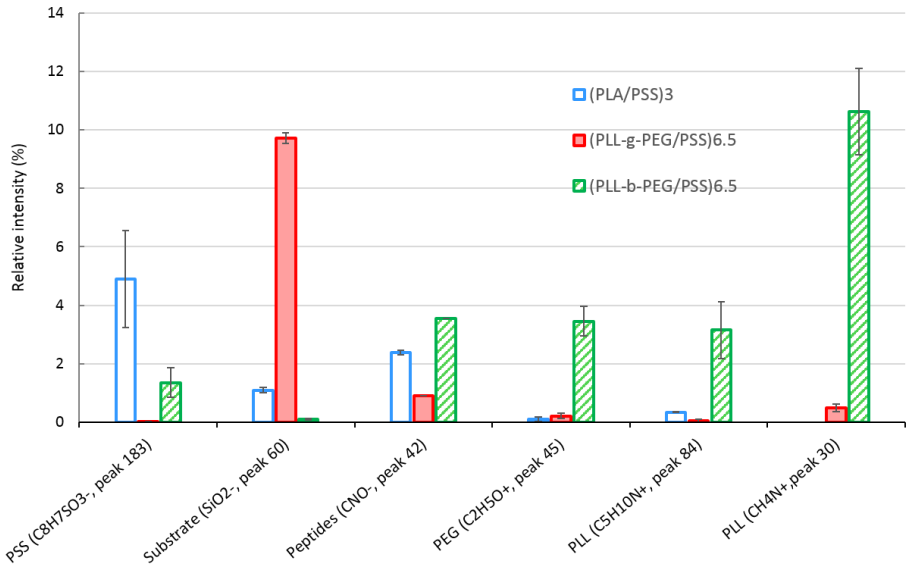

Figure 5.3. Relative intensities of characteristic ToF-SIMS peaks for (left columns) $(PLA/PSS)_3$, (middle columns) $(PLL\text{-}g\text{-}PEG/PSS)_{6.5}$, (right columns) $(PLL_{50}\text{-}b\text{-}PEG/PSS)_{6.5}$ multilayer assembled films deposited on flat silicon substrate.

Relative intensities of characteristic ToF-SIMS peaks for different systems are shown in Figure 5.3. The (PLA/PSS) system presents a noticeable signal for PSS and a smaller signal for peptides, which is related to PLA. It must be noted that SIMS signals are not directly proportional to the composition. (PLL-*g*-PEG/PSS) system has almost no signal related to the building blocks and presents a high signal related to the substrate. These results are in accordance with previous ellipsometry results and prove that there is practically no deposition for (PLL-*g*-PEG/PSS) system. The (PLL_{50}-*b*-PEG/PSS) system has high intensity peaks related to PLL and PEG as well, while the substrate signal is nearly zero, proving the proper deposition of multilayers on the surface. It should be noted that the PSS signal is rather low for this

system, which could be an indication of the presence of PLL_{50}-*b*-PEG as topmost layer in comparison to the (PLA/PSS) multilayers.

Multilayer LBL assembled nanotubes containing graft and block polyelectrolyte-PEG copolymers were fabricated within the pores of a PC membrane. The nanotubes were then released and collected by dissolving the membrane in CH_2Cl_2 and filtering the suspension over a PET filter. The build-up of those nanotubes was compared with the model system $(PLA/PSS)_6$.

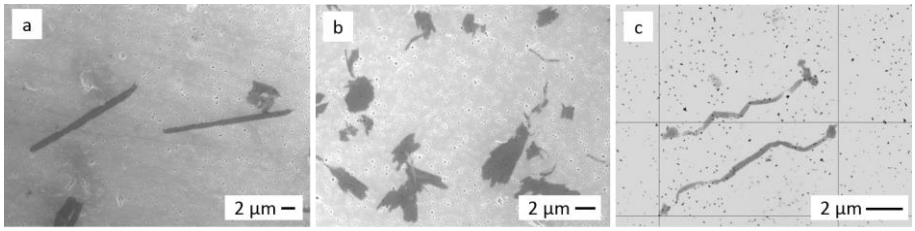

Figure 5.4. SEM images of (a) $(PLA/PSS)_6$, (b) $(PLL\text{-}g\text{-}PEG/PSS)_6$, $(PLL_{50}\text{-}b\text{-}PEG/PSS)_6$ nanotubes on a PET filter.

Figure 5.4 shows SEM images of LbL assembled nanotubes. It is observed that $(PLA/PSS)_6$ nanotubes are properly formed and have a length (~ 20 µm) that corresponds to the thickness of the PC membrane. In contrast, no nanotubes are observed for $(PLL\text{-}g\text{-}PEG/PSS)_6$. Only some patches of matter are found here and there. $(PLL_{50}\text{-}b\text{-}PEG/PSS)_6$ nanotubes are formed within the pores of the PC membrane, however, the nanotubes are rather short (~ 10-15 µm) and seem to have broken into smaller pieces. In addition, they are less rigid compared to (PLA/PSS) nanotubes.

Overall, one can conclude that graft PLL-*g*-PEG copolymer is not incorporated in the structure of the nanotubes or that the first deposited layer of PLL-*g*-PEG is so effectively preventing adsorption that further growth of the

nanotubes is no more possible; this system was thus left aside and no more studied.

Further investigations were carried on for block PLL-*b*-PEG systems with different polyelectrolyte segment length. To this aim, a new system composed of a synthetic (PAH/PSS) core was topped with 1 monolayer of block PLL-*b*-PEG copolymer. The length of the PEG segment was kept constant (113 repeating PEG units) while the length of the PLL segment was varied (10 repeating units vs. 50 repeating units). The thicknesses of these systems were measured by ellipsometry and are reported in Table 5.2.

Table 5.2. Comparing the thickness of multilayered flat films of (PAH/PSS) topped with a monolayer of (PLL-b-PEG) with different PLL segment lengths.

Core system	**No layer on top**	**Topped with**	
		PLL_{10}-b-PEG	PLL_{50}-b-PEG
$(PAH/PSS)_3$	14 nm	18 nm	15 nm
$(PAH/PSS)_6$	35 nm	42 nm	37 nm

According to Table 5.2 deposition of a monolayer of block PLL-*b*-PEG copolymer on (PAH/PSS) multilayers, does not change the thickness drastically. This is acceptable, since there are only 113 repeating units of PEG that will have a length of maximum 5 nm in their very most extremely extended condition.

The surface of the fabricated systems was probed by ToF-SIMS, to verify their chemical composition (Figure 5.5). By comparing ToF-SIMS relative intensities obtained for $(PAH/PSS)_3$ system topped with PLL_{10}-*b*-PEG and

PLL_{50}-*b*-PEG, it is observed that the signals of PSS, substrate and peptides is nearly the same for both cases.

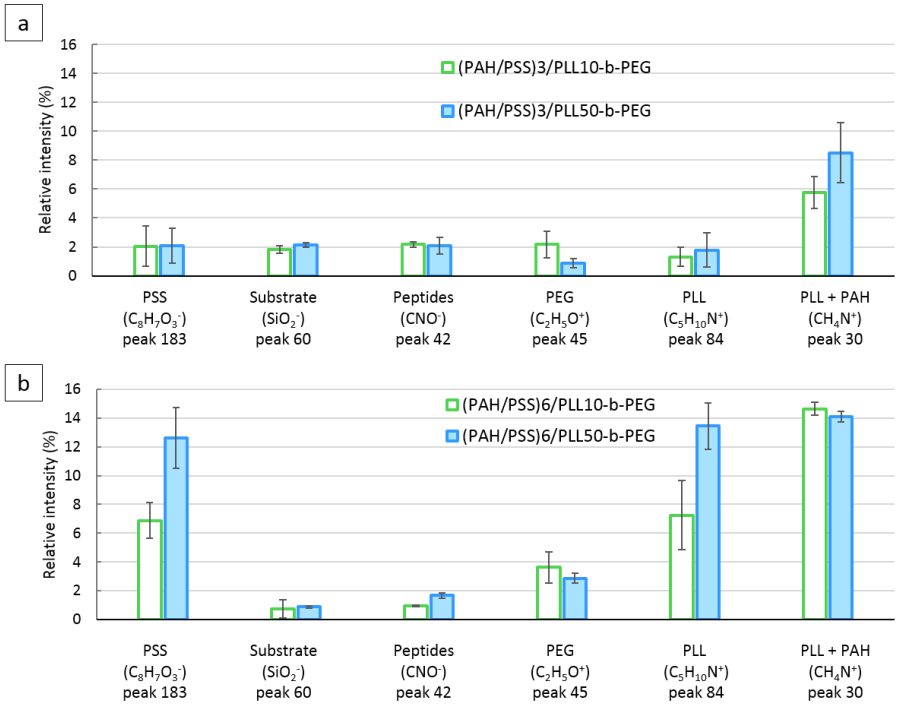

Figure 5.5. Relative intensities of characteristic ToF-SIMS peaks for multilayer assembled films deposited on flat silicon substrates, (a) comparing $(PAH/PSS)_3/PLL_{10}$-*b*-PEG (left columns) with $(PAH/PSS)_3/PLL_{50}$-*b*-PEG (right columns), (b) comparing $(PAH/PSS)_6/PLL_{10}$-*b*-PEG (left columns) with $(PAH/PSS)_6/PLL_{50}$-*b*-PEG (right columns).

Moving forward to thicker systems composed of $(PAH/PSS)_6$, PSS and PLL+PAH signals are strongly increased while substrate signal is decreased. This can be directly related to the effect of increased number of bilayers, since a higher amount of PSS and PAH is present in the structure and the substrate signal is masked by thicker multilayers. Both systems composed of $(PAH/PSS)_6$ topped with PLL-*b*-PEG copolymer show a high signal for PLL with

high error bars. PLL_{50}-*b*-PEG topped system has a higher PLL signal compared to PLL_{10}-*b*-PEG topped system; this is due to the increased length of the PLL block in PLL_{50}-*b*-PEG. Logically, the PLL_{10}-*b*-PEG system presents a higher signal for PEG.

In order to obtain multilayered nanotubes with the PEG chains on their surface and a fluorescent component inside their structure, it was decided to opt for a core-shell structure during the assembly within the pores of PC membrane. The outer shell contains the block polyelectrolyte-PEG copolymer while the core contains a fluorescently tagged polyelectrolyte.

Nanotubes with a core-shell structure composed of either a (PLL_{10}-*b*-PEG/PSS) or (PLL_{50}-*b*-PEG) outer shell and a $(PAH/PSS)_2(PAH\text{-}FITC/PSS)_3$ inner core were fabricated by LbL assembly within the pores of PC membranes. The dry wall thickness of the nanotubes was measured by gas-flow porometry and is reported in Table 5.3. Nanotubes were released and collected by dissolving the PC membrane in CH_2Cl_2 and filtering the suspension through a PET filter (Figure 5.6).

Table 5.3. A summary of core-shell nanotubes and their dry wall thickness measured by gas-flow porometry.

Outer shell	Inner core	Dry wall thickness d_{wall} (nm)
$(PLL_{10}$-b-PEG/PSS$)_1$	$(PAH/PSS)_2/(PAH\text{-}FITC/PSS)_3$	45
$(PLL_{50}$-b-PEG/PSS$)_1$		42

Figure 5.6 shows both epi-fluorescent microscopy and SEM images of core-shell nanotubes composed of PLL-b-PEG copolymers with PLL segments of

different length (10, 50). As observed from Figure 5.6.a and Figure 5.6.b, when a short PLL block (PLL_{10}-*b*-PEG) is used during the assembly, the nanotubes are poorly formed. They do not keep their tubular shape and break into smaller pieces. In contrast, when a long PLL block (PLL_{50}-*b*-PEG) is incorporated during the assembly, the nanotubes hold their tubular structure and their length corresponds to the template thickness (Figure 5.6.c, Figure 5.6.d). In both cases, the nanotubes have a proper fluorescent signal all along the tubes. This indicates that fluorescently tagged polyelectrolytes were able to diffuse through the pores of the PC membrane and those pores were not blocked before incorporating the fluorescent material.

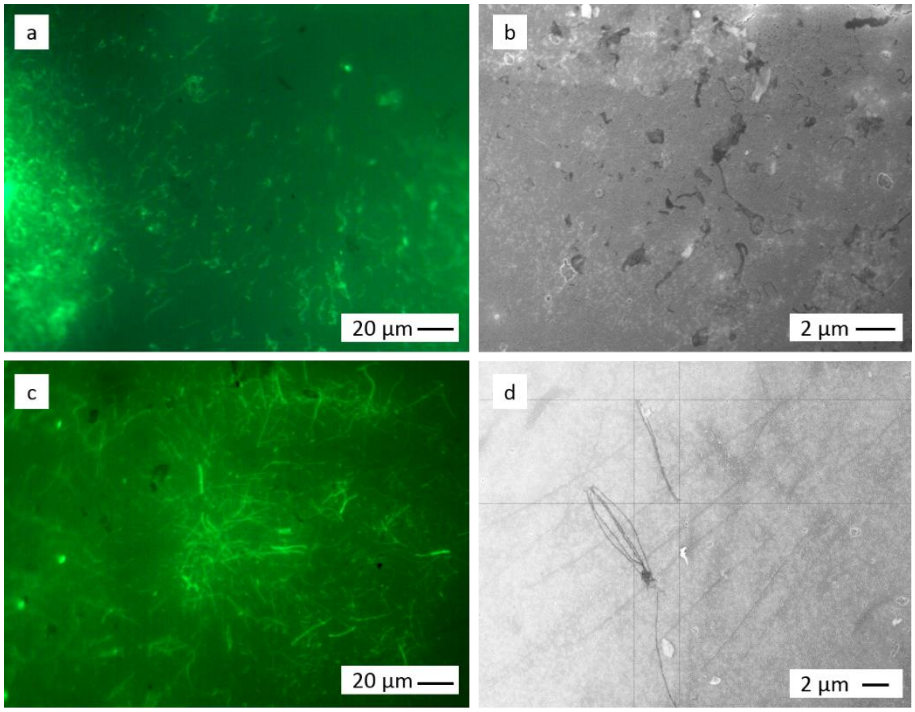

Figure 5.6. left columns (a,c) epi-fluorescent microscopy images of nanotubes filtered over a PET filter, right columns (b,d) SEM images of nanotubes filtered over a metallized PET filter, (a,b) $(PLL_{10}$-*b*-PEG/PSS$)_1$/(PAH/PSS$)_2$/(PAH-FITC/PSS$)_3$, (c,d) $(PLL_{50}$-*b*-PEG/PSS$)_1$/(PAH/PSS$)_2$/(PAH-FITC/PSS$)_3$.

To determine whether PEG chains are available on the surface of the nanotubes, their surface was analyzed by ToF-SIMS in imaging mode. Core-shell nanotubes were released from the PC membrane after dissolving the membrane in CH_2Cl_2. Next, a single drop of obtained suspension was cast over a silicon substrate. Silicon substrates with nanotube deposited on top were probed by ToF-SIMS afterwards (Figure 5.7 and Figure 5.8, for PLL_{10}-*b*-PEG and PLL_{50}-*b*-PEG, respectively.)

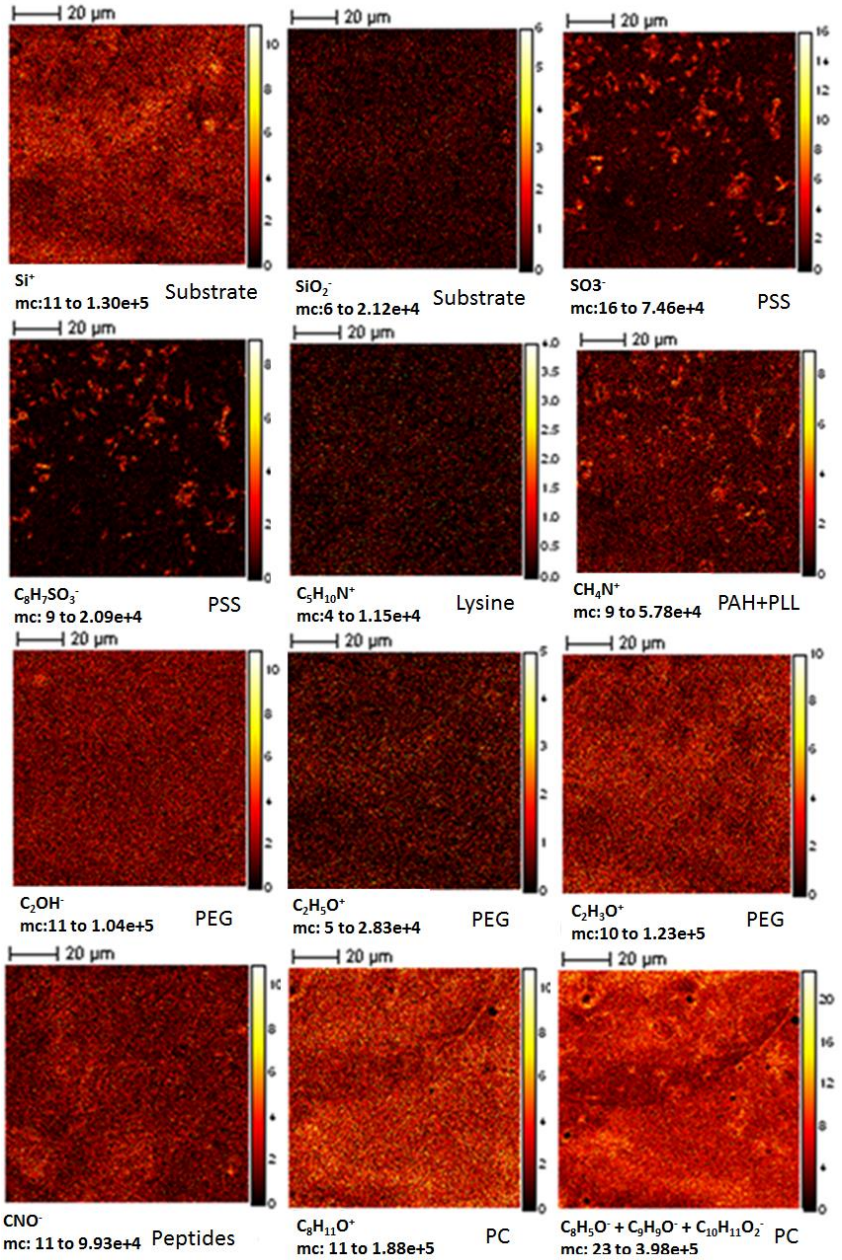

Figure 5.7. ToF-SIMS images (field of view 100 µm^2) of silicon substrate with $(PLL_{10}$-*b*-PEG/PSS$)_1$/$(PAH/PSS)_2$/$(PAH\text{-}FITC/PSS)_3$ nanotubes deposited on top. The scale at the right of each image is from dark (low counts) to bright (high counts). Each image belongs to a specific chemical composition signal (noted below each image on the left) which corresponds to building components of nanotubes (noted below each image on the right).

In Figure 5.7 broken nanotubes are spotted by their strong PSS signal and their PAH+PLL (CH_4N^+) signal as well. However, there is no significant signal for lysine while the PEG signal is not localized on the nanotubes and is found over the surface. This means that strong (CH_4N^+) signal only belongs to PAH, and PLL_{10}-b-PEG is not incorporated in the nanotubes structure. Combined image of negative ion peaks of PC ($C_8H_5O^-$, $C_9H_9O^-$,$C_{14}H_{11}O_2^-$) and positive ion peak of PC ($C_8H_{11}O^+$) show the presence of PC on the surface. This is due to the sample preparation since a drop of nanotubes and dissolved PC suspension in CH_2Cl_2 was dropped over the silicon substrate.

In Figure 5.8 well-formed and unbroken nanotubes are spotted either by negative signals on the substrate or their strong PSS signals. Some signals belonging to PAH+PLL (CH_4N^+) are also available. A weak signal for lysine is found over the nanotubes. In addition, although ($C_2H_5O^+$ and $C_2H_3O^+$) signals for PEG are rather noisy and spread over the whole image, the C_2OH^- signal is stronger over the nanotubes, indicating that PEG blocks are indeed present on the nanotubes surface, albeit to a limited extent.

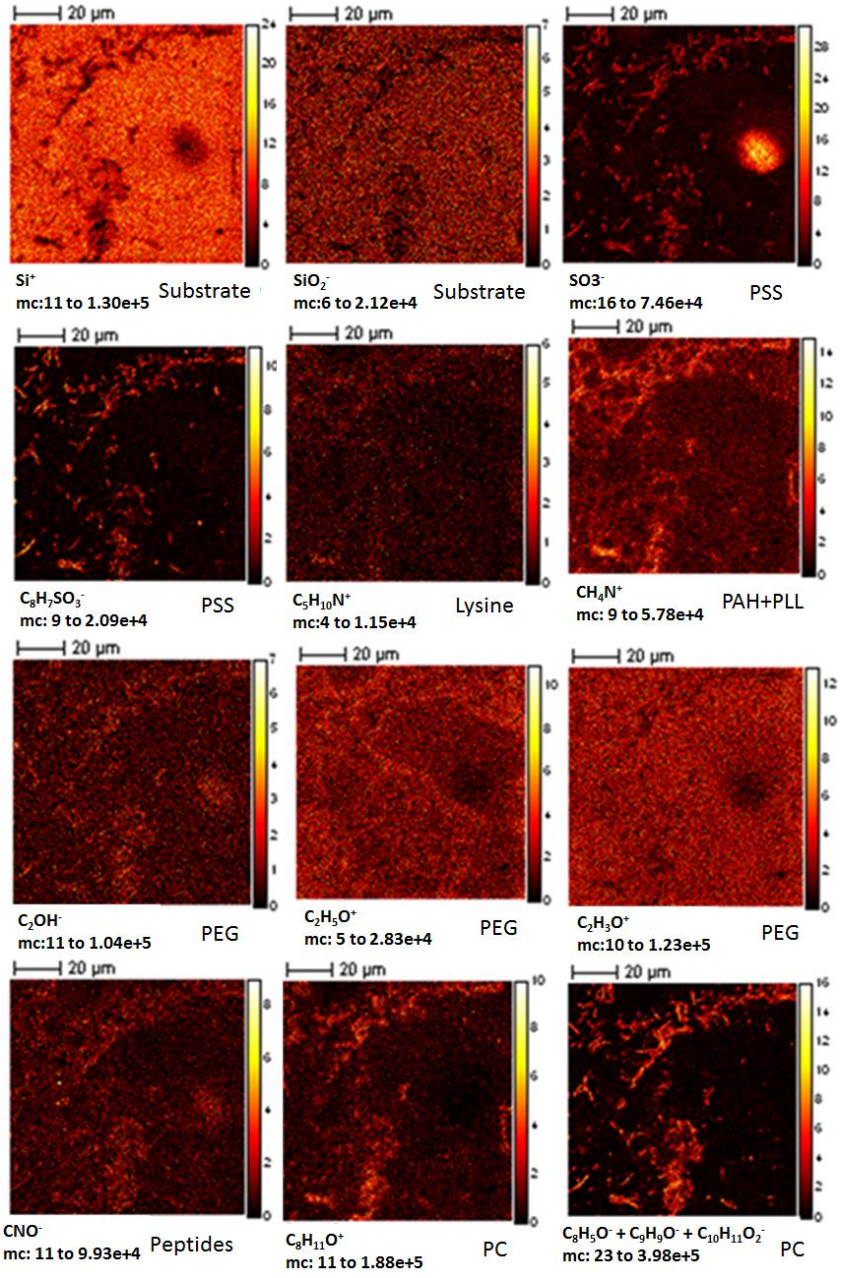

Figure 5.8. ToF-SIMS images (field of view 100 µm^2) of silicon substrate with $(PLL_{50}\text{-b-PEG/PSS})_1/(PAH/PSS)_2/(PAH\text{-FITC/PSS})_3$ nanotubes deposited on top. The scale at the right of each image is from dark (low counts) to bright (high counts). Each image belongs to a specific chemical composition signal (noted below each image on the left) which corresponds to building components of nanotubes (noted below each image on the right).

Considering ToF-SIMS images of nanotubes, one can deduce that there is no PLL-b-PEG shell as the outer layer of nanotubes when the PLL sequence is short, while some PEG is present for the longer PEG block. Previous ToF-SIMS analysis showed that PLL-*b*-PEG interacts with negative charged surface of silicon wafer (Figure 5.5); in addition, there is a noteworthy morphologies difference between nanotubes fabricated after deposition of PLL_{10}-b-PEG and PLL_{50}-b-PEG layer within the pores for PC membrane (Figure 5.6).

A hypothesis is proposed based on the effect of PLL segment size over the configuration of the PEG brush. It has been previously shown that by assembling PLL-*b*-PEG copolymers on spherical nanoparticles, a dense brush of PEG is obtained for short PLL blocks, whereas PEG chains adopt a "mushroom" conformation for larger PLL blocks [32]. Taking this information into account, one can assume that the PLL segment of the block copolymer interacts with the PC membrane and that the PEG segments adopt a different configuration depending on the size of the PLL segment. For both PLL_{10}-*b*-PEG and PLL_{50}-*b*-PEG, PEG chains are extended towards the center of the pore. These chains do not inhibit the diffusion of other polyelectrolytes inside the pores; however, they affect the interaction of diffused PSS with PLL. Those chains block the access to the PLL segment and therefore, there is no interaction between the newly arrived PSS polyelectrolytes and PLL, and thus, a little presence of PLL-*b*-PEG in the structure of nanotubes. For PLL_{10}-*b*-PEG nanotubes, since a dense brush of PEG chains is formed inside the pores, the newly diffused core polyelectrolytes accumulate inside the pores and interact with each other. This results in formation of broken and deformed pieces of fluorescent nanotubes (Figure 5.6.a, Figure 5.6.b). Upon dissolution of the membrane, the PLL_{10}-*b*-PEG brush layer is dissolved and spreads over the whole substrate, providing a homogenous SIMS signal for

the whole image (Figure 5.7). A schematic representation of this hypothesis in demonstrated in Figure 5.9.a.

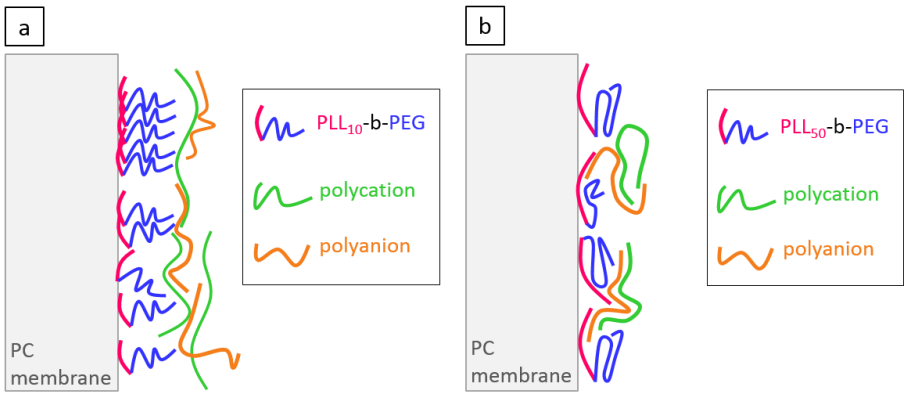

Figure 5.9. . A schematic representation of polyelectrolytes interactions within the pores of a PC membrane (only one side of a pore is illustrated), (a) after deposition of a PLL_{10}-b-PEG monolayer inside the pores, (b) after deposition of a PLL_{50}-b-PEG monolayer inside the pores.

In case of PLL_{50}-b-PEG, it could be assumed that here again PLL block interacts with PC, while PEG chains adopt a "mushroom" conformation, which is less extended towards the center of the PC membrane. Therefore, newly diffused polyelectrolytes can diffuse all through the pores and have a higher chance of forming tubular shaped structures and to complex with the less shielded PLL block (Figure 5.9.b). As observed in Figure 5.6.c and Figure 5.6.d, fluorescent nanotubes were thus successfully formed within the pores of the PC membrane and held their tubular structure after being released from PC membrane. In addition, some PLL_{50}-*b*-PEG chains are incorporated in the structure of tubes as was detected by ToF-SIMS (Figure 5.8).

These nanotubes show that the LbL process strongly depends on the history of the deposition procedure, and this therefore, kinetically controlled. If the copolymer layer is adsorbed first, it will organize so to oppose the formation

of next layers as seen for nanotubes. In contrast, when the copolymer is deposited at the ends of the process, it will make a nice brush layer, as ween for flat multilayers.

Since our previous strategy to fabricate core-shell nanotubes by incorporating PEG-polyelectrolyte copolymers as building block was not successful, it was decided to aim for direct grafting PEG chains on nanotube surface after their fabrication.

5.3.2 Grafting PEG chain by covalent bonding

N-hydroxylsuccinimide (NHS) functionalized polyethylene glycol (PEG-NHS) is an amino reactive PEG derivative that can be used to functionalize any surface with primary amine groups. The reaction between PEG-NHS and primary amines is shown in Figure 5.10.

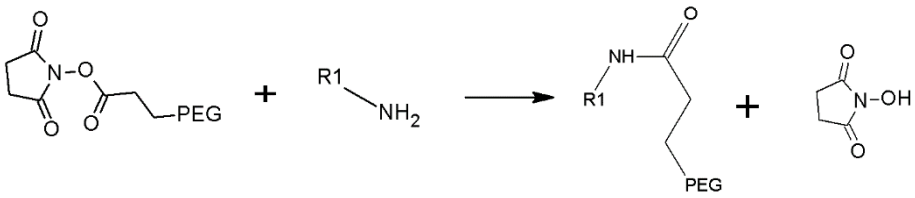

Figure 5.10. The reaction scheme of PEG-NHS with a primary amine, which results in the formation of amide bonds and the conjugation of PEG chain to the amine.

NHS-PEG is soluble in aqueous solutions as well as organic solvents such as chloroform ($CHCl_3$) or dichloromethane (CH_2Cl_2). Therefore, it has a high potential to be used for grafting PEG chains on the amine-bearing surface of multilayer LbL assembled films.

Polyelectrolytes such as PAH and PLL both contain primary amines in their structure, and thus an attempt was made to build multilayer LbL assembled flat films with PAH (or PLL) polyelectrolytes as the uppermost layer, and to

graft PEG chains on their surface by reacting PEG_{2kDa}-NHS with their primary amine groups in organic solvents ($CHCl_3$ or CH_2Cl_2).

Since the length of the PEG segment in (PEG_{2kDa}-NHS) is not very long, no significant changes in the thickness of PEG grafted surfaces is observed by ellipsometry measurements. Therefore, XPS was used to characterize the surface of PEG grafted multilayer flat films to determine whether the grafting reaction has taken place.

Four samples of $(PAH/PSS)_{6.5}$ multilayer flat films were fabricated over silicon substrates. One of them was kept aside, the second sample was only immersed in CH_2Cl_2 for 24 hours at 4 °C, while the third and the fourth samples were reacted with PEG_{2kDa}-NHS in $CHCl_3$ and CH_2Cl_2, respectively (Figure 5.11).

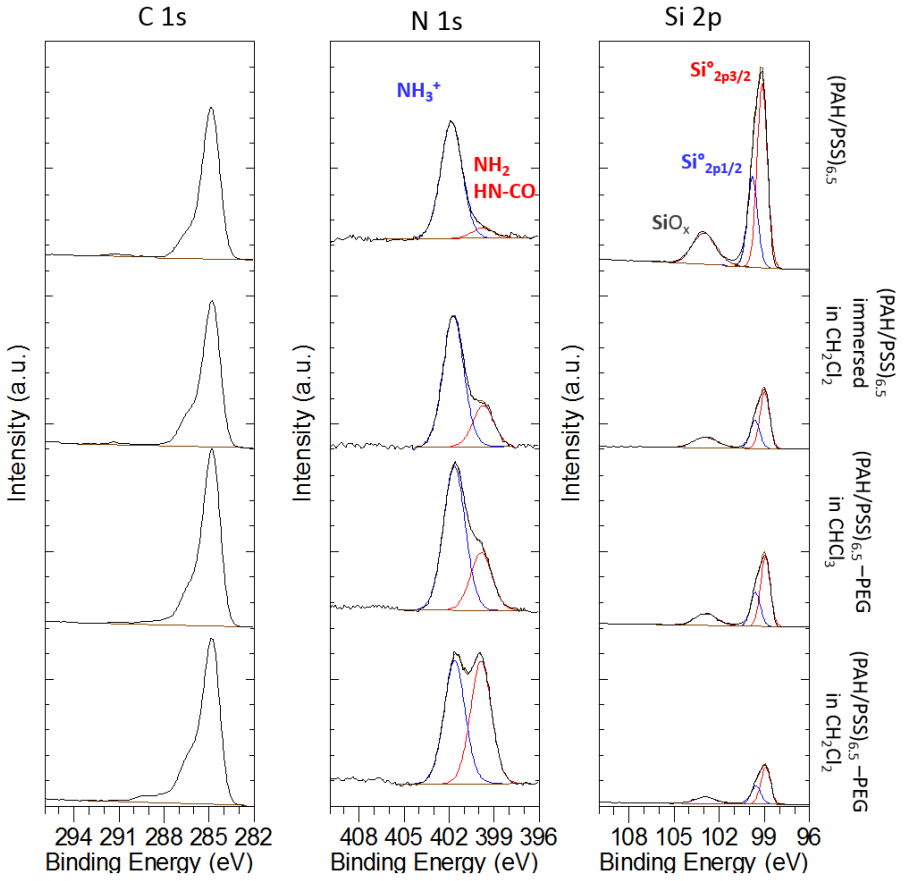

Figure 5.11. C 1s, N 1s and Si 2p peaks, recorded by XPS for different systems, (1st row) $(PAH/PSS)_{6.5}$, (2nd row) $(PAH/PSS)_{6.5}$ only immersed in CH_2Cl_2, (3rd row) PEG grafted $(PAH/PSS)_{6.5}$ in $CHCl_3$, (4th row) PEG grafted $(PAH/PSS)_{6.5}$ in CH_2Cl_2.

Figure 5.11 shows sections of XPS spectra that belong to the main elements of multilayer flat films structures (C 1s, and N 1s); the peaks for the silicon substrate (Si 2p) are presented as well. For C 1s there is no large difference among non-grafted and grafted systems. However, a change is observed in N 1s peaks between different systems. The blue peak (with a binding energy of 401.8 eV) belongs to protonated amines (NH_3^+, from PAH), and the red peak on the right (with a binding energy of 399.8 eV) belongs to unprotonated

nitrogen from amine or amide bonds (NH_2 or HNCO). Unprotonated amine bonds may exist within the structure of multilayers (PAH) and amide bonds are formed due to the PEG grafting reaction. Non-grafted $(PAH/PSS)_{6.5}$ multilayers have a low amount of NH_2 and HNCO groups. However, the amount of these groups increases when the sample is immersed in CH_2Cl_2. The amount of unprotonated nitrogen is also increased after grafting PEG chains on the surface. One can observe that there is a higher amount of unprotonated nitrogen when the grafting is carried out in CH_2Cl_2.

When $(PAH/PSS)_{6.5}$ multilayers come in contact with CH_2Cl_2, the protonation degree of PAH is slightly modified. Such a change in polyelectrolytes ionization degree upon immersion in an aqueous solution has been previously observed by other groups, resulting in partial reconfiguration of the films [33]. Here, the change of protonation is due to the immersion in the organic solvent, presumably affecting the proton equilibrium. Because of the resulting change in charge balance within the film, interactions between PAH and PSS layers may also change and thus, the multilayers undergo a re-configuration. This perturbation in turn affects the silicon signal perceived in XPS. As observed, the Si 2p signal is decreased when multilayers are immersed in CH_2Cl_2. The amount of unprotonated nitrogen for the samples that were grafted with PEG in $CHCl_3$ is almost close to that of non-grafted samples that were only immersed in CH_2Cl_2. The silicon signal is also similar and thus, it is not clear if the grafting has been successful. However, the significant increase in the signal of unprotonated nitrogen for PEG grafted multilayers in CH_2Cl_2 compared to multilayers simply immersed in CH2Cl2, shows that grafting has been successful and amide bonds are formed upon grafting. The presence of grafted matter on the surface is also confirmed since the Si 2p signal is even more decreased for this system. This shows that

indeed some matter is deposited on the surface, which results in increasing the thickness of the layer and masking of the surface signal.

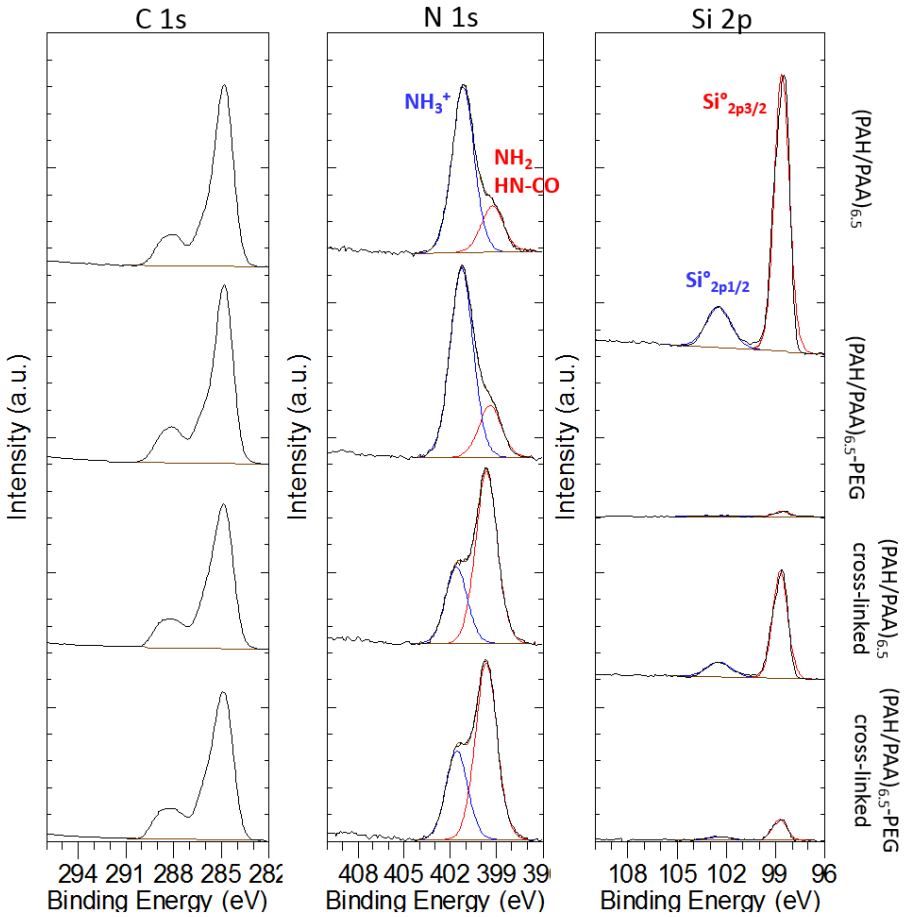

Figure 5.12. C 1s, N 1s and Si 2p peaks, recorded by XPS for different systems, (1st row) $(PAH/PAA)_{6.5}$, (2nd row) PEG grafted $(PAH/PAA)_{6.5}$, (3rd row) crosslinked $(PAH/PAA)_{6.5}$, (4th row) crosslinked and PEG grafted $(PAH/PAA)_{6.5}$.

To study the grafting of multilayers composed of PAH and PAA, flat multilayers of (PAH/PAA) were deposited over silicon substrate. (PAH/PAA) is an interesting system since it can be crosslinked all through the multilayer structure (reacting COOH groups of PAA with NH_2 groups of PAH). In addition,

by terminating the assembly with PAH, primary amines are available on the film surface for further grafting with PEG-NHS.

Figure 5.12 shows XPS recorded C 1s, N 1s and Si 2p peaks for different systems all based on (PAH/PAA). Here again, no significant difference is observed for C 1s peaks. However, there is an increase in unprotonated nitrogen signal for crosslinked samples. This is due to formation of amide bonds as a result of the crosslinking process. However, no significant changes are observed for the N 1s signal prior and after PEG grafting for crosslinked and non-crosslinked systems.

Nevertheless, there is a drastic decrease in the substrate Si 2p signal after grafting PEG over crosslinked and non-crosslinked systems. This can either be attributed to the presence of PEG chains on the surface or can be simply due to changes in multilayers configuration upon immersion in solvent. This possible reconfiguration upon immersion in CH_2Cl_2 prevents us from deciding whether grafting occurred over the non-crosslinked multilayers. However, such a reconfiguration is very unlikely for the crosslinked system, which thus suggests that the decrease of the Si signal would be due to PEG grafting.

To study the effect of PEG grafting on biological (PLA/OVA) system, flat multilayers of (PLA/OVA) topped with primary amine-bearing PLL were prepared and reacted with PEG-NHS in $CHCl_3$ and CH_2Cl_2. However, no significant difference in the elemental peaks was observed (results are not shown). $(PLA/OVA)_6$/PLL systems had a high amount of unprotonated nitrogen (NH_2 or HNCO) which is mainly due to the high amount of amide bonds in OVA. In addition, there was no change in silicon substrate (Si 2p) signal as well. Therefore, it cannot be concluded if the grafting reaction has taken place. It must be noted that the only primary amine-carrying material in this system is the PLL layer that is deposited as a single layer on top of

(PLA/OVA) multilayers. PLL is known for being a very mobile polyelectrolyte which may diffuse through the layers of the system [34,35]. Thus, there is no assurance of the presence of PLL chains on top of the multilayer flat films and thus, there is a chance that the grafting did not take place for this system.

Among all studied systems, (PAH/PSS) multilayers showed promising results for grafting PEG chains by reacting PEG-NHS with the primary amines available on PAH in CH_2Cl_2. To investigate the grafting of PEG chains on the surface of tubes, fluorescently-tagged PEG-NHS reagent (FITC-PEG-NHS) was used to react with (PAH/PSS), crosslinked and non-crosslinked (PAH/PAA) as well as (PAH/OVA) nanotubes.

To this aim, nanotubes were fabricated inside the pores of the PC membrane and then were released from the template by dissolving PC in CH_2Cl_2. Since it was previously shown that the PEG grafting process can successfully be carried on in CH_2Cl_2, FITC-PEG_{2kDa}-NHS reagent was added to the CH_2Cl_2 suspension of released nanotubes and dissolved PC. Nanotubes were then collected by simply filtering the suspension over a PET filter and were then imaged by epi-fluorescence microscopy (Figure 5.13).

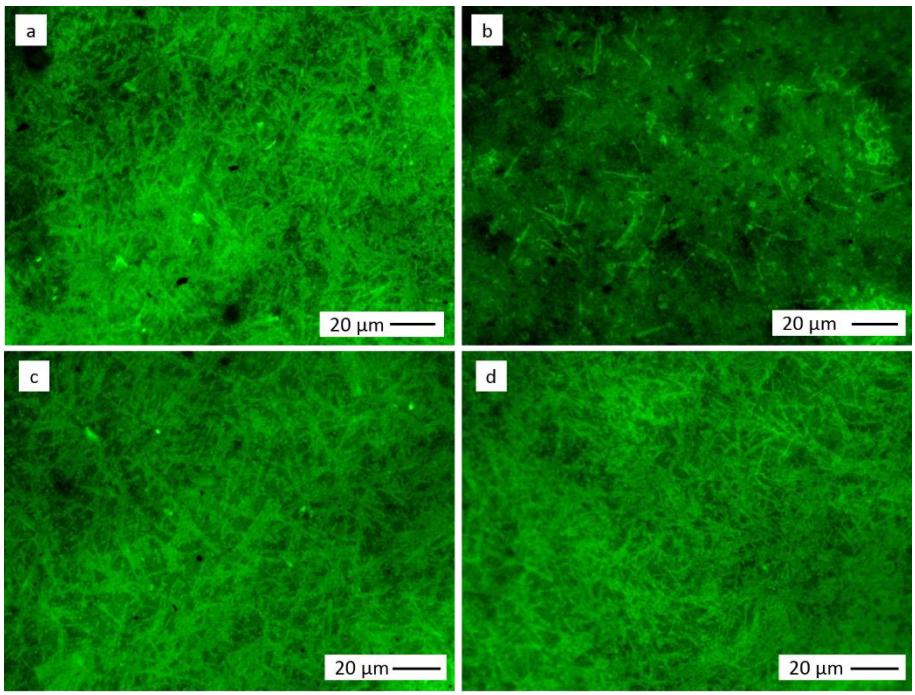

Figure 5.13. Epi-fluorescence images of PEG_{2kDa}-FITC grafted on nanotubes of (a) (PAH/PSS), (b) (non-crosslinked (PAH/PAA), (c) crosslinked (PAH/PAA), (d) (PAH/OVA).(The acquisition conditions of fluorescence images are different and thus, the intensity of the image could not be compared.)

Figure 5.13 shows that a fluorescence signal is observed all along the nanotubes surface for all studied systems. Since the FITC group is directly attached at the end of the PEG chains, one can conclude that nanotubes were grafted with fluorescently-tagged PEG. However, further investigations are needed in order to firmly determine if the grafting has occurred on the surface of the tubes or if the fluorescently-tagged PEG has just entered inside the hollow structure of nanotubes, or was adsorbed within the multilayer wall.

5.4 Conclusion

In this chapter, different methods for introducing PEG chains on the surface of LbL assembled multilayer flat films as well as LbL assembled membrane templated nanotubes were investigated.

Using polyelectrolyte-PEG copolymers seems to be an easy and rapid method to incorporate PEG chains directly into the structure of multilayers during their buildup. However, it is observed that due to the configuration of PEG chains in such copolymers, this is not a highly effective method to construct core-shell nanotubes, with a polyelectrolyte core and a polyelectrolyte-PEG copolymer shell.

On the other hand, PEG chains can be grafted on the surface of the tubes after the release of nanotubes from the membrane by using PEG-NHS reagent which reacts with primary amines available on the surface of nanotubes. XPS data showed that some systems (PAH/PSS) were successfully grafted with PEG while the results were less conclusive for other systems. Epi-fluorescence microscopy images showed that the presence of fluorescence signal along the nanotubes, which can be a sign of successful grafting of fluorescently-tagged PEG chains.

The success of such grafting provides us with many opportunities for further application of PEG grafted multilayer flat films as well as PEG grafted nanotubes. PEG chains should provide antifouling properties to the grafted system and increases their potential as candidates for drug delivery applications.

5.5 Bibliography

(1) Le Droumaguet, B.; Nicolas, J.; Brambilla, D.; Mura, S.; Maksimenko, A.; De Kimpe, L.; Salvati, E.; Zona, C.; Airoldi, C.; Canovi, M.; *et al.* Versatile and Efficient Targeting Using a Single Nanoparticulate Platform: Application to Cancer and Alzheimer's Disease. *ACS Nano* **2012**, *6*, 5866–5879.

(2) Hillaireau, H.; Couvreur, P. Nanocarriers' Entry into the Cell: Relevance to Drug Delivery. *Cell. Mol. Life Sci.* **2009**, *66*, 2873–2896.

(3) Peracchia, M. T.; Fattal, E.; Desmaële, D.; Besnard, M.; Noël, J. P.; Gomis, J. M.; Appel, M.; D'Angelo, J.; Couvreur, P. Stealth PEGylated Polycyanoacrylate Nanoparticles for Intravenous Administration and Splenic Targeting. *J. Control. Release* **1999**, *60*, 121–128.

(4) Couvreur, P.; Gref, R.; Andrieux, K.; Malvy, C. Nanotechnologies for Drug Delivery: Application to Cancer and Autoimmune Diseases. *Prog. Solid State Chem.* **2006**, *34*, 231–235.

(5) Brigger, I.; Dubernet, C.; Couvreur, P. Nanoparticles in Cancer Therapy and Diagnosis. *Adv. Drug Deliv. Rev.* **2012**, *64*, 24–36.

(6) Calvo, P.; Gouritin, B.; Brigger, I.; Lasmezas, C.; Deslys, J.; Williams, A.; Andreux, J. P.; Dormont, D.; Couvreur, P. PEGylated Polycyanoacrylate Nanoparticles as Vector for Drug Delivery in Prion Diseases. *J. Neurosci. Methods* **2001**, *111*, 151–155.

(7) Mura, S.; Couvreur, P. Nanotheranostics for Personalized Medicine. *Adv. Drug Deliv. Rev.* **2012**, *64*, 1394–1416.

(8) Nicolas, J.; Mura, S.; Brambilla, D.; Mackiewicz, N.; Couvreur, P. Design, Functionalization Strategies and Biomedical Applications of Targeted Biodegradable/biocompatible Polymer-Based Nanocarriers for Drug Delivery. *Chem. Soc. Rev.* **2013**, *42*, 1147–1235.

(9) Calvo, P.; Gouritin, B.; Chacun, H.; Desmaele, D.; Angelo, J. D.; Noel, J.; Georgin, D.; Fattal, E.; Andreux, J. P.; Couvreur, P. Polycyanoacrylate Nanoparticles as New Drug Carrier for Brain Delivery. *Pharm. Res.* **2001**, *18*, 1157–1166.

(10) Wattendorf, U.; Koch, M. C.; Walter, E.; Vörös, J.; Textor, M.; Merkle, H. P. Phagocytosis of poly(L-Lysine)-Graft-Poly(ethylene Glycol) Coated Microspheres by Antigen Presenting Cells: Impact of Grafting Ratio and Poly(ethylene Glycol) Chain Length on Cellular Recognition. *Biointerphases* **2006**, *1*, 123–133.

(11) Rabanel, J.-M.; Hildgen, P.; Banquy, X. Assessment of PEG on Polymeric Particles Surface, a Key Step in Drug Carrier Translation. *J. Control. Release* **2014**, *185C*, 71–87.

(12) Zhang, P.; Sun, F.; Tsao, C.; Liu, S.; Jain, P.; Sinclair, A.; Hung, H.-C.; Bai, T.; Wu, K.; Jiang, S. Zwitterionic Gel Encapsulation Promotes Protein Stability, Enhances Pharmacokinetics, and Reduces Immunogenicity. *Proc. Natl. Acad. Sci.* **2015**, *112*, 12046–12051.

(13) Jeon, S. .; Lee, J. .; Andrade, J. .; De Gennes, P. . Protein-Surface Interactions in the Presence of Polyethylene Oxide. *J. Colloid Interface Sci.* **1991**, *142*, 149–158.

(14) Gombotz, W. R.; Wang, G. H.; Horbett, T. A.; Hoffman, A. S. Protein Adsorption to Poly(ethylene Oxide) Surfaces. *J. Biomed. Mater. Res.* **1991**, *25*, 1547–1562.

(15) Kingshott, P.; Griesser, H. J. Surfaces That Resist Bioadhesion. *Curr. Opin. Solid State Mater. Sci.* **1999**, *4*, 403–412.

(16) Holmberg, K.; Tiberg, F.; Malmsten, M.; Brink, C. Grafting with Hydrophilic Polymer Chains to Prepare Protein-Resistant Surfaces. *Colloids Surfaces A Physicochem. Eng. Asp.* **1997**, *123-124*, 297–306.

(17) Elbert, D. L.; Hubbell, J. A. Self-Assembly and Steric Stabilization at

Heterogeneous, Biological Surfaces Using Adsorbing Block Copolymers. *Chem. Biol.* **1998**, *5*, 177–183.

(18) Kenausis, G. L.; Vörös, J.; Elbert, D. L.; Huang, N.; Hofer, R.; Ruiz-Taylor, L.; Textor, M.; Hubbell, J. A.; Spencer, N. D. Poly(L-Lysine)-G-Poly(ethylene Glycol) Layers on Metal Oxide Surfaces: Attachment Mechanism and Effects of Polymer Architecture on Resistance to Protein Adsorption. *J. Phys. Chem. B* **2000**, *104*, 3298–3309.

(19) Blättler, T. M.; Pasche, S.; Textor, M.; Griesser, H. J. High Salt Stability and Protein Resistance of poly(L-Lysine)-G-Poly(ethylene Glycol) Copolymers Covalently Immobilized via Aldehyde Plasma Polymer Interlayers on Inorganic and Polymeric Substrates. *Langmuir* **2006**, *22*, 5760–5769.

(20) Huang, N.-P.; Michel, R.; Voros, J.; Textor, M.; Hofer, R.; Rossi, A.; Elbert, D. L.; Hubbell, J. A.; Spencer, N. D. Poly(L-Lysine)-G-Poly(ethylene Glycol) Layers on Metal Oxide Surfaces: Surface-Analytical Characterization and Resistance to Serum and Fibrinogen Adsorption. *Langmuir* **2001**, *17*, 489–498.

(21) Zahr, A. S.; de Villiers, M.; Pishko, M. V. Encapsulation of Drug Nanoparticles in Self-Assembled Macromolecular Nanoshells. *Langmuir* **2005**, *21*, 403–410.

(22) Zahr, A. S.; Davis, C. A.; Pishko, M. V. Macrophage Uptake of Core-Shell Nanoparticles Surface Modified with Poly(ethylene Glycol). *Langmuir* **2006**, *22*, 8178–8185.

(23) Łukasiewicz, S.; Szczepanowicz, K.; Lukasiewicz, S.; Szczepanowicz, K.; Łukasiewicz, S.; Szczepanowicz, K.; Lukasiewicz, S. In Vitro Interaction of Polyelectrolyte Nanocapsules with Model Cells. *Langmuir* **2014**, *30*, 1100–1107.

(24) Wattendorf, U.; Kreft, O.; Textor, M.; Sukhorukov, G. B.; Merkle, H. P. Stable Stealth Function for Hollow Polyelectrolyte Microcapsules through a Poly(ethylene Glycol) Grafted Polyelectrolyte Adlayer.

Biomacromolecules **2008**, *9*, 100–108.

(25) Johnston, A. P. R.; Cortez, C.; Angelatos, A. S.; Caruso, F. Layer-by-Layer Engineered Capsules and Their Applications. *Curr. Opin. Colloid Interface Sci.* **2006**, *11*, 203–209.

(26) Louguet, S.; Kumar, A. C.; Guidolin, N.; Sigaud, G.; Duguet, E.; Schatz, C. Control of the PEO Chain Conformation on Nanoparticles by Adsorption of PEO-Block-Poly (L -Lysine) Copolymers and Its Significance on Colloidal Stability and Protein Repellency St. *Langmuir* **2011**, *27*, 12891–12901.

(27) Kleim, R.; Kuntzler, L.; Ghemmaz, A. El. Systematic Errors in Rotating-Compensator Ellipsometry. *J. Opt. Soc. Am. A* **1994**, *11*, 2550.

(28) Alem, H.; Blondeau, F.; Glinel, K.; Demoustier-champagne, S.; Jonas, A. M. Layer-by-Layer Assembly of Polyelectrolytes in Nanopores. *Macromolecules* **2007**, *40*, 3366–3372.

(29) Schwarz, S.; Eichhorn, K.-J.; Wischerhoff, E.; Laschewsky, A. Polyelectrolyte Adsorption onto Planar Surfaces: A Study by Streaming Potential and Ellipsometry Measurements. *Colloids Surfaces A Physicochem. Eng. Asp.* **1999**, *159*, 491–501.

(30) Dekeyser, C. M.; Buron, C. C.; Derclaye, S. R.; Jonas, A. M.; Rouxhet, P. G. Degradation of Bare and Silanized Silicon Wafer Surfaces by Constituents of Biological Fluids. *J. Colloid Interface Sci.* **2012**, *378*, 77–82.

(31) Rouxhet, P. G.; Genet, M. J. XPS Analysis of Bio-Organic Systems. *Surf. Interface Anal.* **2011**, *43*, 1453–1470.

(32) Louguet, S.; Kumar, A. C.; Guidolin, N.; Sigaud, G.; Duguet, E.; Lecommandoux, S.; Schatz, C. Control of the PEO Chain Conformation on Nanoparticles by Adsorption of PEO-Block-poly(L-Lysine) Copolymers and Its Significance on Colloidal Stability and

Protein Repellency. *Langmuir* **2011**, *27*, 12891–12901.

(33) Mendelsohn, J. D.; Barrett, C. J.; Chan, V. V.; Pal, a. J.; Mayes, a. M.; Rubner, M. F. Fabrication of Microporous Thin Films from Polyelectrolyte Multilayers. *Langmuir* **2000**, *16*, 5017–5023.

(34) Picart, C.; Mutterer, J.; Richert, L.; Luo, Y.; Prestwich, G. D.; Schaaf, P.; Voegel, J.-C.; Lavalle, P. Molecular Basis for the Explanation of the Exponential Growth of Polyelectrolyte Multilayers. *Proc. Natl. Acad. Sci. U. S. A.* **2002**, *99*, 12531–12535.

(35) Richert, L.; Boulmedais, F.; Lavalle, P.; Mutterer, J.; Ferreux, E.; Decher, G.; Schaaf, P.; Voegel, J.-C.; Picart, C. Improvement of Stability and Cell Adhesion Properties of Polyelectrolyte Multilayer Films by Chemical Cross-Linking. *Biomacromolecules* **2004**, *5*, 284–294.

6 Cellular uptake of multilayer LbL assembled nanotubes

In this study, we report on the stability of template synthesized LbL assembled nanotubes of different chemistries and surface functionalities dispersed in different aqueous medium for different periods. Next, interactions between dendritic cells and nanotubes of different chemistry, size and surface functionality were monitored. Nanotubes were phagocytosed by dendritic cells depending on their chemistry, size and surface function. It was observed that more rigid and shorter nanotubes had a higher chance of being internalized by the cells.

6.1 Introduction

New technical developments in nano engineering have provided tools to fabricate nano-sized particles such as nanospheres, nanowires, nanodisks and nanotubes. These materials are promising for drug delivery applications due to their size and unique characteristics [1–4]. Among all, nanospheres are easier to fabricate and their application has been more studied compared to other more complex structures. However, nanotubes present several advantages as nanocarriers for drug delivery. Briefly, nanotubes have a larger inner volume compared to nanospheres of equal diameter and have interior and exterior surfaces that can be independently functionalized. They also have open ends which help with the loading and delivery process and have longer circulation time in vivo and a higher cell internalization rate [5–7].

Upon different methods to incorporate desired materials in the structure of nanoparticles, LbL assembly is very promising since it is a cheap and extremely versatile method and a broad range of materials such as polymers, lipids, DNAs, proteins and organic or inorganic small molecules can be assembled on different substrates [8]. By combining LbL assembly with template synthesis, tubular nano-objects with a high control over their dimension and composition can be obtained with a high yield [9].

On the route of fabricating new drug delivery systems, studying the interactions between drug carriers and cells is essential. Numerous researches have been dedicated to the uptake of nanoparticles by cells. The pathways and routes that different cell types take while uptaking and phagocytosis of spherical nanoparticles have already been reported [10–15].

Very few studies have been carried out about interactions between cells and template synthesized tubular nanoparticles with aspect ratios ranging

between 1 and 4 [16,17]. Rubner et al. fabricated microtubes of 450 nm outer diameter and 3 µm length comprised of cytophilic and cytophobic surfaces and studied their interaction with immune B-cells [18]. Martin et al also constructed nano test tubes with an aspect ratio of 10 and demonstrated their notable potential for intracellular drug delivery against breast-cancer cells [19,20]. Nanotubes of high aspect ratio containing fibrillar proteins (collagen) have been immobilized on ITO surface and were put in contact with preosteoblast cells by our group. Results showed that nanotubes did not have any cytotoxic effect and the cell but affected cells morphology as well as the length and the thickness of filopodias [21,22].

Among all studied cell types, dendritic cells (DC) are raising a particular interest, as they are known to be the most potent antigen presenting cells (APC) to initiate an adaptive immune response [23,24]. Due to their nature, they have a high phagocytic capacity. In-depth research has been conducted about interactions of LbL assembled hollow capsules containing model antigens with dendritic cells [25–28]. Those studies demonstrated that antigen uptake and delivery are well enhanced and that the intracellular release is well modulated when the antigen is associated with particles having the desired functionalities [29–33].

Interactions between template-synthesized nanotubes and cells have not been studied profoundly due complicated process of releasing those nanotubes from their template and transferring them in a high yield to an aqueous medium suitable for biological applications. This complication is now successfully tackled thanks to our universal method for collection and transferring nanotubes to aqueous medium [34]. Thus, we can move forward with the study of nanotubes interactions with specific cells.

This study provides an insight about the stability of LbL assembled multilayer nanotubes composed of different polyelectrolytes ranging from synthetic to biological protein-based building blocks in different media. Effort will be made to choose the best conditions in order to obtain nanotubes that are stable in cell culture medium for 24 hours.

Afterwards, cellular uptake of these nanotubes by dendritic cells is monitored. It is observed that nanotubes are successfully phagocytosed by dendritic cells. The effect of different parameters such as chemistry, dimension and surface functionalization of nanotubes on their phagocytosis is closely studied as well. Results proved that these nanotubes could indeed be attractive for the delivery of drugs with an intracellular target (such as different proteins or nucleic acids).

6.2 Materials and Methods

6.2.1 Materials

Dichloromethane (CH_2Cl_2), sodium chloride (NaCl), 2-(N-morpholino) ethane sulfonic acid (MES) monohydrate, 4-(2- hydroxyethyl)piperazine-1- ethane sulfonic acid (HEPES), paraformaldehyde, dextran (from Leuconostoc spp., M_W: 40 kDa), N-hydroxy sulfosuccinimide sodium salt (sulfo-NHS),N-(3-Dimethylaminopropyl)-N'-ethylcarbodiimide hydrochloride (EDC), polyallylamine hydrochloride (PAH, M_W: 58 kDa), poly(sodium 4-styrenesulfonate) (PSS, M_W: 70 kDa), polyacrylic acid (PAA, M_W: 100 kDa), poly-L-arginine (PLA, M_W > 70 kDa), ovalbumin (OVA, M_W: 45 kDa) and poly(allylamine hydrochloride) fluorescein isothiocyanate (PAH-FITC, M_W: 15 kDa maximum excitation at 495 nm and an maximum emission at 521 nm) with a monomer to dye ratio (PAH:FITC) of (50:1) were purchased from Sigma-Aldrich. Fluorescent ovalbumin (OVA Alexa Fluor Fluor 488) was purchased from Life Technologies. The Alexa Fluor Fluor 488 fluorophore has a maximum excitation peak at 495 nm and a maximum emission peak at 519 nm. Succinimidyl PEG-NHS (2 kDa) was purchased from NANOCS.

Mouse dendritic cells (DC2.4), Dulbecco's phosphate-buffered saline (DPBS), Dulbecco's modified eagle medium (DMEM), fetal bovine serum (FBS), penicillin-streptomycin (10,000 unit.mL^{-1}), Alexa Fluor 647 and Hoechst staining solutions were purchased from Thermo Fisher Scientific.

Milli-Q water with 18.2 MΩ.cm resistivity was used in all experiments. All products were used as received.

Sheets of track-etched polycarbonate membranes were provided by It4ip (Louvain-la-Neuve, Belgium, http://www.it4ip.be) with pore diameters of namely 500 nm. The pore diameter of the PC membrane is not exactly as

given by the supplier and a 5-10 % variation is observed among the pores. All membranes had a thickness of 21 µm and a pore density of 10^8 pores.cm^{-2}. Hydrophilic poly(ethylene terephthalate) (PET) membranes with a pore size of 200 nm, thickness of 23 µm and pore density of about 5.10^8 pores.cm^{-2} were also provided by It4ip.

6.2.2 Fabrication of LbL assembled nanotubes

All polyelectrolyte solutions were prepared at 1 mg.mL^{-1} concentration except for OVA Alexa Fluor 488 and PAH-FITC polyelectrolytes that were prepared at 0.1 mg.mL^{-1} and 0.5 mg.mL^{-1} concentration respectively. PAH/PSS pairs were prepared in water containing 150 mM NaCl at neutral pH. PAH/PAA pairs were prepared in 150 mM MES at pH = 5.5. PAH/OVA pair was fabricated in 10 mM HEPES buffer at pH = 8 and PLA/OVA pair were prepared in milli-Q water containing 150 mM NaCl at neutral pH. At the end of the LbL deposition process, all samples were rinsed abundantly with milli-Q water to eliminate buffer salts, and dried and stored at room temperature. Optional crosslinking of PAH/PAA and PAH/OVA nanotubes was carried out by immersing the nanotube-containing PC membrane in a 100 mM MES buffer solution (pH = 5.5) containing 25 mM EDC and 48 mM sulfo-NHS for approximately 24 hours at 4 °C. Afterwards, samples were rinsed abundantly with milli-Q water to eliminate buffer salts, and dried and stored at room temperature.

LbL assembly of nanotubes by filtration

A 25 mm diameter piece of nanoporous PC membrane was placed into a stainless steel syringe holder filtration gasket and 3 mL polycation solution was filtered through the membrane with 1 mL.min^{-1} rate by pressure filtration. Excess polyelectrolyte was washed away by filtering the rinsing solution of same ionic strength and composition as used for the

polyelectrolytes was filtered through the membrane with 1 mL.min^{-1} rate. The PC membrane was taken out and the surface of the membrane was rinsed with the rinsing solution and was gently scrubbed with a cell scraper to eliminate any surface adherent layer. Afterwards, 3 mL polyanion solution was filtered through the membrane with 1 mL.min^{-1} rate followed by the same rinsing process. This process was repeated until the desired number of layer pairs (= 3) was achieved. Finally, the PC membrane containing nanotubes was rinsed abundantly with milli-Q water.

Conditioning nanotubes in DPBS

PC membrane containing LbL assembled nanotubes was immersed in DPBS and stirred for 24 hours. Samples were next removed from the buffer, dried and stored at room temperature.

LbL assembly in DPBS buffer (pH = 7.1)

Polyelectrolyte concentration was kept the same. PLA coagulates in DPBS and can only be dissolved in milli-Q water while OVA and PAA are fully soluble in DPBS. In order to have a proper dissolution of PAH in DPBS, an additional 100 mM of NaCl must be added to the solution. The assembly process was carried out as explained previously.

Grafting PEG chains on the surface of nanotubes

Nanotubes with PAH on their outermost layer were capable of further grafting with PEG-NHS ester reagent since succinimidyl group reacts with primary amine, forming amide groups. PC membrane containing nanotubes was dissolved in dichloromethane containing 1 mg.mL^{-1} PEG-NHS ester reagent. The suspension was set aside for 24 hours at 4 °C.

6.2.3 Releasing nanotubes from the template

To release the nanotubes from the template, the PC membrane was dissolved in CH_2Cl_2, resulting in a colloidal suspension of nanotubes and dissolved PC in CH_2Cl_2. The nanotubes were then recovered by filtration of this colloidal suspension over a hydrophilic PET membrane. To maximize the removal of remnant PC, fresh CH_2Cl_2, was flushed through the PET filter for several times.

6.2.4 Checking the stability of nanotubes in aqueous medium

The stability of nanotubes in aqueous medium was checked by dissolving the PC template in CH_2Cl_2 and filtering the resulting suspension over a PET filter. The filter was then immersed in an aqueous medium for 24 hours. Nanotubes deposited on the filter surface were then imaged by epi-fluorescence microscopy prior and after immersion in aqueous medium.

6.2.5 Collection and redispersion in aqueous solution

Dextran powder was used as water-soluble and CH_2Cl_2 -insoluble adjuvant in the nanotube collection process. 20-25 mg of adjuvant was first dispersed in pure CH_2Cl_2 and filtered over a PET filter, leading to formation of a thin porous pellet over the PET filter inside the filtration gasket. This layer aims to mask interactions between the nano-objects and the filter surface. Next, another 20 - 25 mg of adjuvant was added to and dispersed in the colloidal suspension of nanotubes in CH_2Cl_2. The colloidal suspension was filtered through the previously prepared PET filter, thereby building a porous pellet with trapped nanotubes, lying over the pure adjuvant bottom layer. We found that it is crucial to have nanotubes trapped in the whole volume of the pellet. If this step is not followed properly, nanotubes will stack over the surface of the porous adjuvant pellet, resulting in the formation of clusters of nanotubes upon dispersing the pellet in the aqueous solution. To ensure

the total removal of PC traces, CH_2Cl_2 was flushed gently several times through the whole system. The adjuvant pellet was then removed from the filtration gasket and immersed in 2 mL milli-Q water. The aqueous suspension containing the nanotubes and the dissolved adjuvant were then stirred for 15 minutes before being stored at 4 °C.

6.2.6 Checking the stability of free floating nanotubes in DPBS

Nanotubes were collected by dextran adjuvant assisted collection method and were dispersed in DPBS obtaining a solution with a concentration of 5.10^7 nanotubes.mL^{-1}. This solution was mildly stirred for 24 hours and then was filtered through a PET filter for further imaging by epi-fluorescence microscopy.

6.2.7 Cell culture

The DC2.4 cells were cultured in DMEM (Dulbecco's Modified Eagle Medium) supplemented with 10% FBS (fetal bovine serum) and antibiotics (100 units per mL penicillin and 100 $\mu g.mL^{-1}$ streptomycin). Cells were grown at 37 °C in humidified air containing 5 % CO_2.

Cells were seeded at a density of 15000 cells per well (volume of solution per well = 1mL) on WillCo dish for 24 hours and then incubated overnight with 1 mL of nanotubes suspension (5.10^7 nanotubes.mL^{-1} in DPBS). After removing the culture medium, cells were fixed with 4 % PFA (paraformaldehyde) for 35 min at 37 °C. For further imaging purposes, the cell membranes was stained with Alexa Fluor 647-conjugated cholera toxin subunit B (red) and the nuclei was counter-stained with Hoechst (blue).

6.2.8 Characterization methods

Epi-fluorescence microscopy

The suspension of fluorescent-tagged nanotubes was filtered through a PET filter for epi-fluorescence optical microscopy. Fluorescence images were obtained by an Olympus IX2 inverted microscope equipped with a FITC filter set.

Confocal microscopy

Confocal microscopy was carried out on a Leica DMI6000 B inverted microscope equipped with an oil immersion objective (Zeiss, magnification: 63×, numerical aperture: 1.40) and attached to an Andor DSD2 confocal scanner. Images were processed with Image J and Imaris softwares.

Gas-flow porometry

The average diameter of PC membrane pores before and after nanotubes construction was measured by gas flow porometry at room temperature. Air-dried samples were firmly fixed inside the sample holder with an effective section area of 0.396 cm^2. Nitrogen gas was flown upstream with a pressure ranging from 4 - 10 psi. The gas flow rate ($mL.min^{-1}$) downstream from the sample was measured by a flowmeter (Agilent). The inner diameter of the pores was calculated by using Knudsen diffusion and the viscous or Hagen-Poiseuille flow relationship as previously described is Chapter 3.

6.3 Results and Discussion

6.3.1. Build-up of multilayer polyelectrolyte multilayers

Multilayer polyelectrolyte nanotubes were fabricated within the pores of track-etched PC membrane by LbL assembly. Several polyelectrolyte combinations were chosen to fabricate nanotubes of different chemistries ranging from synthetic nanotubes to biological protein-based nanotubes.

Table 5.4. Composition and build-up conditions of the various studied LbL assembled nanotubes. (The pH of buffered solutions is measured by a pH meter (with ± 0.1 error) while the pH of NaCl-containing solutions are assumed to be neutral.)

LbL assembled systems	Polycation	Polyanion	Build-up conditions		
			Construction pH	Construction medium	Amount of buffer or salt
Synthetic	PAH	PSS	Neutral pH	Milli-Q water + NaCl	150 mM NaCl
	PAH	PAA	5.5 ± 0.1 [measured]	MES Buffer	150 mM MES
Protein-based	PAH	OVA	8 ± 0.1 [measured]	HEPES Buffer	10 mM HEPES
	PLA	OVA	Neutral pH	Milli-Q water + NaCl	150 mM NaCl

Table 5.4 is a summary of the studied LbL nanotubes and their fabrication conditions. The choice of build-up conditions (such as buffer, ionic strength, etc.) is explained in detail in chapter 3.

LbL assembly within the pores of the PC membrane was carried out by filtering the polyelectrolyte solutions through the pores (LbL assembly by

filtration). This method was preferred over LbL assembly by immersion since a high number of nanotubes with a similar wall thickness can be assembled in a shorter amount of time and by depositing fewer layers. PC membrane of high pore density (10^8 pores.cm^{-1}) was chosen as a template, in order to have a high amount of nanotubes per PC membrane volume. It must be noted that by increasing the pore density to much higher values (such as 10^9 pores.cm^{-1}) the risk of having interconnected pores increases, which may cause nanotubes aggregation upon release from the PC template. Since a large number of nanotubes were required for cellular uptake tests (~ 10^7 particle.mL^{-1}), 1 cm^2 of PC membrane containing LbL assembled nanotubes was cut out and used for further experiments. The adjuvant-assisted collection method (using dextran powder as adjuvant) was used to transfer nanotubes from the PC template to desired aqueous medium. This method is explained in detail in chapter 4. If the collection is 100 % successful, an aqueous solution containing 5.10^7 nanotubes.mL^{-1} would be obtained.

6.3.1 Stability of free LbL assembled nanotubes in water

Multilayer LbL assembled nanotubes were all made of hydrophilic polyelectrolytes to ensure their stability in aqueous medium. However, prior to the study of cell-nanotube interactions, it is crucial to monitor the long-term integrity of these LbL nanotubes when dispersed in aqueous solutions. As previously reported (see chapter 4.3.1.) (PLA/OVA Alexa Fluor 488)$_6$ nanotubes deposited on a PET filter surface by filtration were stable after mild stirring for 5 days in milli-Q water (Figure 5.14.a and Figure 5.14.b).

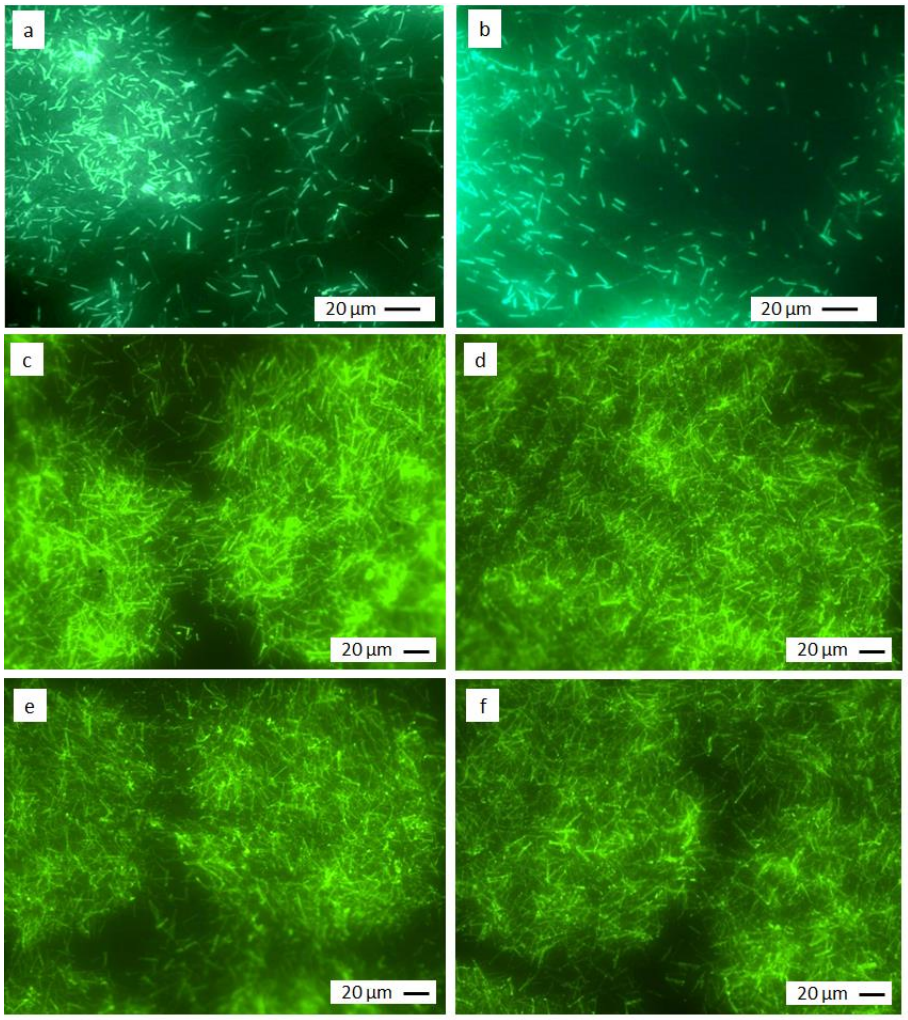

Figure 5.14. Epi-fluorescence microscopy images of (PLA/OVA Alexa Fluor Fluor 488)$_6$ nanotubes, (a) after filtration over a PET filter and prior to immersion in aqueous solution, (b) after immersion in aqueous solution for 5 days, (c, d, e, f) after immersion for 30 minutes in milli-Q water containing (c) no salt, (d) 100mM NaCl, (e) 200 mM NaCl and (f) 500 mM NaCl. (The acquisition conditions of fluorescence images are different and thus, the intensity of the images could not be compared.)

In addition, those nanotubes filtered over PET filter remained stable after being immersed and mildly stirred for 30 minutes in pure water as well as in

aqueous solution of higher ionic strength (up to 500 mM NaCl) (Figure 5.14.c-f). It must be noted that those stability studies were conducted on nanotubes deposited on a supporting PET filter surface and not on free nanotubes suspended in aqueous solution. In the present work, the stability of free-floating nanotubes of different chemistries after a long duration (10 days) of mild stirring in milli-Q water at neutral pH with no additional buffer or salt was verified. LbL assembled nanotubes were collected by dextran-adjuvant assisted method and were dispersed in milli-Q water. Figure 5.15 shows epi-fluorescence microscopy images of dispersed nanotubes after 10 days in milli-Q water.

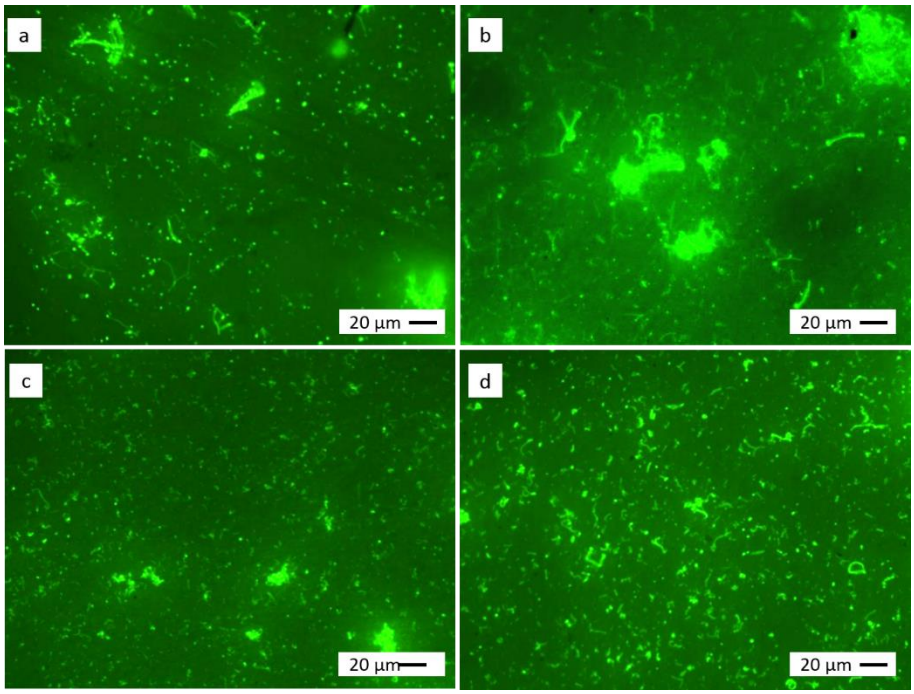

Figure 5.15. Epi-fluorescence microscopy images of (a) $(PAH\text{-}FITC/PSS)_3$, (b) $(PAH\text{-}FITC/PAA)_3$, (c) $(PAH/\ OVA\ Alexa\ Fluor\ 488)_3$, (d) $(PLA/OVA\ Alexa\ Fluor\ 488)_3$ nanotubes dispersed in milli-Q water for 10 days. (The acquisition conditions of fluorescence images are different and thus, the intensity of the images could not be compared.)

To evaluate nanotubes behavior after dispersion in aqueous solution, it was decided to classify different levels of stability after nanotubes dispersion in aqueous solution. Nanotubes are classified to 4 categories, based on their appearance after being dispersed in aqueous solution (Table 5.5).

Table 5.5. Classification of nanotubes into different categories based on the appearance after dispersion in aqueous solution.

Assigned Categories	Nanotubes appearance
1	Nanotubes are intact
2	Nanotubes are swollen
3	Nanotubes are swollen and/or broken into pieces
4	Nanotubes are fully disrupted

As can be seen in Figure 5.15.a. almost all of the nanotubes were fully disrupted. Although some remnants of nanotubes can be seen for (PAH-FITC/PSS)$_3$ and (PAH-FITC/PAA)$_3$ nanotubes, all of studied systems are considered as category 4, fully disrupted.

It should be noted that these observations are limited in some aspects. For instance, nanotubes dispersed in aqueous medium are constantly stirred at a slow rate. Indeed, constant stirring is essential, as nanotubes tend to stick on the bottom and walls of the recipient if left unstirred. High rates of stirring were avoided to protect nanotubes from high mechanical stress. Nevertheless, the stirring may damage the nanotubes. Another experimental limit is due to the observation method. Dispersed nanotubes in aqueous medium are filtered over a virgin PET filter in order to maximize the number of nanotubes available for fluorescence imaging. Attempts to image drops of aqueous medium containing dispersed nanotubes were made but the quality

of these images were lower than images obtained from nanotubes filtered over a PET filter. By filtering highly hydrated, soft nanotubes dispersed in aqueous medium, an external force is exerted over their structure, which might lead to their deformation.

Finally yet importantly, epi-fluorescence images were recorded on dried samples, meaning that nanotubes had lost their water-content prior to observation. As water molecules are eliminated, changes might occur in the structure of the nanotubes. One must therefore keep in mind that the stability comparison of nanotubes is visual and that aforementioned limitations might interfere with the observations.

Nanotubes filtered over a PET filter and then immersed in aqueous solution were much more stable compared to fully dispersed nanotubes in aqueous solution that can freely float in the medium. The former nanotubes benefit from the presence of PET filter as a support, also a mesh of nanotubes is formed as they are filtered and deposited over the PET filter. This network of nanotubes protects them from deformation and prohibits their detachment from the filter surface as explained in chapter 4. Therefore, nanotubes deposited on a filter remained stable even after being immersed for a long duration in aqueous medium. In contrast, dispersed nanotubes in aqueous medium swim around and have no protection from exerted forces. When several nanotubes meet, they tend to stick to each other and form aggregates. This is especially the case for $(PAH\text{-}FITC/PSS)_3$ and $(PAH\text{-}FITC/PAA)_3$ nanotubes as some aggregates are observable. To reinforce the structure of $(PAH\text{-}FITC/PAA)_3$ nanotubes and enhance their stability, the tubes were crosslinked (images not shown). However, no noticeable changes were observable and tubes were still disrupted upon dispersion in aqueous solution.

Protein-based nanotubes are prone to damage, probably due to their soft nature. As discussed in chapter 4, the rigidity degree of protein-based nanotubes was strongly decreased after dispersion in aqueous medium. These soft nanotubes become highly hydrated in aqueous medium and can be easily disrupted upon application of external forces (either during stirring, or during filtration on a PET filter for further imaging).

To prevent nanotubes aggregation in aqueous medium and increase their ability to float in aqueous medium, nanotube surfaces were modified with a highly hydrated PEG corona. The PEG grafting process reported in detail in chapter 5 was carried out on $(PAH\text{-}FITC/PSS)_3$ and $(PAH/OVA\ Alexa\ Fluor\ 488)_3$ nanotubes.

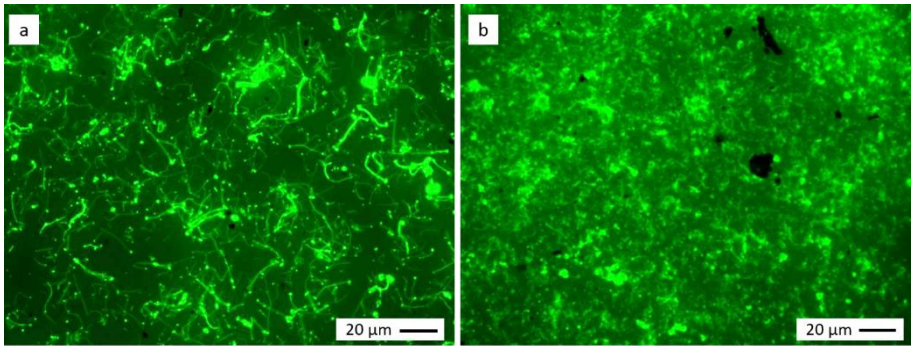

Figure 5.16. Epi-fluorescence microscopy images of (a) PEG-$(PAH\text{-}FITC/PSS)_3$ nanotubes, (b) PEG-$(PAH/OVA\ Alexa\ Fluor\ 488)_3$ nanotubes dispersed in milli-Q water for 24 hours. (The acquisition conditions of fluorescence images are different and thus, the intensity of the images could not be compared.)

Figure 5.16.a shows PEG-grafted nanotubes after dispersion in milli-Q water for 24 hours. PEG-$(PAH\text{-}FITC/PSS)_3$ nanotubes appear to be intact and thus belong to category 1. However, PEG-$(PAH\text{-}FITC/PAA)_3$ nanotubes look disrupted and therefore, these nanotubes are classified in category 4. Such

disruption in nanotubes could be either due to the disassembly of multilayers or due to the soft nature of those nanotubes and their inability to withstand the forces exerted on them during stirring and filtration from aqueous medium. To avoid deformation caused by disassembly of multilayers, (PAH/OVA Alexa Fluor 488)$_3$ nanotubes were first crosslinked. Next, PEG chains were grafted on their surface and afterwards, nanotubes were dispersed in milli-Q water for 24 hours. However, this procedure did not improve the stability of these nanotubes (images not shown). As the nanotubes were crosslinked, disassembly of multilayers can be ruled out and so, the main cause of nanotubes disruption and damage upon dispersion is mostly mechanical. A summary of nanotubes stability in aqueous medium is given in Table 5.6.

Table 5.6. A summary of nanotubes stability in aqueous medium.

System	Stability in aqueous medium	
	10 days	24 hours
(PAH/PSS)	Category 4	n.a.
PEG-(PAH/PSS)	n.a.	Category 1
(PAH/PAA)	Category 4	n.a.
(PAH/OVA)	Category 4	n.a.
PEG-(PAH/OVA)	n.a.	Category 4
(PLA/OVA)	Category 4	n.a.

6.3.2 Stability of free floating LbL assembled nanotubes in culture medium

As nanotubes will be further used for in vitro studies, it is essential to also investigate their stability in the culture medium, which is Dulbecco's phosphate-buffered saline (DPBS). To this aim, nanotubes were collected by dextran-adjuvant assisted collection method and were then dispersed in DPBS at pH = 7.1 and mildly stirred for 24 hours.

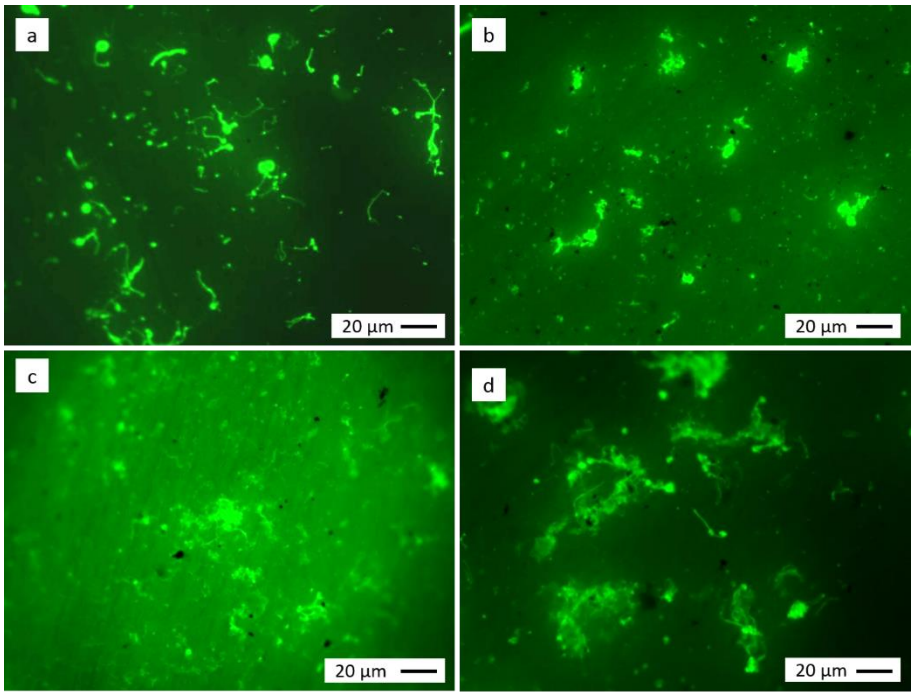

Figure 5.17. Epi-fluorescence microscopy images of (a) $(PAH\text{-}FITC/PSS)_3$, (b) $(PAH\text{-}FITC/PAA)_3$, (c) $(PAH/\ OVA\ Alexa\ Fluor\ 488)_3$, (d) $(PLA/OVA\ Alexa\ Fluor\ 488)_3$ nanotubes dispersed in DPBS for 24 hours. (The acquisition conditions of fluorescence images are different and thus, the intensity of the images could not be compared.)

Figure 5.17, shows nanotubes after being dispersed in DPBS for 24 hours. As can be seen $(PAH\text{-}FITC/PSS)_3$ nanotubes show some signs of disruption (category 3) while other systems such as $(PAH\text{-}FITC/PAA)_3$, $(PAH/OVA\ Alexa\ Fluor\ 488)_3$ and $(PLA/OVA\ Alexa\ Fluor\ 488)_3$ nanotubes are fully disrupted (category 4).

Here again, nanotubes disruption can be related to mechanical forces exerted on soft, hydrated nanotubes. In addition, phosphate ions present in DPBS buffer may also diffuse in nanotubes and may affect the interactions between multilayers, which eventually leads to nanotubes deformation.

(PAH-FITC/PSS)$_3$ nanotubes have a higher tendency to withstand such perturbation, while nanotubes of other chemistries are more vulnerable.

PEG chains were grafted on the surface of nanotubes in order to improve their stability upon dispersion in DPBS buffer.

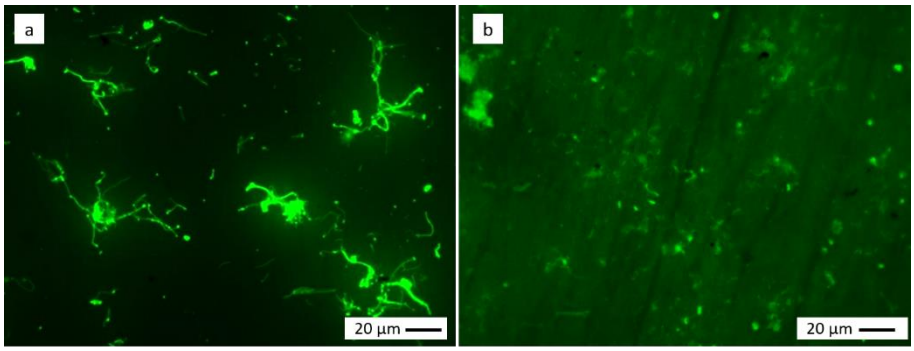

Figure 5.18. Epi-fluorescence microscopy images of (a) PEG-(PAH-FITC/PSS)$_3$ nanotubes, (b) PEG-(PAH/OVA Alexa Fluor 488)$_3$ nanotubes dispersed in DPBS for 24 hours. (The acquisition conditions of fluorescence images are different and thus, the intensity of the images could not be compared.)

Figure 5.18 is shows PEG grafted nanotubes after being dispersed in DPBS for 24 hours. Here, PEG-(PAH-FITC/PSS)$_3$ nanotubes appear to be intact, however, these nanotubes have formed some aggregates (category 1 with some aggregates). PEG-(PAH/OVA Alexa Fluor 488)$_3$ nanotubes were disrupted after being dispersed in DPBS (category 4). The stability of (PAH/OVA Alexa 488)$_3$ nanotubes was not improved when nanotubes were crosslinked prior to PEG grafting.

6.3.3 Fabrication of nanotubes with improved stability in culture medium

Apart from synthetic (PAH/PSS) nanotubes, nanotubes of other chemistries were fully disrupted after being dispersed for 24 hours in DPBS. To improve their stability in DPBS, two different approaches were considered:

1. Conditioning nanotubes in DPBS prior to their dispersion
2. Fabricating the nanotubes in DPBS.

In the first approach, PC membranes containing LbL assembled nanotubes were immersed in DPBS and stirred for 24 hours. Ions present in DPBS buffer can diffuse through the PC membrane pores. The LbL nanotubes have therefore enough time to adapt their structure to the new conditions, while being still embedded and protected by the template. This approach is interesting as it is quite easy to observe if nanotubes disassemble or keep their shape and structure inside the PC membrane after being in contact with DPBS. After being conditioned in DPBS buffer for 24 hours, nanotubes are collected by dextran-adjuvant assisted method and then dispersed in DPBS.

In the second approach, the LbL assembly within the template nanopores is carried out in DPBS. Next, nanotubes are collected by dextran-adjuvant method and then dispersed in DPBS. As nanotubes are directly fabricated in DPBS, there should be no perturbation caused by introduction of new ions upon dispersion.

As $(PAH/PSS)_3$ nanotubes were not fully disrupted after being dispersed in DPBS buffer, aforementioned methods were only carried out on the other systems.

6.3.3.1 1st approach: Conditioning nanotubes in DPBS prior to dispersion

PC membranes containing nanotubes were immersed in DPBS buffer for 24 hours. Afterwards, the membranes were dissolved in PC membrane and the obtained suspension of nanotubes was simply filtered over a PET filter. Nanotubes deposited on the surface of filter were then imaged by epi-fluorescence microscopy.

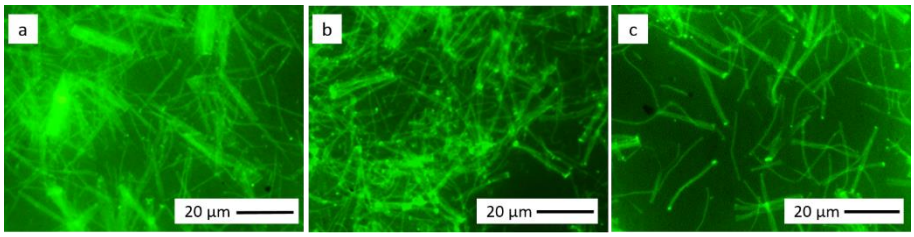

Figure 5.19. Epi-fluorescence microscopy images (a) $(PAH\text{-}FITC/PAA)_3$, (b) $(PAH/OVA\ Alexa\ Fluor\ 488)_3$, (c) $(PLA/OVA\ Alexa\ Fluor\ 488)_3$ nanotubes conditioned in DPBS for 24 hours and released from the membrane. (The acquisition conditions of fluorescence images are different and thus, the intensity of the images could not be compared.)

Figure 5.19 demonstrates that all studied nanotubes kept their tubular shape and their fluorescence signal after being conditioned inside the PC membrane in DPBS buffer for 24 hours, suggesting that DPBS does not disassemble multilayer nanotubes and is indeed a proper medium to disperse nanotubes. Nanotubes were then collected by dextran adjuvant assisted collection method and were dispersed in DPBS and mildly stirred for 24 hours.

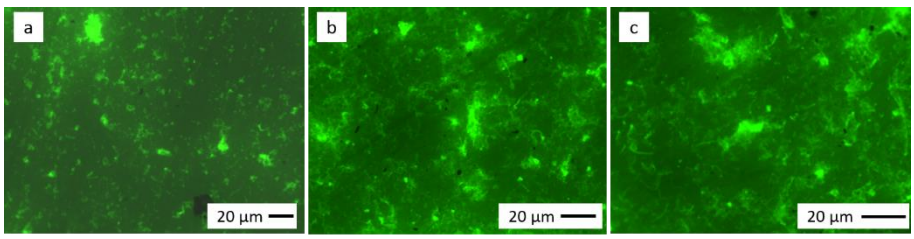

Figure 5.20. Epi-fluorescence microscopy images (a) $(PAH\text{-}FITC/PAA)_3$, (b) $(PAH/OVA\ Alexa\ Fluor\ 488)_3$, (c) $(PLA/OVA\ Alexa\ Fluor\ 488)_3$ nanotubes conditioned in DPBS for 24 hours and dispersed in DPBS for 24 hours. (The acquisition conditions of fluorescence images are different and thus, the intensity of the images could not be compared.)

Figure 5.20 represents epi-fluorescence images of nanotubes that were conditioned for 24 hours in DPBS and further dispersed in DPBS for 24 hours. All studied systems lost their tubular shape, and were disrupted (category 4). Some fluorescent remnants and some aggregates are observed here and there as well.

PEG chains were grafted on the surface of $(PAH\text{-}FITC/PAA)_3$ and $(PAH/OVA\ Alexa\ Fluor\ 488)_3$ nanotubes that were previously conditioned in DPBS, to enhance their stability upon dispersion in DPBS.

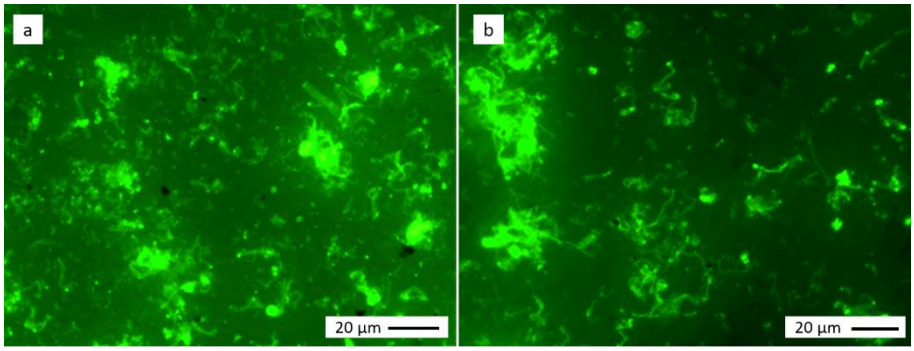

Figure 5.21. Epi-fluorescence microscopy images of (a) PEG-$(PAH\text{-}FITC/PAA)_3$, (b) PEG-$(PAH/OVA\ Alexa\ Fluor\ 488)_3$, nanotubes were previously conditioned in DPBS for 24 hours, then grafted with PEG and afterwards dispersed in DPBS for 24 hours. (The acquisition conditions of fluorescence images are different and thus, the intensity of the images could not be compared.)

As observed in Figure 5.21, grafting PEG chains on the surface of the nanotubes does not significantly enhance their stability and dispersion in DPBS. Here again, broken nanotubes and aggregates are observed. Both PEG-grafted systems belong to category 4.

6.3.3.2 2nd approach: DPBS as LbL assembly medium

The stability of free nanotubes built-up in DPBS with and without further PEG grafting on the outermost layer was checked.

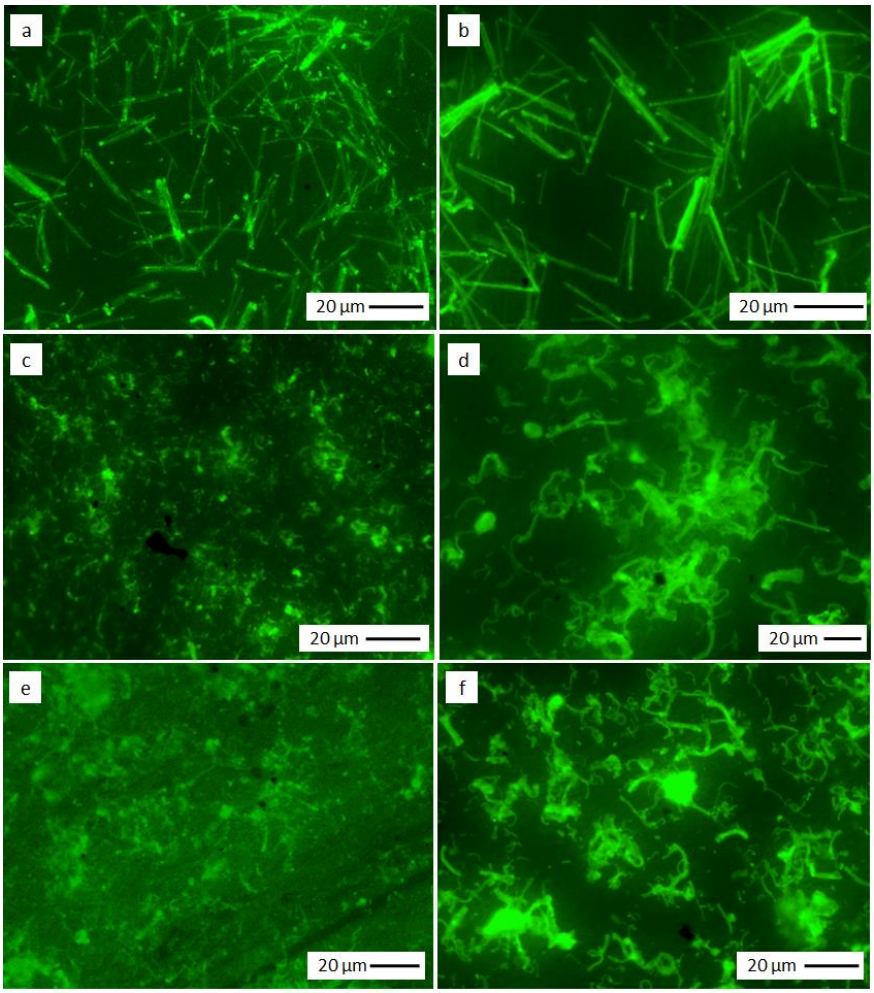

Figure 5.22. Epi-fluorescence images of (a) $(PAH\text{-}FITC/PAA)_3$ and (b) $(PAH/OVA\ Alexa\ Fluor\ 488)_3$ nanotubes assembled in DPBS buffer and imaged directly after being released from the PC template, (c) (PAH-FITC/PAA) and (d) $(PAH/OVA\ Alexa\ Fluor\ 488)_3$ nanotubes assembled in DPBS and dispersed in DPBS for 24 hours, (e) PEG-$(PAH\text{-}FITC/PAA)_3$ and (f) PEG-$(PAH/OVA\ Alexa\ Fluor\ 488)_3$ nanotubes assembled in DPBS, further modified with a PEG corona, and dispersed in DPBS for 24 hours. (The acquisition conditions of fluorescence images are different and thus, the intensity of the images could not be compared.)

Epi-fluorescence microscopy imaging of nanotubes showed that $(PAH\text{-}FITC/PAA)_3$ nanotubes were successfully assembled in DPBS (Figure 5.22.a).

The wall-thickness of those nanotubes was measured by gas-flow porometry and was estimated to be around 45 nm. However, these nanotubes did not keep their tubular shape and were disrupted (category 4) upon dispersion in DPBS (Figure 5.22.c). Grafting PEG chains on the surface of these nanotubes did not significantly improve their stability (Figure 5.22.e).

(PAH/OVA Alexa Fluor 488)$_3$ nanotubes were also successfully fabricated in DPBS buffer (Figure 5.22.b) and their wall thickness was estimated to be about 70 nm by gas-flow porometry measurements. These nanotubes became highly swollen and formed loops upon dispersion in DPBS (category 2) (Figure 5.22.d). Grafting PEG chains on the surface of these nanotubes did not lead to noticeable changes when nanotubes were dispersed in DPBS (Figure 5.22.f). PEG-(PAH/OVA Alexa Fluor 488)$_3$ nanotubes still formed loops and were swollen after being dispersed in DPBS. Some signs of disruption were also observed for these tubes (category 3). A summary of nanotubes stability in DPBS buffer is given in Table 5.7.

Since (PAH-FITC/PAA)$_3$ nanotubes did not keep their shape upon dispersion in DPBS, these nanotubes were not used for any further in-vitro studies.

Table 5.7. A summary of nanotubes stability in DPBS buffer.

System	Adopted process to improve stability		Stability in DPBS
	Conditioning in DPBS	*LbL assembly in DPBS*	
(PAH/PSS)	-	-	Category 1
PEG-(PAH/PSS)	-	-	Category 1
(PAH/PAA)	-	-	Category 4
(PAH/PAA)	**yes**		Category 4
(PAH/PAA)		**yes**	Category 4
PEG-(PAH/PAA)		**yes**	Category 4
(PAH/OVA)	-	-	Category 4
(PAH/OVA)	**yes**		Category 4
PEG-(PAH/OVA)	**yes**		Category 4
(PAH/OVA)		**yes**	Category 2
PEG-(PAH/OVA)		**yes**	Category 3
(PLA/OVA)	-	-	Category 4
(PLA/OVA)	**yes**		Category 4

6.3.4 Cellular uptake of LbL assembled nanotubes

To investigate the interaction between cells and LbL assembled nanotubes, nanotubes of different chemistries as well as different dimensions were brought in contact with mouse dendritic cells DC2.4 for 24 hours in vitro.

Nanotubes chemistries varied from synthetic $(PAH\text{-}FITC/PSS)_3$ to protein-based $(PAH/OVA\ Alexa\ Fluor\ 488)_3$ and biological $(PLA/OVA\ Alexa\ Fluor\ 488)_3$ nanotubes. Nanotubes outer diameter and length varied from 500 nm outer diameter and 21 μm length to 400 nm outer diameter and 10 μm length. PEG chains were grafted on the outer surface of PAH containing nanotubes as well. A summary of all studied nanotubes is presented in Figure 5.23.

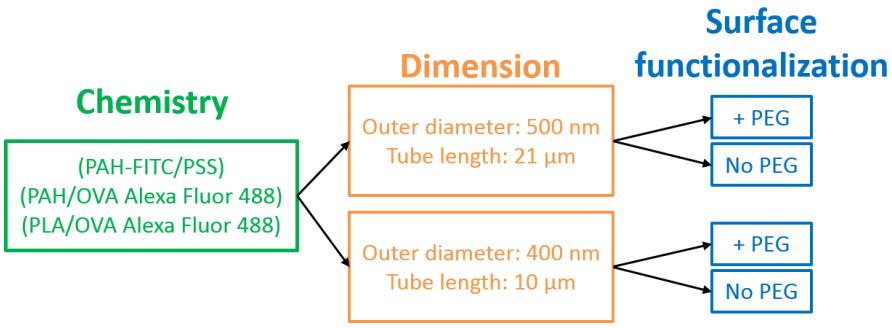

Figure 5.23. A summary of chosen nanotubes of different chemistries, dimensions and surface functionalization used for in vitro cellular uptake studies.

After 24 hours of nanotubes incubation with cells, almost all the cells were viable. Therefore, one can deduce that none of studied systems had toxic effects over the cells.

Figure 5.24 shows confocal microscopy fluorescence overlay images of (PAH-FITC/PSS)$_3$ nanotubes after 24 hours incubation with DC2.4 cells.

As observed in Figure 5.24. both long and short (PAH-FITC/PSS)$_3$ nanotubes were uptaken by the cells (Figure 5.24.a and Figure 5.24.b). The XZ and YZ plane images for long (PAH-FITC/PSS)$_3$ are shown (Figure 5.24.a) and prove that nanotubes have indeed entered the cell membrane. It is observed that a few number of PEG-grafted long nanotubes have also been uptaken by the cells (Figure 5.24.c). A large quantity of short, PEG-grafted (PAH-FITC/PSS) nanotubes is internalized by the cells as observed in Figure 5.24.d.

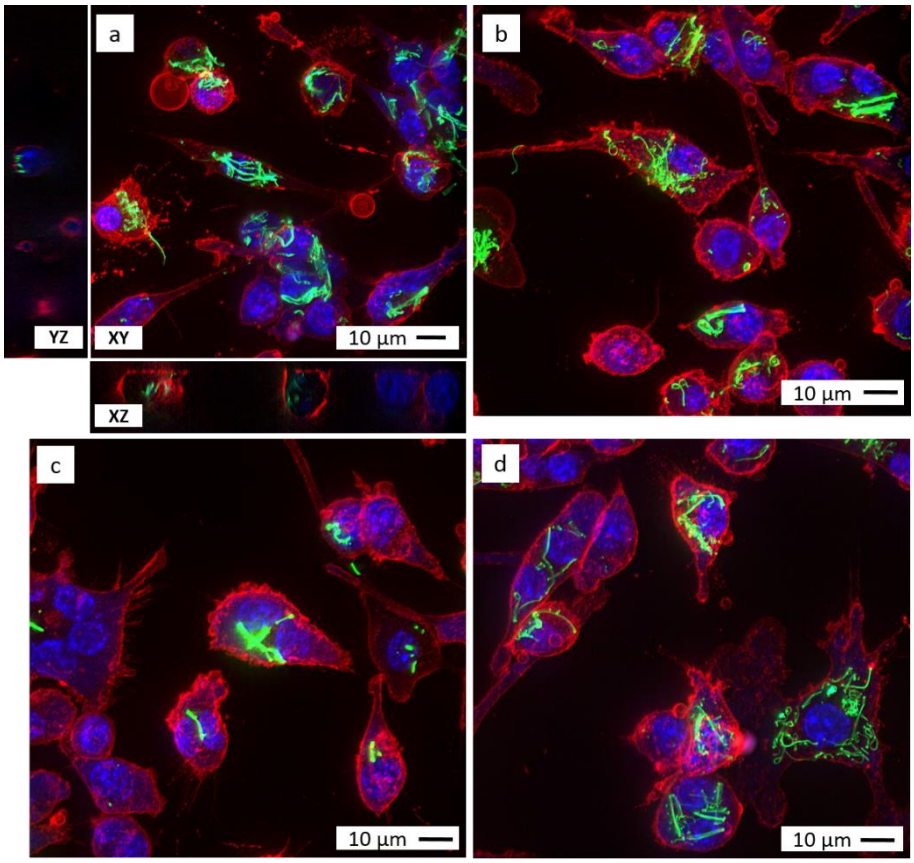

Figure 5.24. Confocal microscopy fluorescence overlay images with maximum intensity projection of Z stacks on XY plane (a) $(PAH\text{-}FITC/PSS)_3$ nanotubes of 500 nm outer diameter and 21 µm length (YZ plane on the left, XZ plane on the bottom and XY plane in the middle), (b) $(PAH\text{-}FITC/PSS)_3$ nanotubes of 400 nm outer diameter and 10 µm length, (c) PEG-$(PAH\text{-}FITC/PSS)_3$ nanotubes of 500 nm outer diameter and 21 µm length, (d) PEG-$(PAH\text{-}FITC/PSS)_3$ nanotubes of 400 nm outer diameter and 10 µm length, after 24 hours incubation with DC2.4 cells. The cells membrane was stained red and the cells nuclei was stained blue. (The analyzed z-axis distance was about 20 µm).

Figure 5.25 shows confocal microscopy fluorescence overlay images of $(PAH/OVA\ Alexa\ Fluor\ 488)_3$ nanotubes after 24 hours incubation with DC2.4 cells. These nanotubes were already swollen and partially disrupted prior to

incubation with DC2.4 cells (Table 5.7). From Figure 5.25, it is observed that a small number of nanotubes have been internalized by the cells. Non-internalized nanotubes did not stick on the surface of the cells and were removed during multiple rinsing steps of the sample preparation process. No significant difference between cellular uptake of PEG-grafted and non-grafted nanotubes is observed

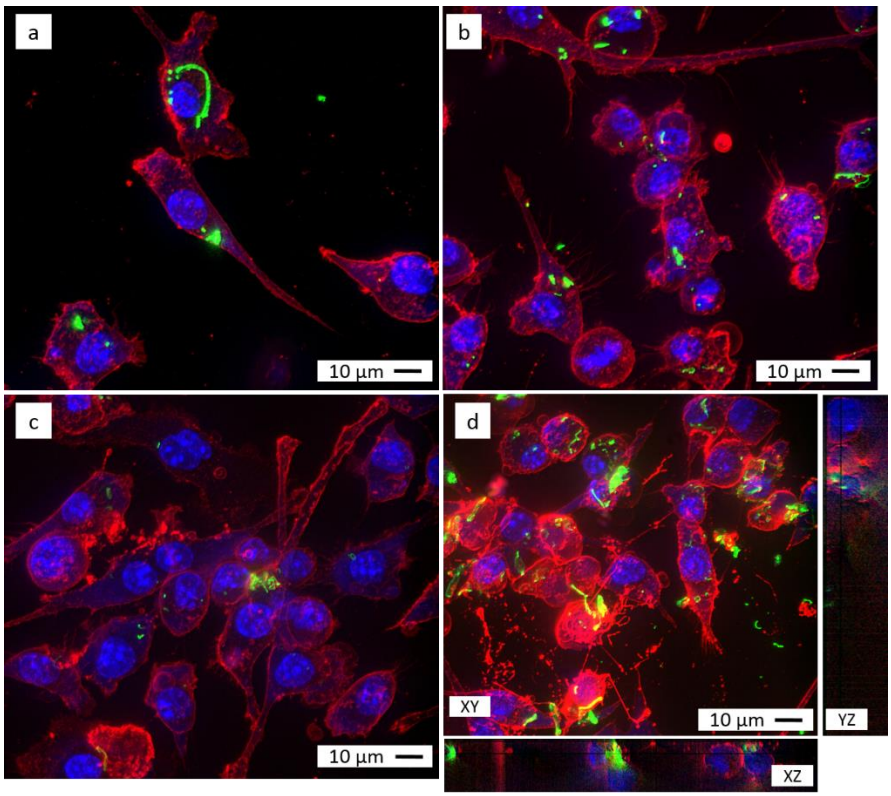

Figure 5.25. Confocal microscopy fluorescence overlay images with maximum intensity projection of Z stacks on XY plane of (a) (PAH/OVA Alexa Fluor 488)$_3$ nanotubes of 500 nm outer diameter and 21 µm length, (b) (PAH/OVA Alexa Fluor 488)$_3$ nanotubes of 400 nm outer diameter and 10 µm length, (c) PEG-(PAH/OVA Alexa Fluor 488)$_3$ nanotubes of 500 nm outer diameter and 21 µm length, (d) PEG-(PAH/OVA Alexa Fluor 488)$_3$ nanotubes of 400 nm outer diameter and 10 µm length (YZ plane on the right, XZ plane on the bottom and XY plane in the middle), after 24 hours incubation with DC2.4 cells. The cells membrane was stained red and the cells nuclei was stained blue. (The analyzed z-axis distance was about 20 µm).

Figure 5.26.a and Figure 5.26.b show confocal microscopy fluorescence overlay images of (PLA/OVA Alexa Fluor 488)$_3$ nanotubes after 24 hours incubation with dendritic cells. Previous stability tests already demonstrated that these nanotubes were disrupted (category 4) upon dispersion in DPBS (Table 5.7). Here, it is observed that although nanotubes are disrupted, their broken pieces are internalized by the cells.

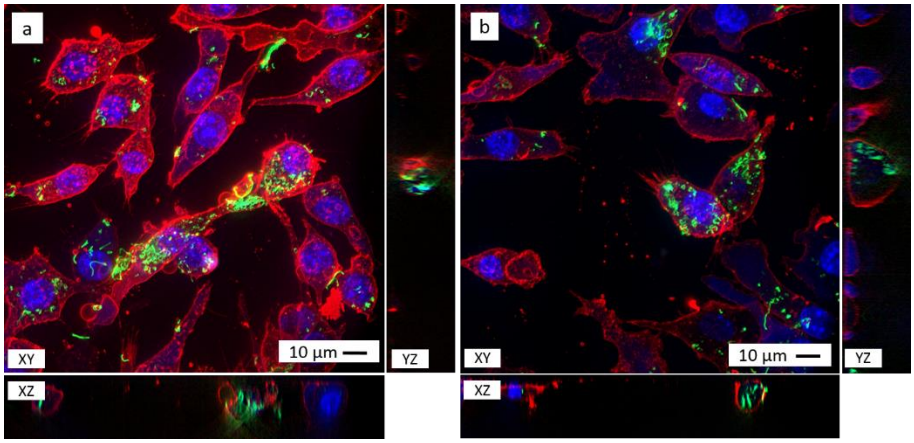

Figure 5.26. Confocal microscopy fluorescence overlay images with maximum intensity projection of Z stacks of two different samples of (PLA/OVA Alexa Fluor 488)$_3$ nanotubes of 500 nm outer diameter and 21 µm length. XY plane in the middle, XZ plane on the bottom and YZ plane on the right. The cells membrane was stained red with and the cells nuclei was stained blue. (The analyzed z-axis distance was about 20 µm).

The difference in cells behavior upon incubation with nanotubes of different chemistries and dimensions should be studied more profoundly. However, from our preliminary experiments, it was concluded that shorter nanotubes have a higher chance of being internalized by the cells. However, we cannot draw any significant conclusions about the antifouling properties of PEG-grafted nanotubes as only a limited number of tests were performed and quantitative data are not available.

It was observed that a higher number of synthetic $(PAH\text{-}FITC/PSS)_3$ nanotubes were uptaken by the cells compared to protein-based $(PAH/OVA\ Alexa\ Fluor\ 488)_3$ and $(PLA/OVA\ Alexa\ Fluor\ 488)_3$. This could be related to the rigidity of these nanotubes. The rigidity degree of nanotubes prior and after dispersion in milli-Q water was previously studied (see Chapter 4, Figure 4.13). The rigidity degree of (PLA/OVA) nanotubes is dropped by 60% while the rigidity degree of (PAH/PSS) and (PAH/OVA) is dropped by 40%. Those rigidity values were calculated by measuring the root-mean-square end-to-end distance of each nanotube as well as their contour length. Therefore, it gives an idea about the rigidity "along" the nanotube structure. However, as observed from Figure 5.22.d, some swelling occurs in "radial direction" for $(PAH/OVA\ Alexa\ Fluor\ 488)_3$ nanotubes. These results indicate that in order to be uptaken by the cells, nanotubes should possess a certain degree of rigidity.

Three-dimensional images obtained from confocal microscopy show that nanotubes have been uptaken by cells and give an idea about nanotubes structure inside the cells (Figure 5.27). The uptake process is indeed phagocytosis.

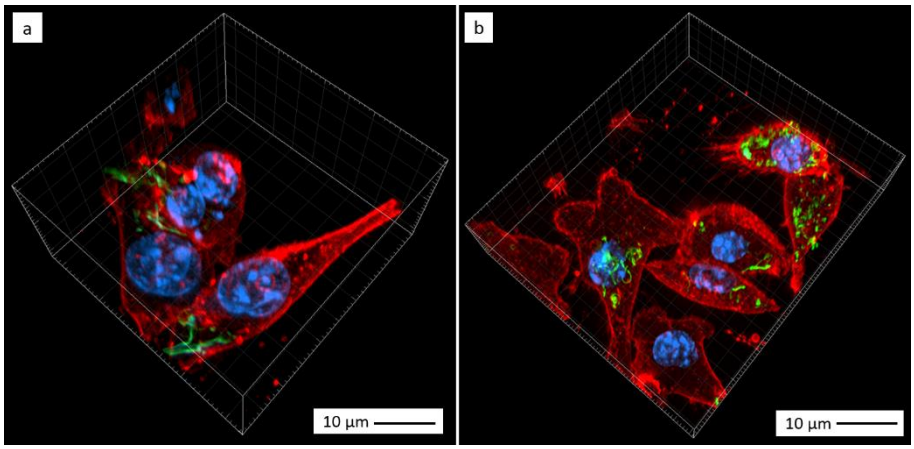

Figure 5.27. 3 dimensional images of nanotubes uptaken by the cells. (a) $(PAH\text{-}FITC/PSS)_3$ nanotubes of 500 nm outer diameter and 21 µm length, (b) $(PLA/OVA\ Alexa\ Fluor\ 488)_3$ nanotubes of 500 nm outer diameter and 21 µm length. The cells membrane was stained red and the cells nuclei was stained blue. (The analyzed z-axis distance was about 20 µm).

6.4 Conclusion

The stability of LbL assembled nanotubes composed of different polyelectrolytes ranging from fully synthetic (PAH/PSS) and (PAH/PAA) to protein-based (PAH/OVA) and biological (PLA/OVA) was checked in milli-Q water and DPBS. It was observed that nanotubes are more stable when they are filtered over a support. Free-floating nanotubes have a higher tendency to disruption and aggregation while being dispersed and stirred in aqueous medium. Since DPBS is going to be used as the cell culture medium for in vitro tests, different strategies such as grafting PEG chains on the surface of the tubes, conditioning the tubes beforehand in DPBS or ultimately constructing tubes in DPBS were developed to improve nanotubes stability in DPBS.

Nanotubes were next incubated with dendritic cells (DC2.4) and their cellular uptake was studied. Shorter nanotubes had a higher chance to be

internalized by the cells. A larger amount of synthetic $(PAH\text{-}FITC/PSS)_3$ nanotubes was uptaken compared to protein-based nanotubes. This could be related to the rigidity degree of nanotubes. Indeed, nanotubes should possess a certain rigidity degree in order to be phagocytosed by the cells. Nanotubes that are soft and highly hydrated are therefore less likely to be uptaken by the cells.

In brief, results obtained in this study demonstrate that LbL assembled nano-objects can be uptaken and internalized by cells and can maintain their structure and morphology after phagocytosis. These key findings pave the way to further use of LbL assembled nanotubes in various biomedical applications and in particular, in the field of drug delivery.

Bibliography

(1) Yan, Y.; Such, G. K.; Johnston, A. P. R.; Lomas, H.; Caruso, F. Toward Therapeutic Delivery with Layer-by-Layer Engineered Particles. *ACS Nano* **2011**, *5*, 4252–4257.

(2) Zhang, X.-Q.; Xu, X.; Bertrand, N.; Pridgen, E.; Swami, A.; Farokhzad, O. C. Interactions of Nanomaterials and Biological Systems: Implications to Personalized Nanomedicine. *Adv. Drug Deliv. Rev.* **2012**, *64*, 1363–1384.

(3) Natarajan, J. V; Nugraha, C.; Ng, X. W.; Venkatraman, S. Sustained-Release from Nanocarriers: A Review. *J. Control. Release* **2014**, *193*, 122–138.

(4) Kamaly, N.; Xiao, Z.; Valencia, P. M.; Radovic-Moreno, A. F.; Farokhzad, O. C. Targeted Polymeric Therapeutic Nanoparticles: Design, Development and Clinical Translation. *Chem. Soc. Rev.* **2012**, *41*, 2971–3010.

(5) Cepak, V. M.; Martin, C. R. Preparation of Polymeric Micro- and Nanostructures Using a Template-Based Deposition Method. *Chem. Mater.* **1999**, *11*, 1363–1367.

(6) Gratton, S. E. A.; Ropp, P. A.; Pohlhaus, P. D.; Luft, J. C.; Madden, V. J.; Napier, M. E.; DeSimone, J. M. The Effect of Particle Design on Cellular Internalization Pathways. *Proc. Natl. Acad. Sci. U. S. A.* **2008**, *105*, 11613–11618.

(7) Komatsu, T. Protein-Based Nanotubes for Biomedical Applications. *Nanoscale* **2012**, *4*, 1910–1918.

(8) Hammond, P. T. Polyelectrolyte Multilayered Nanoparticles: Using Nanolayers for Controlled and Targeted Systemic Release. *Nanomedicine (Lond).* **2012**, *7*, 619–622.

(9) Azzaroni, O.; Lau, K. H. A. Layer-by-Layer Assemblies in Nanoporous Templates: Nano-Organized Design and Applications of Soft Nanotechnology. *Soft Matter* **2011**, *7*, 8709–8724.

(10) Hillaireau, H.; Couvreur, P. Nanocarriers' Entry into the Cell: Relevance to Drug Delivery. *Cell. Mol. Life Sci.* **2009**, *66*, 2873–2896.

(11) Johnston, A. P. R. R.; Such, G. K.; Ng, S. L.; Caruso, F. Challenges Facing Colloidal Delivery Systems : From Synthesis to the Clinic. *Curr. Opin. Colloid Interface Sci.* **2011**, *16*, 171–181.

(12) Vergaro, V.; Scarlino, F.; Bellomo, C.; Rinaldi, R.; Vergara, D.; Maffia, M.; Baldassarre, F.; Giannelli, G.; Zhang, X.; Lvov, Y. M.; *et al.* Drug-Loaded Polyelectrolyte Microcapsules for Sustained Targeting of Cancer Cells. *Adv. Drug Deliv. Rev.* **2011**, *63*, 847–864.

(13) Kastl, L.; Sasse, D.; Wulf, V.; Hartmann, R.; Mircheski, J.; Ranke, C.; Carregal-Romero, S.; Martínez-López, J. A.; Fernández-Chacón, R.; Parak, W. J.; *et al.* Multiple Internalization Pathways of Polyelectrolyte Multilayer Capsules into Mammalian Cells. *ACS Nano* **2013**, *7*, 6605–6618.

(14) Yameen, B.; Choi, W. Il; Vilos, C.; Swami, A.; Shi, J.; Farokhzad, O. C. Insight into Nanoparticle Cellular Uptake and Intracellular Targeting. *J. Control. Release* **2014**, *190*, 485–499.

(15) Łukasiewicz, S.; Szczepanowicz, K.; Lukasiewicz, S.; Szczepanowicz, K.; Łukasiewicz, S.; Szczepanowicz, K.; Lukasiewicz, S. In Vitro Interaction of Polyelectrolyte Nanocapsules with Model Cells. *Langmuir* **2014**, *30*, 1100–1107.

(16) Zhang, Y.; Tekobo, S.; Tu, Y.; Zhou, Q.; Jin, X.; Dergunov, S. a; Pinkhassik, E.; Yan, B. Permission to Enter Cell by Shape: Nanodisk vs Nanosphere. *ACS Appl. Mater. Interfaces* **2012**.

(17) Shimoni, O.; Yan, Y.; Wang, Y.; Caruso, F. Shape-Dependent Cellular

Processing of Polyelectrolyte Capsules. *ACS Nano* **2013**, *7*, 522–530.

(18) Gilbert, J. B.; O'Brien, J. S.; Suresh, H. S.; Cohen, R. E.; Rubner, M. F.; Brien, J. S. O. Orientation-Specific Attachment of Polymeric Microtubes on Cell Surfaces. *Adv. Mater.* **2013**, *25*, 5948–5952.

(19) Buyukserin, F.; Medley, C. D.; Mota, M. O.; Kececi, K.; Rogers, R. R.; Tan, W.; Martin, C. R. Antibody-Functionalized Nano Test Tubes Target Breast Cancer Cells. *Nanomedicine (Lond).* **2008**, *3*, 283–292.

(20) Perry, J. L.; Guo, P.; Johnson, S. K.; Mukaibo, H.; Stewart, J. D.; Martin, C. R. Fabrication of Biodegradable Nano Test Tubes by Template Synthesis. *Nanomedicine (Lond).* **2010**, *5*, 1151–1160.

(21) Kalaskar, D. M.; Demoustier-champagne, S.; Dupont-Gillain, C. C. Interaction of Preosteoblasts with Surface-Immobilized Collagen-Based Nanotubes. *Colloids Surfaces B Biointerfaces* **2013**, *111*, 134–141.

(22) Kalaskar, D. M.; Poleunis, C.; Dupont-Gillain, C.; Demoustier-Champagne, S. Elaboration of Nanostructured Biointerfaces with Tunable Degree of Coverage by Protein Nanotubes Using Electrophoretic Deposition. *Biomacromolecules* **2011**, *12*, 4104–4111.

(23) Keselowsky, B. G.; Xia, C. Q.; Clare-Salzler, M. Multifunctional Dendritic Cell-Targeting Polymeric Microparticles. *Hum. Vaccin.* **2011**, *7*, 37–44.

(24) Silva, A. L.; Rosalia, R. A.; Varypataki, E.; Sibuea, S.; Ossendorp, F.; Jiskoot, W. Poly-(lactic-Co-Glycolic-Acid)-Based Particulate Vaccines: Particle Uptake by Dendritic Cells Is a Key Parameter for Immune Activation. *Vaccine* **2015**, *33*, 847–854.

(25) De Koker, B. S.; De Geest, B. G.; Singh, S. K. K.; Van Kooyk, Y.; De Meester, J.; De Smedt, S. C.; Grooten, J. Polyelectrolyte

Microcapsules as Antigen Delivery Vehicles towards Dendritic Cells: Uptake , Processing and Cross-Presentation of Encapsulated Antigens. *Angew. Chem. Int. Ed. Engl.* **2009**, *48*, 8485–8489.

(26) De Koker, S.; De Cock, L. J.; Rivera-Gil, P.; Parak, W. J.; Auzély Velty, R.; Vervaet, C.; Remon, J. P.; Grooten, J.; De Geest, B. G. Polymeric Multilayer Capsules Delivering Biotherapeutics. *Adv. Drug Deliv. Rev.* **2011**, *63*, 748–761.

(27) De Cock, L. J.; De Koker, S.; De Geest, B. G.; Grooten, J.; Vervaet, C.; Remon, J. P.; Sukhorukov, G. B.; Antipina, M. N.; Cock, L. J. De; Koker, S. De; *et al.* Polymeric Multilayer Capsules in Drug Delivery. *Angew. Chem. Int. Ed. Engl.* **2010**, *49*, 6954–6973.

(28) De Koker, S.; Lambrecht, B. N.; Willart, M. A.; Van Kooyk, Y.; Grooten, J.; Vervaet, C.; Remon, J.-P.; De Geest, B. G. Designing Polymeric Particles for Antigen Delivery. *Chem. Soc. Rev.* **2011**, *40*, 320–339.

(29) De Geest, B. G.; Sanders, N. N.; Sukhorukov, G. B.; Demeester, J.; De Smedt, S. C.; Geest, B. G. De; Smedt, S. C. De. Release Mechanisms for Polyelectrolyte Capsules. *Chem. Soc. Rev.* **2007**, *36*, 636–649.

(30) De Geest, B. G.; Vandenbroucke, R. E.; Guenther, A. M.; Sukhorukov, G. B.; Hennink, W. E.; Sanders, N. N.; Demeester, J.; De Smedt, S. C. Intracellularly Degradable Polyelectrolyte Microcapsules. *Adv. Mater.* **2006**, *18*, 1005–1009.

(31) Dierendonck, M.; De Koker, S.; Vervaet, C.; Remon, J. P.; De Geest, B. G. Interaction between Polymeric Multilayer Capsules and Immune Cells. *J. Control. Release* **2012**, *161*, 592–599.

(32) De Temmerman, M.-L.; Rejman, J.; Vandenbroucke, R. E.; De Koker, S.; Libert, C.; Grooten, J.; Demeester, J.; Gander, B.; De Smedt, S. C. Polyelectrolyte LbL Microcapsules versus PLGA Microparticles for Immunization with a Protein Antigen. *J. Control. Release* **2012**, *158*, 233–239.

(33) De Geest, B. G.; De Koker, S.; Demeester, J.; De Smedt, S. C.; Hennink, W. E. Self-Exploding Capsules. *Polym. Chem.* **2010**, *1*, 137.

(34) Saghazadeh, S.; Zhang, S.; Lefèvre, D.; Le Beulze, A.; Jonas, A. M.; Demoustier-Champagne, S. Universal Method to Transfer Membrane-Templated Nano-Objects to Aqueous Solutions. *Langmuir* **2015**, *31*, 7264–7273.

7 Conclusions and perspectives

In this work, we aimed to push the boundaries of nanoparticle-based drug delivery systems by fabricating multilayer assembled tubular nano-objects of different compositions, transferring them from organic solvent medium to aqueous medium, functionalizing their surface with antifouling moieties and studying their interactions with model immune cells while addressing the challenges arose at each step.

First, LbL assembled multilayer flat films and nanotubes were fabricated either by LbL deposition over a flat substrate or combining LbL assembly with template synthesis method. Template synthesis method provided us the possibility to fine-tune the dimensions of nanotubes and LbL assembly and gave us the opportunity to use a wide range of materials as building blocks of the nanotubes.

Studied systems had different chemistry ranging from strong to weak polyelectrolytes and up to biological macromolecules. We observed that the growth of multilayers in geometrically confined nanostructures differs from that of flat surfaces, which is in accordance with previous studies. We also observed the flattening of protein containing nanotubes upon drying. As it turns out, the soft nature of these tubes is indeed a crucial point that will affect their further application.

Next, different strategies to efficiently collect and disperse nanotubes in water were explored. Among them, the adjuvant-assisted filtration approach, using dextran as adjuvant, was particularly efficient and allowed the collection and dispersion in aqueous solution of all nanotubes studied in this work. This method is universal and independent of the chemistry of nano-objects and has been successful for collection and dispersion of other

tubular nano-objects such as polypyrrole nanotubes and gold nanowires in aqueous medium. Second, the method gives the opportunity of collecting a large number of nanotubes in one single filtration process. This method is especially applicable and interesting for systems where there is only a small amount of nanotubes to collect (for instance, a low amount of nanotubes composed of expensive molecules). The morphology of nanotubes was characterized prior to and after their immersion in water, revealing that the rigidity degree of LbL nanotubes strongly decreases after being in contact with water, leading to highly swollen and flexible nanotubes in aqueous solution.

Afterwards, on our route to approach an ideal drug carrier, we aimed to add antifouling PEG chains on the surface of nanotubes. We used block and graft polyelectrolyte-PEG copolymers both on flat surfaces and inside the pores. We found that depending on the conformation that PEG chains might adopt, further assembly could be partially or completely inhibited. Therefore, we aimed for covalently grafting PEG chains on the surface of the tubes after their release from the template. Primary amines available on nanotubes surface were shown to react successfully with NHS-PEG.

Our final step was to incubate dendritic cells with LbL assembled nanotubes to observe their interaction with cells and verify if the nanotubes are uptaken by phagocytosis. To this aim, the stability of nanotubes in milli-Q water as well as in cell culture medium (which is DPBS buffer, pH = 7.1) was studied. We found out that some nanotubes were less stable in DPBS compared to others. Therefore, different strategies were developed to improve the stability of nanotubes in culture medium. It was observed that short synthetic nanotubes had a higher chance of being phagocytosed by the cells. Such a difference in phagocytosis is probably due to difference in nanotubes

rigidity degree. Nanotubes maintained their structure inside the cells after being internalized.

We are certain that these key findings shed some light on further use of template synthesized LbL assembled nanotubes in various biomedical applications. Nevertheless, many challenges are yet to overcome and many parameters have still to be studied.

For instance, tubular nano objects of shorter length and smaller diameter can be fabricated. In the present study, the shortest tubes were 10 µm long and had an outer diameter of 400 nm. Fabricating shorter nanotubes means using thinner PC templates that are extremely fragile and difficult to manipulate. An interesting alternative would be the use of nanoporous PC membranes with one closed surface. Such templates can have a thickness of 10 – 20 µm while the depth of the pores inside them reaches maximum 5 µm. Those templates are easy to manipulate and give the opportunity to fabricate nanotubes with one open and one closed end. In other terms, nano test tubes can be fabricated by this process. Up to now, only silica nano test tubes and chitosan nano test tubes were fabricated using alumina templates. Promising results were recently obtained in our group by fabricating (PAH/PSS) nano test tubes of 5 µm length and 300 nm pore diameter.

More profound and detailed studies should be conducted on nanotubes behavior in aqueous medium in order to have a quantitative evaluation of nanotubes stability. Interactions between cells and nanotubes should be studied at different time intervals to observe nanotubes/cells interaction overtime. In addition, quantitative evaluation of nanotubes uptaken by the cells should also be performed.

Another aspect worth investigation is the use of degradable components in nanotubes structure. This is particularly interesting for studying the kinetics

of drug release inside or outside of the cells. Well-known examples of hydrolytically degradable synthetic polycations are the members of poly(beta-amino ester)s family. Amino acid containing nanotubes can also be degraded by protease. By combining such elements, nanotubes providing sustained release of their cargo can be fabricated.

On our way to fabricate multifunctional nanotubular drug delivery systems, the surface of nanotubes plays a pivotal role and there is still a lot to be done in respect of nanotubes surface functionalization. An in-depth study of the density of grafted PEG chains per surface area is essential. In addition, functionalizing nanotubes surface with other components, such as targeting moieties, is also very interesting and worthy of investigation. Sophisticated systems with different functional groups on nanotubes ends and surface are also extremely intriguing.

Template synthesized LbL assembled nanotubes have a promising future in the development of therapeutic carriers and further studies is required to fully understand them as well as to optimize them towards real applications. It is a hope that this thesis inspires further research dedicated to tubular nano-objects for biomedical applications.

Appendix

A summary of composition and build-up conditions of the various studied LbL assembled nanotubes in each chapter.

Chapter 3.

Polycation	Polyanion	Construction medium	Amount of salt or buffer	Construction pH	Assembling method	Crust removal
PAH	PSS	milli-Q water	150 mM NaCl	neutral	LbL by dipping	After each bilayer
					LbL by filtration	After each layer
PAH	PAA	MES buffer	150 mM MES	5.5 ± 0.1	LbL by dipping	After each bilayer
					LbL by filtration	After each layer
PAH	OVA	HEPES buffer	10 mM HEPES	8 ± 0.1	LbL by dipping	After each bilayer
					LbL by filtration	After each layer
PLA	OVA	milli-Q water	150 mM NaCl	neutral	LbL by dipping	After each bilayer
					LbL by filtration	After each layer

Chapter 4.

Polycation	Polyanion	Construction medium	Amount of salt or buffer	Construction pH	Assembling method	Crust removal
PAH	PSS	milli-Q water	150 mM NaCl	neutral	LbL by dipping	After each bilayer
PAH	PAA	MES buffer	150 mM MES	5.5 ± 0.1	LbL by dipping	After each bilayer
PAH	OVA	HEPES buffer	10 mM HEPES	8 ± 0.1	LbL by dipping	After each bilayer
PLA	OVA	milli-Q water	150 mM NaCl	neutral	LbL by dipping	After each bilayer

Chapter 5.

polycation		polyanion	Construction medium	amount of salt or buffer	construction pH	Assembling method	Crust removal
PAH		PSS	milli-Q water	150 mM NaCl	neutral	LbL by dipping	After each bilayer
PAH		PAA	MES buffer	150 mM MES	5.5 ± 0.1	LbL by dipping	After each bilayer
PAH		OVA	HEPES buffer	10 mM HEPES	8 ± 0.1	LbL by dipping	After each bilayer
PLA		OVA	milli-Q water	150 mM NaCl	neutral	LbL by dipping	After each bilayer
PLA		PSS	milli-Q water	150 mM NaCl	neutral	LbL by dipping	After each bilayer
PLL-g-PEG		PSS	milli-Q water	150 mM NaCl	neutral	LbL by dipping	After each bilayer
PLL-b-PEG		PSS	milli-Q water	150 mM NaCl	neutral	LbL by dipping	After each bilayer
Shell	PLL-b-PEG	PSS	milli-Q water	150 mM NaCl	neutral	LbL by dipping	After each bilayer
Core	PAH	PSS					

Chapter 6.

polycation	polyanion	Construction medium	amount of salt or buffer	construction pH	Assembling method	Crust removal
PAH	PSS	milli-Q water	150 mM NaCl	neutral	LbL by filtration	After each layer
PAH	PAA	MES buffer	150 mM MES	5.5 ± 0.1	LbL by filtration	After each layer
PAH	OVA	HEPES buffer	10 mM HEPES	8 ± 0.1	LbL by filtration	After each layer
PLA	OVA	milli-Q water	150 mM NaCl	neutral	LbL by filtration	After each layer
PAH	PAA	DPBS buffer	150 mM DPBS	7.1 ± 0.1	LbL by filtration	After each layer
PAH	OVA	DPBS buffer	150 mM DPBS	7.1 ± 0.1	LbL by filtration	After each layer

Dissemination

Publications

- Saghazadeh, S.; Zhang, S.; Lefèvre, D.; Le Beulze, A.; Jonas, A. M.; Demoustier-Champagne, S. Universal Method to Transfer Membrane-Templated Nano-Objects to Aqueous Solutions. *Langmuir* **2015**, *31*, 7264–7273.
- Saghazadeh, S.; De Geest, B.; A.; Jonas, A. M.; Demoustier-Champagne, S. Surface Functionaliation of Multilayer Assembled Nanotubes and their Cellular Uptake (in preparation)

Communications

- **Layer-by-Layer Self-Assembled Nanotubes for Drug Delivery Applications**
  Saghazadeh, S.; De Geest, B.; Jonas, A. M.; Demoustier-Champagne, S.
  15th Conference of International Association of Colloid and Interface Scientists (IACIS), **2015**, Mainz, Germany
  (Oral presentation)
- **Layer-by-Layer Assembled Nanotubes for Drug Delivery Applications**
  Saghazadeh, S., Zhang, S.; De Geest, B.; Jonas, A. M.; Demoustier-Champagne, S
  Annual PhD Student Day by IMCN-UCL, 22 May **2015**,
  Louvian-la-Neuve, Belgium
  (Oral presentation)
- **Layer-by-Layer Assemblies in Nanoporous Templates: A « Gentle yet Versatile » Method toward Functional Nanotubes for Bio-related Applications**
  Saghazadeh, S.; Lefèvre, D.; Ramirez-Wong, D.; Zhang, S; Roy, C,; Kalaskar, D.; Landoulsi, J.; Doupont, C; Jonas, A. M,; Demoustier-Champagne, S.
  IMCN Institute Scientific Advisory Committee Visit, 13-14 March **2014**, Louvain-la-Neuve, Belgium
  (Poster presentation)

- **Self Assembled Layer by Layer Nanotubes for Drug Delivery Applications**
  Saghazadeh, S.; De Geest, B.; Jonas, A. M.; Demoustier-Champagne, S.
  Responsive Materials for Biological Applications: From Drug Delivery to Cell Culture Workshop, 17 March **2014**, Spa, Belgium
  (Poster presentation)
- **Polyelectrolyte Multilayered Tubular Nanocarriers for Drug Delivery Applications**
  Saghazadeh, S.; De Geest, B.; Jonas, A. M.; Demoustier-Champagne, S.
  Annual Meeting of Belgian Polymer Group (BPG), 16-17 May **2013**, Houffalize, Belgium
  (Poster presentation)
- **Polyelectrolyte Multilayered Tubular Nanocarriers for Drug Delivery Applications**
  Saghazadeh, S.; De Geest, B.; Jonas, A. M.; Demoustier-Champagne, S.
  Annual PhD Student Day by IMCN-UCL, 18 May **2013**,
  Louvain-la-Neuve, Belgium
  (Poster presentation)